
FINAL REPORT

**U.F. Project No: 00108015
FDOT Project No: BDV31-977-07**

MAXIMUM HEAT OF MASS CONCRETE – PHASE 2

**Mang Tia
Adrian Lawrence
Tu Anh Do
David Verdugo
Sangyoung Han
Mohammed Almarshoud
Brandon Ferrante
Ananya Markandeya**

November 2016

**Department of Civil and Coastal Engineering
Engineering School of Sustainable Infrastructure and Environment
College of Engineering
University of Florida
Gainesville, Florida 32611-6580**

DISCLAIMER

The opinions, findings, and conclusions expressed in this publication are those of the authors and not necessarily those of the State of Florida Department of Transportation or the U.S. Department of Transportation.

Prepared in cooperation with the State of Florida Department of Transportation and the U.S. Department of Transportation.

SI (MODERN METRIC) CONVERSION FACTORS (from FHWA)

APPROXIMATE CONVERSIONS TO SI UNITS

SYMBOL	WHEN YOU KNOW	MULTIPLY BY	TO FIND	SYMBOL
LENGTH				
in	inches	25.4	millimeters	mm
ft	feet	0.305	meters	m
yd	yards	0.914	meters	m
mi	miles	1.61	kilometers	km

SYMBOL	WHEN YOU KNOW	MULTIPLY BY	TO FIND	SYMBOL
AREA				
in²	square inches	645.2	square millimeters	mm ²
ft²	square feet	0.093	square meters	m ²
yd²	square yard	0.836	square meters	m ²
ac	acres	0.405	hectares	ha
mi²	square miles	2.59	square kilometers	km ²

SYMBOL	WHEN YOU KNOW	MULTIPLY BY	TO FIND	SYMBOL
VOLUME				
fl oz	fluid ounces	29.57	milliliters	mL
gal	gallons	3.785	liters	L
ft³	cubic feet	0.028	cubic meters	m ³
yd³	cubic yards	0.765	cubic meters	m ³

NOTE: volumes greater than 1000 L shall be shown in m³

SYMBOL	WHEN YOU KNOW	MULTIPLY BY	TO FIND	SYMBOL
MASS				
oz	ounces	28.35	grams	g
lb	pounds	0.454	kilograms	kg
T	short tons (2000 lb)	0.907	megagrams (or "metric ton")	Mg (or "t")

SYMBOL	WHEN YOU KNOW	MULTIPLY BY	TO FIND	SYMBOL
TEMPERATURE (exact degrees)				
°F	Fahrenheit	5 (F-32)/9 or (F-32)/1.8	Celsius	°C

SYMBOL	WHEN YOU KNOW	MULTIPLY BY	TO FIND	SYMBOL
ILLUMINATION				
fc	foot-candles	10.76	lux	lx
fl	foot-Lamberts	3.426	candela/m ²	cd/m ²

SYMBOL	WHEN YOU KNOW	MULTIPLY BY	TO FIND	SYMBOL
FORCE and PRESSURE or STRESS				
lbf	poundforce	4.45	newtons	N
kip	kilo poundforce	4.45	kilo newtons	kN
lbf/in²	poundforce per square inch	6.89	kilopascals	kPa

APPROXIMATE CONVERSIONS TO SI UNITS

SYMBOL	WHEN YOU KNOW	MULTIPLY BY	TO FIND	SYMBOL
LENGTH				
mm	millimeters	0.039	inches	in
m	meters	3.28	feet	ft
m	meters	1.09	yards	yd
km	kilometers	0.621	miles	mi

SYMBOL	WHEN YOU KNOW	MULTIPLY BY	TO FIND	SYMBOL
AREA				
mm²	square millimeters	0.0016	square inches	in ²
m²	square meters	10.764	square feet	ft ²
m²	square meters	1.195	square yards	yd ²
ha	hectares	2.47	acres	ac
km²	square kilometers	0.386	square miles	mi ²

SYMBOL	WHEN YOU KNOW	MULTIPLY BY	TO FIND	SYMBOL
VOLUME				
mL	milliliters	0.034	fluid ounces	fl oz
L	liters	0.264	gallons	gal
m³	cubic meters	35.314	cubic feet	ft ³
m³	cubic meters	1.307	cubic yards	yd ³

SYMBOL	WHEN YOU KNOW	MULTIPLY BY	TO FIND	SYMBOL
MASS				
g	grams	0.035	ounces	oz
kg	kilograms	2.202	pounds	lb
Mg (or "t")	megagrams (or "metric ton")	1.103	short tons (2000 lb)	T

SYMBOL	WHEN YOU KNOW	MULTIPLY BY	TO FIND	SYMBOL
TEMPERATURE (exact degrees)				
°C	Celsius	1.8C+32	Fahrenheit	°F

SYMBOL	WHEN YOU KNOW	MULTIPLY BY	TO FIND	SYMBOL
ILLUMINATION				
lx	lux	0.0929	foot-candles	fc
cd/m²	candela/m ²	0.2919	foot-Lamberts	fl

SYMBOL	WHEN YOU KNOW	MULTIPLY BY	TO FIND	SYMBOL
FORCE and PRESSURE or STRESS				
N	newtons	0.225	poundforce	lbf
kPa	kilopascals	0.145	poundforce per square inch	lbf/in ²

*SI is the symbol for International System of Units. Appropriate rounding should be made to comply with Section 4 of ASTM E380.

(Revised March 2003)

TECHNICAL REPORT DOCUMENTATION PAGE

1. Report No.	2. Government Accession No.	3. Recipient's Catalog No.	
4. Title and Subtitle Maximum Heat of Mass Concrete – Phase 2		5. Report Date <p style="text-align: center;">September 2016</p>	
		6. Performing Organization Code	
7. Author(s) M. Tia, A. Lawrence, T. Do, D. Verdugo, S. Han, M. Almarshoud, B. Ferrante, and A. Markandeya		8. Performing Organization Report No. <p style="text-align: center;">00108015</p>	
9. Performing Organization Name and Address Department of Civil and Coastal Engineering Engineering School of Sustainable Infrastructure & Environment University of Florida 365 Weil Hall – P.O. Box 116580 Gainesville, FL 32611-6580		10. Work Unit No. (TRAIS)	
		11. Contract or Grant No. <p style="text-align: center;">BDV31-977-07</p>	
12. Sponsoring Agency Name and Address Florida Department of Transportation 605 Suwannee Street, MS 30 Tallahassee, FL 32399		13. Type of Report and Period Covered <p style="text-align: center;">Final Report 05/21/13 – 11/30/16</p>	
		14. Sponsoring Agency Code	
15. Supplementary Notes <p style="text-align: center;">Prepared in cooperation with the U.S. Department of Transportation and the Federal Highway Administration</p>			
16. Abstract The main findings and recommendations from this study are as follows: <ol style="list-style-type: none"> (1) The database of adiabatic temperature rise tables which was developed in this study can be used in the DIANA software for the modeling of mass concrete structures. (2) Classification of segmental bridge sections should be based on local volume-to-area ratio (V/A), which excludes extremities, when it is used to identify if a certain segmental bridge section is considered as a mass concrete structure. (3) Recommended values for thermal properties of various insulating materials and soils to be used in thermal analysis of mass concrete structures are given. (4) The results of thermal analysis indicate that a typical drilled shaft with a diameter of over 4 feet would have a maximum temperature differential that exceeded the limit of 35 °F (19.4 °C) set by the FDOT. However, the four drilled shafts placed in this study did not show any visible cracks in spite of the high temperature differential, both calculated and measured. It is recommended that further investigation be undertaken to determine if the criterion for mass concrete could be relaxed for drilled shafts. (5) Prediction equations for estimating 28-day compressive strength from compressive strength at other curing times for ternary blend mixes were recommended. It is recommended a more extensive testing program be conducted to verify and refine the developed equations. (6) It is recommended that the developed interface software DIANA Input File Generator (DIFG) be used by Florida Department of Transportation (FDOT) personnel for quick thermal analysis of rectangular concrete footings and cylindrical concrete drilled shafts. 			
17. Key Words Mass concrete; thermal analysis; isothermal calorimetry; drilled shaft; soil foundation; R-value; temperature differential; temperature monitoring; insulation; temperature logger; TNO DIANA; ternary blend mix; interface software.		18. Distribution Statement <p style="text-align: center;">No restrictions.</p>	
19. Security Classif. (of this report) <p style="text-align: center;">Unclassified</p>	20. Security Classif. (of this page) <p style="text-align: center;">Unclassified</p>	21. No. of Pages <p style="text-align: center;">416</p>	22. Price

ACKNOWLEDGMENTS

The Florida Department of Transportation (FDOT) is gratefully acknowledged for providing the financial support for this study. The FDOT Materials Office provided the additional testing equipment, materials, and personnel needed for this investigation. Sincere thanks go to the project manager, Mr. Michael Bergin, for providing his technical coordination and advice throughout the project. The valuable technical advice and support from Dr. Harvey Deford and Messrs. Richard DeLorenzo, Shelby Brothers, Patrick Carlton, and Gwendolyn Cochran of FDOT are duly acknowledged. Sincere appreciation also goes to W.R. Grace and Company for providing the admixtures and to Argos USA Corporation for providing the cement, slag, and fly ash for the laboratory study.

EXECUTIVE SUMMARY

Main Objectives of the Study

This research study addressed several key issues in the area of mass concrete structures in Florida. The specific objectives of the study were as follows:

- (1) To build a database of rate of heat production of different cement blends used in mass concrete in Florida so that this needed information for thermal analysis of mass concrete would be readily available.
- (2) To evaluate typical segmental bridge pier segments used in Florida to determine whether some of them need to be treated as mass concrete.
- (3) To investigate the insulating properties of different types of soil and under various moisture conditions to be used in thermal analysis of mass concrete placed on them.
- (4) To evaluate typical drilled shafts used in Florida to determine whether some of them need to be treated as mass concrete.
- (5) To study the strength development of ternary blend concrete mixes in Florida to develop equations for determining 28-day compressive strength from the strength of concrete that is older than 28 days.
- (6) To develop user-friendly interface software for thermal analysis of mass concrete so that this needed analysis can be performed readily.

Work Accomplished and Main Findings

Development of Database of Rate of Heat Production of Cement Blends

FDOT mix designs that are classified for use in mass concrete applications were identified. Samples of the cementitious components from these identified concrete mixes were tested for their heat of hydration using the isothermal calorimetry test. The results were used to develop a database of adiabatic temperature rise tables which can be readily used in the DIANA software for thermal analysis of mass concrete structures.

Thermal Analysis of Segmental Bridge Structures

Thermal analysis using the DIANA software was performed on typical segmental bridge pier segments used in Florida to evaluate their temperature development and distribution during construction. The main findings are as follows:

- (1) Classification of segmental bridge sections as mass concrete structures, based on overall volume-to-area (V/A) ratio, is not adequate. Bridge sections with V/A ratios less than 1.0 foot could produce maximum temperature differentials which failed limits set by FDOT.
- (2) Local V/A ratio, which excludes extremities, is more appropriate in classifying and identifying segmental bridge sections as mass concrete structures.
- (3) Maximum temperatures and maximum temperature differentials of segmental bridge sections are greatly influenced by the heat of hydration of the cementitious materials used in the concrete.
- (4) Use of high-strength concrete in analysis produced the highest temperatures and temperature differentials.

- (5) Use of pozzolanic cementitious material replacement, in particular HVFA, greatly reduces the maximum temperature and maximum temperature differential in segmental bridge sections.

Determination of Thermal Properties of Soils in Different Moisture Conditions

A laboratory testing program was conducted to determine the R-values of several typical soils in Florida under varying moisture conditions. The test results show that moisture content is the main factor affecting the insulation property of soils. The R-value of soil decreases sharply as the moisture content increases. Variation in temperature has minimal effects on the R-value of soil.

Analytical Evaluation of Drilled Shafts

Finite element models using the DIANA software were developed to analyze the temperature development of drilled shafts under dry and wet conditions. The main findings are summarized as follows:

- (1) All concrete mixtures which were used in this study to model the thermal behavior of a drilled shaft with a diameter of over 4 feet produced maximum temperature differentials that exceeded the limit of 19.4 °C (35.0 °F) set by the FDOT.
- (2) For drilled shafts with diameters less than 6 feet, the maximum concrete temperature and the maximum concrete temperature differential were not significantly affected by the depth of the drilled shaft.
- (3) The use of pozzolanic material as replacement for Portland cement reduced the maximum temperature and maximum temperature difference in the drilled shaft.
- (4) A shaft with centroid void is a viable alternative shaft design for controlling not only the maximum temperature but also the maximum temperature difference of mass concrete drilled shafts.

Field Evaluation of Drilled Shafts

Four concrete drilled shafts, which were six feet in diameter and seven feet in length, were placed in a Florida soil to a depth of six feet to evaluate the temperature development in the concrete at early age subject to the effects of concrete mixes used and the moisture condition of the surrounding soil. The two concrete mixes used were a slag-cement concrete mix with a relatively low heat of hydration and a pure Portland cement concrete mix with a high heat of hydration. The two soil conditions used were a dry condition and a wet condition.

The results of the study show that the use of slag-cement concrete mix had substantially reduced the maximum temperature differential in the drilled shafts. However, the maximum temperature differentials in all four shafts exceeded the maximum allowable limit of 19.4 °C (35.0 °F) according to FDOT specifications for mass concrete. For the two shafts which used a pure cement concrete mix, the maximum allowable temperature of 82.2 °C (180.0 °F) according to FDOT specifications for mass concrete was also exceeded.

For the four shafts tested, there was no significant difference between effects of the wet soil and dry soil environment. This was due to the fact that there was no difference in the first four feet of soil, and the difference in moisture condition of the soil beyond four feet depth was not enough to cause any noticeable difference in the developed temperature in the shafts.

Thermal analysis using the developed DIANA finite element model was performed to determine the temperature development of these four drilled shafts at early age. The computed temperatures were found to match fairly well with the measured temperature values. This indicates that the finite element thermal analysis model used in this study can make fairly accurate predictions of temperature development in concrete drilled shafts at early age.

Laboratory Study on Strength Development of Ternary Blend Concrete Mixes

A laboratory testing program was conducted to study the strength development of ternary blend concrete mixes in Florida. Statistical analyses were performed to develop predictions which can be used for determining 28-day compressive strength from the strength of concrete that is older than 28 days. Based on the strength gain characteristics of ternary blend mixes as evaluated by their strength gaining factor ($f'_c(t)/f'_c(28)$) in this laboratory study, the ternary blend mixes in Florida can be divided into 4 categories and a separate prediction equation can be used for each category of mix for estimation of 28-day compressive strength from compressive strength at other curing time. The recommended prediction equations for estimating 28-day compressive strength from compressive strength at other curing times are presented in Table 7-32 (in Chapter 7). Prediction equations were also developed for relating compressive strength to the elastic modulus, splitting tensile strength, and flexural strength of ternary blend mixes in Florida. The equations are presented in Equations 7-1, 7-2, and 7-3 (in Chapter 7).

Development of User-Friendly Interface Software for Mass Concrete Analysis

A user-friendly interface software, Diana Input File Generator (DIFG), was developed for use in thermal analysis of (1) rectangular concrete footings and (2) cylindrical concrete drilled shafts using the DIANA software. This developed interface software makes it possible for someone without extensive training in finite element method or the DIANA software to perform thermal analysis of these two types of mass concrete structures in Florida.

Recommendations

The following recommendations are made based on the findings from this study:

- (1) The database of adiabatic temperature rise tables which was developed in this study can be used in the DIANA software for the modeling of mass concrete structures. It is recommended that this database be expanded to include ternary blend mixes which are viable mix designs for mass concrete application.
- (2) Classification of segmental bridge sections should be based on local V/A ratio, which excludes extremities, when it is used to identify if a certain segmental bridge section is considered as a mass concrete structure. A thermal analysis should be performed if the LOCAL V/A ratio is very close to or exceeds 1.0 foot. A field study should be conducted to monitor the temperature development in segmental bridge sections during construction in order to validate the analytical results from the thermal analysis using the DIANA software.
- (3) Based on the results from the laboratory testing program and literature review, the recommended thermal properties of various insulating materials and soils to be used in thermal analysis of mass concrete structures are presented in Table 8-2.
- (4) The results of thermal analysis indicate that a typical drilled shaft with a diameter of over 4 feet would have a maximum temperature differential that exceeded the limit of 19.4 °C (35.0 °F) set by the FDOT, and thus should be considered as mass concrete. However, the four drilled shafts placed in this study did not show any visible cracks in spite of the high temperature differential, both calculated and measured. It is recommended that further investigation be undertaken to determine if the criterion for mass concrete could be relaxed for drilled shafts.

- (5) Prediction equations for estimating 28-day compressive strength from compressive strength at other curing times for ternary blend mixes were recommended. However, since the developed prediction equations were based on a limited testing program on only 14 concrete mixes, it is recommended that a more extensive testing program be conducted to verify and refine the developed equations.
- (6) It is recommended that the developed interface software DIFG be used by FDOT personnel for quick thermal analysis of rectangular concrete footings and cylindrical concrete drilled shafts. After some period of evaluation of the software, further refinement and upgrade of the software can be done based on the needs of FDOT.

TABLE OF CONTENTS

	<u>page</u>
DISCLAIMER	ii
SI (MODERN METRIC) CONVERSION FACTORS (from FHWA)	iii
TECHNICAL REPORT DOCUMENTATION PAGE	v
ACKNOWLEDGMENTS	vi
EXECUTIVE SUMMARY	vii
Main Objectives of the Study	vii
Work Accomplished and Main Findings	viii
Development of Database of Rate of Heat Production of Cement Blends.....	viii
Thermal Analysis of Segmental Bridge Structures	viii
Determination of Thermal Properties of Soils in Different Moisture Conditions.....	ix
Analytical Evaluation of Drilled Shafts	ix
Field Evaluation of Drilled Shafts	x
Laboratory Study on Strength Development of Ternary Blend Concrete Mixes.....	xi
Development of User-Friendly Interface Software for Mass Concrete Analysis.....	xi
Recommendations.....	xii
LIST OF TABLES	xxi
LIST OF FIGURES	xxviii
CHAPTER	
1 INTRODUCTION	1
1.1 Background and Research Needs	1
1.1.1 Need for Data Base of Rate of Heat Production of Different Cement Blends	3
1.1.2 Need for Investigation on Segmental Bridge Pier Segments	3
1.1.3 Need for Investigation of Soil as an Insulator	4
1.1.4 Need for Extension of Mass Concrete Research to Drilled Shafts.....	5
1.1.5 Need for Study of Strength Development of Ternary Blend Concrete Mixes	6
1.1.6 Need for Development of the User-Friendly Software for Mass Concrete Analysis.....	6
1.2 Objectives of Study.....	7
1.3 Approach and Scope of Research	8
2 DEVELOPMENT OF DATABASE OF RATE OF HEAT PRODUCTION OF CEMENT BLENDS FOR MASS CONCRETE.....	10
2.1 Introduction.....	10

2.2	Isothermal Calorimetry Test Equipment	10
2.3	Isothermal Calorimetry Testing Procedure.....	15
2.3.1	Determination of Temperature Rise Inputs	17
2.3.2	Estimating Degree of Hydration.....	18
2.3.3	Determination of Activation Energy	20
2.4	Results of Isothermal Calorimetry Tests	21
2.4.1	Mix Design and Proportioning of Concrete Mixes Tested.....	21
2.4.2	Method for Presentation and Interpretation of Test Results.....	23
2.4.3	Tests Conducted on Paste Fractions without Admixtures	24
2.4.4	Tests on Cementitious Systems with Admixtures	25
2.5	Tables of Heat of Hydration and Temperature Rise Inputs	29
2.6	Activation Energy and Arrhenius Constant for Cement Blends.....	38
2.7	Database Interface Program for Mass Concrete Mixes	38
3	THERMAL ANALYSIS OF SEGMENTAL BRIDGE STRUCTURES	40
3.1	Overview.....	40
3.2	Description of Finite Element Model	40
3.3	Results of Thermal Analysis.....	44
3.3.1	Parametric Studies	44
3.3.2	Effect of V/A Ratio on Temperature Development	44
3.3.3	Effect of Heat of Hydration on Temperature Development	47
3.4	Summary of Findings	52
4	DETERMINATION OF THERMAL PROPERTIES OF SOILS IN DIFFERENT MOISTURE CONDITIONS	53
4.1	Introduction.....	53
4.2	Results of Laboratory Testing Program.....	53
4.2.1	Materials Tested	53
4.2.2	R-value of Soils as Affected by Moisture and Temperature	56
4.2.3	R-value of Muck as Affected by Temperature	65
4.2.4	R-value of Lime Rock as Affected by Moisture and Temperature	66
4.2.5	R-value of Concrete as Affected by Temperature	67
5	EVALUATION OF DRILLED SHAFTS FOR CONSIDERATION AS MASS CONCRETE STRUCTURES.....	68
5.1	Introduction.....	68
5.1.1	Background and Research Needs	68
5.1.2	Current Standards and Specifications.....	69
5.1.3	Objectives	69
5.2	Description of Finite Element Model Used for Thermal Analysis.....	70
5.2.1	Overview of Finite Element Model.....	70
5.2.2	Element Selection.....	70
5.2.3	Parametric Input Values	71
5.2.4	Model Geometry.....	75

5.3	Parametric Thermal Analysis	76
5.3.1	Solid Drilled Shafts of Varying Diameters in Soils of Varying Moisture Levels	76
5.3.2	Concretes of Different Cementitious Compositions.....	78
5.4	Results of Thermal Analysis of Drilled Shaft.....	79
5.4.1	Effects of Length and Diameter of Solid Drilled Shafts	79
5.4.2	Effects of Cementitious Composition of Concrete.....	83
5.4.3	Effect of Using Centroid Void in Drilled Shafts	87
5.5	Summary of Findings	90
6	FIELD EVALUATION OF DRILLED SHAFT	91
6.1	Introduction.....	91
6.2	Mix Designs and Properties of Concrete Used in Drilled Shafts	92
6.3	Moisture Level and R-Value of Soil Surrounding the Four Drilled Shafts	93
6.4	Measured Temperature Distributions in the Drilled Shafts.....	94
6.5	Thermal Analysis of the Four Drilled Shafts.....	107
6.5.1	Overview	107
6.5.2	Finite Element Model for the Four Drilled Shafts.....	107
6.5.3	Heat of Hydration and Thermal Properties of Concrete.....	108
6.5.4	Results of Thermal Analysis of the Four Drilled Shafts	110
6.6	Summary of Findings	110
7	LABORATORY STUDY ON STRENGTH DEVELOPMENT OF TERNARY BLEND CONCRETE MIXES	112
7.1	Introduction.....	112
7.2	Laboratory Testing Program.....	113
7.2.1	Design of Experiment.....	113
7.2.2	Materials	117
7.2.2.1	Aggregates.....	117
7.2.2.2	Portland Cement	121
7.2.2.3	Fly Ash	124
7.2.2.4	Ground Blast-Furnace Slag	125
7.2.2.5	Silica Fume.....	126
7.2.2.6	Admixtures	126
7.3	Test Results.....	127
7.3.1	Fresh Concrete Properties.....	127
7.3.2	Results of Hardened Concrete Tests.....	129
7.3.2.1	Compressive Strength	129
7.3.2.2	Splitting Tensile Strength.....	133
7.3.2.3	Flexural Strength	136
7.3.2.4	Modulus of Elasticity	139
7.4	Developed Prediction Equations.....	142
8	DEVELOPMENT OF USER-FRIENDLY SOFTWARE FOR THERMAL ANALYSIS OF MASS CONCRETE	144

8.1 Introduction.....	144
8.2 Overview of DIFG.....	145
8.2.1 Three Main Steps in Thermal Analysis Using DIANA.....	145
8.2.2 Main Functions of DIFG.....	145
8.3 Needed Inputs for Running of DIFG.....	148
8.3.1 Introduction.....	148
8.3.2 Needed information for Thermal Analysis of Rectangular Footing.....	148
8.3.3 Needed information for Thermal Analysis of Drilled Shaft.....	152
8.4 An Example of Thermal Analysis of a Drilled Shaft Using DIFG.....	153
8.4.1 Input Information for the Drilled Shaft TO BE Analyzed.....	153
8.4.2 Output Files from DIFG.....	155
9 FINDINGS AND RECOMMENDATIONS.....	158
9.1 Summary of Work Accomplished and Main Findings.....	158
9.1.1 Development of Database of Rate of Heat Production of Cement Blends.....	158
9.1.2 Thermal Analysis of Segmental Bridge Structures.....	158
9.1.3 Determination of Thermal Properties of Soils in Different Moisture Conditions.....	159
9.1.4 Analytical Evaluation of Drilled Shafts.....	159
9.1.5 Field Evaluation of Drilled Shafts.....	160
9.1.6 Laboratory Study on Strength Development of Ternary Blend Concrete Mixes.....	161
9.1.7 Development of User-Friendly Interface Software for Mass Concrete Analysis.....	161
9.2 Recommendations.....	162
LIST OF REFERENCES.....	164
APPENDIX	
A TYPICAL HIGH-STRENGTH CONCRETE DIANA INPUT FILE.....	169
B DEVELOPMENT of MIX DESIGN DATABASE 1.0.....	173
B.1 Introduction.....	173
B.2 Overview of Database Applications.....	173
B.2.1 Types of Databases.....	174
B.3 Database Architecture.....	174
B.3.1 General Structure.....	175
B.3.2 The User Interface (UI).....	175
B.3.3 The Data Source and Dataset.....	176
B.4 Database Interface Program.....	178
B.5 Example: How To Find a Mix Design Based on W/C Ratio.....	180
B.5.1 Step 1.....	180
B.5.2 Step 2.....	180
B.6 Example: How To Find a Mix Design Based on Mix Number.....	181
B.6.1 Step 1.....	181

B.6.2 Step 2	181
B.7 Example: How To Change Mix Design Information.....	182
B.7.1 Step 1	182
B.7.2 Step 2	183
B.7.3 Step 3	183
B.8 Example: How To Add New Mix Designs into the Database	184
B.8.1 Step 1	184
B.8.2 Step 2	185
B.8.3 Step 3	185
 C CODES OF DATABASE MIX DESIGN DATABASE 1.0 FOR VISUAL STUDIO.....	186
 D EQUIPMENT AND TEST PROCEDURE FOR EVALUATION OF INSULATION PROPERTIES OF SOIL.....	191
D.1 Materials Tested.....	191
D.2 Testing Equipment and Procedures	193
D.2.1 Thermal Properties Analyzer.....	193
D.2.2 Temperature Control Box.....	195
D.2.3 Sample Container for Soil Samples.....	200
D.2.4 Glass Jars for Holding Samples.....	201
D.2.5 Treatment of Test Samples	202
D.2.6 Testing Procedures of the Thermal Properties Analyzer.....	206
 E CONSTRUCTION AND INSTRUMENTATION OF DRILLED SHAFTS	208
E.1 Overview	208
E.2 Mix Designs of Concrete Used in Drilled Shafts.....	209
E.3 Installation of Temperature Data Loggers	211
E.4 Dewatering of Soil	215
E.5 Pouring of Concrete	222
 F TESTING EQUIPMENT AND PROCEDURES FOR STUDY ON TERNARY BLEND CONCRETE MIXES.....	225
F.1 Fresh Concrete Tests (Plastic Properties).....	225
F.1.1 Slump	225
F.1.2 Unit Weight.....	227
F.1.3 Air Content.....	227
F.1.4 Temperature of Freshly Mixed Hydraulic-Cement Concrete	228
F.2 Hardened Concrete Tests (Mechanical Properties).....	230
F.2.1 Compressive Strength for 4” X 8” Cylindrical Concrete Specimens.....	230
F.2.2 Modulus of Elasticity (MOE).....	233
F.2.3 Splitting Tensile Strength Test.....	235
F.2.4 Flexural Strength of Concrete	237
 G STATISTICAL ANALYSIS OF DATA FROM TERNARY BLEND MIX STUDY	239

G.1	Analysis of Compressive Strength Data	239
G.1.1	Existing Models for Estimating Compressive Strength	239
G.1.2	Normalization of Data	241
G.1.3	Accuracy Measures.....	245
G.1.4	Results of Regression Analysis	245
G.1.4.1	Freiesleben Model	246
G.1.4.2	Modified CEB-FIP Model.....	259
G.1.4.3	Modified Hyperbolic Model.....	271
G.1.4.4	Second Degree Hyperbolic Model,	285
G.1.5	Comparison of Standard Error of Estimate for All Models.....	294
G.2	Analysis of Modulus of Elasticity Data	297
G.3	Analysis of Flexural Strength Data.....	299
G.4	Analysis of Splitting Tensile Strength Data	301
H	STRENGTH DATA FROM TERNARY BLEND MIX STUDY.....	303
H.1	Compressive Strength Data.	303
H.2	Modulus of Elasticity Data	317
H.3	Splitting Tensile Strength Data.....	324
H.4	Flexural Strength Data	331
I	DIFG BATCH FILE	338
J	DIFG PRE-PROCESSING FILE	339
K	DIFG COMMAND FILE	342
L	POST-PROCESSING FILE	343
M	CONCRETE.DAT FILE.....	346
N	USER MANUAL FOR DIFG FOR THERMAL ANALYSIS OF MASS CONCRETE	347
N.1	Introduction.....	347
N.2	Running DIFG and DIANA for Thermal Analysis of a Rectangular Footing.....	349
N.2.1	STEP 1: Installing Matlab Compiler Runtime	349
N.2.2	STEP 2: Opening DIANA Input File Generator (DIFG)	350
N.2.3	STEP 3: Inputting Parametric Values on DIFG Interface	351
N.2.4	STEP 4: Saving Output Files and Closing DIFG	354
N.2.5	STEP 5: Pre-Setting before Operating DIANA.....	356
N.2.6	STEP 6: Running DIANA Automatically	357
N.2.7	STEP 7: Reading the Output Files from DIANA Post-Processing	360
N.3	Thermal Analysis of Drilled Shaft.....	365
N.3.1	STEP 1: Installing Matlab-Language Operating File	365
N.3.2	STEP 2: Opening DIANA Input File Generator (DIFG)	365
N.3.3	STEP 3: Inputting Parametric Values on DIFG Interface	366
N.3.4	STEP 4: Saving Output Files and Closing DIFG	369
N.3.5	STEP 5: Pre-Setting before Operating DIANA.....	371

N.3.6 STEP 6: Running DIANA Automatically	372
N.3.7 STEP 7: Reading the Output Files from DIANA Post-Processing	375

LIST OF TABLES

<u>Table</u>	<u>page</u>
Table 2-1. Specific heats of materials used.	15
Table 2-2. List of mixes included in this study.....	21
Table 2-3. Paste fractions of mixes tested in this study.....	22
Table 2-4. Paste fractions tested with admixtures.	22
Table 2-5. Dosages of admixture used.....	26
Table 2-6. Heat of hydration for the cement blends.	30
Table 2-7. Temperature rise input for selected mixes.....	34
Table 2-8. Chemical composition of cement blends in the study.....	39
Table 2-9. Computed activation energies and arrhenius constants for cement blends.	39
Table 3-1. Width dimensions used for parametric study of segmental bridges.....	45
Table 3-2. Maximum temperature and temperature differentials calculated by DIANA using varying V/A ratios.....	47
Table 3-3. Properties of FDOT mixes used in parametric study.	48
Table 3-4. Maximum temperature and temperature differentials calculated by DIANA using FDOT mix designs.....	51
Table 4-1. Designation and origination of materials tested.	55
Table 4-2. R-values of soil samples at different moisture and temperature conditions.....	64
Table 5-1. Paste fractions tested for each mixture.	72
Table 5-2. Thermal properties of concrete used in FE models.	74
Table 5-3. Geometry of the drilled shafts studied.....	77
Table 5-4. Concrete mixtures used in parametric study.	78
Table 5-5. Heat energy of cementitious mixture obtained from isothermal calorimetry.....	83
Table 5-6. Dimensions of drilled shafts with centroid void analyzed.	87
Table 6-1. Mix designs and plastic properties of concrete used in each drilled shaft.	93

Table 6-2. R-values of drilled shaft soil at different moisture levels.....	94
Table 6-3. Elevation of temperature sensors in each drilled shaft and surrounding soil.	95
Table 6-4. Thermal properties and initial temperatures of the four drilled shaft concretes.....	109
Table 7-1. Classifications of ternary blend mixes evaluated.	113
Table 7-2. Mix designs of ternary blend mixes evaluated.	114
Table 7-3. Fresh concrete property tests.	116
Table 7-4. Hardened concrete property tests.	116
Table 7-5. Physical properties of silica sand used.	117
Table 7-6. Physical properties of Miami Oolite aggregate.	119
Table 7-7. Brooksville aggregate physical properties.....	120
Table 7-8. Chemical compositions of the cements used.....	122
Table 7-9. Physical properties of the cements used.....	123
Table 7-10. Fly ash chemical and physical properties.....	124
Table 7-11. Slag physical and chemical properties.	125
Table 7-12. Chemical composition of the silica fume used.....	126
Table 7-13. The plastic properties of slag and fly ash ternary blend concrete mixes containing Miami Oolite coarse aggregate.	127
Table 7-14. The plastic properties of silica fume and fly ash ternary blend concrete mixes containing Miami Oolite coarse aggregate.	128
Table 7-15. The plastic properties of slag and fly ash ternary concrete mixes containing Brooksville limestone aggregate.....	128
Table 7-16. Compressive strength test results for slag and fly ash ternary blend concrete mixes with W/C higher than 0.4.	129
Table 7-17. Compressive strength test results for slag and fly ash ternary blend concrete mixes with W/C lower than 0.4.	130
Table 7-18. Compressive strength test results for silica fume and fly ash ternary blend concrete mixes containing Type I/II Portland cement.	130

Table 7-19. Compressive strength test results for silica fume and fly ash ternary blend concrete mixes containing Type III Portland cement.	131
Table 7-20. Splitting tensile test results for slag and fly ash ternary blend concrete mixes with W/C higher than 0.4.....	134
Table 7-21. Splitting tensile test results for slag and fly ash ternary blend concrete mixes with W/C lower than 0.4.....	134
Table 7-22. Splitting tensile test results for silica fume and fly ash ternary blend concrete mixes containing Type I/II Portland cement.....	135
Table 7-23. Splitting tensile test results for silica fume and fly ash ternary blend concrete mixes containing Type III Portland cement.....	135
Table 7-24. Flexural strength test results for slag and fly ash ternary blend concrete mixes with W/C higher than 0.4.....	136
Table 7-25. Flexural strength test results for slag and fly ash ternary blend concrete mixes with W/C lower than 0.4.....	137
Table 7-26. Flexural strength test results for silica fume and fly ash ternary blend concrete mixes with W/C containing Type I/II Portland cement.....	137
Table 7-27. Flexural strength test results for silica fume and fly ash ternary blend concrete mixes containing Types III Portland cement.	138
Table 7-28. MOE test results for slag and fly ash ternary blend concrete mixes with W/C higher than 0.4.	139
Table 7-29. MOE test results for slag and fly ash ternary blend concrete mixes with W/C lower than 0.4.....	140
Table 7-30. MOE test results for silica fume and fly ash ternary blend concrete mixes with W/C containing Type I/II Portland cement.....	140
Table 7-31. MOE test results for silica fume and fly ash ternary blend concrete mixes with W/C containing Type III Portland cement.....	141
Table 7-32. Recommended equations for estimating compressive strength at other curing time from 28-day compressive strength.....	142
Table 7-33. Recommended equations for estimating 28-day compressive strength from compressive strength at other curing time.	143
Table 8-1. Monthly mean ambient temperature (°C) in North, Central, and South Florida from 1981 to 2010.....	151
Table 8-2. Thermal properties of various insulating materials and soils.....	151

Table B-1. List of mixes included in this study.	177
Table B-2. Paste fractions of mixes tested in this study.	177
Table D-1. Designation and origination of materials tested.	191
Table D-2. Standard tests used to characterize soil, muck, and lime rock samples.....	192
Table D-3. Properties of the soil samples,	193
Table D-4. Properties and composition of concrete tested.	193
Table E-1. Mix proportions of the concretes used.....	210
Table E-2. Concrete plastic property test results for each shaft.	211
Table G-1. The strength factor for all concrete mixes.	241
Table G-2. Comparison between the actual and Freiesleben model predicted compressive strength for slag and fly ash mixes with W/C more than 0.4.....	249
Table G-3. Comparison between the actual and Freiesleben model predicted compressive strength for slag and fly ash mixes with W/C less than 0.4.....	251
Table G-4. Comparison between the actual and Freiesleben model predicted compressive strength for silica fume, fly ash and Type I/II cement mixes.	254
Table G-5. Comparison between the actual and Freiesleben model predicted compressive strength for silica fume, fly ash and Type III cement mixes.	257
Table G-6. Comparison between the actual and modified CEB-FIP model predicted compressive strength for slag and fly ash mixes with W/C more than 0.4.....	262
Table G-7. Comparison between the actual and modified CEB-FIP model predicted compressive strength for slag and fly ash mixes with W/C less than 0.4.....	264
Table G-8. Comparison between the actual and modified CEB-FIP model predicted compressive strength for silica fume, fly ash and Type I/II cement mixes.	267
Table G-9. Comparison between the actual and modified CEB-FIP model predicted compressive strength for silica fume, fly ash and Type III cement mixes.	270
Table G-10. Comparison between the actual and modified hyperbolic model predicted compressive strength for slag and fly ash mixes with W/C more than 0.4.....	275
Table G-11. Comparison between the actual and modified hyperbolic model predicted compressive strength for slag and fly ash mixes with W/C less than 0.4.....	278

Table G-12. Comparison between the actual and modified hyperbolic model predicted compressive strength for silica fume, fly ash and Type I/II cement mixes.	281
Table G-13. Comparison between the actual and modified hyperbolic model predicted compressive strength for silica fume, fly ash and Type III cement mixes.	284
Table G-14. Comparison between the actual and 2nd degree hyperbolic predicted compressive strength for slag and fly ash mixes with W/C more than 0.4.....	287
Table G-15. Comparison between the actual and 2nd degree hyperbolic predicted compressive strength for slag and fly ash mixes with W/C less than 0.4.....	289
Table G-16. Comparison between the actual and 2nd degree hyperbolic predicted compressive strength for silica fume, fly ash, and type I/II cement mixes.....	291
Table G-17. Comparison between the actual and 2nd degree hyperbolic predicted compressive strength for silica fume, fly ash, and Type III cement mixes.	293
Table G-18. Comparison of standard error of estimate for all models.	295
Table G-19. Results of regression analysis relating MOE to compressive strength.....	298
Table G-20. Results of regression analysis relating flexural strength to compressive strength.....	300
Table G-21. Results of regression analysis relating splitting tensile strength to compressive strength.....	302
Table H-1. Compressive strength data of mix 1.	303
Table H-2. Compressive strength data of mix 2.	304
Table H-3. Compressive strength data of mix 3.	305
Table H-4. Compressive strength data of mix 4.	306
Table H-5. Compressive strength data of mix 5.	307
Table H-6. Compressive strength data of mix 6.	308
Table H-7. Compressive strength data of mix 7.	309
Table H-8. Compressive strength data of mix 8.	310
Table H-9. Compressive strength data of mix 9.	311
Table H-10. Compressive strength data of mix 10.	312
Table H-11. Compressive strength data of mix 11.	313

Table H-12. Compressive strength data of mix 12.	314
Table H-13. Compressive strength data of mix 13.	315
Table H-14. Compressive strength data of mix 14.	316
Table H-15. Modulus of elasticity data of mix 1.	317
Table H-16. Modulus of elasticity data of mix 2.	317
Table H-17. Modulus of elasticity data of mix 3.	318
Table H-18. Modulus of elasticity data of mix 4.	318
Table H-19. Modulus of elasticity data of mix 5.	319
Table H-20. Modulus of elasticity data of mix 6.	319
Table H-21. Modulus of elasticity data of mix 7.	320
Table H-22. Modulus of elasticity data of mix 8.	320
Table H-23. Modulus of elasticity data of mix 9.	321
Table H-24. Modulus of elasticity data of mix 10.	321
Table H-25. Modulus of elasticity data of mix 11.	322
Table H-26. Modulus of elasticity data of mix 12.	322
Table H-27. Modulus of elasticity data of mix 13.	323
Table H-28. Modulus of elasticity data of mix 14.	323
Table H-29. Splitting tensile strength data of mix 1.	324
Table H-30. Splitting tensile strength data of mix 2.	324
Table H-31. Splitting tensile strength data of mix 3.	325
Table H-32. Splitting tensile strength data of mix 4.	325
Table H-33. Splitting tensile strength data of mix 5.	326
Table H-34. Splitting tensile strength data of mix 6.	326
Table H-35. Splitting tensile strength data of mix 7.	327
Table H-36. Splitting tensile strength data of mix 8.	327

Table H-37. Splitting tensile strength data of mix 9.....	328
Table H-38. Splitting tensile strength data of mix 10.....	328
Table H-39. Splitting tensile strength data of mix 11.....	329
Table H-40. Splitting tensile strength data of mix 12.....	329
Table H-41. Splitting tensile strength data of mix 13.....	330
Table H-42. Splitting tensile strength data of mix 14.....	330
Table H-43. Flexural strength data of mix 1.....	331
Table H-44. Flexural strength data of mix 2.....	331
Table H-45. Flexural strength data of mix 3.....	332
Table H-46. Flexural strength data of mix 4.....	332
Table H-47. Flexural strength data of mix 5.....	333
Table H-48. Flexural strength data of mix 6.....	333
Table H-49. Flexural strength data of mix 7.....	334
Table H-50. Flexural strength data of mix 8.....	334
Table H-51. Flexural strength data of mix 9.....	335
Table H-52. Flexural strength data of mix 10.....	335
Table H-53. Flexural strength data of mix 11.....	336
Table H-54. Flexural strength data of mix 12.....	336
Table H-55. Flexural strength data of mix 13.....	337
Table H-56. Flexural strength data of mix 14.....	337

LIST OF FIGURES

<u>Figure</u>	<u>page</u>
Figure 1-1. Stress vs. time plot showing time of crack initiation.	2
Figure 1-2. Segmental bridge pier segment with the core highlighted for concrete volume-to-surface area ratio calculation highlighted.	4
Figure 2-1. TAM Air calorimeter.	13
Figure 2-2. Admix. ampoule with the test sample and stirrer-syringe assembly.	16
Figure 2-3. Loaded calorimetry blocks.	16
Figure 2-4. Heat of hydration vs. time for eight paste fractions.	24
Figure 2-5. Temperature rise inputs for the nine mixes in the study.	25
Figure 2-6. Degree of hydration vs. time for HVFA1.	26
Figure 2-7. Degree of hydration vs. time for TB1.	27
Figure 2-8. Degree of hydration vs. time for FB2.	27
Figure 2-9. Degree of hydration vs. time for SB1/SB2.	28
Figure 3-1. General design of complete interior pier diaphragm segment.	41
Figure 3-2. Dimensions used in DIANA FE model (mm).	42
Figure 3-3. Interior pier segment recommended width measurements (mm).	42
Figure 3-4. FE model mesh of one-quarter concrete bridge pier segment used in analysis.	43
Figure 3-5. Temperature development of segmental bridge sections with varying V/A ratios.	46
Figure 3-6. Temperature differential development of segmental bridge sections with varying V/A ratios.	46
Figure 3-7. Temperature development of segmental bridge sections with varying FDOT mix designs.	50
Figure 3-8. Temperature differential development of segmental bridge sections with varying FDOT mix designs.	50
Figure 4-1. Measured R-values of soil sample 1 under different moisture and temperature conditions.	56

Figure 4-2. Measured R-Values of soil sample 2 under different moisture and temperature conditions.....	57
Figure 4-3. Measured R-Values of soil sample 3 under different moisture and temperature conditions.....	58
Figure 4-4. Measured R-Values of soil sample 4 under different moisture and temperature conditions.....	59
Figure 4-5. Measured R-Values of DS1 soil sample under different moisture conditions.....	61
Figure 4-6. Measured R-Values of DS2 soil sample under different moisture conditions.....	61
Figure 4-7. Measured R-Values of DS3 soil sample under different moisture conditions.....	62
Figure 4-8. Measured R-Values of DS4 soil sample under different moisture conditions.....	62
Figure 4-9. Measured R-Values of all DS soil samples under different moisture conditions.	63
Figure 4-10. R-Values of composite DS soil sample under different moisture conditions.	63
Figure 4-11. Measured R-Values of muck under different temperature conditions.	65
Figure 4-12. Measured R-Values of lime rock under different moisture and temperature conditions.....	66
Figure 4-13. Measured R-values of concrete under different temperatures.	67
Figure 5-1. Thermal analysis modeling elements.....	71
Figure 5-2. Input data obtained from isothermal calorimetry testing.	73
Figure 5-3. Geometry and boundary conditions of pilot FE model.....	76
Figure 5-4. Maximum temperature versus shaft diameter.....	80
Figure 5-5. Maximum temperature differential versus shaft diameters.....	81
Figure 5-6. Maximum temperature versus curing time.	85
Figure 5-7. Maximum temperature differential versus curing time.....	86
Figure 5-8. Maximum temperature and maximum temperature difference on centroid void drilled shafts.....	89
Figure 6-1. Temperature sensor positions in a drilled shaft and surrounding soil.....	95
Figure 6-2. Measured temperatures in drilled shaft 1 along the center line under wet soil.....	97

Figure 6-3. Measured temperatures in drilled shaft 1 along the middle line under wet soil,	97
Figure 6-4. Measured temperatures in drilled shaft 1 along the edge line under wet soil.	98
Figure 6-5. Measured temperatures in drilled shaft 2 along the center line under wet soil.	98
Figure 6-6. Measured temperatures in drilled shaft 2 along the middle line under wet soil.	99
Figure 6-7. Measured temperatures in drilled shaft 2 under along the edge line wet soil.	99
Figure 6-8. Measured temperatures in drilled shaft 3 along the center line under dry soil.	100
Figure 6-9. Measured temperatures in drilled shaft 3 along the middle line under dry soil.	100
Figure 6-10. Measured temperatures in drilled shaft 3 along the edge line under dry soil.	101
Figure 6-11. Measured temperatures in drilled shaft 4 along the center line under dry soil.	101
Figure 6-12. Measured temperatures in drilled shaft 4 along the middle line under dry soil.	102
Figure 6-13. Measured temperatures in drilled shaft 4 along the edge line under dry soil.	102
Figure 6-14. Maximum temperature and temperature differentials after missing data imputation for drilled shafts 2 and 4.	103
Figure 6-15. Measured and computed maximum temperature and temperature differentials in drilled shafts.	105
Figure 6-16. Measured and computed maximum temperature and temperature differentials in drilled shafts.	106
Figure 6-17. Axis-symmetric FE model for thermal analysis of the four drilled shafts.	108
Figure 6-18. Adiabatic temperature rise data for the four drilled shaft concrete mixes.	109
Figure 7-1. Gradation of silica sand.	118
Figure 7-2. Gradation of Miami Oolite aggregate.	119
Figure 7-3. Gradation of Brooksville limestone aggregate.	120
Figure 7-4. Strength factor versus age for all 14 concrete mixes.	132
Figure 7-5. Compressive strength versus age for all 14 concrete mixes.	132
Figure 7-6. Splitting tensile strength versus age.	133
Figure 7-7. Flexural strength versus age.	136

Figure 7-8. Modulus of elasticity versus age.	139
Figure 8-1. Screen display upon running of DIFG interface software.	145
Figure 8-2. Flow chart showing main steps performed by DIFG and DIANA	147
Figure 8-3. Geometry of the rectangular footing and needed inputs for thermal analysis	149
Figure 8-4. Various insulation for rectangular footing.	150
Figure 8-5. Geometry of the cylindrical drilled shaft and needed inputs for thermal analysis...	153
Figure 8-6. Grouping boxes in DIFG.....	154
Figure 8-7. Locations of coldest and hottest points in rectangular footing and drilled shaft.	156
Figure 8-8. Content of Hot.PRT from analysis of example drilled shaft.....	156
Figure 8-9. Temperature contour plot from Day1.PS.....	157
Figure 8-10. Close-up view of the temperature contour plot from Day1.PS.....	157
Figure B-1. Database architecture.....	175
Figure B-2. Interface of database program for organizing FDOT mix designs.....	178
Figure B-3. Isolation of data for concrete mix design.	179
Figure B-4. Message indicating error in user entry or unavailability of data.	179
Figure B-5. Selection of data by W/C ratio.	180
Figure B-6. Selection of data by mix number.....	181
Figure B-7. Selection of a mix design to be edited.....	182
Figure B-8. Highlighting a property to be edited.....	183
Figure B-9. Entering a new mix design entry (step 1).....	184
Figure B-10. Entering a new mix design entry (step 2).....	185
Figure D-1. KD2Pro thermal properties analyzer probes used.....	194
Figure D-2. KD2Pro thermal properties analyzer data recorder.....	194
Figure D-3. Artic Silver thermal compound and pilot pins used.....	195
Figure D-4. Temperature-control box used.	196

Figure D-5. Switched outlet, transformer, thermostat, and relay used	197
Figure D-6. Porcelain light fixture used.	198
Figure D-7. Entire setup of the temperature control box.	199
Figure D-8. PVC pipe epoxied to a wooden board.	200
Figure D-9. The PVC pipe with soil sample and TR1 probe in a 75° F testing condition.	201
Figure D-10. Glass jar used to hold soil sample.	201
Figure D-11. A concrete cylinder used in testing with pilot pin partially inserted.	203
Figure D-12. Insulation mat material tested in the study.	204
Figure D-13. TR1 Probe used.	206
Figure D-14. KS1 Probe used.	206
Figure E-1. Four-inch spacing between data logger and casing inside shaft.	212
Figure E-2. Six-inch spacing between data logger in soil and casing.	212
Figure E-3. Temperature loggers attached to steel frame.	213
Figure E-4. Layout for frame for temperature logger attachment for shafts 2 to 4.	214
Figure E-5. Mammoth Constructor’s drilling truck.	215
Figure E-6. Installation of casing.	216
Figure E-7. Baler.	216
Figure E-8. Backhoe driving casing.	217
Figure E-9. Water table inside casing.	218
Figure E-10. Well point.	219
Figure E-11. Well field.	220
Figure E-12. Engine-driven diaphragm water pump.	220
Figure E-13. FDOT geotechnical drilling truck.	221
Figure E-14. Tremie pipe.	222
Figure E-15. Removal of casing.	223

Figure E-16. Installation of beauty ring.....	223
Figure E-17. Close-up of beauty ring.	224
Figure F-1. Performing the slump test.	226
Figure F-2. Dimensions of the slump test mold.....	226
Figure F-3. Conducting unit weight test.	227
Figure F-4. Air content test.....	228
Figure F-5. Thermometer used in the temperature test.....	229
Figure F-6. The Forney testing machine used for the compressive strength testing.	230
Figure F-7. Grinding each side of the specimens and keeping the specimens moisturized until the test is completed.	231
Figure F-8. Specimen measurement and alignment.....	232
Figure F-9. The Forney testing machine.....	233
Figure F-10. The compressometer (electronic sensor connected to the Forney software).	234
Figure F-11. The aligning jig for the splitting tensile strength test before and after placing the concrete specimen.	235
Figure F-12. Splitting tensile strength test specimen after conducting the test.	236
Figure F-13. Testing machine for flexural strength test before and after installing concrete beam.....	237
Figure F-14. A fractured flexure beam specimen.	238
Figure G-1. The compressive strength test results before normalization.	242
Figure G-2. The strength factor for all concrete mixes.....	242
Figure G-3. The strength factors for slag and fly ash mixes with W/C more than 0.4.....	243
Figure G-4. The strength factors for slag and fly ash mixes with W/C less than 0.4.	243
Figure G-5. The strength factors for silica fume, fly ash and Type I/II Portland cement mixes.	244
Figure G-6. The strength factors for silica fume, fly ash and Type III Portland cement mixes.....	244

Figure G-7. Sample plot of linearized Freiesleben model.	247
Figure G-8. Comparison between actual and predicted strength factors from Freiesleben model for slag and fly ash mixes with W/C more than 0.4.....	248
Figure G-9. Comparison between actual and predicted strength factors from Freiesleben model for slag and fly ash mixes with W/C less than 0.4.....	252
Figure G-10. Comparison between actual and predicted strength factors from Freiesleben model for silica fume, fly ash and Type I/II cement mixes.	255
Figure G-11. Comparison between actual and predicted strength factors from Freiesleben model for silica fume, fly ash and Type III cement mixes.	258
Figure G-12. Sample plot of linearized modified CEB-FIP model.	260
Figure G-13. Comparison between actual and predicted strength factors from modified CEB-FIP model for slag and fly ash mixes with W/C more than 0.4.....	261
Figure G-14. Comparison between actual and predicted strength factors from modified CEB-FIP model for slag and fly ash mixes with W/C less than 0.4 modified.	265
Figure G-15. Comparison between actual and predicted strength factors from modified CEB-FIP model for silica fume, fly ash and Type I/II cement mixes.	268
Figure G-16. Comparison between actual and predicted strength factors from modified CEB-FIP model for silica fume, fly ash and Type III cement mixes.	271
Figure G-17. Sample plot of linearized modified hyperbolic model.	272
Figure G-18. Comparison between actual and predicted strength factors from modified hyperbolic model for slag and fly ash mixes with W/C more than 0.4.	274
Figure G-19. Comparison between actual and predicted strength factors from modified hyperbolic model for slag and fly ash mixes with W/C less than 0.4.....	277
Figure G-20. Comparison between actual and predicted strength factors from modified hyperbolic model for silica fume, fly ash and Type I/II cement mixes.	280
Figure G-21. Comparison between actual and predicted strength factors from modified hyperbolic model for silica fume, fly ash and Type III cement mixes.	283
Figure G-22. Comparison between actual and predicted strength factors from 2nd degree hyperbolic model for slag and fly ash mixes with W/C more than 0.4.	288
Figure G-23. Comparison between actual and predicted strength factors from 2nd degree hyperbolic model for slag and fly ash mixes with W/C less than 0.4.....	290

Figure G-24. Comparison between actual and predicted strength factors from 2nd degree hyperbolic model for silica fume, fly ash and Type I/II cement mixes	292
Figure G-25. Comparison between actual and predicted strength factors from 2nd degree hyperbolic model for silica fume, fly ash and Type III cement mixes.	294
Figure G-26. Plot of MOE versus compressive strength.	297
Figure G-27. Plot of flexural strength versus compressive strength.....	300
Figure G-28. Plot of splitting tensile strength versus compressive strength.....	301
Figure N-1. Main steps in the use of DIFG and DIANA in performing a thermal analysis.....	348
Figure N-2. Provided files for running DIFG software.	349
Figure N-3. Running of MCR_R2013a_win64_installer.....	350
Figure N-4. Creating the folder and saving DIFG.EXE in it.	350
Figure N-5. Screen display upon running of DIFG interface software.....	351
Figure N-6. Inputting title name for analysis.....	351
Figure N-7. Structure selection of rectangular foundation.	352
Figure N-8. Inputting parametric values for Rectangular foundation.....	353
Figure N-9. Inputting the name of concrete data file.....	353
Figure N-10. Generating four input files and closing DIFG software.....	354
Figure N-11. Saving the generated input files in initial setting directory.....	355
Figure N-12. Setting iDIANA in the initial directory where all files are located.....	356
Figure N-13. All needed files for running thermal analysis using DIANA.....	357
Figure N-14. Starting DIANA initially.....	358
Figure N-15. Starting DIANA for pre-processing.	358
Figure N-16. Starting DIANA for analyzing.	359
Figure N-17. Starting DIANA for post-processing.....	359
Figure N-18. Locations of coldest and hottest points in rectangular footing.....	360
Figure N-19. Screen display showing all output files from DIANA.	361

Figure N-20. Content of tabulation from analysis of example rectangular footings.	362
Figure N-21. Temperature contour view.	364
Figure N-22. Creating the folder and saving DIFG.EXE in it.	365
Figure N-23. Screen display upon running of DIFG interface software.....	366
Figure N-24. Inputting title name for analysis.	366
Figure N-25. Structure selection of drilled shaft.	367
Figure N-26. Inputting parametric values for drilled shaft.	368
Figure N-27. Inputting the name of concrete data file.	368
Figure N-28. Generating four input files and closing DIFG.....	369
Figure N-29. Saving and generated input files in initial setting directory.....	370
Figure N-30. Setting iDIANA in the initial directory where all files are located.....	371
Figure N-31. All needed files for running thermal analysis using DIANA.	372
Figure N-32. Starting DIANA initially.	373
Figure N-33. Starting DIANA for pre-processing.	373
Figure N-34. Starting DIANA for analyzing.	374
Figure N-35. Starting DIANA for post-processing.....	374
Figure N-36. Locations of coldest and hottest points in drilled shaft.....	375
Figure N-37. Screen display showing all output files from DIANA.	376
Figure N-38. Content of tabulation from analysis of example drilled shafts.....	377
Figure N-39. Temperature contour view.	379

CHAPTER 1 INTRODUCTION

1.1 Background and Research Needs

Whenever fresh concrete is used in the construction of large homogeneous structures such as foundations and dams, consideration is always given to the amount of heat that will be generated and the resulting volume change. Volume changes occur due to temperature changes in the structure which initially increase as the concrete hydrates and decrease as the reaction is exhausted. Temperature difference per unit distance between one point and another in a structure is called a thermal gradient. Temperature gradients are produced when the heat being generated in the concrete is dissipated to the surrounding environment causing the temperature at the surface of the concrete to be lower than the temperature at the interior of the concrete. This temperature drop at the surface results in the contraction of the concrete. With the interior of the concrete being more mature than the surface, it acts as a restraint against the contraction, creating tensile stresses in the surface.

The magnitude of the tensile stress is dependent on the thermal differential in the mass concrete, the coefficient of thermal expansion, modulus of elasticity, creep or relaxation of the concrete, and the degree of restraint in the concrete. Since the concrete is still in its early age, its full tensile strength is not developed, and if the tensile stresses are larger than the early age tensile strength, cracking will occur (ACI 207.1R; ACI 207.2R) as depicted in Figure 1-1. If cracking does occur, it will ultimately affect the ability of the concrete to withstand its design load, and allow the infiltration of deleterious materials which undermine durability.

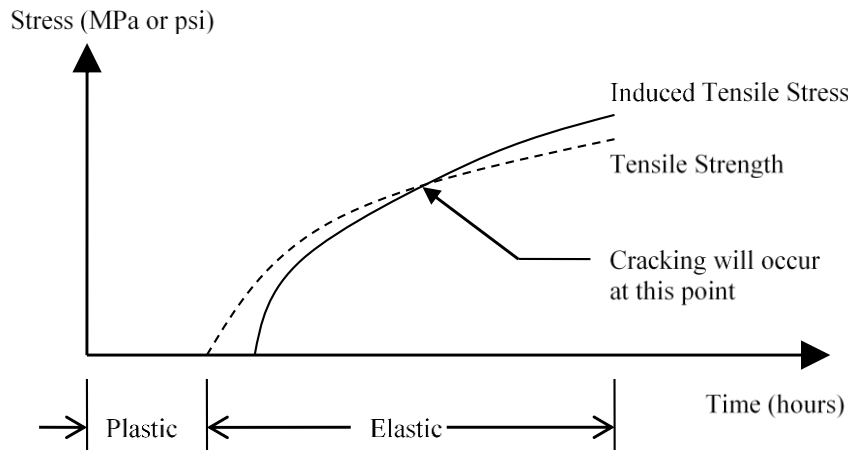


Figure 1-1. Stress vs. time plot showing time of crack initiation.

FDOT currently defines mass concrete as all bridge components (except drilled shafts and segmental superstructure pier and expansion joint segments) with one or both of the following geometric parameters:

1. Minimum dimension ≥ 3 ft. (914 mm).
2. Ratio of concrete volume to the surface area >1 ft. (305 mm).

Once a concrete structure is defined as mass concrete, FDOT mandates that a contractor must submit a temperature differential control plan which models the temperature distribution of the concrete, and describes the measures that will be taken to prevent exceedance of the temperature differential limit of 19.4 °C (35.0 °F), the maximum allowed concrete temperature of 82.2 °C (180.0 °F). Section 346-3.3 of the Florida Department of Transportation (FDOT) Standard Specification for Road and Bridge Construction currently requires that the analysis of the anticipated thermal developments in mass concrete elements is done following the procedure known as the Schmidt method which is outlined in Section 207 of the American Concrete Institute (ACI) Manual of Concrete Practice.

A previous FDOT-funded study of mass concrete structures in the field has shown that finite element modeling of the expected temperature distribution of hydrating concrete, using the energy data obtained from conducting isothermal calorimetric tests on its cementitious components, is a workable and viable option in predicting the expected temperature distribution of the concrete. Results from the study showed that the Schmidt method consistently underestimated the temperatures in the concrete while the temperature profiles calculated by the finite element model closely agreed with the temperature profiles measured at all the locations monitored.

1.1.1 Need for Data Base of Rate of Heat Production of Different Cement Blends

One of the needed inputs to the finite element modeling of mass concrete is the rate of heat production of the cementitious materials used in the concrete mix. The rate of heat production of the cementitious material can be obtained from isothermal calorimetric testing. If a database of rate of heat production of the different cement blends used in typical mass concrete is available, the thermal analysis of a mass concrete structure can be performed readily without having to wait for the results from the isothermal calorimetric test to be obtained first. This is especially useful if several different concrete mixes are to be evaluated for use in the structure. There is a need to conduct a laboratory testing program to generate the needed data to build up such a database.

1.1.2 Need for Investigation on Segmental Bridge Pier Segments

The FDOT Construction office has been faced with possible issues with Segmental Bridge Structures that use high strength concrete. One particular structure used segmental bridge pier segments with a volume-to-surface area ratio, calculated using the core concrete area highlighted in Figure 1-2, of 0.97 feet. Although these segments' volume-to-surface area ratios were less than 1.0 feet, and therefore not considered mass concrete, thermal cracking occurred.

Because these segmental structures were not classified as mass concrete, measures were not taken to determine the maximum temperature and temperature differential realized in the structure. The question thus arises: should the V/A threshold of 1.0 feet be reduced when high strength mixes are used, and what should that threshold be? Additional detailed thermal stress analysis in conjunction with some field monitoring of typical segmental bridge pier segments are needed to answer this question.

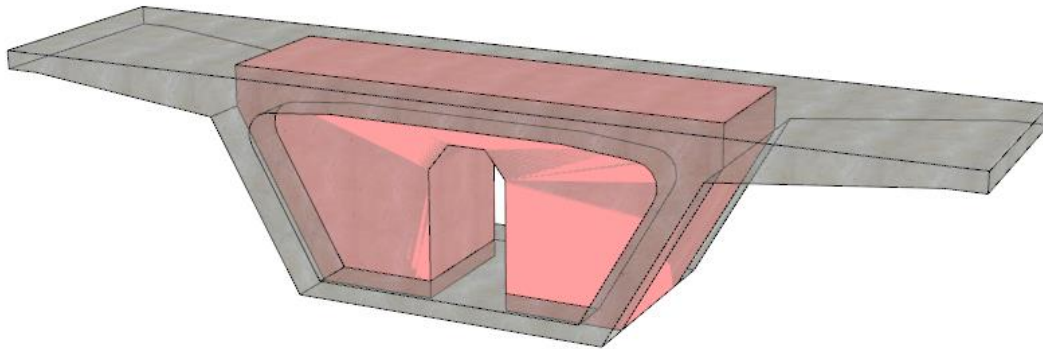


Figure 1-2. Segmental bridge pier segment with the core highlighted for concrete volume-to-surface area ratio calculation highlighted.

1.1.3 Need for Investigation of Soil as an Insulator

Contractors often complain about the requirement of installing insulation between the bottom surface of a mass concrete footer and soil. The argument is posited that when mass concrete is placed directly on top of a soil layer, additional insulation is not needed at the bottom of the concrete as the soil on which the concrete is being placed is already an insulating material. However, after attempts by two separate contractors on two separate projects to prove that soil does provide insulating properties when mass concrete footers are placed directly on top of the soil, both cases experienced temperature differentials exceeding the maximum allowable limit of 19.4 °C (35.0 °F) within the first 24 hours. It was then concluded that at locations with a high water table (above the footer bottom) soil could not be relied on as a good insulator. Subsequent

to these two incidents, a preliminary finite element model using typical soil properties suggests that dry soil may be an appropriate insulating material in mass concrete footer applications. Further investigation is needed by using the actual measured properties of the in situ soil to answer the question of whether or not the absence of an insulating layer between mass concrete foundations and dry soil may cause a problem with cracking of the concrete at early age.

1.1.4 Need for Extension of Mass Concrete Research to Drilled Shafts

The Florida Department of Transportation's Structures Design Guidelines specify that all drilled shafts with diameters greater than 6 feet shall be designated as mass concrete and a Technical Special Provision (TSP) shall be required. The TSP in this particular instance generally takes the form of a mass concrete temperature control plan.

It has recently come to the attention of the FDOT that drilled shaft contractors often use temporary casings that are larger in diameter than called for in the design when performing drilling operations for the construction of drilled shafts. This is done to allow enough space for the auger to operate without taking extra care within the casing. As a result, drilled shafts designed as having 6 feet diameters, and therefore not being classified as mass concrete, end up being as large as 7 feet in diameter when constructed.

The following question has therefore been asked: Should miscellaneous drilled shaft contractors be required to comply with the mass concrete requirements when temporary casings larger than 6 feet in diameter are used? There is a need to extend the mass concrete research to answer the above question.

1.1.5 Need for Study of Strength Development of Ternary Blend Concrete Mixes

Based on past research (such as FDOT contract BD545-35), it has been determined that ternary blend concretes can provide a 100 year service life of structures in Florida. Since the ternary blends only have 30 to 40 % Portland cement, they also help to reduce initial heat generation which may reduce the need for temperature control models for some structures that might typically require methods to control heat development.

The revised Section 346 of the 2016 FDOT Standard Specification for Road and Bridge Construction will include language to allow the ternary blends in all classes of concrete. However, the equations needed to assist in resolving low strength issues between the contractor and the Department as defined in Section 346-11 have been neglected. Thus, there is a need to study the strength development of ternary blend concretes so that equations for determining 28-day compressive strength from the strength of concrete that is older than 28 days can be developed.

1.1.6 Need for Development of the User-Friendly Software for Mass Concrete Analysis

The DIANA computer software is a versatile finite-element program, which has been effectively used in thermal analysis of mass-concrete structures in research projects conducted by the University of Florida (UF) for the Florida Department of Transportation (FDOT). While the DIANA software is a powerful tool for performing thermal analysis of mass-concrete structures, the users of this software need to have a good knowledge of finite-element method, and the commands and procedures of the DIANA software. There was a need to develop a user-friendly interface software, so that someone without extensive training in finite-element method or the DIANA software can also perform thermal analysis of typical mass-concrete structures in Florida.

1.2 Objectives of Study

The specific objectives of this research project are as follows:

1. To build a data base of rate of heat production of different cement blends used in mass concrete in Florida.
2. To evaluate typical segmental bridge pier segments used in Florida to determine whether some of them need to be treated as mass concrete.
3. To investigate the insulating properties of different types of soil and under various moisture conditions to be used in thermal analysis of mass concrete placed on them.
4. To evaluate typical drilled shafts used in Florida to determine whether some of them need to be treated as mass concrete.
5. To study the strength development of ternary blend concrete mixes in Florida to develop equations for determining 28-day compressive strength from the strength of concrete that is older than 28 days.
6. To develop user-friendly interface software for thermal analysis of mass concrete.

1.3 Approach and Scope of Research

The main objectives of this study were accomplished through the following tasks:

1. Development of Data Base of Rate of Heat Production of Cement Blends for Mass Concrete in Florida.

FDOT mix designs that are classified for use in mass concrete applications were identified. Samples of their cementitious components from these identified concrete mixes were tested for their heat of hydration using the isothermal calorimetry chamber. The results from these isothermal calorimetry tests were then used to build a suitable data base of adiabatic temperature rise tables that can be used in the DIANA software for the modeling of mass concrete structures. The work performed in this task is presented in Chapter 2.

2. Thermal Analysis of Segmental Bridge Structures

Thermal analysis using the DIANA software were performed on typical segmental bridge pier segments used in Florida to evaluate their temperature development and distribution during construction. The work performed in this task is presented in Chapter 3.

3. Determination of Thermal Properties of Soils in Different Moisture Conditions

A laboratory testing program was conducted to determine the R-values of several typical soils in Florida under varying moisture conditions. The work performed in Task 3 is presented in Chapter 4.

4. Evaluation of Drilled Shafts for Consideration as Mass Concrete Structures

Finite element models using the DIANA software were developed to analyze the temperature development of drilled shaft under dry and wet conditions. The model developed was used to determine the effect the volume-to-surface area ratio of a drilled shaft, as well as the cementitious composition of the concrete mixture has on its thermal behavior. The temperature development of drilled shafts with centroid voids was also evaluated. A field testing program

was also performed to record the actual temperature development and distributions in four concrete drilled shafts placed under soils of different moisture conditions to evaluate the actual effects of the soils of different moisture conditions on mass concrete. The analytical work performed is presented in Chapter 5, while the field testing program is presented in Chapter 6.

5. Laboratory Study on Strength Development of Ternary Blend Concrete Mixes

A laboratory testing program was conducted to study the strength development of ternary blend concrete mixes in Florida. Statistical analyses were performed to develop predictions which can be used for determining 28-day compressive strength from the strength of concrete that is older than 28 days. The laboratory study is presented in Chapter 7.

6. Development of User-Friendly Interface Software for Mass Concrete Analysis

A user-friendly interface software was developed for use in thermal analysis of (1) rectangular concrete footings and (2) cylindrical concrete drilled shafts using the DIANA software. This interface software is described in Chapter 8.

7. Conclusions and Recommendations

Finally, conclusions and recommendations are presented in Chapter 9.

CHAPTER 2
DEVELOPMENT OF DATABASE OF RATE OF HEAT PRODUCTION
OF CEMENT BLENDS FOR MASS CONCRETE

2.1 Introduction

One of the needed inputs to the finite element modeling of mass concrete is the rate of heat production of the cementitious materials used in the concrete mix. The rate of heat production of the cementitious material can be obtained from isothermal calorimetric testing. If a database of rate of heat production of the different cement blends used in typical mass concrete is available, the thermal analysis of a mass concrete structure can be performed readily without having to wait for the results from the isothermal calorimetric test to be obtained first. To meet this need, a laboratory testing program was conducted to generate the needed data to build up such a database. This chapter presents the laboratory testing program and the development of the database of rate of heat production of cement blends for mass concrete in Florida.

2.2 Isothermal Calorimetry Test Equipment

Rate of heat production of cement blends is measured by means of an isothermal calorimeter. A typical isothermal conduction calorimeter setup consists of two cells; one cell is designed for the cement/mortar sample under study, and the other for placement of an inert material (both of which are placed in ampoules). These cells are connected to a heat sink containing a semiconductor device. This assembly is located inside a chamber where a thermostat is used to help maintain a constant temperature. The progression of an exothermic or endothermic reaction causes a difference in heat to occur across the two cells, which creates a voltage difference across these cells. This phenomenon is attributed to the 'Seebeck Effect', which is prevalent due to the presence of the semiconducting piles in the heat sink (Wadso, 2001). The primary function of the heat sink is to conduct heat away from the instrument in order to ensure, working in tandem with the thermostat, that isothermal condition is maintained.

Measurement of the voltage created across the cells can be used to calculate the thermal power, which is integrated with respect to time to obtain energy, as expressed by the following equation:

$$Q = \int_0^t p \cdot dt \quad (2-1)$$

Where

Q is the cumulative energy,

p is the power,

t is the time.

The term ‘isothermal’ may be a little misleading as the conditions in the chamber can be best described as ‘essentially isothermal’, which is indicative of conditions where the temperature differences are usually found to be on the order of 10 mK above or below the given reference temperature (Wadso, 2010). The heat generated is continuously conducted away by the heat sink to maintain an almost constant temperature. The voltage used to calculate power is set up due to a temperature differential that is created across the two cells. It is therefore necessary that the reference sample and the study sample have similar thermal characteristics or masses and that the reference sample does not produce any heat. A simple method to accomplish this is to ensure that their heat capacities are the same and by selecting an inert material such as glass to be placed in a reference cell. The required mass of the reference sample can be calculated using the following equation (Wadso, 2010):

$$M_c = \sum \frac{m_i \cdot c_i}{c_R} \quad (2-2)$$

Where

M_c is the mass of the reference sample,

c_R is the specific heat capacity of the reference sample,

c_i is the specific heat of the i^{th} constituent,

m_i is the mass of the i^{th} constituent.

This computation would have to include the heat capacity of sand if a mortar fraction is being tested. The instrument used for testing is calibrated by passing a known thermal power through the instrument. In the heat of hydration testing of cement, the critical coefficients are the calibration coefficient ‘ \mathcal{E} ’ and the baseline voltage. The instrument used in this study for testing is the TAM Air 8-channel Calorimeter (Figure 2-1), which allows the testing of 8 paste/mortar samples simultaneously. The calorimeter is placed in a temperature controlled environment where the temperature is set at 23.0 °C. However, given the fact that the channels partially share the heat sink, if all of the 8 cells are loaded for testing, it is likely that ‘crosstalk’ could occur (Wadso, 2010). Crosstalk can be described as a situation where the thermal activity in one set of cells might affect the surrounding cells. The procedures for the testing of cement paste or mortar using Isothermal Calorimetry for the determination of heat of hydration has been formalized in ASTM C1702 Standard Test Method while ASTM C1679 Standard Practice gives guidelines for measuring the hydration kinetics. Experiments conducted during our study are primarily concerned with the determination of heat of hydration.



Figure 2-1. TAM Air calorimeter.

The internal mixing procedure specified in ASTM C1702 was used in conducting the isothermal calorimetry test. In the internal mixing procedure, the specified amount of water is added after the admix-ampoule containing the paste or the mortar mix is placed in the isothermal calorimeter channel or cell. The water is added in the stirrer-syringe assembly of the admix ampoule and then weighed. The internal mixing procedure allows the first hydration peak associated with initial hydrolysis of cement to be captured. In external mixing, typically the paste or mortar is mixed outside the instrument using a blender and placed in the ampoule after the mixing has been completed. A correction is applied for the heat liberated during the initial hydration.

The testing program consists of the following sets of experiments:

1. Tests conducted on pastes without admixtures
2. Tests conducted on pastes with admixtures

The first set of tests was conducted on paste fractions of the selected set of mass concrete mix designs. The second round of testing was conducted on four paste fractions representing a range of w/b ratio in order to assess the possibility of incorporating admixtures in future testing programs.

De-ionized water was used during the testing program. For pastes tested with admixtures, a representative amount of chemical admixture is added to the mix water in conformance with the mix design specifications. Four replicates are tested in the first round of testing with the number being reduced to 2 for the second round of testing. The procedure adopted during the program to calculate the weights of the cement pastes is described as follows:

1. Glass beads weighing 13.3 g are placed in an ampoule. This ampoule containing the glass beads is placed in the reference cell.
2. The heat capacity (thermal mass) of the glass beads in the reference ampoule is to be balanced by the mass of cement paste. To achieve this balance, the required mass of the constituents of the cementitious system is calculated by applying the law of mixtures to determine the heat capacity of the paste.

The determination of the weight masses of the constituents of the cementitious paste is done in two steps. In the first step, the weight of each constituent for a unit mass of the cementitious paste is computed based on the w/b ratio and SCM replacement percentage. The mass of glass beads that would correspond to the same heat capacity as the unit mass of the cementitious system is found by using Equation 2-2. Then, the total mass of the cementitious system that corresponds to heat capacity of 13.3 g of glass beads is calculated. The total mass is broken down into masses of various constituents (Portland cement, SCMs, and water) using the fractional percentages calculated previously. The specific heat capacities used during these computations are listed in Table 2-1.

Table 2-1. Specific heats of materials used.

Material	Specific Heat (J/g·°K)
Glass	0.840 (Wadso, 2001)
Portland Cement	0.750 (TAM Air Manual)
Fly ash	0.720 (Wadso, 2001)
Slag	0.711 (Bentz, 2009)
Water	4.190 (Engineering Toolbox)
Metakaolin	0.938 (Burgess Pigment)
Coarse Aggregate (Limestone)	0.840 (Engineering Toolbox)
Fine Aggregate (Silica Sand)	0.800 (Engineering Toolbox)

2.3 Isothermal Calorimetry Testing Procedure

The procedure for the isothermal calorimetry test can be summarized as follows:

1. The TAM Air instrument is calibrated and is set at a suitable temperature. The chosen temperature of the chamber can be set between 23.0 - 60.0 °C. A reference temperature of 23.0 °C was used in this testing program.
2. The constituents of the paste (Portland cement, SCMs, and water) are weighed to the nearest 0.001g in an ampoule.
3. The water that is to be added is taken in the syringes of the stirrer-syringe assembly. If an admixture is to be added, then a representative volume of the water containing the admixture is taken. The mass proportions of the mixed water and admixture were calculated based on the proportioning of the mix ingredients of the concrete mix design.
4. The stirrer-syringe assembly is attached to the ampoules containing the Portland cement and SCMs. A gluing substance is used to ensure that the assembly fits tightly with the ampoule (Figure 2-2).
5. The admix-ampoule (the stirrer-syringe assembly attached to the ampoule) is lowered into the appropriate cell/channel of the instrument (Figure 2-3).
6. The internal mixing procedure described in ASTM C1702 is used. After the voltage reading in the data logger for all sample cells is close to or almost zero, i.e. the voltage stabilizes, the syringe lever is pressed down to release the water. The stirrer is then used to mix the sample thoroughly for about 2-3 minutes.



Figure 2-2. Admix. ampoule with the test sample and stirrer-syringe assembly.

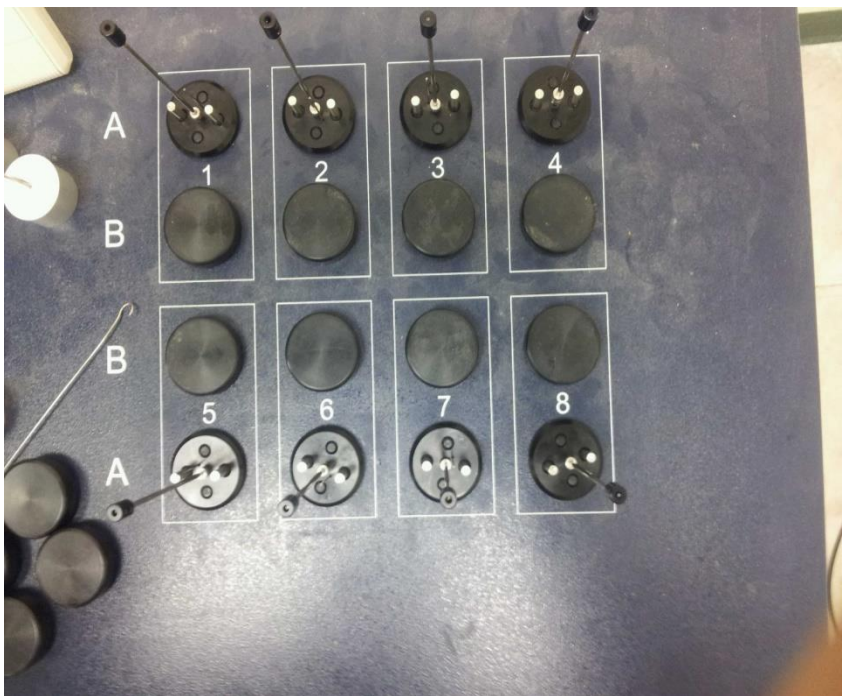


Figure 2-3. Loaded calorimetry blocks.

TAM Air has a compatible data logging system installed on a work station where the relevant inputs are entered before starting the test and where the power and heat of hydration measurements can be tabulated. Most of the tests are run for 168 hours, which is 7 days. The data logging software generates tables for voltage, rate of heat generation, and cumulative heat of hydration data which are normalized (based on the data entered in the % cementitious materials field).

2.3.1 Determination of Temperature Rise Inputs

The rationale behind the method used to determine the temperature rise in the work by Lawrence (2009) using Isothermal Calorimetric HOH (Heat of Hydration data) was to ensure consistency between the various types of calorimetry used during the study with the assumption being that the energy rise curve is similar to that which would be derived under adiabatic conditions. The method used for the determination of temperature rise input from HOH data is as follows:

1. The weight of a unit volume of concrete (1 m³) is determined from the unit weight given in the specifications.
2. The heat capacity of this unit volume is calculated by finding the product of the masses of the various constituents and their specific heat capacities by applying the law of mixtures:

$$H_{cp}^{concrete} = \sum M_i \cdot C_i \quad (2-3)$$

Where

M_i is the mass of the ith constituent of concrete,

C_i is the specific heat capacity of the ith constituent of concrete.

Applying Equation 2-3, we get:

$$H_{cp}^{concrete} = M_{hcp} \cdot C_p^{comenipaste} + M_{cag} \cdot C_p^{coarseagg} + M_{fag} \cdot C_p^{fineagg} \quad (2-4)$$

Using the 1st law of thermodynamics, temperature rise during each step increment is given by following formula:

$$\Delta T = \frac{\Delta Q}{C_p \cdot M} \quad (2-5)$$

Where

ΔT is the temperature rise in (°C),

C_p is the specific heat capacity of the mix (J/g·°C),

M is the mass of 1 m³ of the concrete mix (g),

ΔQ is the energy increment.

The product of C_p and M gives the volumetric heat capacity. The placement temperature is taken as 23.0 °C.

2.3.2 Estimating Degree of Hydration

Here the process of approximating the degree of hydration using cumulative heat generated during an isothermal calorimetry test is briefly described. The equation used is as follows:

$$a_t = \frac{H_t}{H_u} \quad (2-6)$$

Where

a_t is the degree of hydration at time t,

H_t is the heat generated at time t (J/g),

H_u is the heat generated at the ultimate degree of hydration (J/g).

The calculation of the ultimate heat of hydration is determined based on: (1) Chemical Composition of cement and (2) SCM replacement levels. The following Equations from Schindler and Folliard (2005) and Ferraro (2009) were used to calculate the heat of hydration:

$$H_{cem} = 500 \cdot pC_3S + 260 \cdot pC_2S + 866 \cdot pC_3A + 420 \cdot pC_4AF + 624 \cdot pSO_3 + 1186 \cdot pFreeCaO + 850 \cdot pMgO \quad (2-7)$$

Where

H_{cem} is the total heat available within Portland cement (J/g) at $\alpha = 1$,

pI is the percentage fraction of the i^{th} compounds as determined from Bogue's data.

To account for heat of hydration from SCMs, the following equations (Schindler and Folliard, 2005) are used:

$$H_U = P_{cem} \cdot H_{cem} + P_{slag} \cdot H_{slag} + P_{flyash} \cdot H_{flyash} \quad (2-8)$$

Where

H_{slag} is the heat of hydration of slag (550J/g for 120 grade slag),

H_{flyash} is the heat of hydration of fly ash (1800·pCaO J/g or 209 J/g),

P_{flyash} is the percentage fraction of fly ash,

P_{slag} is the percentage fraction of slag.

The heat of hydration of metakaolin (Mk) is taken as $1.125 \cdot H_{cem}$ (Gajda, 2007)

2.3.3 Determination of Activation Energy

The following relationship derived in Poole (2007) was used to estimate activation energy:

$$41230 + 1416000 \cdot [C_3A + C_4AF] \cdot P_{cement} \cdot SO_3 \cdot P_{cement} - 347000 \cdot Na_2eq - 19.8 \cdot Blaines + 29600 \cdot P_{flyash} \cdot P_{caoflyash} - 16200 \cdot P_{GGBS} \quad (2-9)$$

Where

P_{cement} is % cement in mixture,

P_{flyash} is % fly ash in mixture,

$P_{caoflyash}$ is % CaO in fly ash,

P_{GGBS} is % GGBF slag in mixture,

$Blaines$ is Blaine fineness of cement,

Na_2eq is % Na_2eq in cement,

C_3A is % C_3A in cement,

C_4AF is % C_4AF in cement,

SO_3 is % SO_3 in cement.

2.4 Results of Isothermal Calorimetry Tests

2.4.1 Mix Design and Proportioning of Concrete Mixes Tested

The mix design details of the mass concrete mixes whose paste fractions are a part of the laboratory testing program are listed in Table 2-2. The details of the paste fractions tested are provided in Tables 2-3 and 2-4. All of the mixes listed in Table 2-2 satisfy requirements for FDOT Class IV structural concrete and Mass Concrete. Some of the salient provisions are as follows:

1. Minimum cementitious content of 658 lb./yd³ (Class IV Structural)
2. Maximum cementitious content of 752 lb./yd³ (Mass Concrete)
3. Maximum w/b ratio of 0.41 (Class IV Structural)
4. A maximum w/b ratio of 0.35 when incorporating metakaolin or ultrafine fly ash

Table 2-2. List of mixes included in this study.

MIX.	Cement (lb./yd ³)	SCMs(lb./yd ³)			Fine Aggregate (lb./yd ³)	Coarse Aggregate (lb./yd ³)	w/b ratio	Unit Weight (lb./yd ³)
		Fly ash	Slag	Mk				
HVFA 1	365.0	365.0	-	-	1075.0	1770.0	0.30	140.6
HVFA 2	365.0	365.0	-	-	1079.5	1770.0	0.30	140.7
TB1	396.0	263.0	-	93.0	1125.0	1660.0	0.34	138.7
TB2	280.0	280.0	140.0	-	1058.0	1720.0	0.41	139.4
SB1	330.0	-	330.0	-	1062.0	1780.0	0.40	139.5
SB2	330.0	-	330.0	-	1103.0	1710.0	0.40	138.5
FB1	489.0	263.0	-	-	1082.0	1702.0	0.36	141.0
FB2	467.0	278.0	-	-	967.0	1778.0	0.37	139.4
FB3	455.0	245.0	-	-	1198.0	1600.0	0.38	139.4

Table 2-3. Paste fractions of mixes tested in this study.

Mix	w/b ratio	Cement (g)	Fly Ash (g)	(%)	Slag (g)	(%)	MK (g)	Water (g)	Total (g)	% Material
07-0852 (SB1)	0.40	2.305	-	-	2.305	50%	-	1.863	6.473	71.2%
01-0550 (SB2)	0.40	2.305	-	-	2.305	50%	-	1.863	6.473	71.2%
03-1870 (FB1)	0.36	3.230	1.739	35%	-	-	-	1.789	6.759	73.5%
06-1202 (FB2)	0.37	3.059	1.821	37%	-	-	-	1.806	6.686	73.0%
01-1149 (TB1)	0.34	2.686	1.788	35%	-	-	0.633	1.737	6.844	74.6%
051526 (HVFA1)	0.30	2.804	2.804	50%	-	-	-	1.683	7.291	76.9%
061103 (HVFA2)	0.30	2.804	2.804	50%	-	-	-	1.683	7.291	76.9%
01-1099 (TB2)	0.41	1.827	0.913	20%	1.827	40%	-	1.872	6.439	70.9%
06-0531 (FB3)	0.38	3.114	1.677	35%	-	-	-	1.821	6.612	72.5%

Table 2-4. Paste fractions tested with admixtures.

Mix	w/b ratio	Cement (g)	Fly Ash (g)	(%)	Slag (g)	(%)	MK (g)	Admix + Water (g)	Total (g)	% Material
SB1/2	0.40	2.305	-	-	2.305	50%	-	-	1.880	6.490
FB2	0.37	3.059	1.821	37%	-	-	-	-	1.829	6.709
TB1	0.34	2.686	1.788	35%	-	-	0.633	-	1.737	6.844
HVFA1	0.30	2.804	2.804	50%	-	-	-	-	1.683	7.291

2.4.2 Method for Presentation and Interpretation of Test Results

The current method uses the first law of thermodynamics to convert the normalized heat of hydration trend to temperature rise at a particular time as specified in Lawrence (2009) and Do (2013). The assumption implicit in this conversion is that the cumulative energy-rise curve obtained is representative of that obtained in adiabatic conditions. The computed temperature rise data are referred to as ‘temperature rise input’.

The expression for temperature rise is given below:

$$\Delta T = H \cdot M_p \quad (2-10)$$

where H is expressed in the heat of hydration increment (J/g) and M_p is a multiplication factor based on mix proportions and thermal properties of the concrete mix constituents ($\text{g} \cdot ^\circ\text{C}/\text{J}$) since heat capacity is assumed to be a constant.

The multiplication factor is given by:

$$M_p = \frac{\gamma_w}{H_c} \cdot C \quad (2-11)$$

Where

γ_w is unit weight or specific weight of concrete (g/m^3),

H_c is the volumetric heat capacity of concrete ($\text{J}/\text{m}^3 \cdot ^\circ\text{C}$),

C is the mass fraction of the cementitious paste (decimal).

2.4.3 Tests Conducted on Paste Fractions without Admixtures

The objective of this phase of the testing program pertains to characterizing temperature rise inputs for the nine FDOT-approved mass concrete mixes that were identified for this project. SB1/SB2 constitute the same cement blend whilst having distinctive mix designs. It is to be noted that though four replicate tests were run for each mix design, only the result with highest HOH was presented for each blend. This was done so that the most conservative values of HOH could be used for thermal analysis of concrete.

Figure 2-4 shows the plots of HOH versus time for the eight cement blends tested.

Figure 2-5 shows the plots of computed temperature rise data for the nine concrete mixes.

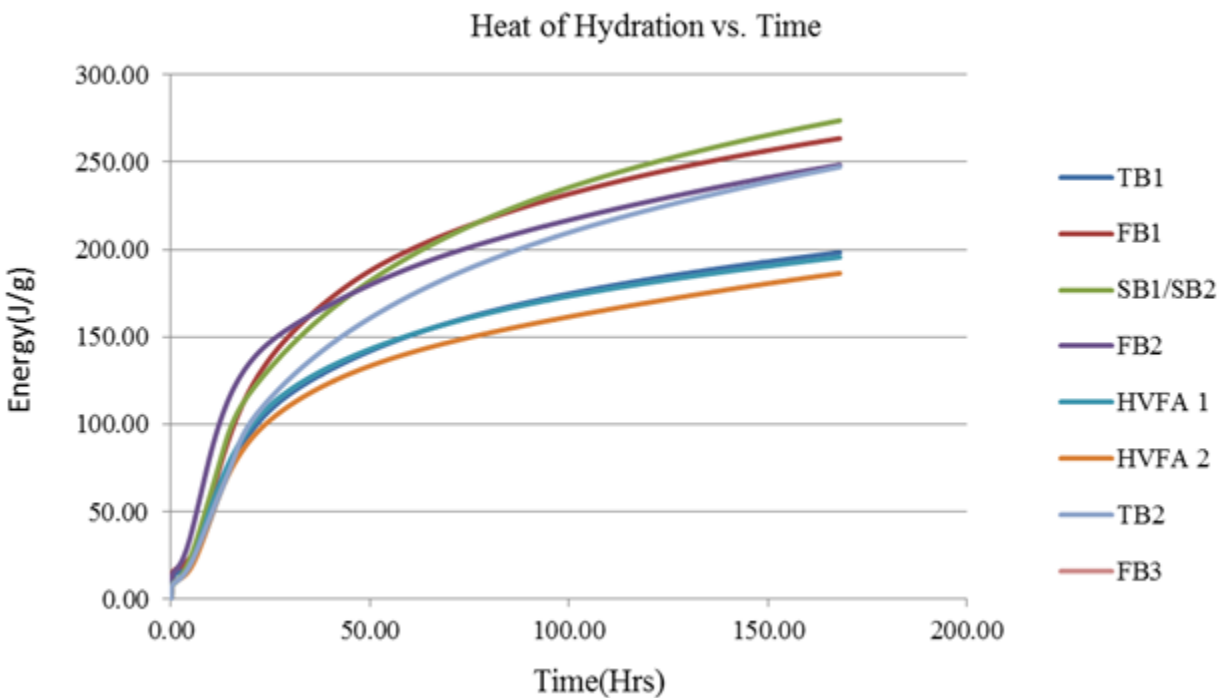


Figure 2-4. Heat of hydration vs. time for eight paste fractions.

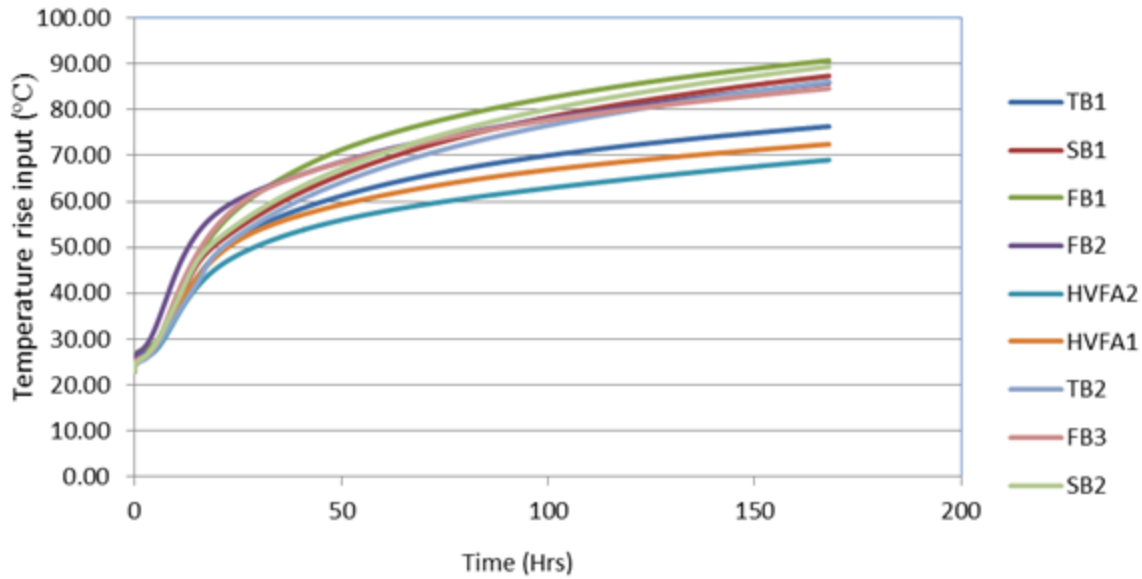


Figure 2-5. Temperature rise inputs for the nine mixes in the study.

2.4.4 Tests on Cementitious Systems with Admixtures

This phase of the testing program attempts to explore the possibility of incorporating a representative volume of admixtures during the testing of the paste fractions. The main hypotheses underlying the possible need for testing with admixtures are as follows:

1. The likely retarding and dispersing effects induced by the addition of HRWRs and WRRETs needs to be captured.
2. The energy rise and curing history would be different when accounting for the effects of (1).
3. The addition of water reducers and superplasticizers ensures greater consistency in mixing especially for the pastes with low w/b ratios.

The blends tested with admixtures for the current study incorporate admixtures that were specified in the selected mixes. The admixture designations are:

1. Type A&D (Water reducing and retarding/ Water Reducing) - Admixture ADM1.
2. Type B&D (Water Reducing and Retarding / Retarding) - Admixture ADM2.
3. Type F (Superplasticizers) -Admixture ADM3 & ADM4.

The following mixes were tested during this program: TB1, FB2, SB1 and HVFA1.

These mixes were chosen due to the fact that they represent a suitable range of w/b ratios. The dosages of admixtures used are shown in Table 2-5. Anticipating effects (1) through (3), the most convenient method to study changes in the hydration behavior of these mixes induced by the addition of chemical admixtures would be to plot the degree of hydration against time.

Table 2-5. Dosages of admixture used.

Cementitious Blend	Admixture 1	Admixture 2
TB1	ADM1(0.391)*	ADM 3(0.424)
FB2	ADM1(0.471)	-
SB1	ADM1(0.365)	-
HVFA1	ADM2(0.517)	ADM4(0.677)

(Note: * Dosage in terms of % by weight of cement)

The plots of degree of hydration obtained for the three mixes tested with and without admixtures are given in Figures 2-6 through 2-9.

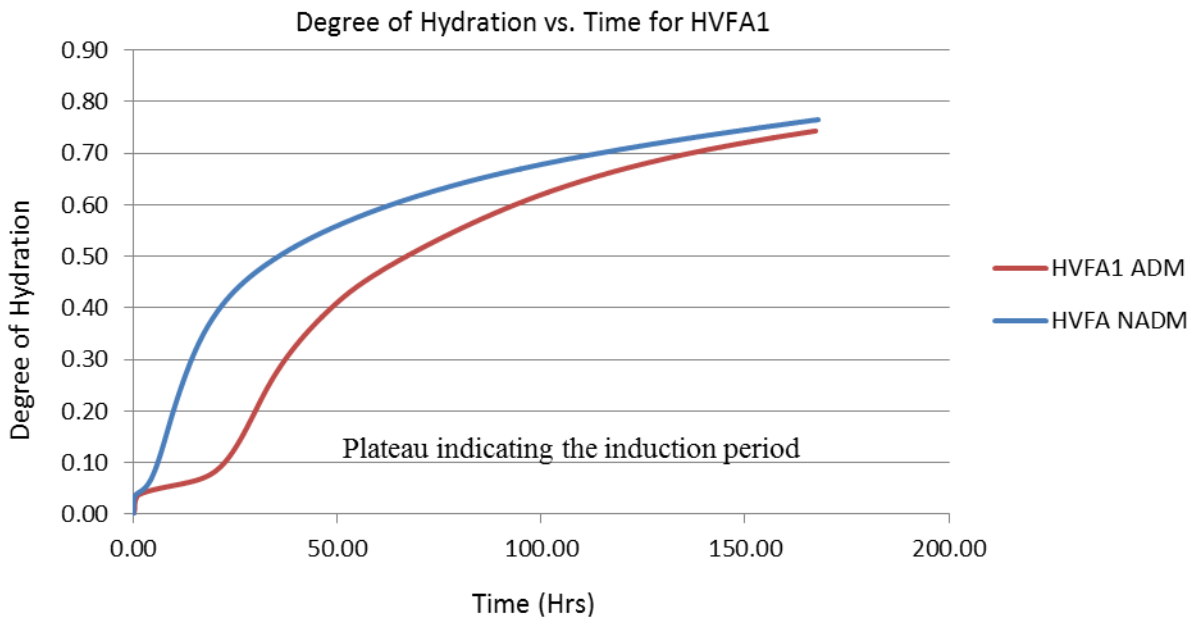


Figure 2-6. Degree of hydration vs. time for HVFA1.

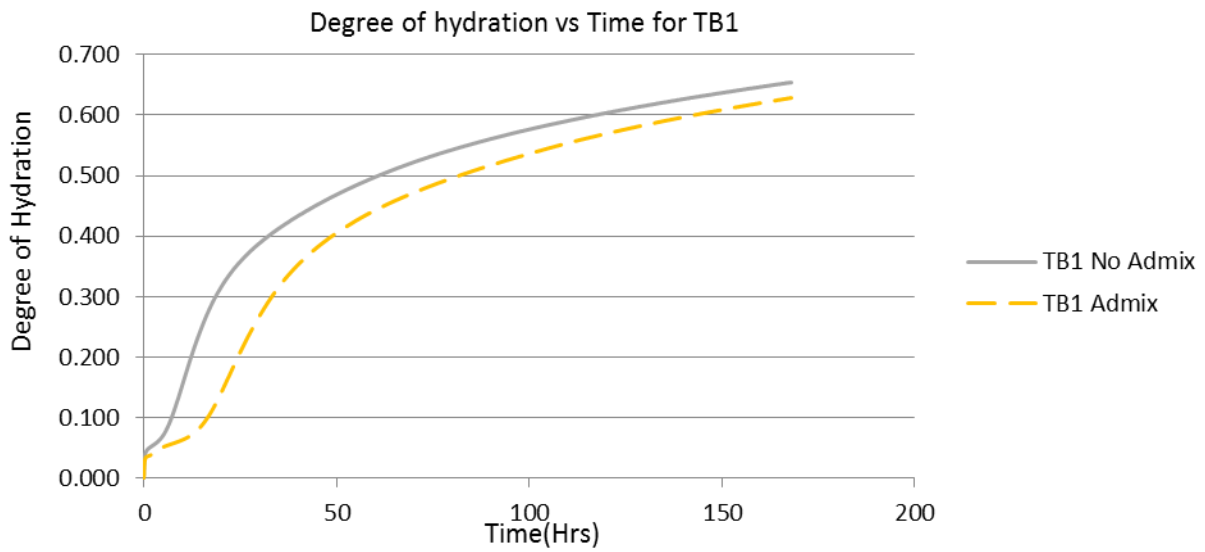


Figure 2-7. Degree of hydration vs. time for TB1.

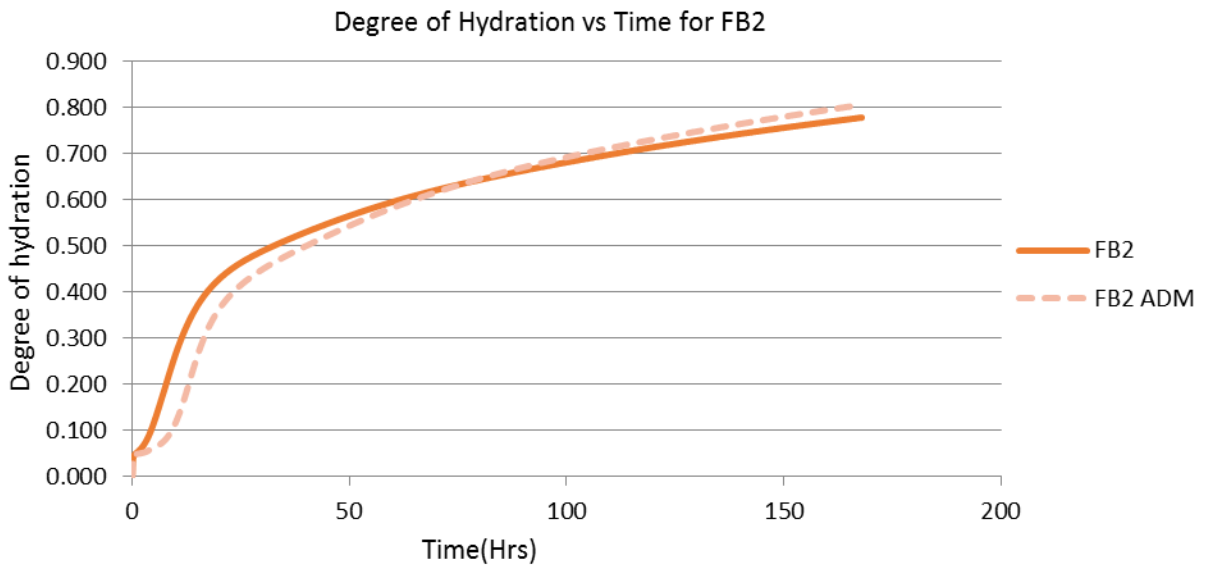


Figure 2-8. Degree of hydration vs. time for FB2.

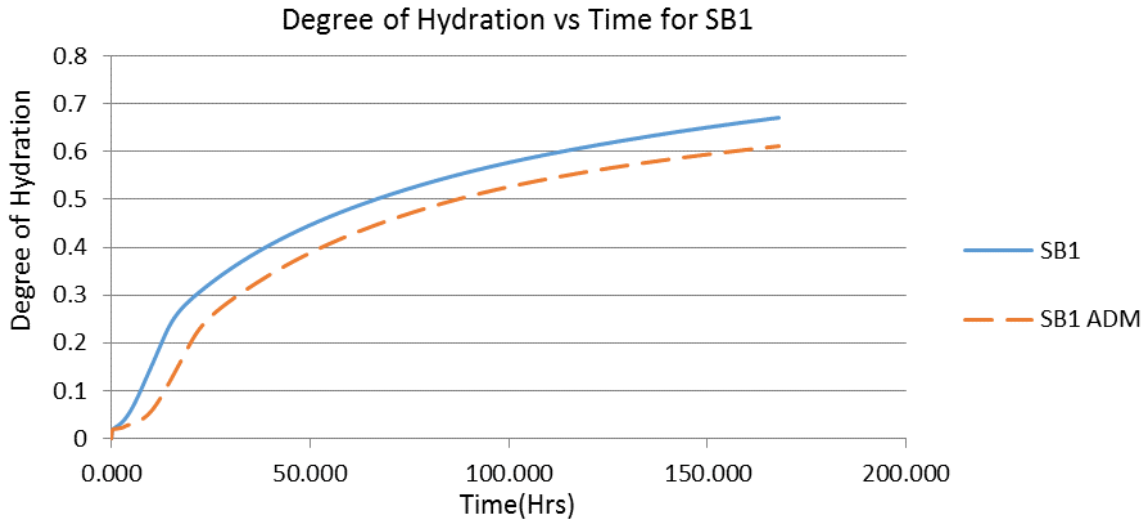


Figure 2-9. Degree of hydration vs. time for SB1/SB2.

From these four figures, the extension of the dormant period in the hydration of the cement can be seen in all the cement blends with admixtures. This is due to the effects of the retarding admixture. The behavior of FB2 incorporating the same retarder as SB1 is worth noting. For FB2, the normalized HOH at 7 days, and by consequence the temperature, is higher for the paste incorporating the retarding admixture. Some authors have previously noted the effect of increased dispersion in cement pastes due to the addition of a retarding admixture leading to higher rates of hydration after the end of the dormant period (Poole, 2007; Ramachandran, 1996). In the instance of FB2, one can observe a crossover as early as 80 hours. In this respect, the behavior of FB2 is somewhat anomalous because a slightly higher degree of hydration is reached within the duration of a 7-day test. The hydration behavior of paste SB1 is also interesting in that the main hydration peak for the paste incorporating retarder is much lower. It might also be worth noting that the largest cumulative and percentage decrease in HOH or temperature rise input was seen in SB1. Moreover, SB1 has the lowest admixture dosage for the pastes tested. It would appear that, apart from some obvious effects such as the extension of

a dormant period and the lowering of cumulative HOH at early ages, the testing of pastes with type A&D WRRETs and HRWRs does not reveal any salient trends. A larger testing program which includes testing of pastes at different dosages might be required to investigate further the effects of different types of admixtures on the pastes included in this study.

2.5 Tables of Heat of Hydration and Temperature Rise Inputs

Since the admixtures which were used in the concrete mixes in this testing program contained some retarders, the rate of hydration of the cement blend with admixtures was generally lower as compared with that of the corresponding cement blend without admixture. In order to be able to do a more conservative thermal analysis of mass concrete, the heat of hydration from the cement blends without admixture was used to develop the database of rate of heat production of cement blends for mass concrete. In the running of the DIANA software for thermal analysis of mass concrete, an input file containing the material properties of the concrete is needed. The required material properties and the required format for this input file are presented in Appendix A. Part of this concrete input file requires specifying temperature rise inputs at intervals of 1 hour for the duration of the analysis period. Table 2-6 presents the heat of hydration of the eight cement blends tested at 1 hour time increments. Table 2-7 presents computed temperature rise inputs for the nine selected concrete mixes. It is to be noted that two of the concrete mixes use the same cement blend.

Table 2-6. Heat of hydration for the cement blends.

Time (Hours)	FB1 (J/g)	TB1 (J/g)	SB1/2 (J/g)	HVFA1 (J/g)	FB2 (J/g)	HVFA1 (J/g)	FB3 (J/g)	TB2 (J/g)
1	0.000	0.000	0.000	0.000	0.000	0.000	0.019	0.000
2	0.196	0.010	0.003	0.028	0.085	0.175	2.176	0.051
3	2.114	0.296	0.153	0.558	1.246	1.781	10.577	0.858
4	6.941	1.573	1.024	2.472	4.781	5.679	23.322	3.532
5	14.164	4.288	3.202	6.041	10.712	11.387	37.480	8.253
6	22.788	8.369	6.843	10.959	18.342	18.105	51.423	14.532
7	32.005	13.493	11.774	16.770	26.934	25.215	64.457	21.769
8	41.291	19.305	17.688	23.074	35.928	32.326	76.357	29.476
9	50.339	25.507	24.273	29.574	44.952	39.217	87.113	37.313
10	58.985	31.876	31.268	36.069	53.779	45.773	96.799	45.057
11	67.153	38.253	38.466	42.431	62.276	51.944	105.519	52.575
12	74.817	44.531	45.715	48.582	70.373	57.718	113.383	59.790
13	81.981	50.641	52.906	54.478	78.042	63.102	120.493	66.662
14	88.665	56.542	59.963	60.099	85.276	68.114	126.942	73.179
15	94.898	62.210	66.837	65.436	92.087	72.780	132.809	79.339
16	100.709	67.633	73.495	70.494	98.491	77.123	138.164	85.154
17	106.132	72.809	79.918	75.281	104.510	81.171	143.069	90.637
18	111.197	77.742	86.097	79.808	110.169	84.946	147.575	95.807
19	115.933	82.439	92.030	84.089	115.491	88.473	151.726	100.682
20	120.368	86.907	97.718	88.138	120.501	91.772	155.562	105.281
21	124.527	91.159	103.167	91.968	125.220	94.863	159.117	109.623
22	128.432	95.204	108.383	95.595	129.671	97.763	162.418	113.725
23	132.104	99.054	113.376	99.032	133.872	100.489	165.493	117.605
24	135.563	102.720	118.155	102.290	137.843	103.054	168.362	121.278
25	138.825	106.213	122.729	105.382	141.600	105.471	171.046	124.757
26	141.905	109.541	127.109	108.319	145.159	107.753	173.561	128.058
27	144.818	112.717	131.303	111.112	148.534	109.910	175.922	131.192
28	147.577	115.748	135.321	113.770	151.739	111.951	178.144	134.171
29	150.192	118.643	139.173	116.301	154.784	113.886	180.238	137.006
30	152.675	121.410	142.867	118.715	157.681	115.722	182.215	139.705
31	155.035	124.057	146.411	121.018	160.441	117.466	184.083	142.278
32	157.281	126.592	149.814	123.217	163.072	119.125	185.852	144.733
33	159.420	129.019	153.082	125.320	165.583	120.705	187.530	147.079
34	161.460	131.347	156.223	127.332	167.981	122.211	189.122	149.321
35	163.407	133.580	159.244	129.258	170.275	123.648	190.636	151.466
36	165.268	135.723	162.150	131.105	172.469	125.021	192.077	153.520
37	167.047	137.783	164.948	132.875	174.571	126.333	193.450	155.489
38	168.751	139.763	167.644	134.575	176.586	127.589	194.760	157.377
39	170.383	141.667	170.242	136.207	178.519	128.793	196.011	159.190

Table 2-6. Continued.

Time (Hours)	FB1 (J/g)	TB1 (J/g)	SB1/2 (J/g)	HVFA1 (J/g)	FB2 (J/g)	HVFA1 (J/g)	FB3 (J/g)	TB2 (J/g)
40	171.948	143.501	172.747	137.776	180.375	129.947	197.207	160.932
41	173.450	145.267	175.164	139.286	182.158	131.054	198.351	162.606
42	174.893	146.969	177.498	140.739	183.873	132.117	199.447	164.217
43	176.280	148.611	179.752	142.138	185.523	133.138	200.498	165.768
44	177.614	150.195	181.930	143.487	187.112	134.121	201.506	167.262
45	178.899	151.724	184.036	144.788	188.643	135.067	202.474	168.702
46	180.136	153.201	186.074	146.043	190.120	135.978	203.404	170.091
47	181.328	154.629	188.045	147.255	191.544	136.856	204.299	171.431
48	182.479	156.011	189.955	148.426	192.919	137.702	205.160	172.726
49	183.589	157.347	191.804	149.558	194.247	138.519	205.989	173.977
50	184.661	158.640	193.597	150.653	195.530	139.308	206.788	175.187
51	185.697	159.893	195.334	151.712	196.771	140.070	207.559	176.357
52	186.698	161.107	197.020	152.738	197.972	140.807	208.303	177.489
53	187.667	162.284	198.656	153.732	199.135	141.519	209.021	178.585
54	188.605	163.426	200.244	154.694	200.261	142.209	209.716	179.648
55	189.513	164.533	201.787	155.628	201.351	142.877	210.387	180.677
56	190.393	165.608	203.285	156.534	202.409	143.523	211.036	181.676
57	191.246	166.652	204.742	157.412	203.435	144.150	211.664	182.645
58	192.073	167.667	206.158	158.265	204.430	144.758	212.272	183.585
59	192.875	168.652	207.536	159.094	205.396	145.348	212.862	184.498
60	193.654	169.611	208.876	159.899	206.335	145.920	213.433	185.384
61	194.410	170.543	210.181	160.682	207.246	146.476	213.987	186.246
62	195.145	171.450	211.451	161.443	208.132	147.016	214.525	187.084
63	195.859	172.333	212.689	162.183	208.994	147.541	215.046	187.899
64	196.553	173.192	213.894	162.903	209.832	148.050	215.553	188.691
65	197.228	174.029	215.069	163.605	210.647	148.546	216.045	189.463
66	197.885	174.845	216.215	164.287	211.441	149.029	216.523	190.214
67	198.525	175.640	217.332	164.953	212.214	149.499	216.989	190.946
68	199.147	176.415	218.422	165.601	212.967	149.956	217.441	191.658
69	199.754	177.171	219.485	166.233	213.701	150.401	217.881	192.353
70	200.344	177.908	220.523	166.849	214.416	150.835	218.310	193.030
71	200.920	178.628	221.537	167.450	215.113	151.258	218.727	193.690
72	201.482	179.330	222.527	168.036	215.793	151.670	219.133	194.335
73	202.029	180.016	223.494	168.609	216.457	152.072	219.529	194.963
74	202.564	180.686	224.438	169.167	217.104	152.464	219.915	195.577
75	203.085	181.340	225.362	169.713	217.736	152.847	220.291	196.176
76	203.594	181.979	226.265	170.246	218.353	153.220	220.658	196.761
77	204.091	182.604	227.148	170.766	218.956	153.585	221.016	197.332
78	204.576	183.215	228.011	171.275	219.545	153.941	221.366	197.891
79	205.050	183.812	228.856	171.773	220.121	154.289	221.707	198.437
80	205.514	184.397	229.683	172.259	220.684	154.629	222.040	198.970
81	205.966	184.968	230.492	172.735	221.234	154.962	222.365	199.492
82	206.409	185.528	231.284	173.200	221.772	155.286	222.683	200.003

Table 2-6. Continued.

Time (Hours)	FB1 (J/g)	TB1 (J/g)	SB1/2 (J/g)	HVFA1 (J/g)	FB2 (J/g)	HVFA1 (J/g)	FB3 (J/g)	TB2 (J/g)
83	206.842	186.076	232.060	173.655	222.298	155.604	222.994	200.502
84	207.266	186.612	232.820	174.101	222.813	155.915	223.298	200.991
85	207.681	187.137	233.564	174.537	223.317	156.219	223.594	201.469
86	208.086	187.651	234.293	174.964	223.811	156.517	223.885	201.938
87	208.483	188.155	235.008	175.383	224.294	156.808	224.169	202.396
88	208.872	188.648	235.709	175.793	224.767	157.093	224.447	202.846
89	209.253	189.132	236.395	176.194	225.231	157.373	224.719	203.286
90	209.626	189.606	237.069	176.588	225.685	157.646	224.985	203.717
91	209.991	190.071	237.730	176.973	226.130	157.914	225.246	204.140
92	210.350	190.527	238.378	177.351	226.566	158.177	225.502	204.554
93	210.701	190.975	239.013	177.722	226.994	158.434	225.752	204.960
94	211.045	191.413	239.637	178.086	227.413	158.687	225.997	205.358
95	211.382	191.844	240.250	178.443	227.825	158.934	226.237	205.749
96	211.713	192.266	240.851	178.793	228.228	159.177	226.473	206.132
97	212.038	192.681	241.441	179.136	228.624	159.415	226.704	206.509
98	212.356	193.088	242.020	179.473	229.012	159.648	226.930	206.878
99	212.668	193.488	242.590	179.804	229.393	159.877	227.152	207.240
100	212.975	193.880	243.149	180.129	229.768	160.102	227.370	207.596
101	213.276	194.265	243.698	180.448	230.135	160.323	227.584	207.945
102	213.572	194.644	244.238	180.761	230.496	160.539	227.793	208.288
103	213.862	195.016	244.768	181.069	230.850	160.752	227.999	208.624
104	214.147	195.382	245.289	181.371	231.198	160.961	228.201	208.955
105	214.427	195.741	245.802	181.668	231.540	161.166	228.400	209.280
106	214.702	196.094	246.306	181.960	231.876	161.368	228.594	209.600
107	214.972	196.441	246.801	182.247	232.206	161.566	228.786	209.914
108	215.238	196.782	247.288	182.529	232.530	161.760	228.974	210.222
109	215.499	197.118	247.767	182.806	232.849	161.952	229.158	210.525
110	215.755	197.448	248.239	183.079	233.163	162.140	229.340	210.824
111	216.007	197.773	248.703	183.347	233.471	162.325	229.518	211.117
112	216.255	198.092	249.159	183.611	233.774	162.506	229.693	211.405
113	216.499	198.406	249.608	183.870	234.073	162.685	229.865	211.689
114	216.739	198.716	250.050	184.125	234.366	162.861	230.035	211.968
115	216.975	199.020	250.485	184.376	234.655	163.034	230.201	212.243
116	217.207	199.319	250.913	184.624	234.939	163.204	230.365	212.513
117	217.436	199.614	251.335	184.867	235.218	163.371	230.526	212.779
118	217.660	199.904	251.750	185.106	235.493	163.536	230.685	213.041
119	217.882	200.190	252.159	185.342	235.764	163.698	230.841	213.299
120	218.099	200.472	252.562	185.574	236.030	163.858	230.994	213.552
121	218.314	200.749	252.959	185.803	236.293	164.015	231.145	213.802
122	218.525	201.022	253.349	186.028	236.551	164.169	231.294	214.048
123	218.733	201.291	253.734	186.249	236.806	164.322	231.440	214.290
124	218.937	201.556	254.114	186.468	237.056	164.472	231.584	214.529
125	219.139	201.817	254.488	186.683	237.303	164.619	231.726	214.764

Table 2-6. Continued.

Time (Hours)	FB1 (J/g)	TB1 (J/g)	SB1/2 (J/g)	HVFA1 (J/g)	FB2 (J/g)	HVFA1 (J/g)	FB3 (J/g)	TB2 (J/g)
126	219.338	202.074	254.856	186.895	237.547	164.765	231.865	214.996
127	219.533	202.327	255.219	187.103	237.786	164.908	232.003	215.224
128	219.726	202.577	255.577	187.309	238.022	165.049	232.138	215.449
129	219.916	202.823	255.930	187.512	238.255	165.188	232.272	215.670
130	220.103	203.066	256.278	187.712	238.484	165.326	232.403	215.889
131	220.288	203.305	256.622	187.909	238.710	165.461	232.533	216.104
132	220.469	203.541	256.960	188.103	238.933	165.594	232.660	216.316
133	220.649	203.774	257.294	188.295	239.153	165.725	232.786	216.525
134	220.825	204.004	257.623	188.484	239.370	165.855	232.910	216.732
135	220.999	204.230	257.948	188.670	239.583	165.982	233.032	216.935
136	221.171	204.453	258.268	188.854	239.794	166.108	233.153	217.136
137	221.341	204.673	258.584	189.035	240.002	166.232	233.272	217.334
138	221.508	204.891	258.896	189.214	240.207	166.354	233.389	217.529
139	221.672	205.105	259.204	189.390	240.409	166.475	233.504	217.721
140	221.835	205.317	259.508	189.564	240.608	166.594	233.618	217.911
141	221.995	205.525	259.808	189.736	240.805	166.712	233.730	218.099
142	222.154	205.731	260.103	189.905	240.999	166.828	233.841	218.284
143	222.310	205.935	260.395	190.072	241.191	166.942	233.950	218.466
144	222.464	206.135	260.684	190.237	241.380	167.055	234.058	218.647
145	222.616	206.334	260.969	190.400	241.566	167.166	234.165	218.824
146	222.766	206.529	261.250	190.561	241.750	167.276	234.270	219.000
147	222.914	206.722	261.527	190.720	241.932	167.384	234.373	219.173
148	223.060	206.913	261.801	190.876	242.112	167.491	234.475	219.344
149	223.205	207.101	262.072	191.031	242.289	167.597	234.576	219.513
150	223.347	207.287	262.339	191.184	242.464	167.702	234.676	219.680
151	223.488	207.471	262.603	191.335	242.637	167.805	234.774	219.845
152	223.627	207.652	262.864	191.484	242.807	167.906	234.871	220.007
153	223.764	207.832	263.122	191.631	242.976	168.007	234.967	220.168
154	223.900	208.009	263.377	191.776	243.142	168.106	235.062	220.327
155	224.033	208.183	263.628	191.920	243.307	168.204	235.155	220.483
156	224.166	208.356	263.877	192.062	243.469	168.301	235.248	220.638
157	224.296	208.527	264.122	192.202	243.630	168.396	235.339	220.791
158	224.425	208.696	264.365	192.341	243.788	168.491	235.429	220.942
159	224.553	208.862	264.605	192.477	243.945	168.584	235.518	221.092
160	224.679	209.027	264.842	192.613	244.100	168.677	235.606	221.239
161	224.803	209.190	265.077	192.746	244.252	168.768	235.692	221.385
162	224.926	209.351	265.308	192.878	244.404	168.858	235.778	221.529
163	225.048	209.510	265.537	193.009	244.553	168.947	235.863	221.672
164	225.168	209.667	265.764	193.138	244.701	169.035	235.947	221.812
165	225.286	209.823	265.988	193.266	244.847	169.122	236.029	221.951
166	225.404	209.977	266.209	193.392	244.991	169.207	236.111	222.089
167	225.520	210.129	266.428	193.517	245.134	169.292	236.192	222.225
168	225.635	210.279	266.645	193.640	245.275	169.376	236.272	222.360

Table 2-7. Temperature rise input for selected mixes.

Time (Hours)	FB1 (J/g)	TB1 (J/g)	SB1/2 (J/g)	HVFA1 (J/g)	FB2 (J/g)	HVFA1 (J/g)	FB3 (J/g)	TB2 (J/g)
1	23.000	23.000	23.000	23.000	23.000	23.000	23.000	23.005
2	23.048	23.003	23.001	23.007	23.001	23.022	23.043	23.555
3	23.519	23.076	23.036	23.138	23.038	23.320	23.441	25.680
4	24.705	23.406	23.241	23.613	23.253	24.228	24.407	28.893
5	26.480	24.108	23.752	24.497	23.792	25.752	25.822	32.453
6	28.599	25.163	24.608	25.716	24.693	27.712	27.486	35.954
7	30.864	26.486	25.767	27.156	25.913	29.919	29.248	39.223
8	33.145	27.988	27.157	28.718	27.376	32.230	31.010	42.206
9	35.368	29.591	28.704	30.328	29.005	34.548	32.718	44.901
10	37.493	31.237	30.348	31.938	30.736	36.816	34.342	47.326
11	39.499	32.884	32.040	33.514	32.517	38.999	35.872	49.509
12	41.382	34.507	33.743	35.039	34.310	41.079	37.302	51.476
13	43.143	36.086	35.433	36.500	36.089	43.049	38.637	53.255
14	44.785	37.611	37.091	37.892	37.835	44.907	39.879	54.868
15	46.316	39.075	38.707	39.215	39.535	46.657	41.035	56.335
16	47.744	40.476	40.271	40.469	41.183	48.302	42.111	57.674
17	49.077	41.814	41.781	41.655	42.772	49.849	43.114	58.900
18	50.321	43.089	43.233	42.776	44.300	51.302	44.050	60.027
19	51.485	44.302	44.627	43.837	45.768	52.670	44.924	61.064
20	52.574	45.457	45.964	44.841	47.175	53.957	45.741	62.023
21	53.596	46.555	47.244	45.790	48.523	55.169	46.507	62.911
22	54.556	47.601	48.470	46.689	49.814	56.312	47.226	63.736
23	55.458	48.596	49.643	47.540	51.049	57.392	47.901	64.504
24	56.308	49.543	50.766	48.347	52.232	58.412	48.537	65.221
25	57.109	50.445	51.841	49.114	53.363	59.377	49.136	65.892
26	57.866	51.306	52.871	49.842	54.447	60.291	49.701	66.520
27	58.582	52.126	53.856	50.534	55.484	61.158	50.236	67.110
28	59.260	52.909	54.801	51.192	56.479	61.982	50.741	67.665
29	59.902	53.657	55.706	51.819	57.431	62.764	51.221	68.188
30	60.512	54.372	56.574	52.417	58.345	63.508	51.676	68.681
31	61.092	55.056	57.407	52.988	59.222	64.217	52.108	69.148
32	61.644	55.711	58.206	53.533	60.064	64.893	52.519	69.590
33	62.170	56.339	58.974	54.054	60.872	65.538	52.911	70.009
34	62.671	56.940	59.712	54.553	61.650	66.154	53.284	70.406
35	63.149	57.517	60.422	55.030	62.397	66.744	53.640	70.784
36	63.606	58.071	61.105	55.488	63.116	67.307	53.980	71.144
37	64.044	58.603	61.763	55.926	63.808	67.847	54.305	71.487
38	64.462	59.115	62.396	56.348	64.475	68.365	54.617	71.814
39	64.863	59.607	63.007	56.752	65.118	68.862	54.915	72.127

Table 2-7. Continued.

Time (Hours)	FB1 (J/g)	TB1 (J/g)	SB1/2 (J/g)	HVFA1 (J/g)	FB2 (J/g)	HVFA1 (J/g)	FB3 (J/g)	TB2 (J/g)
40	65.248	60.081	63.596	57.141	65.738	69.338	55.201	72.425
41	65.617	60.537	64.164	57.515	66.336	69.797	55.475	72.711
42	65.971	60.977	64.712	57.875	66.913	70.237	55.739	72.984
43	66.312	61.401	65.242	58.222	67.471	70.661	55.992	73.247
44	66.640	61.810	65.754	58.556	68.010	71.069	56.235	73.498
45	66.955	62.205	66.249	58.878	68.531	71.462	56.470	73.740
46	67.259	62.587	66.727	59.189	69.035	71.842	56.695	73.972
47	67.552	62.956	67.191	59.490	69.522	72.208	56.913	74.196
48	67.835	63.313	67.639	59.780	69.995	72.561	57.123	74.411
49	68.108	63.658	68.074	60.061	70.452	72.902	57.325	74.618
50	68.371	63.993	68.495	60.332	70.896	73.232	57.520	74.817
51	68.626	64.316	68.904	60.594	71.326	73.551	57.709	75.009
52	68.872	64.630	69.300	60.848	71.743	73.859	57.892	75.195
53	69.110	64.934	69.684	61.095	72.148	74.158	58.068	75.375
54	69.340	65.229	70.057	61.333	72.540	74.447	58.239	75.548
55	69.563	65.515	70.420	61.565	72.922	74.727	58.405	75.715
56	69.780	65.793	70.772	61.789	73.293	74.999	58.565	75.877
57	69.989	66.063	71.114	62.007	73.653	75.262	58.720	76.034
58	70.192	66.325	71.447	62.218	74.004	75.518	58.871	76.186
59	70.389	66.580	71.771	62.423	74.344	75.766	59.017	76.333
60	70.581	66.827	72.086	62.623	74.676	76.007	59.159	76.476
61	70.767	67.068	72.393	62.817	74.999	76.242	59.297	76.614
62	70.947	67.303	72.691	63.006	75.313	76.469	59.431	76.748
63	71.123	67.531	72.982	63.189	75.619	76.691	59.561	76.878
64	71.293	67.753	73.265	63.367	75.917	76.906	59.687	77.005
65	71.459	67.969	73.541	63.541	76.208	77.115	59.810	77.128
66	71.620	68.180	73.810	63.710	76.492	77.319	59.929	77.247
67	71.777	68.385	74.073	63.875	76.768	77.518	60.046	77.363
68	71.930	68.586	74.329	64.036	77.038	77.711	60.159	77.476
69	72.079	68.781	74.579	64.192	77.301	77.900	60.269	77.586
70	72.225	68.972	74.823	64.345	77.557	78.083	60.377	77.693
71	72.366	69.157	75.061	64.494	77.808	78.263	60.482	77.797
72	72.504	69.339	75.294	64.639	78.053	78.437	60.584	77.898
73	72.639	69.516	75.521	64.781	78.292	78.608	60.683	77.997
74	72.770	69.689	75.743	64.920	78.526	78.774	60.781	78.093
75	72.898	69.858	75.960	65.055	78.755	78.936	60.875	78.187
76	73.023	70.023	76.172	65.187	78.978	79.095	60.968	78.279
77	73.145	70.185	76.380	65.316	79.196	79.250	61.058	78.368
78	73.264	70.343	76.583	65.442	79.410	79.401	61.147	78.456
79	73.381	70.497	76.781	65.565	79.619	79.549	61.233	78.541
80	73.495	70.648	76.975	65.686	79.824	79.694	61.317	78.624
81	73.606	70.796	77.166	65.804	80.024	79.835	61.399	78.705
82	73.715	70.940	77.352	65.919	80.220	79.973	61.480	78.784

Table 2-7. Continued.

Time (Hours)	FB1 (J/g)	TB1 (J/g)	SB1/2 (J/g)	HVFA1 (J/g)	FB2 (J/g)	HVFA1 (J/g)	FB3 (J/g)	TB2 (J/g)
83	73.821	71.082	77.534	66.032	80.412	80.108	61.559	78.862
84	73.925	71.220	77.713	66.142	80.600	80.241	61.636	78.938
85	74.027	71.356	77.888	66.250	80.784	80.370	61.711	79.012
86	74.127	71.489	78.059	66.356	80.964	80.497	61.785	79.084
87	74.224	71.619	78.227	66.460	81.141	80.621	61.857	79.155
88	74.320	71.747	78.392	66.561	81.314	80.743	61.928	79.225
89	74.413	71.872	78.553	66.661	81.484	80.862	61.997	79.292
90	74.505	71.994	78.711	66.758	81.651	80.978	62.065	79.359
91	74.595	72.114	78.866	66.854	81.814	81.093	62.131	79.424
92	74.683	72.232	79.019	66.948	81.975	81.205	62.196	79.488
93	74.769	72.348	79.168	67.040	82.132	81.315	62.260	79.550
94	74.854	72.461	79.315	67.130	82.286	81.422	62.323	79.611
95	74.937	72.572	79.459	67.218	82.438	81.528	62.384	79.671
96	75.018	72.682	79.600	67.305	82.586	81.632	62.444	79.730
97	75.098	72.789	79.739	67.390	82.732	81.733	62.503	79.788
98	75.176	72.894	79.875	67.473	82.876	81.833	62.561	79.844
99	75.253	72.997	80.009	67.555	83.017	81.931	62.618	79.900
100	75.328	73.099	80.140	67.636	83.155	82.027	62.673	79.954
101	75.402	73.198	80.269	67.715	83.291	82.122	62.728	80.007
102	75.475	73.296	80.396	67.793	83.424	82.214	62.782	80.060
103	75.546	73.392	80.520	67.869	83.556	82.305	62.834	80.111
104	75.616	73.487	80.643	67.944	83.685	82.395	62.886	80.161
105	75.685	73.579	80.763	68.017	83.811	82.483	62.937	80.211
106	75.752	73.671	80.882	68.090	83.936	82.569	62.987	80.259
107	75.819	73.760	80.998	68.161	84.059	82.654	63.036	80.307
108	75.884	73.849	81.113	68.231	84.179	82.737	63.084	80.354
109	75.948	73.935	81.225	68.299	84.298	82.819	63.132	80.400
110	76.011	74.021	81.336	68.367	84.414	82.900	63.178	80.445
111	76.073	74.104	81.445	68.433	84.529	82.979	63.224	80.490
112	76.134	74.187	81.552	68.499	84.642	83.057	63.269	80.534
113	76.194	74.268	81.658	68.563	84.753	83.133	63.313	80.577
114	76.253	74.348	81.762	68.626	84.862	83.209	63.357	80.619
115	76.311	74.427	81.864	68.688	84.970	83.283	63.400	80.660
116	76.368	74.504	81.965	68.750	85.076	83.356	63.442	80.701
117	76.424	74.580	82.064	68.810	85.180	83.428	63.483	80.742
118	76.479	74.655	82.161	68.869	85.283	83.498	63.524	80.781
119	76.534	74.729	82.257	68.928	85.384	83.568	63.564	80.820
120	76.587	74.802	82.352	68.985	85.484	83.636	63.604	80.858
121	76.640	74.873	82.445	69.042	85.582	83.704	63.643	80.896
122	76.692	74.944	82.537	69.098	85.679	83.770	63.681	80.933
123	76.743	75.014	82.628	69.153	85.774	83.835	63.719	80.970
124	76.793	75.082	82.717	69.207	85.868	83.900	63.756	81.005
125	76.842	75.149	82.805	69.260	85.960	83.963	63.793	81.041

Table 2-7. Continued.

Time (Hours)	FB1 (J/g)	TB1 (J/g)	SB1/2 (J/g)	HVFA1 (J/g)	FB2 (J/g)	HVFA1 (J/g)	FB3 (J/g)	TB2 (J/g)
126	76.891	75.216	82.891	69.312	86.051	84.026	63.829	81.076
127	76.939	75.281	82.977	69.364	86.141	84.087	63.864	81.110
128	76.987	75.346	83.061	69.415	86.230	84.148	63.899	81.144
129	77.033	75.410	83.144	69.465	86.317	84.208	63.934	81.177
130	77.079	75.472	83.225	69.515	86.403	84.267	63.968	81.210
131	77.125	75.534	83.306	69.564	86.488	84.325	64.001	81.242
132	77.169	75.595	83.386	69.612	86.572	84.382	64.034	81.274
133	77.213	75.655	83.464	69.659	86.655	84.438	64.067	81.305
134	77.257	75.715	83.541	69.706	86.736	84.494	64.099	81.336
135	77.300	75.773	83.618	69.752	86.816	84.549	64.130	81.367
136	77.342	75.831	83.693	69.798	86.896	84.603	64.162	81.397
137	77.383	75.888	83.767	69.843	86.974	84.656	64.192	81.427
138	77.424	75.944	83.841	69.887	87.051	84.709	64.223	81.456
139	77.465	75.999	83.913	69.931	87.127	84.761	64.253	81.485
140	77.505	76.054	83.984	69.974	87.202	84.812	64.282	81.513
141	77.544	76.108	84.055	70.017	87.276	84.863	64.311	81.541
142	77.583	76.161	84.124	70.058	87.350	84.913	64.340	81.569
143	77.622	76.214	84.193	70.100	87.422	84.962	64.368	81.596
144	77.659	76.265	84.261	70.141	87.493	85.010	64.396	81.623
145	77.697	76.317	84.328	70.181	87.564	85.058	64.424	81.649
146	77.734	76.367	84.394	70.221	87.633	85.106	64.451	81.676
147	77.770	76.417	84.459	70.260	87.702	85.152	64.478	81.701
148	77.806	76.466	84.523	70.299	87.770	85.199	64.504	81.727
149	77.841	76.515	84.587	70.338	87.837	85.244	64.531	81.752
150	77.876	76.563	84.650	70.375	87.903	85.289	64.556	81.777
151	77.911	76.611	84.712	70.413	87.968	85.333	64.582	81.801
152	77.945	76.657	84.773	70.450	88.033	85.377	64.607	81.826
153	77.979	76.704	84.834	70.486	88.096	85.421	64.632	81.850
154	78.012	76.749	84.894	70.522	88.159	85.463	64.657	81.873
155	78.045	76.795	84.953	70.558	88.222	85.505	64.681	81.897
156	78.077	76.839	85.011	70.593	88.283	85.547	64.705	81.920
157	78.110	76.883	85.069	70.628	88.344	85.588	64.729	81.942
158	78.141	76.927	85.126	70.662	88.404	85.629	64.752	81.965
159	78.173	76.970	85.182	70.696	88.463	85.669	64.775	81.987
160	78.204	77.013	85.238	70.729	88.522	85.709	64.798	82.009
161	78.234	77.055	85.293	70.763	88.580	85.748	64.821	82.031
162	78.264	77.096	85.347	70.795	88.637	85.787	64.843	82.052
163	78.294	77.137	85.401	70.828	88.694	85.826	64.865	82.073
164	78.324	77.178	85.455	70.860	88.750	85.864	64.887	82.094
165	78.353	77.218	85.507	70.891	88.805	85.901	64.908	82.115
166	78.382	77.258	85.559	70.922	88.860	85.938	64.930	82.135
167	78.410	77.297	85.611	70.953	88.914	85.975	64.951	82.155
168	78.438	77.336	85.662	70.984	88.968	86.011	64.971	82.175

2.6 Activation Energy and Arrhenius Constant for Cement Blends

Two other properties of the cement blends which are needed along with the temperature rise inputs for thermal analysis by DIANA are (1) activation energy and (2) Arrhenius constant. The activation energy of each cement blend was computed from its chemical composition by using Equation 2-9. The chemical compositions of the cement blends for the nine concrete mixes in the testing program are shown in Table 2-8. The Arrhenius constant for each cement blend is computed by dividing its activation energy by the universal gas constant R (which is equal to $8.314 \text{ J/K}\cdot\text{mol}$). The computed activation energies and Arrhenius constants for the eight cement blends are presented in Table 2-9.

2.7 Database Interface Program for Mass Concrete Mixes

A database interface program for managing and retrieving FDOT mass concrete mix design information was developed as part of the work in this task. The developed database interface program, which is named Mix Design Database (MMD) 1.0 is presented in Appendix B. The computer codes for the MMD 1.0 software is shown in Appendix C. Table 2-8 Chemical composition of cement blends in the study.

Table 2-8. Chemical composition of cement blends in the study.

Component	07-0852 (SB1)	01-0550 (SB2)	06-1202 (FB1)	06-0531- 02 (FB3)	05-1526- 01 (HVFA1)	06-1033 (HVFA2)	01-1099 (TB2)	03-1870 (FB2)	01-1149 (TB2)
Cement	FLROCK	FLROCK	Cemex- Miami	TITAN	TITAN	TITAN	American	Suwanee	FLROCK
Fly ash	-	-	Boral Bowan	ST JACK	ST JACK	ST-BB	ST-BB	ST-CR	ST-CR
Slag	Supercem	Supercem	-	-	-	-	Vulcan	-	-
w/b ratio	0.400	0.400	0.370	0.380	0.300	0.300	0.410	0.360	0.340
Blaines Fineness	413.000	413.000	387.500	399.000	399.000	399.000	412.000	430.000	413.000
C3S	0.640	0.640	0.585	0.610	0.610	0.610	0.550	0.575	0.640
C2S	0.061	0.061	0.141	0.100	0.100	0.100	0.130	0.151	0.061
C3A	0.060	0.060	0.070	0.070	0.070	0.070	0.080	0.080	0.060
C4AF	0.131	0.131	0.110	0.120	0.120	0.120	0.130	0.097	0.131
SO3	0.031	0.031	0.028	0.029	0.029	0.029	0.035	0.031	0.031
PFreeCaO	0.0080	0.0080	0.0090	0.0137	0.0137	0.0137	0.0130	0.0200	0.0080
PMgO	0.010	0.010	0.009	0.009	0.009	0.009	0.010	0.008	0.010
Pggbs	0.500	0.500	-	-	-	-	0.400	-	-
Pflyash	-	-	0.373	0.350	0.500	0.500	0.200	0.350	0.350
Pmeta	-	-	-	-	-	-	-	-	0.124
Pcement	0.500	0.500	0.627	0.650	0.500	0.500	0.400	0.650	0.526
Na20eq	0.0026	0.0026	0.0035	0.0035	0.0035	0.0035	0.0038	0.0033	0.0026
PCaoflyash	-	-	0.0150	0.0143	0.0143	-	-	0.0626	0.0626

(Note: Bogues compounds and SCM replacement levels are given in terms of their weight ratios)

Table 2-9. Computed activation energies and arrhenius constants for cement blends.

Mix	Activation Energy(J/mol)	Arrhenius Constant(°K)
TB1	36,430.10	4,381.78
FB1	35,529.89	4,273.50
SB1/2	42,346.43	5,093.38
FB2	35,036.43	4,214.15
FB3	35,529.89	4,273.50
HVFA1	34,277.48	4,122.86
HVFA2	34,277.48	4,122.86
TB2	44,616.21	5,366.39

CHAPTER 3 THERMAL ANALYSIS OF SEGMENTAL BRIDGE STRUCTURES

3.1 Overview

Recently, the FDOT Construction Office has faced issues with segmental bridge structures that use high strength concrete. One particular structure that used segmental bridge pier segments had a volume-to-surface area ratio of 0.97 foot. Although these segments' volume-to-surface area ratios were less than 1.0 foot, and therefore not considered mass concrete, thermal cracking occurred. Because these segmental structures were not classified as mass concrete, measures were not taken to determine the maximum temperature and temperature differential realized in the structure. The question thus arises: should the V/A threshold of 1.0 foot be reduced when high strength mixes are used, and what should that threshold be? In order to address this question, research was conducted to study the effects of a segmental bridge section's dimensions and the effects of heat of hydration of the cementitious materials of the concrete on the maximum temperature and temperature differential in the segmental bridge structure. This chapter presents the results of this investigation.

3.2 Description of Finite Element Model

A concrete pier bridge segment has a complex geometric shape characterized by its flange and web elements as shown in Figure 3-1. The flange and web elements are described as extremities in practice (shown in red). These elements help create a torsionally stiff box which is required to handle the torsional moments incurred when attaching the cables to the bridge's centerline — thus securing it in place.

The general finite element model developed in this study consists of a concrete interior pier segment diaphragm used in segmental bridge construction. The interior pier segment diaphragm was designed based on girder standards set by the American Segmental Bridge

Institute (ASBI), the American Association of State Highway and Transportation Officials (AASHTO) and the Precast/Prestressed Concrete Institute (PCI).

Dimensions for the interior pier segment resemble those typically used in Florida for the construction of segmental bridges. A detailed section drawing of the full segment with dimensions used is shown in Figure 3-2. It is important to note that units are labeled in millimeters. Width dimensions follow standards set by AASHTO, PCI and ASBI for section type 1800-1. A cross sectional drawing with recommended width values established by AASHTO, PCI and ASBI for interior pier bridge segments is shown on Figure 3-3.

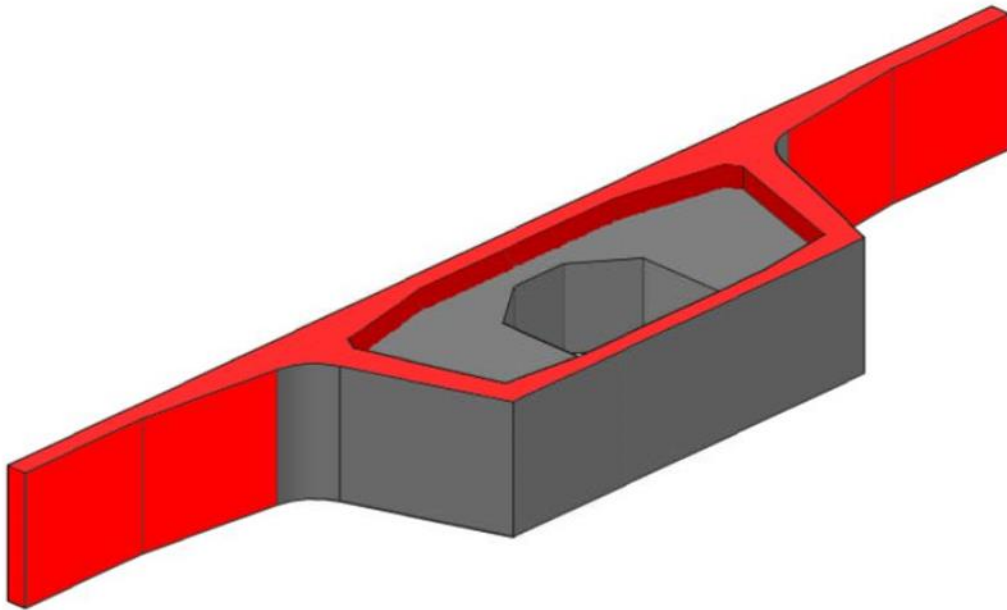


Figure 3-1. General design of complete interior pier diaphragm segment.

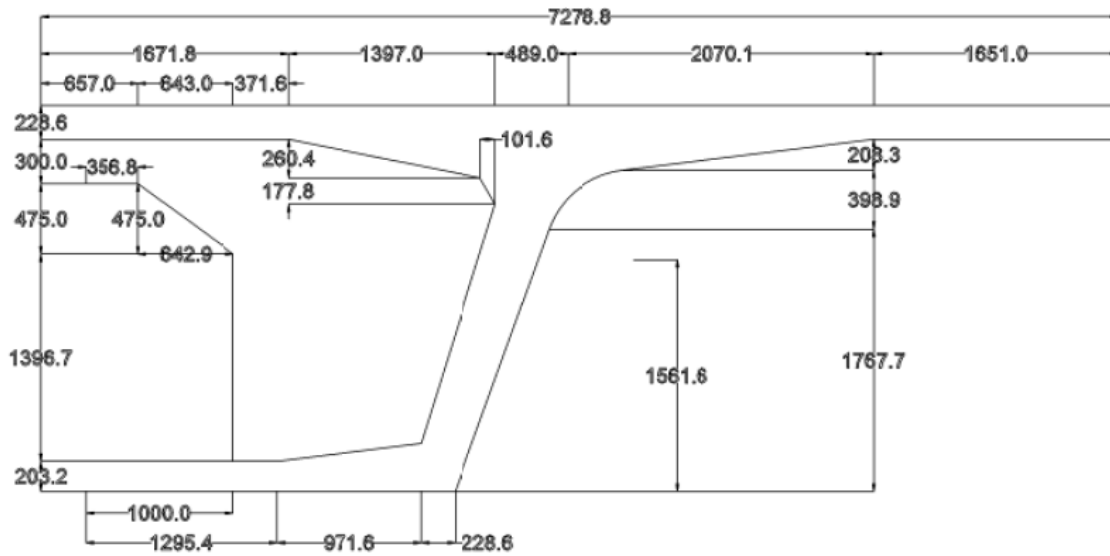


Figure 3-2. Dimensions used in DIANA FE model (mm).

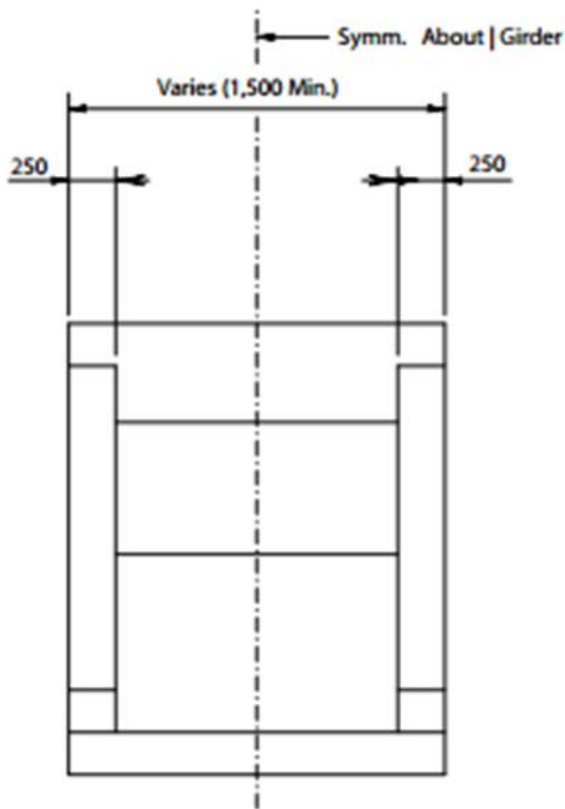


Figure 3-3. Interior pier segment recommended width measurements (mm).

Based on the symmetry of the diaphragm segment, one-quarter of the whole segment without flanges was modeled in an effort to reduce computation time and the output file size from the DIANA software. The finite element mesh of one-quarter concrete bridge pier segment is shown in Figure 3-4.

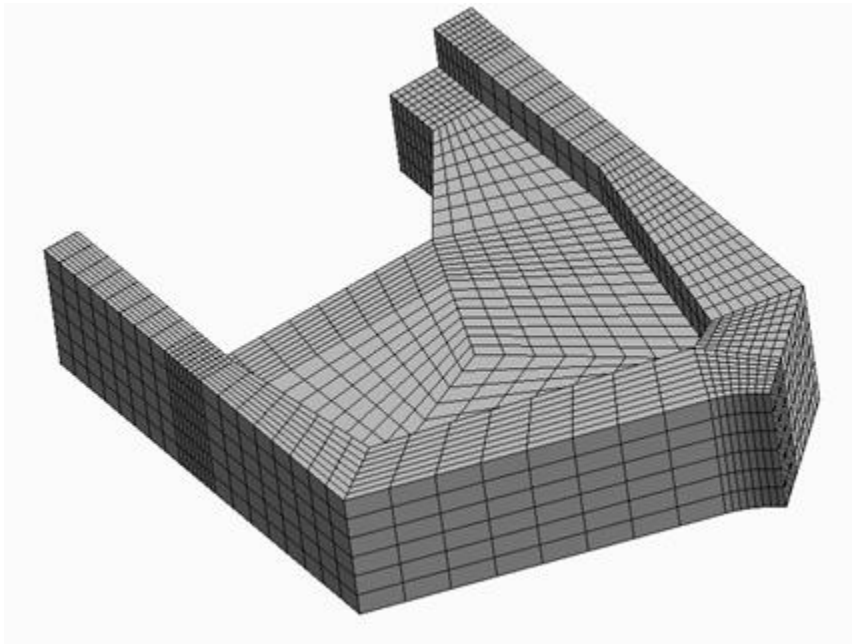


Figure 3-4. FE model mesh of one-quarter concrete bridge pier segment used in analysis.

A DIANA thermal analysis was performed using adiabatic temperature rise data for a typical Florida high-strength concrete with design strength of 8,500 psi. The adiabatic temperature rise data file used is shown in Appendix A. The model was exposed to the environment during analysis at a constant temperature of 23.0 °C (73.4 °F). The model was analyzed over a 167 hour period.

3.3 Results of Thermal Analysis

3.3.1 Parametric Studies

Two parametric studies were conducted. The first focuses on analyzing the effect of V/A ratio of segmental bridge sections on temperature differential by adjusting the width of the segment, thus changing the V/A ratio. The second analyzes the effect of different heat of hydrations of concrete, resulting from analyzing different FDOT approved concrete mixes, on temperature differential of segmental bridge sections.

3.3.2 Effect of V/A Ratio on Temperature Development

The analysis discussed in this section was performed on the quarter model no-flange segment discussed above. The analysis was performed using concrete adiabatic temperature rise data corresponding to a typical FDOT high-strength concrete with a compressive strength of 8,500 psi.

Dimensions for the bridge pier segment were based on box girder standards set by the American Segmental Bridge Institute (ASBI), the American Association of State Highway, Transportation Officials (ASSHTO), and the Precast/Prestressed Concrete Institute (PCI). For this analysis, the only parameter that was altered was the width of the segment, in order to achieve different V/A ratios.

Table 3-1 shows the dimensions used in this analysis and the corresponding V/A ratio and local V/A ratio of each trial. The local V/A ratio represents the ratio calculated from the core segment, not including flange or web elements. True width relates to the actual width of the true, real-sized segment, while model width relates to the width of the quarter model used for thermal analysis in DIANA.

Table 3-1. Width dimensions used for parametric study of segmental bridges.

Trial	V/A (ft.)	Local V/A (ft.)	1/4 model Width (ft.)	True Width (ft.)	Trial
1	0.8	1.06	2.46	4.92	1
2	0.9	1.20	3.18	6.36	2
3	1.0	1.30	3.94	7.87	3
4	1.1	1.37	4.79	9.58	4
5	1.2	1.45	6.07	12.14	5

Trial 1 represents the minimum width dimensions allowed by ASSHTO, ASBI and PCI standards for interior pier segmental sections. Per specifications, an interior bridge pier segment cannot be smaller than the one presented as Trial 1.

Figure 3-5 presents the maximum temperatures for the five trials tested with V/A ratios of: 0.8, 0.9, 1.0, 1.1 and, 1.2 feet. Figure 5-1 also shows that as the V/A ratio of a trial increases, the maximum temperature recorded for that trial also increases. This is attributed to the increase in volume of bridge section as the width is increased which consequently results in additional generation of heat from hydration of cement. In addition, it is clear that the highest temperatures for all trials calculated by DIANA occur within the first 50 hours of placement.

Figure 3-6 shows the temperature differential development for the five trials tested with V/A ratios of: 0.8, 0.9, 1.0, 1.1 and, 1.2 feet. The figure shows that the maximum temperature differentials for all trials occur within the first 50 hours of placement.

Table 3-2 summarizes the maximum temperature and maximum temperature differential calculated for each trial by DIANA thermal analysis. The V/A ratios range from 0.80 to 1.20 feet while the local V/A ratios range from 1.06 to 1.45 feet.

Based on DIANA thermal analyses results, the maximum temperature differential values calculated for all trials exceed the allowable temperature differential limits set by FDOT. Florida Department of Transportation (2015) specifies that a maximum allowable temperature of 82.2°C

(180.0 °F) and differential between the concrete core and the exterior surface of 19.4 °C (35.0 °F) be not exceeded.

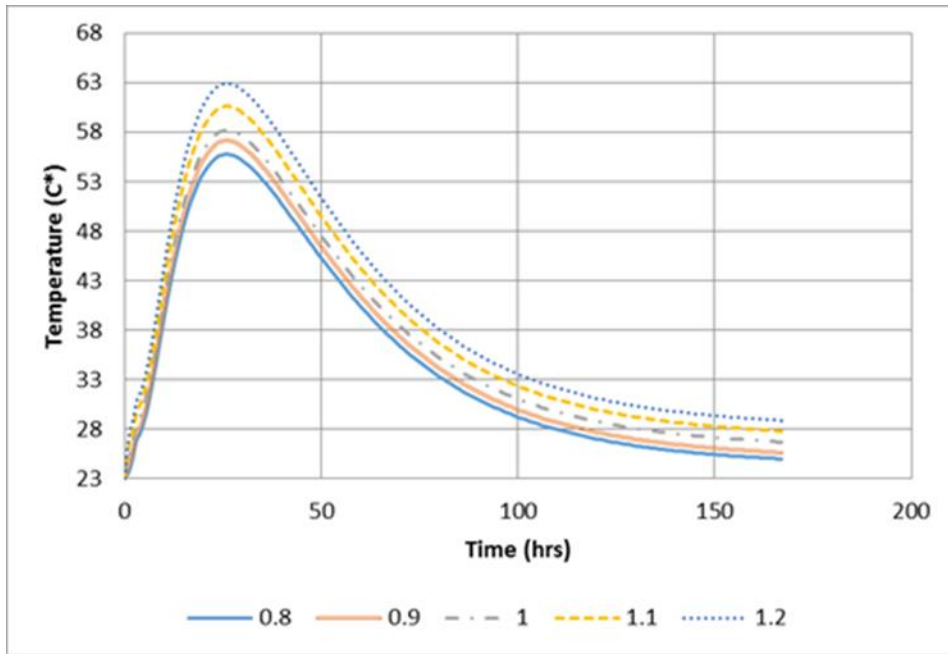


Figure 3-5. Temperature development of segmental bridge sections with varying V/A ratios.

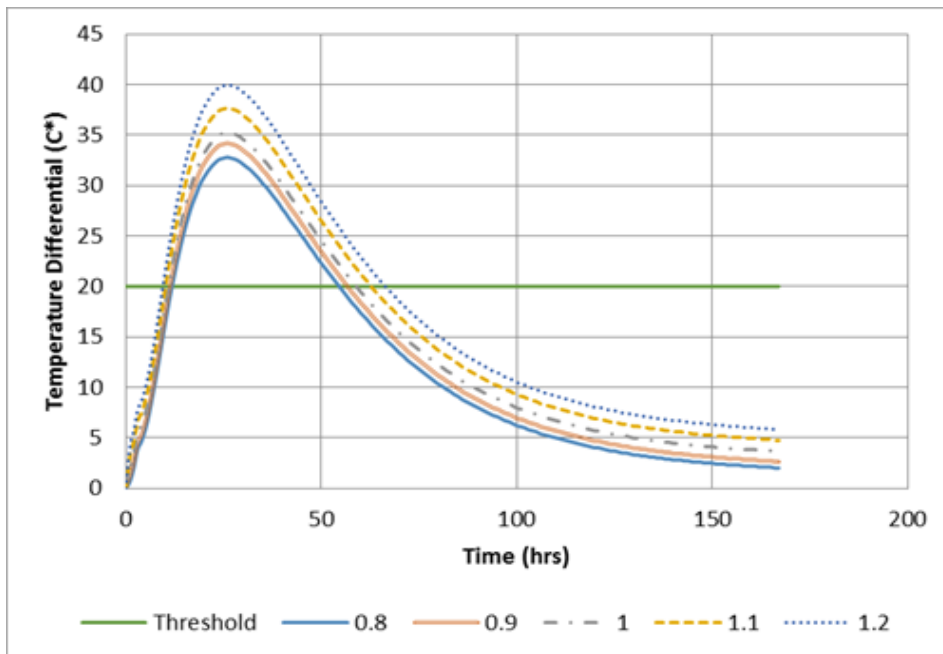


Figure 3-6. Temperature differential development of segmental bridge sections with varying V/A ratios.

Table 3-2. Maximum temperature and temperature differentials calculated by DIANA using varying V/A ratios.

Trial	V/A (ft.)	Local V/A (ft.)	Max. Temperature (°C)	Max. Temp. Difference (°C)
1	0.80	1.06	55.8	32.8
2	0.90	1.20	57.2	34.2
3	1.00	1.30	58.2	35.2
4	1.10	1.37	60.7	37.7
5	1.20	1.45	63.0	40.0

In addition, Florida Department of Transportation (2014) states that a bridge section is to be considered mass concrete when the minimum width dimension of the concrete [bridge segment] exceeds 3 feet and the ratio of volume of concrete to the surface area is greater than 1 feet. However, Table 3-2 shows that trials 1 and 2 — having a V/A ratio lower than 1.0 feet — had maximum temperature differentials higher than those allowed by FDOT.

It is important to note that the local V/A ratio — not including flange or web elements — for all trials was higher than 1.0 feet. Therefore, local V/A ratio was more appropriate in classifying bridge sections as mass concrete than overall V/A ratio.

3.3.3 Effect of Heat of Hydration on Temperature Development

The thermal analysis was performed using concrete adiabatic temperature rise data corresponding to several different FDOT concrete mix designs used for construction in Florida.

A typical high-strength concrete Florida concrete (8,500 psi) was used as a control for the analysis. In addition to the control mix, four other FDOT approved concrete mix designs were used for this parametric study. The additional mix designs analyzed were:

- Ternary Blend (TB) – FDOT Mix: 01-1149.
- Slag Blend (SB) – FDOT Mix: 07-0852.
- High-Volume Fly Ash (HVFA) – FDOT Mix: 05-1526.
- Fly Ash Blend (FB) – FDOT Mix: 03-1870.

Table 3-3 shows the mix design properties for the mix designs selected for this parametric analysis. The mixes selected represent actual FDOT mix designs used in concrete structure applications and they represent a suitable range of water-to-cement (W/C) ratios for analysis. Temperature rise data for FDOT mixes was retrieved using the mix design database program presented in the report for Subtask 1C of this research study. It is important to mention that the selected mixes are not commonly used for segmental bridge applications, yet they are mixes used in other mass concrete applications. These mixes are composed of pozzolanic materials mixed with Portland cement. Pozzolanic materials are known to lower the heat generated due to hydration when used as Portland cement replacements (Markandeya, 2014).

Table 3-3. Properties of FDOT mixes used in parametric study.

FDOT Mix No.	Designation	W/C	Cement (g)	Fly Ash (g)	(%)	Slag (g)	(%)	Metakaolin (g)	Water (g)
07-0852	SB	0.4	2.305	-	-	2.305	50%	-	1.863
03-1870	FB	0.36	3.23	1.739	35%	-	-	-	1.789
01-1149	TB	0.34	2.686	1.788	35%	-	-	0.633	1.737
05-1526	HVFA	0.3	2.804	2.804	50%	-	-	-	1.683

The cement blends for the concrete mixes were tested in a calorimetry machine to measure the heat of hydration. The first law of thermodynamics was then used to convert the normalized heat of hydration values into temperature rise values that can be used by DIANA as inputs for thermal analysis using the equation below.

$$\Delta T = H \cdot M_p \tag{3-1}$$

Where

H is Heat of Hydration (J/g),

M_p is Multiplication Factor – Based on Mix proportion and Thermal properties of the concrete’s constituents (J·°C/g).

Dimensions for the bridge pier segment were based on girder standards set by the American Segmental Bridge Institute (ASBI), the American Association of State Highway, and Transportation Officials (AASHTO), and the Precast/Prestressed Concrete Institute (PCI). The dimensions for the quarter model in this analysis were fixed; the model used has a V/A ratio of 0.80 feet, a local V/A ratio of 1.06 feet.

Figure 3-7 presents the temperature development results of the five concrete mix designs tested: control mix, TB, FB, SB, and HVFA. As shown, the highest temperature is recorded in the bridge segment using the control mixture. This is attributed to the fact that the control mixture is a typical high-strength concrete mix composed primarily of Portland cement, thus generating more heat than mixes that combine pozzolanic materials. The lowest temperatures are calculated when using the HVFA mix. The HVFA mix is composed of 50 % replacement of Portland cement with fly ash. This represents a high Portland cement replacement value, as a result the heat of hydration, and subsequent temperature rise is limited and thus lower. These results are expected from practice and are evident from DIANA thermal analysis results. Additionally, the highest temperatures recorded occur during the first 50 hours after placement.

Figure 3-8 presents the temperature differential development results of the five concrete mix designs tested: control mix, TB, FB, SB, and HVFA. The trend follows that of the before-mentioned results. The highest temperature differentials are calculated when using the control mix — a result of the additional heat generated due to hydration of high-strength concrete. The lowest temperature differential is calculated when using the HVFA mix — a result of the large percentage of Portland cement replacement with fly ash.

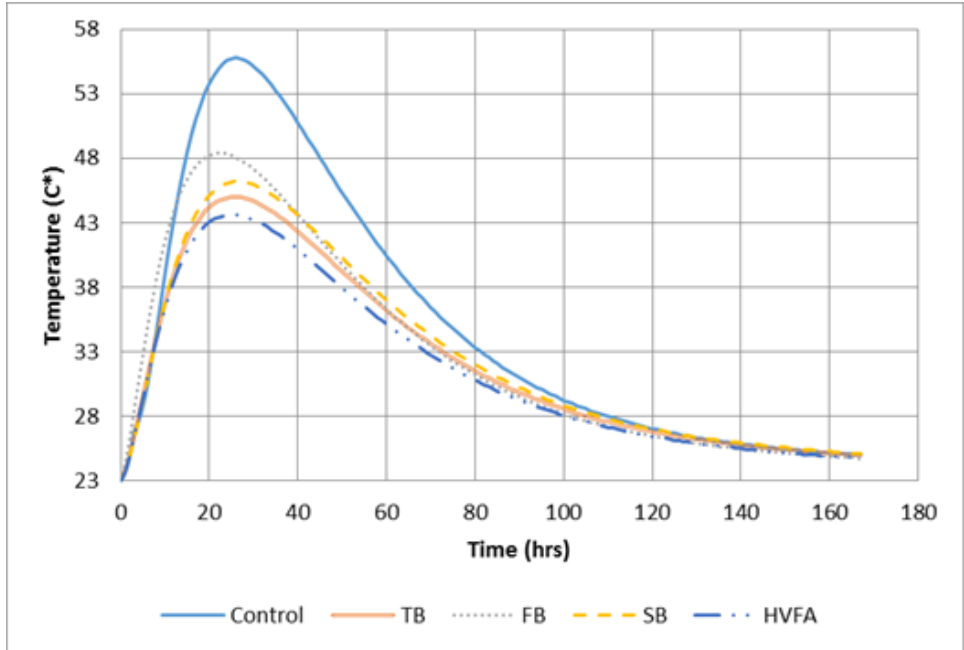


Figure 3-7. Temperature development of segmental bridge sections with varying FDOT mix designs.

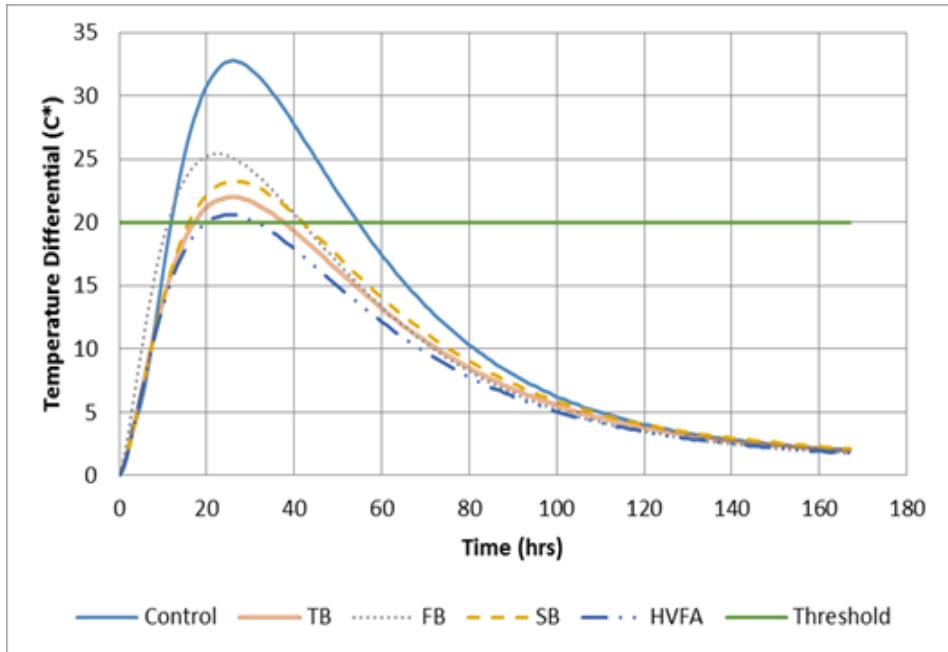


Figure 3-8. Temperature differential development of segmental bridge sections with varying FDOT mix designs.

Table 3-4 summarizes the maximum temperature and maximum temperature differential calculated for each trial by the DIANA thermal analysis. Based on the DIANA thermal analyses results, the maximum temperature differential values calculated for all trials exceed the allowable temperature differential limits set by FDOT. Florida Department of Transportation (2015) specifies that a maximum allowable temperature of 82.2 °C (180.0 °F) and differential between the concrete core and the exterior surface of 19.4 °C (35.0 °F) be not exceeded. However, use of ternary blends and pozzolanic materials greatly reduced the heat generated due to hydration in segmental bridges, as calculated by DIANA. There is a 28 % difference in maximum temperature calculated by the DIANA analysis between the highest temperature yielding mix and the lowest temperature yielding mix, namely Control mix and HVFA, respectively.

Table 3-4. Maximum temperature and temperature differentials calculated by DIANA using FDOT mix designs.

FDOT Mix No.	Designation	Max. Temperature (°C)	Max. Temp. Difference (°C)
N/A	Control	55.8	32.8
03-1870	FB	48.4	25.4
07-0852	SB	46.3	23.3
01-1149	TB	45.0	22.0
05-1526	HVFA	43.6	20.6

In addition, the DIANA results shows that mix HVFA produced a maximum temperature differential value of 20.6 °C (69.6 °F). This value closely approximates the limit set by FDOT of a maximum temperature differential of 19.4 °C (35.0 °F).

3.4 Summary of Findings

1. Classification of segmental bridge sections, as mass concrete structures, based on overall V/A ratio, is not adequate. Bridge sections with V/A ratios less than 1.0 feet could produce maximum temperature differentials which failed limits set by FDOT.
2. Local V/A ratio, which excludes extremities, is more appropriate in classifying and identifying segmental bridge sections as mass concrete structures.
3. Maximum temperatures and maximum temperature differentials of segmental bridge sections are greatly influenced by the heat of hydration of the cementitious materials used in the concrete.
4. Use of high-strength concrete in analysis produced the highest temperatures and temperature differentials.
5. Use of pozzolanic cementitious material replacement, in particular HVFA, greatly reduces the maximum temperature and maximum temperature differential in segmental bridge sections.

CHAPTER 4
DETERMINATION OF THERMAL PROPERTIES OF SOILS IN
DIFFERENT MOISTURE CONDITIONS

4.1 Introduction

The main objective of this research task was to investigate the insulating properties of different soils and under various moisture conditions to be used in thermal analysis of mass concrete placed on them. A laboratory testing program was performed to evaluate the insulating properties of several typical soils present in Florida and the effects of varying moisture content on them. A field testing program was also performed to record the actual temperature development and distributions in four concrete drilled shafts placed under soils of different moisture conditions to evaluate the actual effects of the soils of different moisture conditions on mass concrete. This chapter presents the results of the laboratory testing program. The detailed description of the equipment and test procedures used are presented in Appendix D. The field testing program is presented in Chapter 5.

4.2 Results of Laboratory Testing Program

4.2.1 Materials Tested

In the State of Florida, the majority of mass concrete poured in contact with the ground is found in bridge foundation projects. These foundation elements are normally poured in areas that have either been partially dewatered for construction, such as with coffer dams, areas where water has been diverted, or areas seasonally flooded.

Many riparian environments and river bottoms have soils largely composed of sandy materials and clay materials. Undesirable soils with high organic percentages are usually removed; however, some high organic materials may still remain. When fill is needed below the mass concrete structure, lime rock is often used if local soils are not desirable or unavailable. The soils selected for study were soils indicative of riparian environments. These sandy clay

soils will be encountered in various moisture contents depending upon the efforts to dewater the site during construction. Muck was also studied because of its possible existence in a riparian site where mass concrete might be poured.

Four soil samples (samples 1-4) and the muck tested in this project were acquired from the Florida Department of Transportation Materials Lab and originated from a road widening project in Nassau County, Florida. Four additional soil samples (samples 5-8) were taken from the field testing site in Gainesville during construction of the four drilled shafts that were part of this research. The lime rock tested also came from the FDOT Materials Lab, but originated in Duval County, Florida. Concrete samples 1 and 2 originated in Lafayette County, Florida, whereas concrete sample 3 contained granite aggregate from Washington County, Florida. The insulation mat material tested was acquired from the State Materials Office. The designations and sources of the materials tested are listed in Table 4-1.

Table 4-1. Designation and origination of materials tested.

Material	Designation	Origination
Soil Sample 1	A-3	US 17 Nassau Co.
Soil Sample 2	A-7-5	US 17 Nassau Co.
Soil Sample 3	A-7-6	US 17 Nassau Co.
Soil Sample 4	A-2-4	US 17 Nassau Co.
Muck	77.59 % Organic content	US 17 Nassau Co.
Lime rock	-	Duval Co.
Concrete 1	Limestone, 57 stone	Lafayette Co.
Concrete 2	Limestone, 89 stone	Lafayette Co.
Concrete 3	Granite	Washington Co.
Insulation Mat	Polyethylene	FDOT SMO
Soil Sample 5	A-3	Alachua Co.
Soil Sample 6	A-3	Alachua Co.
Soil Sample 7	A-3	Alachua Co.
Soil Sample 8	A-3	Alachua Co.

4.2.2 R-value of Soils as Affected by Moisture and Temperature

Soil sample 1 is a predominately sandy material with 90 % total sand. This sample displayed a marked difference between the high and low moisture test results with very little difference due to changes in temperature. The sample at dry condition had an insulation property of 2.5 to 2.8 R-value/inch, while the sample at wet condition (15.4 % moisture) had a value of 0.8 to 1.0 R-value/inch. The test results for soil sample 1 are shown in Figure 4-1.

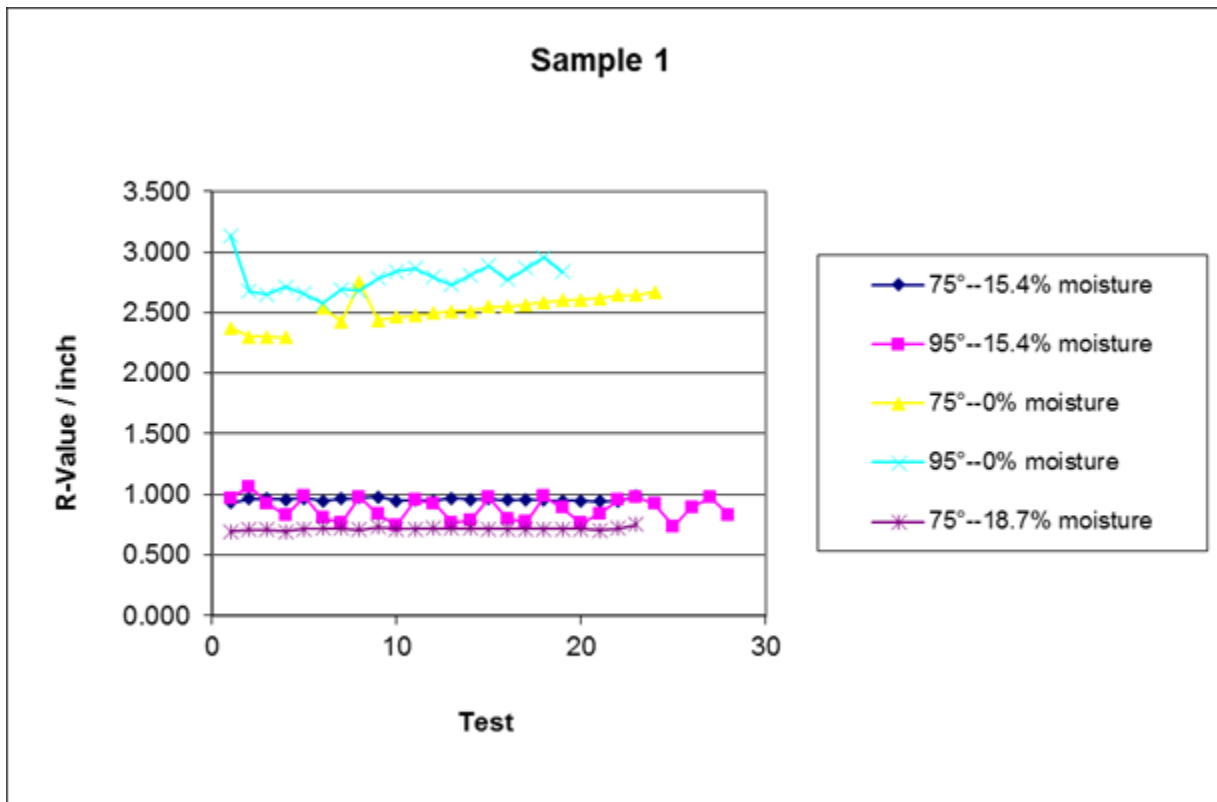


Figure 4-1. Measured R-values of soil sample 1 under different moisture and temperature conditions.

Soil sample 2 is a predominately clay-like material with 35 % clay and 52 % sand. As shown in Figure 4-2, when soil sample 2 was moist and at high or low temperature, the test yielded relatively low insulation property of 0.8 to 1.5 R-value/inch. Conversely, when the moisture content was 0 %, the measured insulation values were substantially higher, at 7.5 to 8.0 R-value/inch.

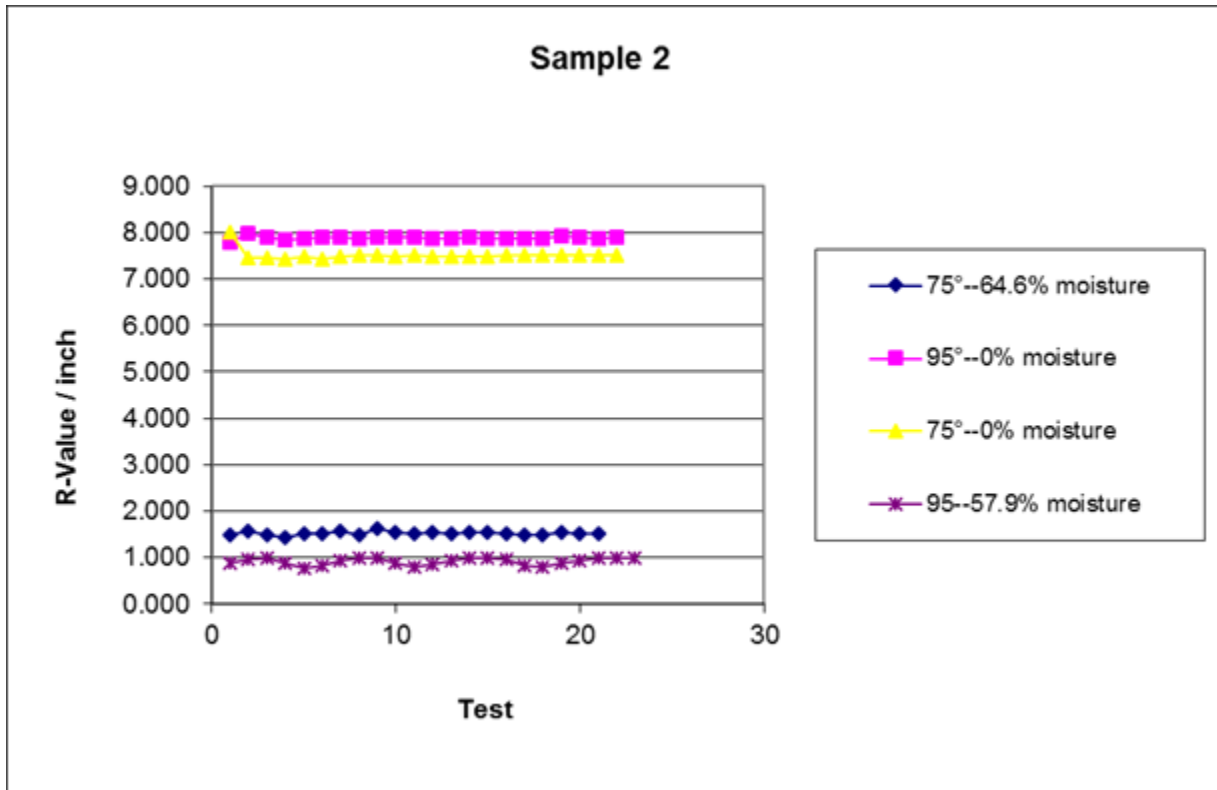


Figure 4-2. Measured R-Values of soil sample 2 under different moisture and temperature conditions.

Soil sample 3 is similar in composition to sample 2 in that it has 31 % clay and 54 % sand. Again it can be noted that the measured insulation values were substantially lower at high moisture content, at approximately 1.2 R-value/inch, as can be seen from Figure 4-3. When the moisture content was low (0 and 5 %), the measured insulation values were much higher, at 8.0 to 9.5 R-value/inch.

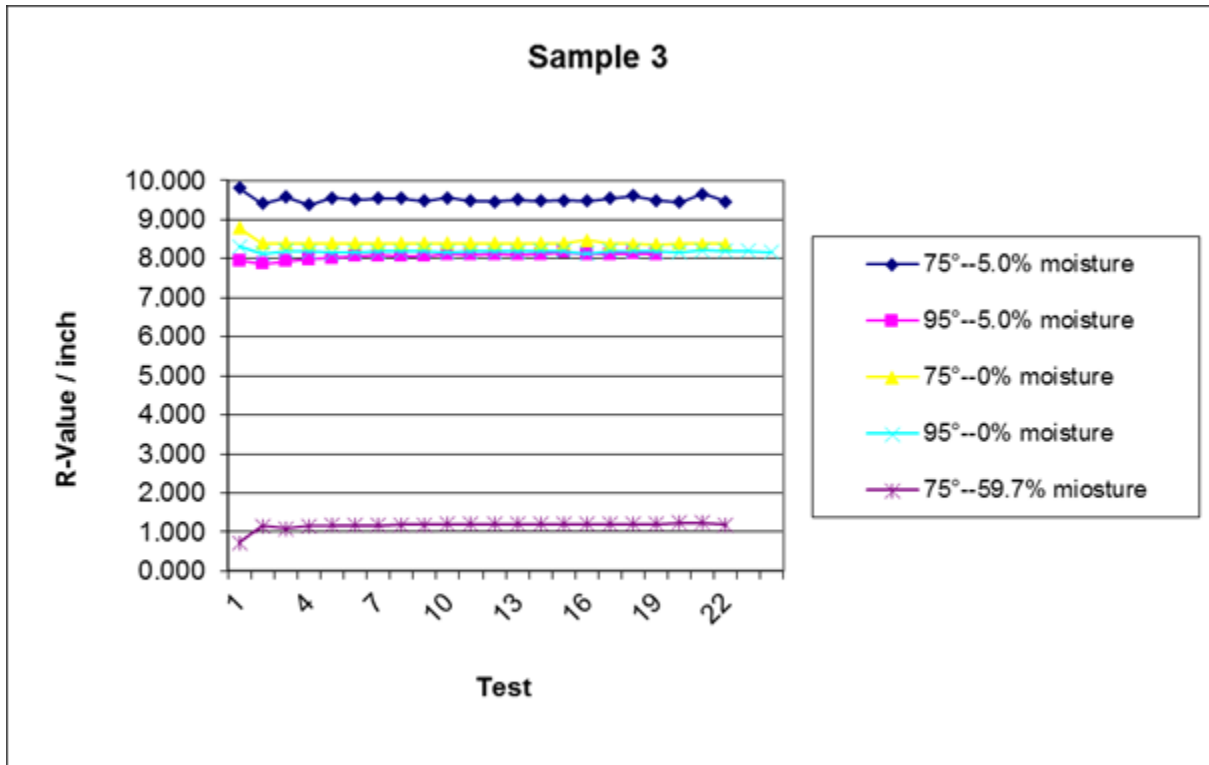


Figure 4-3. Measured R-Values of soil sample 3 under different moisture and temperature conditions.

Soil sample 4 is a very sandy material with 90 % sand. The measured insulation values are plotted in Figure 4-4. At low moisture content (0 and 9.4 %) and at both test temperatures, the measured insulation values were 7.5 to 8.0 R-value/inch. However, at the high moisture content of 24.9 %, the measured insulation values were 0.8 to 0.9 R-value/inch.

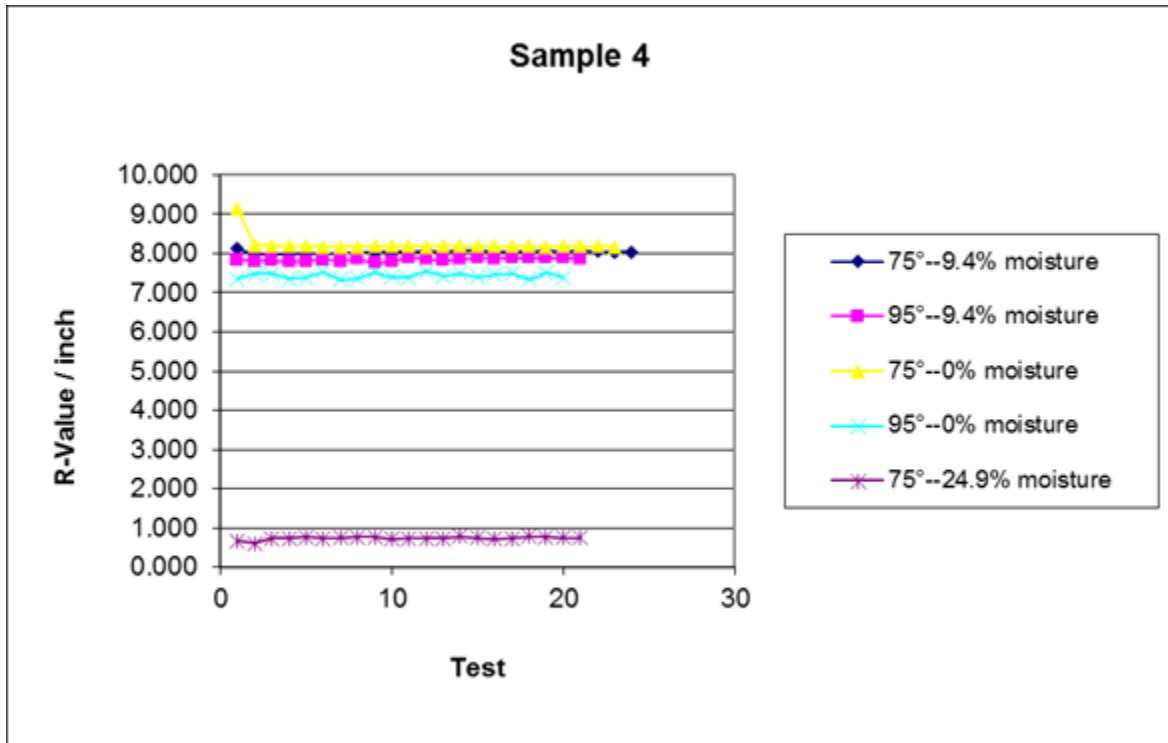


Figure 4-4. Measured R-Values of soil sample 4 under different moisture and temperature conditions.

Figures 4-5 through 4-8 show plots of measured insulation property of the four soil samples collected from the locations where the four drilled shafts were constructed as part of the field testing program. Since the four drilled shafts were located in close proximity to one another, it is expected that the measured soil properties would be similar. The four soil samples, which were tested separately, showed almost identical results. For comparison purpose, the test results from the four soil samples are shown together in Figure 4-9. At high moisture content between 15.4 % and 17.9 %, the average measured insulation value was 0.78 R-value/inch. At moisture content of less than 1.0 %, the average measured insulation value was 5.32 R-value/inch.

Since the property of the soils at the locations of the four drilled shafts is so markedly similar, the four soil samples were combined into a composite sample and tested at various moisture contents in order to develop an R-value/ inch versus moisture curve as shown in Figure 4-10. It can be seen that the R-value decreases sharply with increase in moisture content until it reaches a moisture content of around 6 %, at which point the insulation value reaches its lowest value and remains unchanged with further increase in moisture content.

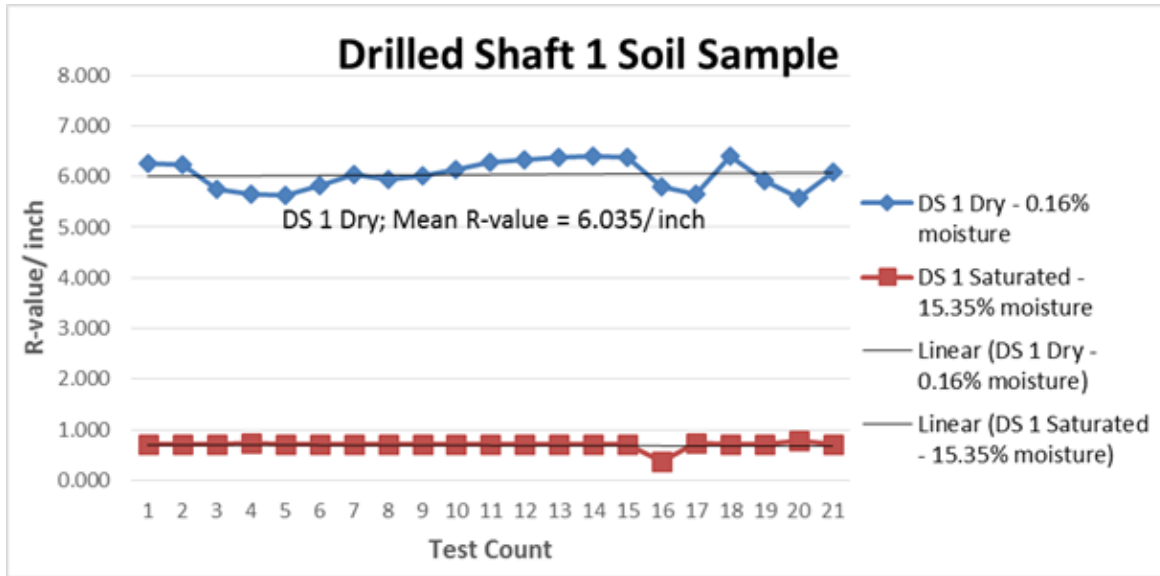


Figure 4-5. Measured R-Values of DS1 soil sample under different moisture conditions.

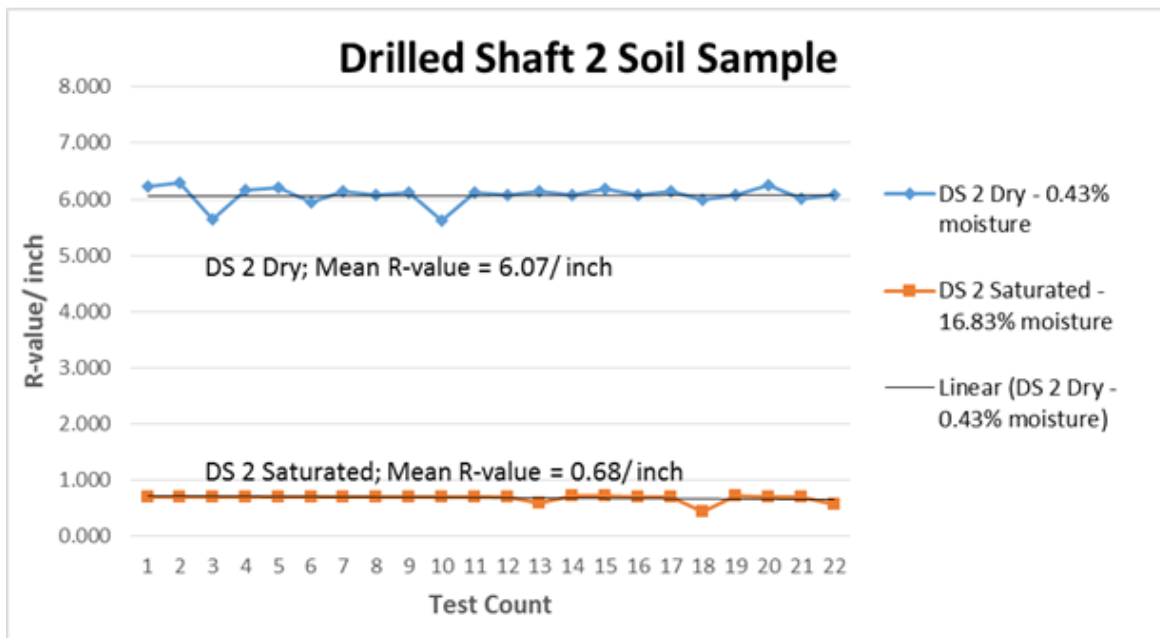


Figure 4-6. Measured R-Values of DS2 soil sample under different moisture conditions.

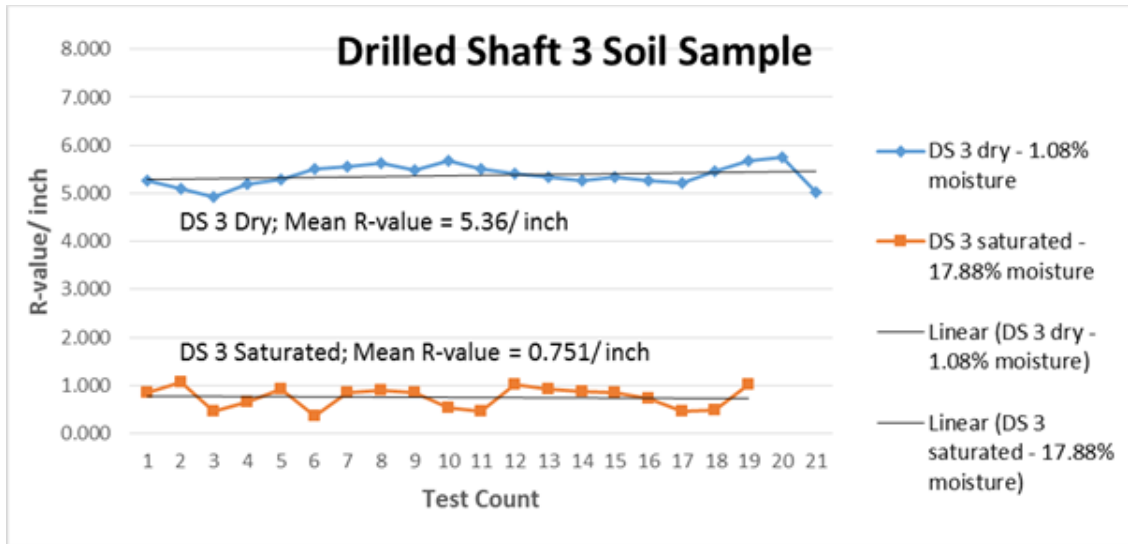


Figure 4-7. Measured R-Values of DS3 soil sample under different moisture conditions.

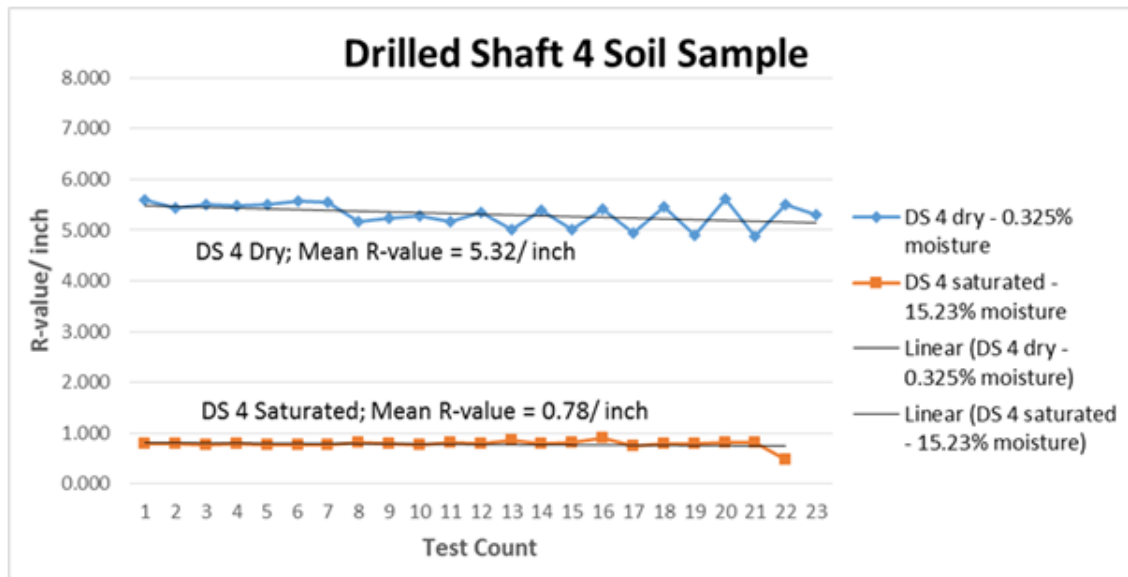


Figure 4-8. Measured R-Values of DS4 soil sample under different moisture conditions.

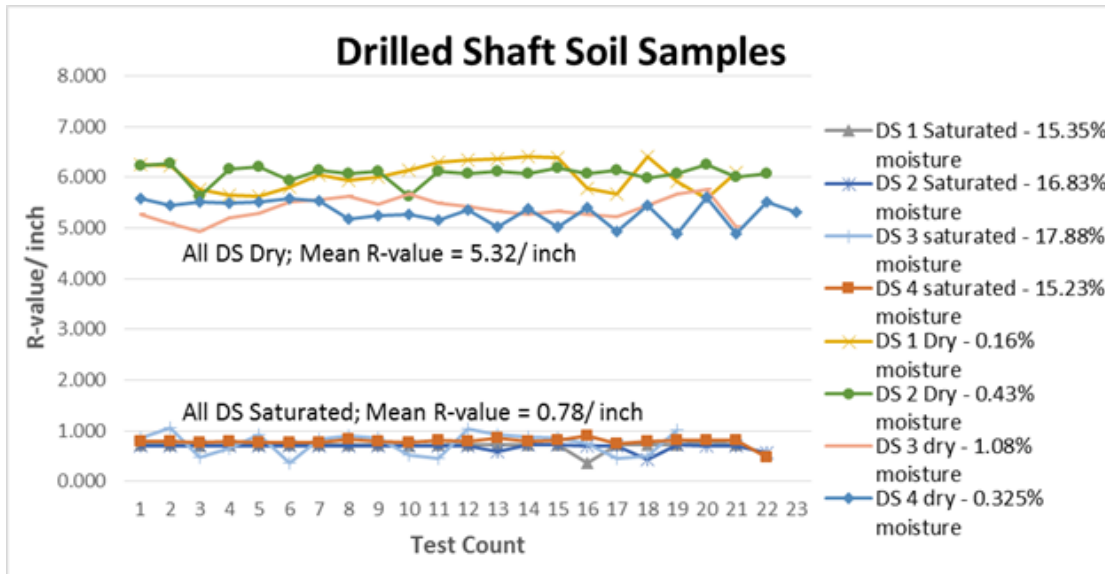


Figure 4-9. Measured R-Values of all DS soil samples under different moisture conditions.

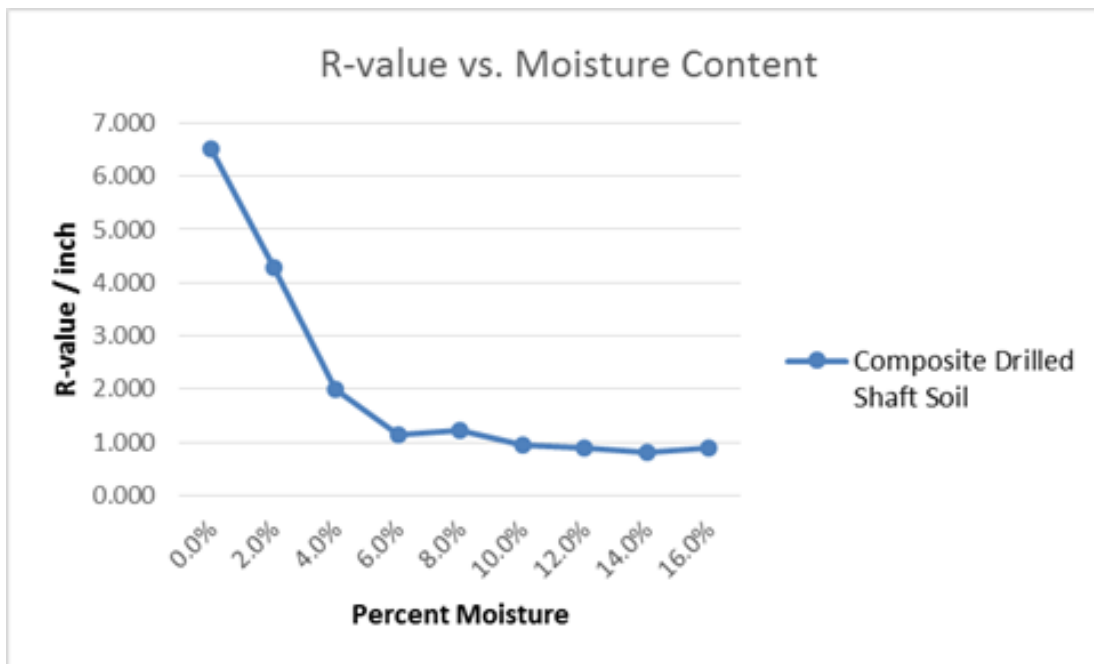


Figure 4-10. R-Values of composite DS soil sample under different moisture conditions.

The average measured R-values of the eight soil samples under different moisture and temperature conditions are summarized in Table 4-2. It can be seen that moisture content is the main factor affecting the insulation property of soils. The R-value of soil decreases sharply as the moisture content increases. Variation in temperature has minimal effects on the R-value of soil.

Table 4-2. R-values of soil samples at different moisture and temperature conditions.

Soil Samples	#1	#2	#3	#4	#5	#6	#7	#8					
Temp. (°F)	75.0	95.0	75.0	95.0	75.0	95.0	75.0	95.0	75.0	95.0	75.0	75.0	
Moisture %	< 1.0 %	2.52*	2.78	7.52	7.89	8.41	8.19	8.23	7.44	6.04	6.07	5.36	5.32
	5.0 %					9.52	8.06						
	14-17 %	0.96	0.90					0.80	0.78	0.70	0.68	0.75	0.78
	24.9 %							0.73					
	57.9 %											1.17	
	64.6 %			1.53	0.91								

(Note: * in units of R-value/inch.)

4.2.3 R-value of Muck as Affected by Temperature

Testing on muck was limited to the moist condition. When the muck was received, the moisture content was 243.1 % as determined by drying in a 230 °F oven. The volume of water lost generated a sample too small for adequate dry-condition testing to be conducted. It was able to be determined, however, that in a saturated state at low temperatures, the R-value/inch is higher (6.3 average) than that when the temperature is high (4.8 average). The results of tests on muck at two different temperatures are shown in Figure 4-11.

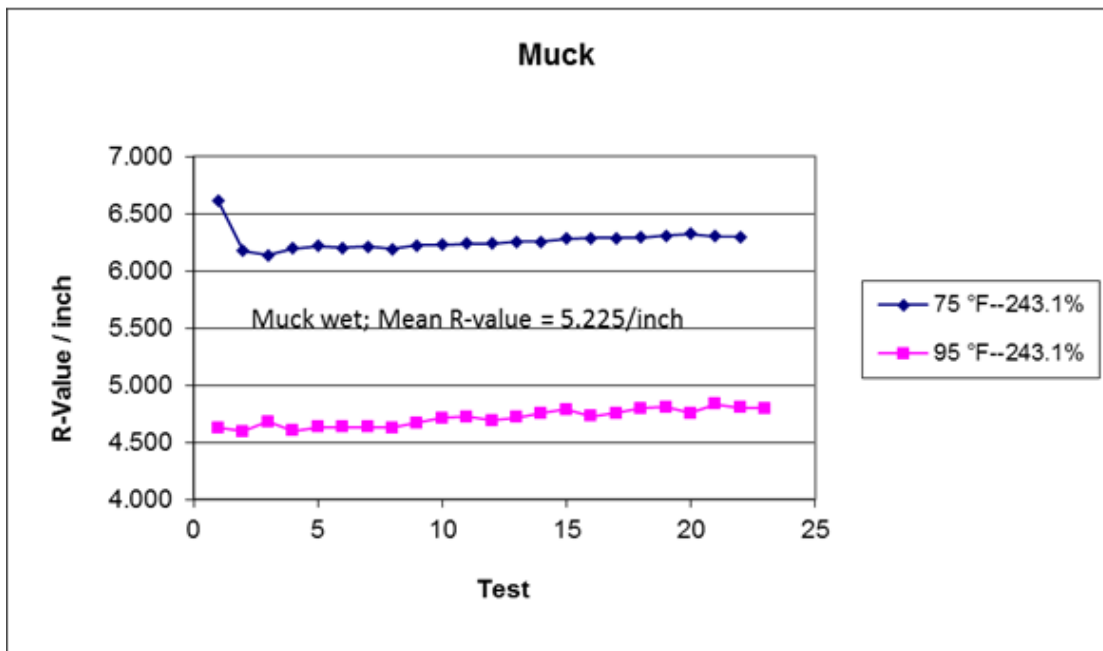


Figure 4-11. Measured R-Values of muck under different temperature conditions.

4.2.4 R-value of Lime Rock as Affected by Moisture and Temperature

Figure 4-12 shows the plots of insulation values of lime rock at different moisture and temperature conditions. At the low moisture contents of 0 and 3.3 % and at both testing temperatures, the insulation values of the lime rock do not vary much and are from 5.5 to 6.5 R-value/inch. At the high moisture content of 23.3 %, the insulation value of the lime rock drops to approximately 1.0 R-value/inch. Variation in temperature has minimal effects on the R-value of lime rock.

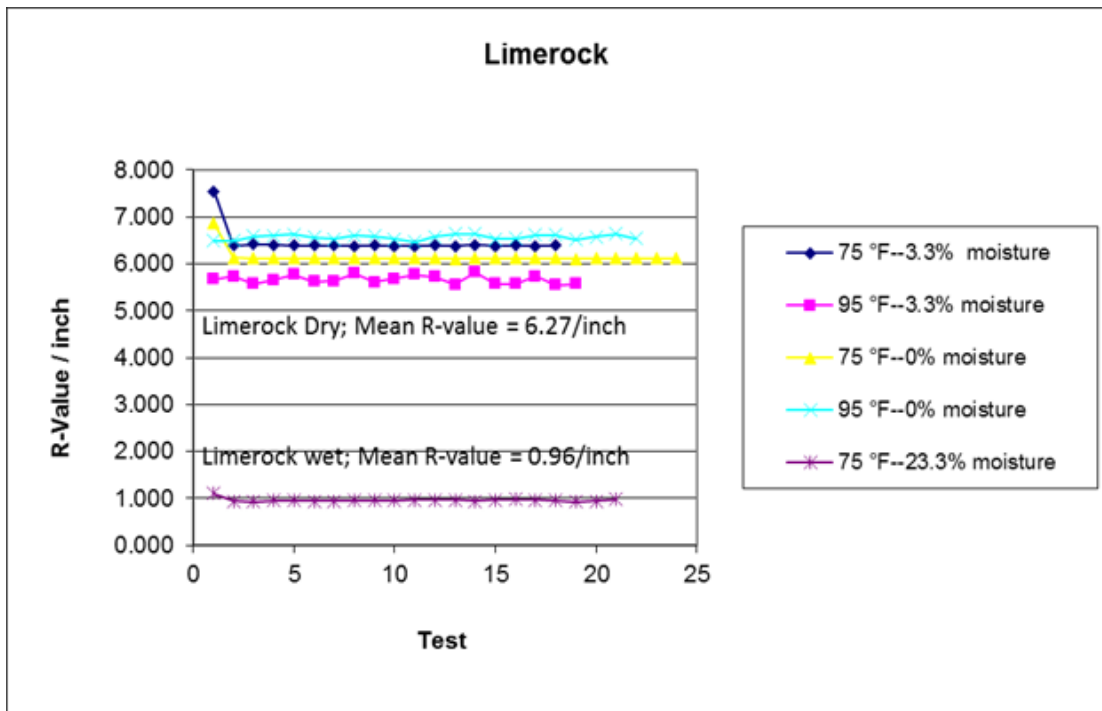


Figure 4-12. Measured R-Values of lime rock under different moisture and temperature conditions.

4.2.5 R-value of Concrete as Affected by Temperature

Figure 4-13 shows the plots of insulation values of the three concretes tested at different temperatures conditions. Variation in temperature appears to have little effect on the R-value of the different concretes, while the aggregate type appears to have more significant effects. The concrete samples made with granite have an average insulation value of 0.94 R-value/inch, while the concrete samples made with limestone have an average insulation value of 0.82 R-value/inch.

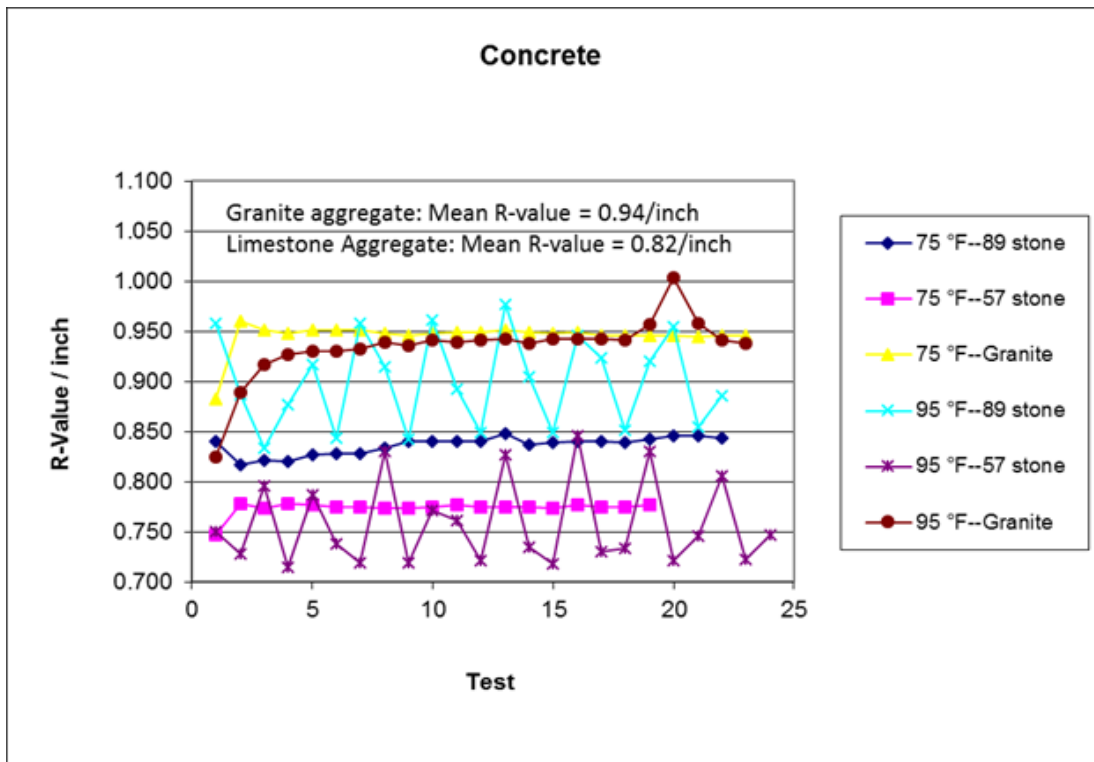


Figure 4-13. Measured R-values of concrete under different temperatures.

CHAPTER 5
EVALUATION OF DRILLED SHAFTS FOR CONSIDERATION AS MASS CONCRETE
STRUCTURES

5.1 Introduction

5.1.1 Background and Research Needs

Thermal cracking in mass concrete has long concerned researchers and engineers, in particular its effects on the durability, serviceability, and aesthetics of concrete (ACI 207.1R; ACI 207.2R; Tia et al., 2010). When Portland cement is mixed with water, heat is generated due to the exothermic chemical reaction that occurs during the early hardening phase. During this early hardening stage, the temperatures within a concrete structure, particularly between its core and its surface, will vary due to different rates of heat dissipation. This usually results in volume change and the inducement of tensile stress on the surface which in turn may cause thermal cracking (Mehta and Monteiro, 2014).

There is a need for further research into the relationship between the volume-to-surface area ratio of a concrete drilled shaft and its thermal profile. Currently, the Florida Department of Transportation (FDOT) Structures Design Guidelines designates a concrete drilled shaft as mass concrete based on its diameter. Recently concern has been expressed on whether the current minimum diameter of 6 feet is adequately accounting for the possible occurrence of thermal cracking. A literature review has revealed that not many studies have been conducted on the issue of thermal cracking in drilled shafts. This chapter presents the findings of the relationship between the diameter of a drilled shaft and its potential for thermal cracking using finite element modeling.

An additional factor that should be considered when assessing the vulnerability of a drilled shaft to thermal cracking is the moisture content of the soil into which the shaft is being placed. In a previous study (Tia et al., 2013), it was found that foundation footings constructed

in saturated sand, without adequate protective insulation between the soil and its outside surfaces, had the highest probability of experiencing thermal cracking. The findings of the study on foundation footings raises questions of thermal cracking in drilled shafts because all surfaces are surrounded by soil, and in most cases in Florida, by saturated soil.

5.1.2 Current Standards and Specifications

To mitigate against thermal cracking in concrete drilled shafts, the FDOT defines mass concrete in drilled shafts as: “all drilled shafts with diameters greater than 6 feet shall be designated as mass concrete” (FDOT Structures Design Guidelines, 2016, page 1-15.). Any drilled shaft with a diameter greater than 6 feet would therefore require the submission of a technical special methods report.

To prevent mass concrete thermal cracking, the American Concrete Institute (ACI) recommends a maximum concrete temperature of 70.0 °C (158.0 °F) and a maximum internal concrete temperature difference of 19.4 °C (35.0 °F) in mass concrete (ACI 301, 2010). This is similar to the FDOT Standard Specification for Road and Bridge Construction which requires the maximum concrete temperature to be no higher than 82.2 °C (180.0 °F) and the maximum concrete temperature difference no higher than 19.4 °C (35.0 °F, FDOT, 2016).

5.1.3 Objectives

The specific objectives of this research task were to:

1. Evaluate the FDOT’s definition of a mass concrete drilled shaft based on the shaft’s diameter.
2. Analyze drilled shafts constructed in the field for calibration of the Finite Element (FE) model.
3. Develop a viable solution that will aid in the reduction of thermal cracking in mass concrete drilled shafts.

5.2 Description of Finite Element Model Used for Thermal Analysis

5.2.1 Overview of Finite Element Model

The modeling of the early age thermal behavior of concrete in this study was conducted with the aid of the commercially available TNO DIANA 9.4.4 (2011) software package. This software package was selected because it offers a wide range of material models for the analysis of non-linear concrete material behavior, including the behavior of early age concrete. Most importantly, DIANA can make the assessment of the temperature development due to cement hydration and determine the temperature differentials in modeled structures. The DIANA's main modeling features utilized in this study were the equivalent age calculation and the temperature- and time-dependent material properties.

The finite element analysis for all cases utilized DIANA's 'Heat-flow Staggered Axisymmetric' feature, which performs a thermal analysis on a given model. Researchers were interested only in the effects on the transfer of the thermal energy generated by the concrete. Although reinforcing steel conducts heat rapidly, in mass concrete drilled shafts, the volume of reinforcement is small relative to the volume of concrete in the shaft; therefore the high conductivity of the reinforcement will not significantly affect the thermal behavior of the concrete. We could therefore simplify the drill shaft model by omitting the reinforcing steel.

5.2.2 Element Selection

For this analysis, a four-node Q4AHT isoparametric axisymmetric solid ring element was selected for the thermal analysis of the drilled shaft and soil mass. In addition, a two-node B2AHT isoparametric axisymmetric boundary element was used to model the thermal flow transfer. The Q4AHT solid ring element and the B2AHT boundary element are shown in Figure 5-1.

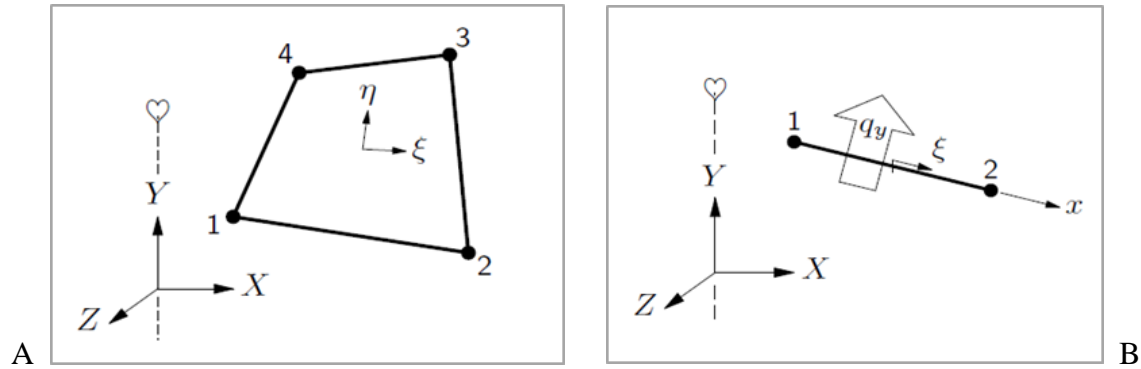


Figure 5-1. Thermal analysis modeling elements. A) Q4AHT isoparametric and B) B2AHT isoparametric.

Elements Q4AHT are effective in simulating the phenomenon of convection-diffusion, and are especially useful for the analysis of heat transfer problems. The elements utilize linear interpolation and Gauss integration. For the model described in this report, both the conductivity and heat capacity were modeled as constant. The boundary convection was modeled using B2AHT element, which is specially used to describe boundaries in axial symmetry thermal analyses. The two nodes in this element were modeled to coincide with the corner nodes of the surface of the line elements they lie on.

5.2.3 Parametric Input Values

In order to analyze the thermal behavior via the FE models, it was necessary to input values for (1) the heat produced during the hydration of concrete, (2) the thermal properties of concrete and, (3) the environmental conditions such as ambient temperature and soil moisture content.

For this finite element analysis, the preprocessing method was selected, and the input data, adiabatic temperature rise of the concrete, are obtained by conversion using the concrete hydration heat produced and measured during isothermal calorimetry testing.

The concrete mixtures selected for this mass concrete drilled shaft study were control mixes of (1) Trial 1 – 30 % Type 1 Portland cement plus 70 % slag and (2) Trial 2 – Type 1 Portland cement with no supplementary cementitious material. Three additional Florida concrete mixtures typically used in drilled shaft concrete construction which were measured during a previous project (Tia et al., 2013) were also used. Table 5-1 shows the composition and proportioning of the mixtures used in the isothermal calorimetry testing.

Table 5-1. Paste fractions tested for each mixture.

Mixture	Cement (g)	Slag (g)	Fly Ash (g)	Metakaolin (g)	Water (g)	Admix. (g)	W/C Ratio	Total (g)
Trial 1	1.2085	2.8198	-	-	1.6516	0.014	0.41	5.6939
Trial 2	4.0837	-	-	-	1.6743	0.014	0.41	5.7720
FB1	3.230	-	1.739	-	1.789	-	0.36	6.759
TB1	2.686	-	1.788	0.633	1.737	-	0.34	6.844
HVFA1	2.804	-	2.804	-	1.683	-	0.30	7.291

As stated previously, the heat energy generated during the isothermal calorimetry tests is converted to the adiabatic temperature rise of the concrete mixture as expressed by Equation 5-1. The conversion is graphically depicted in Figure 5-2(A).

$$\Delta Q = m \cdot C_p \cdot \Delta T \quad (5-1)$$

Where

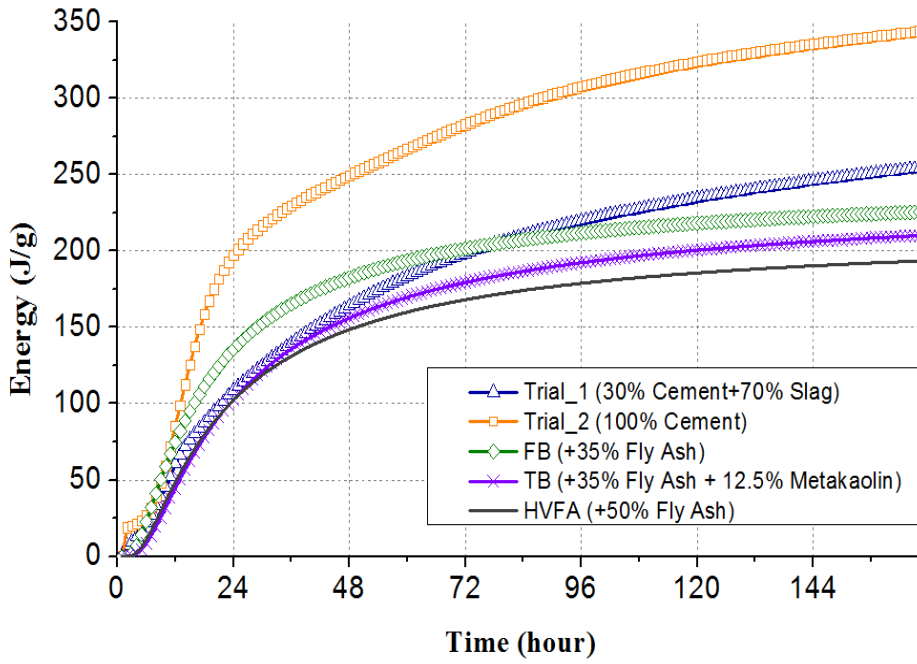
ΔQ is energy rise (J),

m is mass of concrete (g),

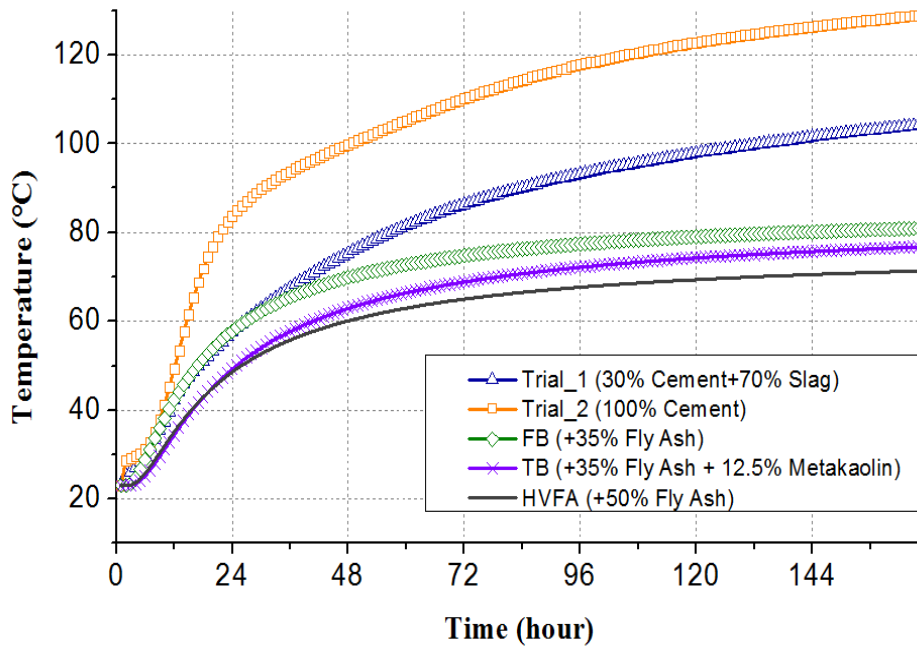
C_p is specific heat capacity (J/g-°C),

ΔT is change in temperature or temperature rise (°C).

Figure 5-2(B) shows the temperature rise with respect to equivalent age for each mixtures.



A



B

Figure 5-2. Input data obtained from isothermal calorimetry testing. A) energy rise of each mixture and B) adiabatic temperature of each mixture.

To accurately model thermal behavior of concrete, input values for thermal conductivity and heat capacity were required. The concrete's heat capacity was calculated by multiplying its specific heat by its total mass. The thermal conductivity is directly related to the type of aggregate used and the density of the concrete. ACI 207.2R recommends that for concrete with limestone aggregate, the value for thermal conductivity ranges from 2.6 to 3.3 J/m·s·°C. However, these recommended values are for concrete consisting of 100% Portland cement and do not take into account the effect admixtures and supplementary cementitious materials have on concrete density. Therefore, in the previous research conducted by Tia et al. (2013), the thermal conductivity was experimentally measured and found to be approximately 2.2 J/m·s·°C. The values of thermal properties used in drilled shaft models are summarized in Table 5-2.

Table 5-2. Thermal properties of concrete used in FE models.

Mixture	Specific Heat (J/g·°C)	Heat Capacity (J/m ³ ·°C)	Thermal Conductivity (J/m·s·°C)	Density (g/m ³)
Trial 1	1.152	2,453,380	2.20	2,130,444
Trial 2	1.145	2,549,932	2.20	2,226,554
FB	1.045	2,375,706	2.20	2,273,529
TB	1.038	2,321,351	2.20	2,236,443
HVFA	1.000	2,266,665	2.20	2,267,079

The boundary load conditions imposed for thermal analysis consisted of (1) an initial temperature of concrete, (2) a fixed environmental temperature of side and bottom soil, and (3) an external ambient temperature. An initial temperature of 26.0 °C (78.8 °F) was set for the models. An initial and constant soil temperature of 23.0 °C (73.4 °F) was also set based on the assumption that the soil around the drilled would maintain a stable temperature. The external temperature was applied to all the exposed surfaces of the model, taking into consideration that these surfaces are also affected by air convection, and are exposed to the environment. For this research, ambient temperature was set at a constant 20.0 °C (68.0 °F).

5.2.4 Model Geometry

The finite element models developed in this study consist of a drilled shaft with surrounding soil. The soil surrounding the shafts were modeled as being 12 feet thick from the outer surface of the shafts, in order to fully dissipate heat from the drilled shaft. The shaft structure was modeled as having a total length of 7 feet with 6 feet drilled into soil and the upper one foot being above the ground surface. The shaft had a diameter of 6 feet to comply with the Florida Department of Transportation's specifications which state that drilled shafts with a diameter of 6 feet and above must be designated as mass concrete and comply with the special technical provisions. Due to the cylindrical shape of a drilled shaft, the accuracy of the axial symmetry analysis results would be the same with three-dimensional analysis. Since axial symmetry analysis is more time-efficient, the models were simplified into two-dimensional geometry as illustrated in Figure 5-3.

dimensions to determine the diameter at which the allowable maximum temperature of 82.2 °C (180.0 °F), and the maximum temperature difference of 19.4 °C (35.0 °F) will be exceeded. The results of this investigation may provide the verifying definition for the size of drilled shaft that should be considered as mass concrete.

For this parametric study, ten (10) FE models of drilled shafts with the different volume-to-surface area ratio were constructed. The ten FE models were analyzed with two geometry components; diameters of 6 feet, 8 feet, 10 feet, and 12 feet, and depths of 7 feet and 13 feet respectively. The diameter and height of drilled shafts for all cases studied are given in Tables 5-3. Except for the variations in drilled shaft diameter and depth (volume-to-surface ratio), all thermal and boundary conditions of the FE models are fixed and remain the same. Two concrete mix designs were used – Trial 1 (30 % Type 1 Portland cement with 70 % slag) and Trial 2 (100 % Type 1 Portland cement).

Table 5-3. Geometry of the drilled shafts studied.

Trial	1	2	3	4	5	6	7	8	9	10
Shaft diameter (ft.)	4	4	6	6	8	8	10	10	12	12
Drilled depth (ft.)	6	12	6	12	6	12	6	12	6	12
Total height (ft.)	7	13	7	13	7	13	7	13	7	13
V/A area ratio (ft.)	0.78	0.87	1.05	1.22	1.27	1.53	1.46	1.81	1.62	2.05

Two moisture levels were applied to the soil surrounding the drilled shaft models, namely dry (Thermal conductivity: 0.27 J/s·m·°C, Heat capacity: 1.212 x 10⁶ J/m³·°C) and wet (Thermal conductivity: 2.0 J/s·m·°C, Heat capacity: 1.560 x 10⁶ J/m³·°C) (Tia et al., 2013).

5.3.2 Concretes of Different Cementitious Compositions

The heat of hydration is one of the most important parametric values that determine the thermal behavior of a concrete mix design (Riding et al., 2012). This parametric study was conducted using the adiabatic temperature rise data obtained from concrete mix designs typically used for construction in Florida. To develop the FE model, concrete mix designs Trial 1 (30 % Portland cement plus 70 % slag) and Trial 2 (100 % Portland cement) were used as control mixes to establish base lines for the analysis. In addition to the control mixes, three other concrete mix designs typical for drilled shaft construction in Florida were used for this parametric study. The additional mixtures were:

- Fly Ash Blend (FB) – FDOT Mix: 03-1870.
- Ternary Blend(TB) – FDOT Mix: 01-1149.
- High-Volume Fly Ash (HVFA) – FDOT Mix: 05-1526.

Table 5-4 shows the concrete properties for the mix designs selected for this parametric analysis. The mixes selected represent actual FDOT mix designs used in mass concrete applications and they represent a suitable range of water-to-cementitious content (W/C) ratio for analysis. As previously stated, in order to get the adiabatic temperature rise input data for the FE model, the isothermal calorimetry test was conducted on representative cementitious paste samples to measure their respective heats of hydration. The first law of thermodynamics is then used to convert the normalized heat of hydration values into temperature rise values that can be used by DIANA as inputs for thermal analysis.

Table 5-4. Concrete mixtures used in parametric study.

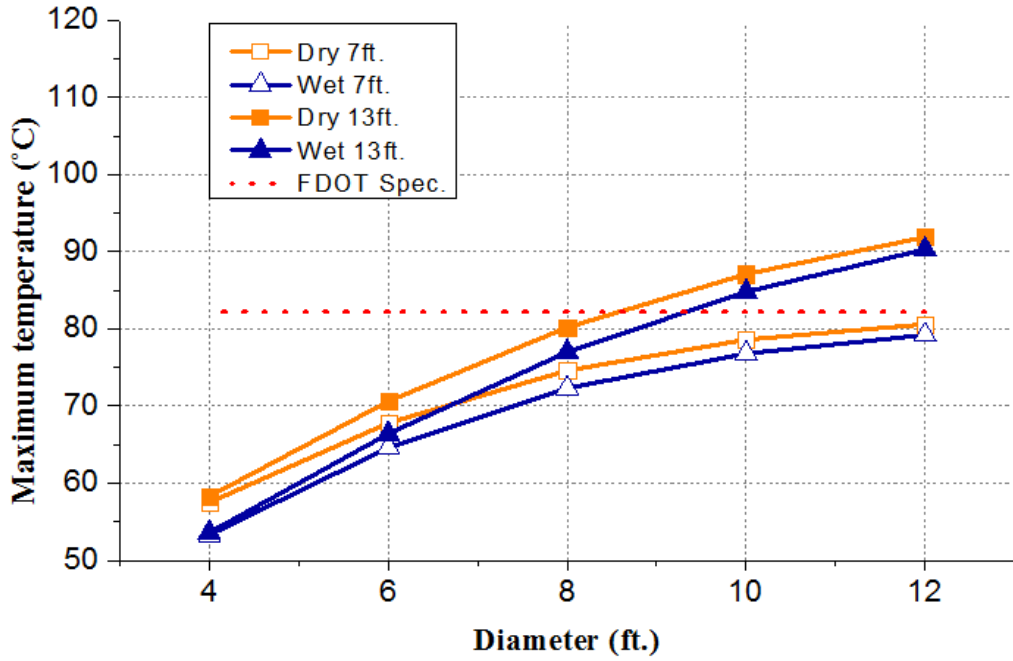
Mixtures	W/C Ratio	Cement (lb./yd ³)	Fly Ash (lb./yd ³)	Slag (lb./yd ³)	Metakaolin (lb./yd ³)	CA (lb./yd ³)	FA (lb./yd ³)
Trial 1	0.41	282	-	658	-	1,200	1,072
Trial 2	0.41	940	-	-	-	1,200	1,238
FB	0.36	489	263	-	-	1,702	1,082
TB	0.34	396	263	-	93	1,660	1,125
HVFA	0.30	365	365	-	-	1,770	1,075

5.4 Results of Thermal Analysis of Drilled shaft

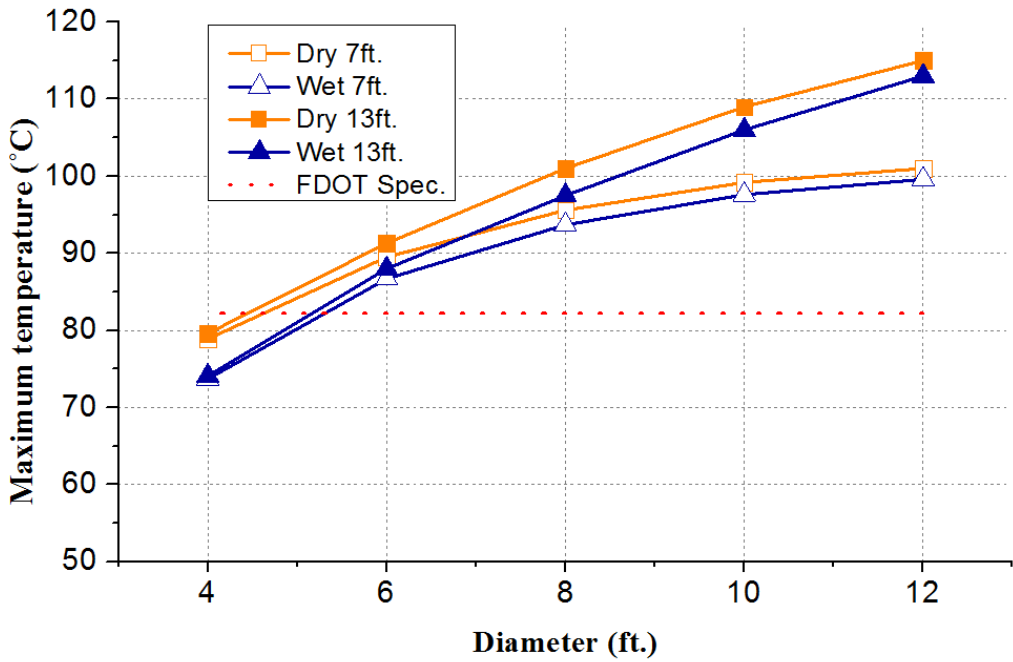
5.4.1 Effects of Length and Diameter of Solid Drilled Shafts

Figure 5-4 presents the maximum temperatures for the ten trials tested with diameters of 4, 6, 8, 10, and 12 feet respectively, each modeled twice with depths of 7 and 13 feet. Using the control concrete mixtures Trial 1 and Trial 2, the temperatures calculated by DIANA showed that increasing the volume of the drilled shaft by holding the shaft depth constant but increasing the shaft diameter resulted in an increase in the maximum concrete temperature. As the concrete volume increases, so too does the generation of heat due to the concrete hydration process. High levels of heat created large temperature differentials that can undermine the drilled shaft's integrity.

Figure 5-5 presents the temperature differential development for the ten drilled shaft models analyzed with V/A ratios of 0.78, 1.05, 1.27, 1.46, and 1.62 feet (depth of 7 feet), and 0.87, 1.22, 1.53, 1.81, and 2.05 feet with (depth of 13 feet). The lowest temperature differential values, calculated by DIANA, using the control concrete mixtures Trial 1 and Trial 2, corresponded with the drilled shaft with the smallest diameter of 4 feet. The highest temperature difference calculated by DIANA corresponded to the drilled shaft with the largest diameter of 12 feet.

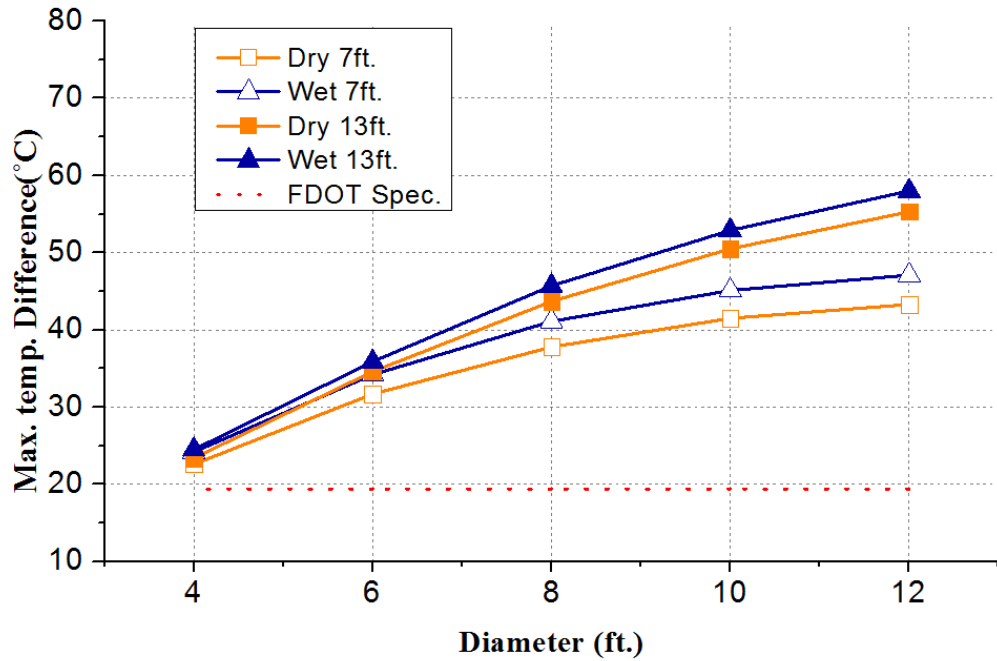


A

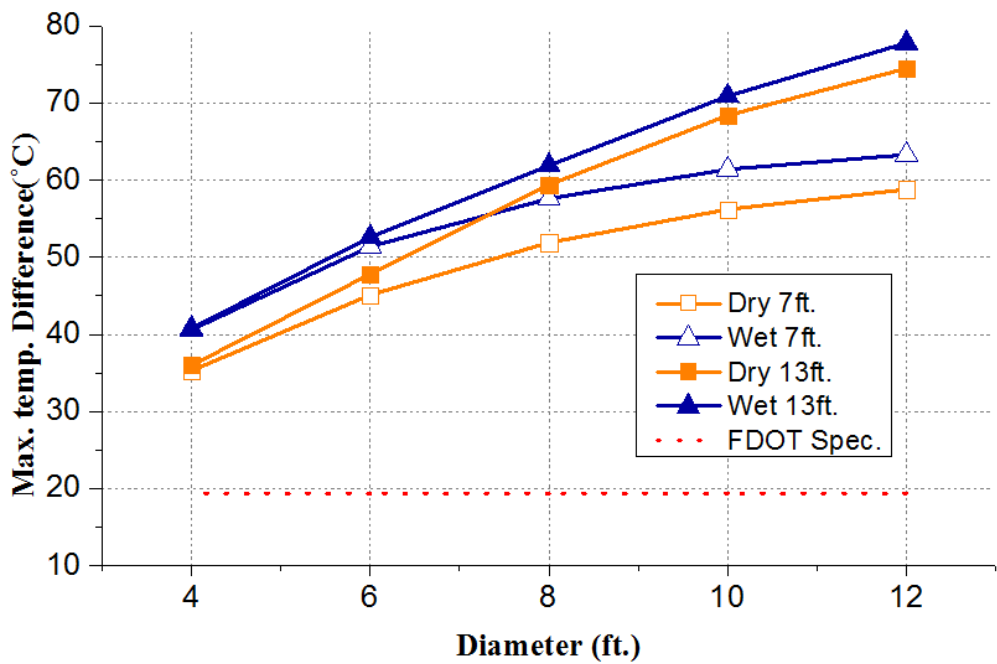


B

Figure 5-4. Maximum temperature versus shaft diameter. A) concrete mixture of Trial 1 and B) concrete mixture of Trial 2.



A



B

Figure 5-5. Maximum temperature differential versus shaft diameters. A) concrete mixture of Trial 1 and B) concrete mixture of Trial 2.

Based on the DIANA thermal analysis results, the maximum temperature differential values calculated for all trials exceeded the 19.4 °C (35.0 °F) allowable temperature difference limit set by the FDOT. A result of particular interest was that although the FDOT Structures Design Guide (2016) states that a drilled shaft is to be considered mass concrete when its diameter exceeds 6 feet, the 4 feet diameter drilled shafts modeled with mix designs Trial 1 and Trial 2 experienced maximum temperature differentials higher than 19.4 °C (35.0 °F), as shown in Figure 5-5.

Also observed from the analyses was that increasing the depths of the drilled shafts from 7 to 13 feet did not significantly change the temperature profile of the drilled shaft up to a diameter of 6 feet. This finding can be attributed to the fact that the volume-to-surface ratio of the drilled shafts significantly increased when the diameter surpassed a value of six feet.

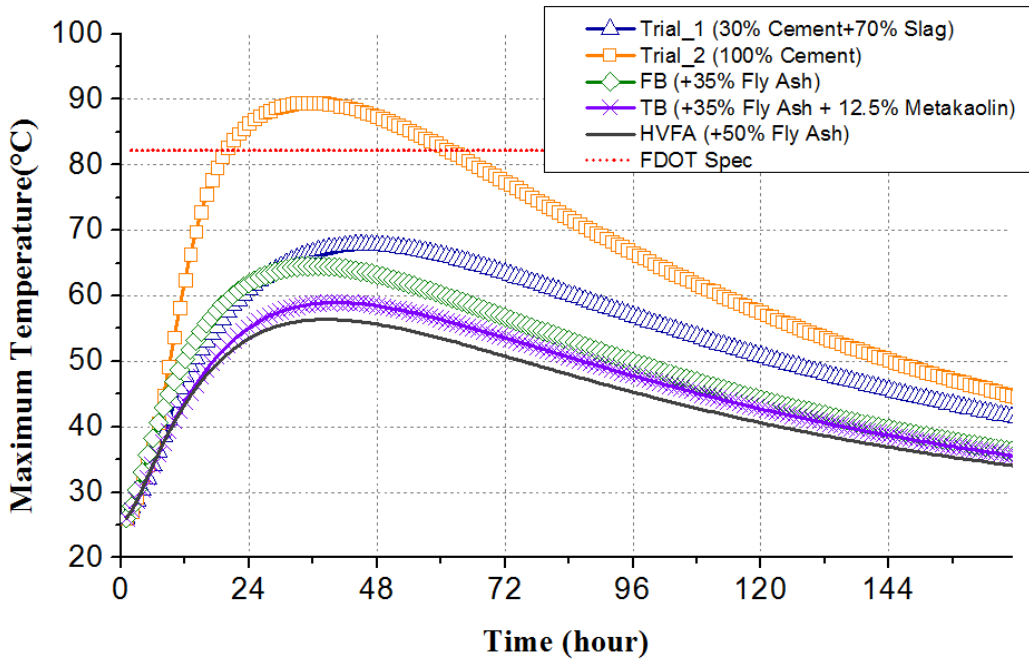
5.4.2 Effects of Cementitious Composition of Concrete

Figure 5-6 presents the temperature development results of the five concrete mix designs tested: Trial 1, Trial 2, FB, TB, and HVFA. As shown, the highest temperature was recorded in the drilled shaft using Trial 2 (Pure Portland cement Type 1). This was attributed to the fact that the control mixture of Trial 2 was composed of 100% Portland cement and produced the highest heat of hydration – the final energy indicated the value of 344.5 J/g. The lowest temperatures were calculated when mixtures TB and HVFA were used. These mixtures had the lowest total cementitious content and contained pozzolanic supplementary cementitious materials. As a result, the heat of hydration and subsequent temperature rise were lower. An interesting result was seen in that mixture FB showed a relatively high temperature rise even though the total generated energy was within the same range as the other mixtures in Table 5-5. Additionally, the highest temperatures recorded occurred during the first 24 hours after placement. This was attributed to mixture FB having a higher rate of early age hydration than the other mixtures except for mixture Trial 1 with 100 % Portland cement. Controlling the rate of heat dissipation is difficult since insulating all external surfaces of drilled shafts is not possible, therefore limiting the amount of early age heat is the most effective method that can be used to manage the thermal profile in drilled shafts.

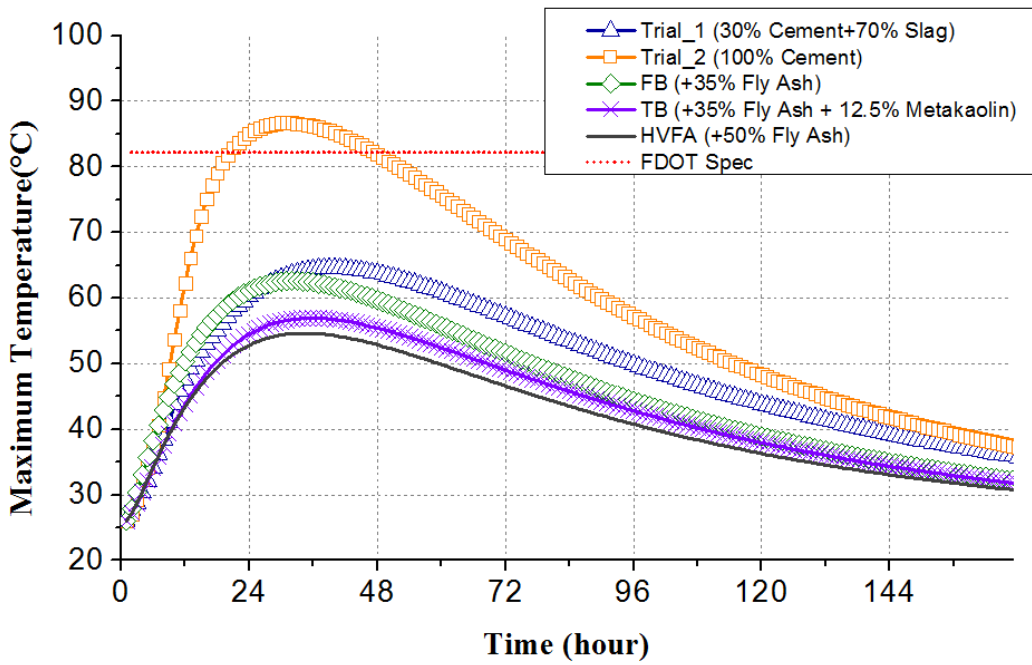
Table 5-5. Heat energy of cementitious mixture obtained from isothermal calorimetry.

Time after Placement	Trial 1 (J/g)	Trial 2 (J/g)	FB (J/g)	TB (J/g)	HVFA (J/g)
24 (hours)	108.6	197.2	135.5	102.7	102.3
48 (hours)	163.9	249.5	182.5	156.0	148.4
72 (hours)	198.2	282.9	201.5	179.3	168.0
168 (hours)	254.9	344.5	225.6	210.3	193.6

Figure 5-7 presents the temperature differential results for the five concrete mix designs tested: Trial 1, Trial 2, FB, TB and HVFA. These represented the highest and the lowest temperature values, as calculated by the DIANA software. Results of FE models showed that mixture FB produced a maximum temperature differential value of 32.2 °C (58.0 °F), mixture TB produced a maximum temperature differential value of 27.6 °C (49.7 °F), and mixture HVFA produced a maximum temperature differential value of 25.7 °C (46.3 °F). These mixtures were expected to be the coolest and therefore the best for maintaining relatively low temperature differentials. However, the maximum temperature differential calculated for each of these mixtures exceeded 19.4 °C (35.0 °F), and therefore would not conform to the FDOT mass concrete specifications.

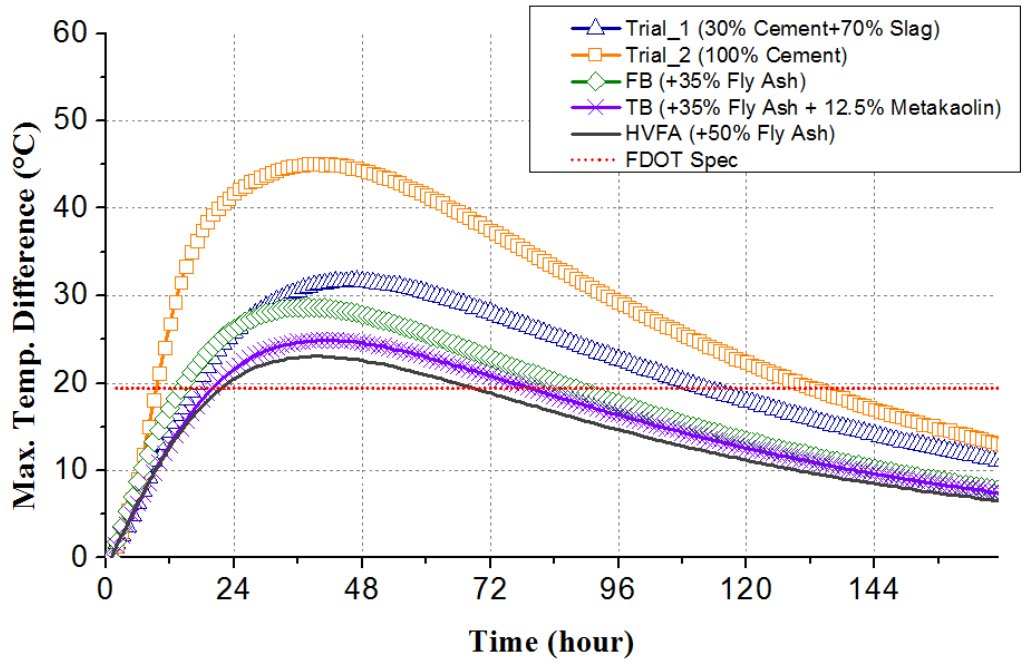


A

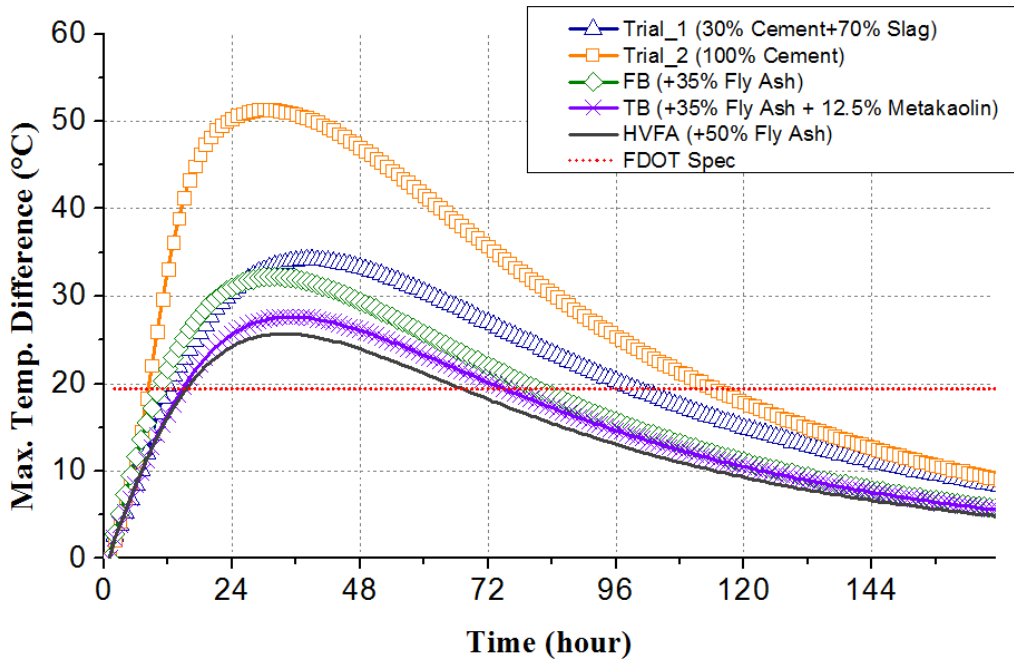


B

Figure 5-6. Maximum temperature versus curing time. A) fully dry soil condition and B) wet soil condition.



A



B

Figure 5-7. Maximum temperature differential versus curing time. A) fully dry soil condition and B) wet soil condition.

All DIANA results showed the maximum temperature differential values calculated for all mixtures exceeded the allowable temperature differential limits set by FDOT. The main reason for this is that while the temperature of the concrete at the shaft's core will rise relatively in sync with its adiabatic condition, given that the shaft surfaces are not insulated, heat dissipation from near surface concrete will occur at a fast rate. Therefore, even though the maximum concrete temperature calculated in any of the mixtures was only 54.6 °C (130.3 °F), special measures for the mitigation of concrete temperatures would need to be undertaken to ensure that the maximum concrete temperature difference does not exceed 19.4 °C (35.0 °F).

5.4.3 Effect of Using Centroid Void in Drilled Shafts

Similar thermal analysis was performed to evaluate the possible effects of inclusion of a centroid void in the construction of the drilled shaft on its temperature development. Table 5-6 shows the dimensions of the various drilled shafts with centroid void which were analyzed. The reference drilled shaft was a solid shaft with a radius of 3 feet and a cross sectional area of 28.26 ft². The other drilled shafts with centroid void which were analyzed all had the same cross-sectional area, but different radius and thickness. Two concrete mixes Trial 1 and Trial 2, which were used in the previous analysis as presented in Section 4.2 were used. The same soil and environmental conditions which were used in the previous analysis were also used. Each shaft analyzed was 7 feet long with 6 feet of it under soil.

Table 5-6. Dimensions of drilled shafts with centroid void analyzed.


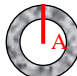
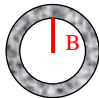
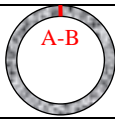
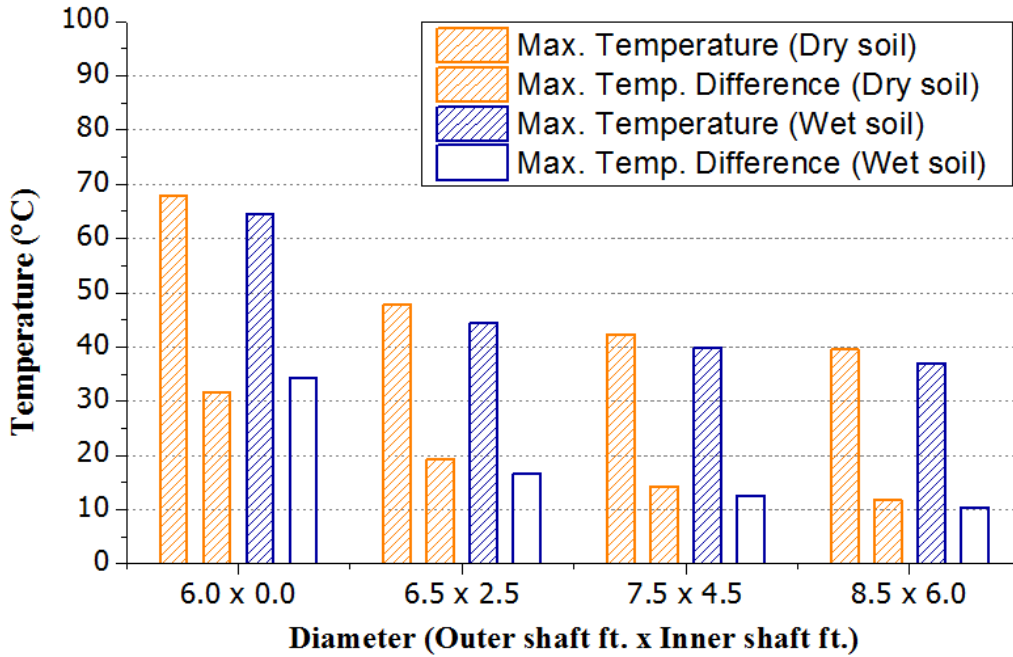
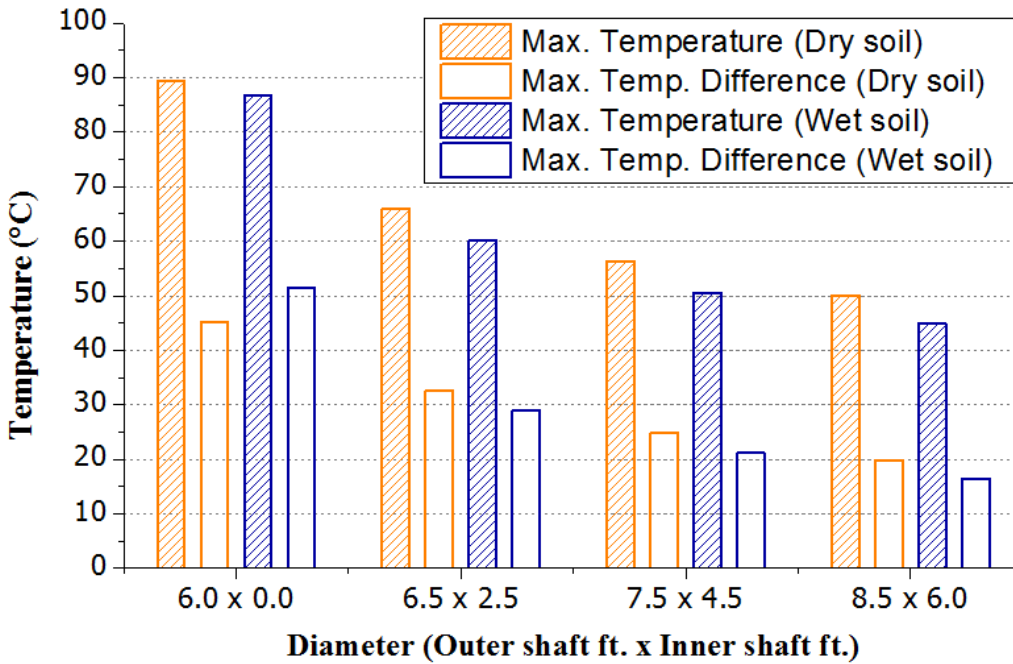
Cross-section shape of Drilled shafts				
Outer shaft radius (ft.)	3.00	4.00	5.00	6.00
Inner void shaft radius (ft.)	-	2.65	4.00	5.20
A-B) Thickness of cross-section (ft.)	3.00	1.35	1.00	0.80
Cross-section area (Square ft.)	28.26	28.26	28.26	28.26
Volume-to-surface area ratio (ft.)	1.05	0.57	0.44	0.36

Figure 5-8 presents the results of the thermal analysis in terms maximum temperature and maximum temperature differentials in the various drilled shafts with centroid void using concrete mixes Trial 1 and Trial 2, and under both dry and wet soil conditions. It can be seen that the use of centroid void has resulted in a significant decrease in both the maximum temperature and the maximum temperature differentials in the shaft for both concrete mixtures Trial 1 and Trial 2. The maximum temperature decreased due to two main reasons. The first reason is that the wide surface area of the exposed concrete in the void increased the “concrete core’s” ability to dissipate the heat easily, therefore preventing the maximum concrete temperature from attaining the values seen in the solid drilled shaft (Trial 1 – 68.6 °C and Trial 2 – 86.0 °C). This finding is in accordance with the previous findings on the effects of different volume-to-surface area ratios in mass concrete foundation footings (Tia et al., 2013).

Secondly, due to the centroid void, the location of the maximum concrete temperature shifted towards the outer shaft as presented in Table 5-6 where it is seen that the thickness of the void shaft’s cross section decreased to 1.5 feet from the 6 feet calculated for the solid drilled shaft. Therefore, it can be said that geometric redesign converted the structure from being a mass concrete structure to being a normal concrete structure, for which thermal cracking is not a concern.



A



B

Figure 5-8. Maximum temperature and maximum temperature difference on centroid void drilled shafts. A) Trial 1 mixture and B) Trial 2 mixture.

5.5 Summary of Findings

FE models were developed to analyze the thermal behavior of drilled shaft under two different soil conditions, dry and wet. The model developed was used to determine the effect the volume-to-surface area ratio of a drilled shaft, as well as the cementitious composition of the concrete mixture has on its thermal behavior. The main findings are summarized as follows:

1. All concrete mixtures used in this study model the thermal behavior of a drilled shaft with a diameter of over four feet produced the maximum temperature differentials that exceeded the limit set by the FDOT.
2. For drilled shafts with diameters less than six feet, the maximum concrete temperature, and the maximum concrete temperature differential were not significantly affected by the depth of the drilled shaft.
3. The use of pozzolanic material as replacement for Portland cement (Trial 1, TB and HVFA) reduced the maximum temperature and maximum temperature difference in the drilled shaft.
4. Mixture FB produced a relatively rapid early age hydration reaction which resulted in a higher temperature profile compared to other mixtures that also contained pozzolanic material.
5. All concrete mix designs produced maximum temperature differentials which exceeded the 19.4 °C (35.0 °F) limit set by the FDOT.
6. In binary mixtures, the application of centroid shaft void caused a significant decrease in both the maximum temperature and the maximum temperature difference.
7. A shaft with centroid void is a viable alternative shaft design for controlling not only the maximum temperature but also the maximum temperature difference of mass concrete drilled shafts.

CHAPTER 6 FIELD EVALUATION OF DRILLED SHAFT

6.1 Introduction

A field study was conducted to evaluate the actual temperature development in four test drilled shafts and to compare the measured temperatures with the analytical values as computed by the DIANA finite element model for thermal analysis as presented in Chapter 5. The results from this field evaluation served to validate the analytical model used.

A total of four concrete drilled shafts, which were 6 feet in diameter and 7 feet in length, were placed in a natural Florida soil (with an AASHTO classification of A-3) to a depth of 6 feet. Two of the drilled shafts (Shafts 1 & 2) were intended to be placed in a wet soil environment, while the other two shafts (Shafts 3 & 4) were intended to be placed in a dry soil environment. Among the two drilled shafts placed in the wet soil, one (Shaft 1) used a slag-cement concrete mix with a relatively low heat of hydration, and the other (Shaft 2) used a pure Portland cement concrete mix with a high heat of hydration. Similarly, among the two drilled shafts placed in the dry soil, one (Shaft 3) used a slag-cement concrete mix with a relatively low heat of hydration, and the other (Shaft 4) used a pure Portland cement concrete mix with a high heat of hydration.

Temperature data loggers were installed at various locations in the concrete drilled shafts and in the surrounding soil to monitor the temperature development and distribution during the early age of the concrete. Temperatures at the various sensor locations were monitored for at least seven days after concrete placement. Thermal analysis using the developed DIANA finite element model was performed to determine the temperature development of these four drilled shafts at early age, and the calculated temperatures were compared with the measured ones to assess the validity of the developed finite element model.

The detailed description of the construction of the four drilled shafts is presented in Appendix E. This report presents the analysis of the data collected and the thermal analysis using the developed DIANA finite element model.

6.2 Mix Designs and Properties of Concrete Used in Drilled Shafts

Table 6-1 presents the mix designs and the fresh concrete properties of the concrete used in the four drilled shafts. The concrete used in shafts #2 and #4 represents a typical drilled shaft mix used in Florida. They had a cement content of 942 and 959 lb. of Type I/II Portland cement per cubic yard of concrete. The concrete used in shafts #1 and #3 had the same cementitious materials content as the concrete for shafts #2 and #4, but 70 % of the Portland cement was replaced with ground blast-furnace slag. Thus, this concrete had relatively lower heat of hydration.

Table 6-1. Mix designs and plastic properties of concrete used in each drilled shaft.

Shaft No.	Drilled shaft 1	Drilled shaft 2	Drilled shaft 3	Drilled shaft 4
Cement (lb./yd. ³)	279.0	942.0	282.0	959.0
Slag (lb./ yd. ³)	654.0	-	659.0	-
89 Stone (lb./ yd. ³)	1,220.0	1,217.0	1,213.0	1,220.0
Sand (lb./ yd. ³)	1,127.0	1,299.0	1,122.0	1,299.0
Water (lb./ yd. ³)	273.0	274.0	283.0	233.0
Air Entraining Admixture (oz./ yd. ³)	-	0.32	-	0.21
Water Reducing Admixture (oz./ yd. ³)	113.3	112.6	112.6	112.6
Actual Slump (in)	9.8	9.5	10.3	8.0
Temperature (°F)	76.0	76.0	71.0	82.0
Actual Air (%)	3.5	4.0	3.5	2.7
Unit Weight (lb./ft ³)	134	136	132	138
W/C	0.29	0.29	0.30	0.24

6.3 Moisture Level and R-Value of Soil Surrounding the Four Drilled Shafts

The R-value of the soil surrounding the four drilled shafts as a function of moisture content has been evaluated in Subtask 3B. Table 6-2 presents the R-values of the soil at various moisture levels. Results of soil investigation indicated that for shafts 1 & 2, the soil was dry to a depth of four feet, and was saturated beyond a depth of 4 feet. For shafts 3 & 4, the soil was dry to a depth of four feet, and was in a drained condition beyond a depth of 4 feet. For the dry condition, the soil can be considered to have a moisture level close to 0 % and R-value/inch of

6.5. For the drained condition, the soil can be considered to have a moisture level of around 6.0% and R-value/inch of 1.142. For the saturated condition, the soil can be considered to have a moisture content of around 16.0 % and R-value/inch of 0.89.

Table 6-2. R-values of drilled shaft soil at different moisture levels.

Moisture level in soil (%)	0.0	4.0	6.0	8.0	12.0	16.0
Soil R-Value (hr·ft·°F/BTU)	6.507	2.003	1.142	1.215	0.903	0.887
Thermal conductivity (J/m·s·°C)	0.266	0.863	1.5141	1.4226	1.915	1.949
Heat Capacity (J/m ³ ·°C)	1.212×10 ⁶	1.325×10 ⁶	1.448×10 ⁶	1.431×10 ⁶	1.524×10 ⁶	1.564×10 ⁶

6.4 Measured Temperature Distributions in the Drilled Shafts

Command Center temperature data loggers (by Transtec Group, Inc.) were installed at various locations in the concrete drilled shafts and in the surrounding soil to monitor the temperature development and distribution during the early age of the concrete. A total of twenty seven (27) temperature data loggers were used for each drilled shaft. Figure 6-1 shows the locations of the temperature sensors in a drilled shaft and its surrounding soil.

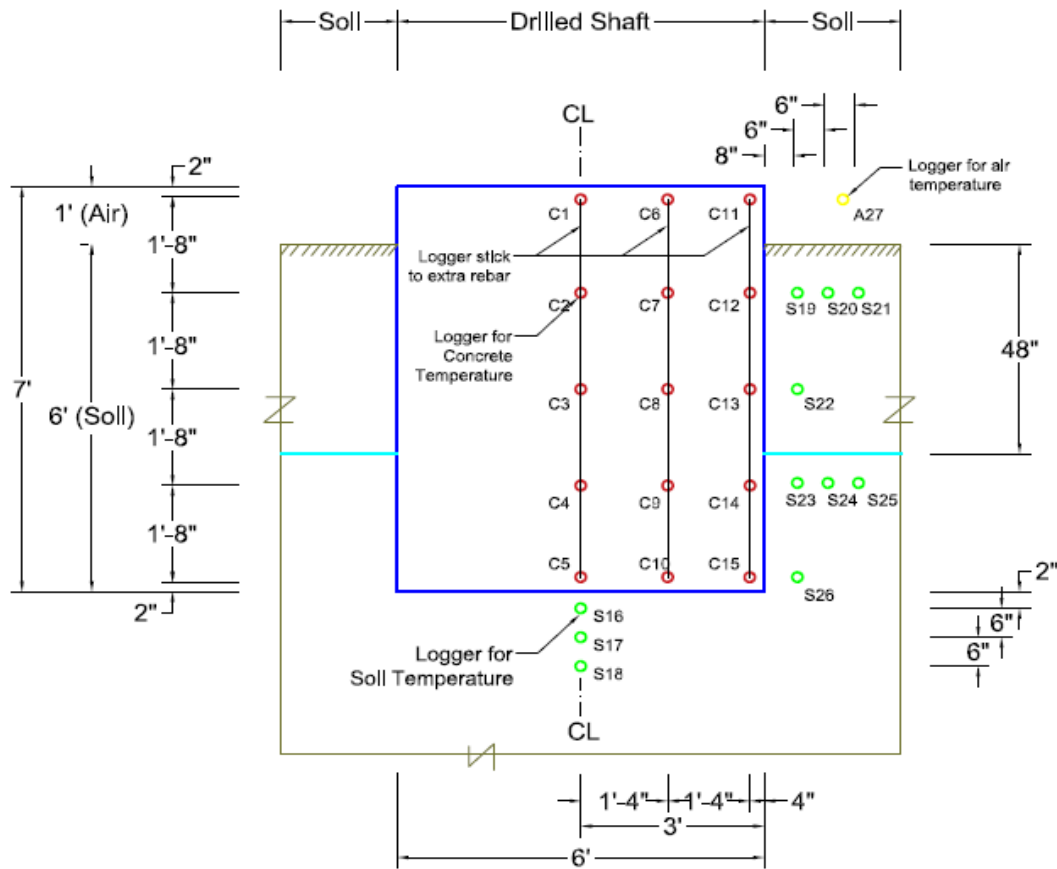


Figure 6-1. Temperature sensor positions in a drilled shaft and surrounding soil.

Sensors 1 through 5 were placed along the vertical centerline. Sensors 6 through 10 were placed along the middle line between the center and near surface. Sensors 11 through 15 were placed 4 inch (10.16 cm) from the surface. The information on the sensors' vertical locations are given in Table 6-3.

Table 6-3. Elevation of temperature sensors in each drilled shaft and surrounding soil.

Sensor No.	Distance from Bottom (in.)	Distance from Top (in.)
1, 6 and 11	82.0	2.0
2, 7 and 12	62.0	22.0
3, 8 and 13	42.0	42.0
4, 9 and 14	22.0	62.0
5, 10 and 15	2.0	82.0

The temperatures measured by the sensors in each drilled shafts are presented in Figures 6-2 to 6-13. The temperatures at sensor C3, which was located at the center of the shaft, showed the highest values. The lowest temperatures below soil were measured at sensor C15, which was located near the bottom surface of the shaft. The maximum temperature differential in each shaft can be taken to be the difference between the temperature at C3 and the temperature at C15. It is to be noted that the temperature data loggers which were used in this study had a maximum limiting value of 85.0 °C (185.0 °F), and temperatures over this value were recorded as 85.0 °C (185.0 °F). This limiting value can be noted to be reached for the following cases:

1. Sensors C2, C3, and C4 in shaft 2.
2. Sensors C2, C3, C4, C7, C8, and C9 in shaft 4.

In order to determine the maximum temperatures and temperature differentials in shafts 2 and 4, the maximum temperatures at C3 need to be estimated. The missing data for sensor C3 were estimated using a statistical method called Multiple Imputation Method in the SPSS software. The multiple imputation method uses a regression model to predict missing values. In order to impute the missing data that occurred at a specific measurement point, it was necessary to find another (Hair et al., 2009) measurement point whose temperature data would constitute a valid reference to develop the regression model. Since the thermal properties within the adiabatic material of concrete were equivalent, it was considered appropriate to designate the closest sensor to C3 as the referential point of measurement. Thus, the temperature data recorded by sensor C8 were used in the Multiple Imputation Method of SPSS to impute the missing temperature data for sensor C3.

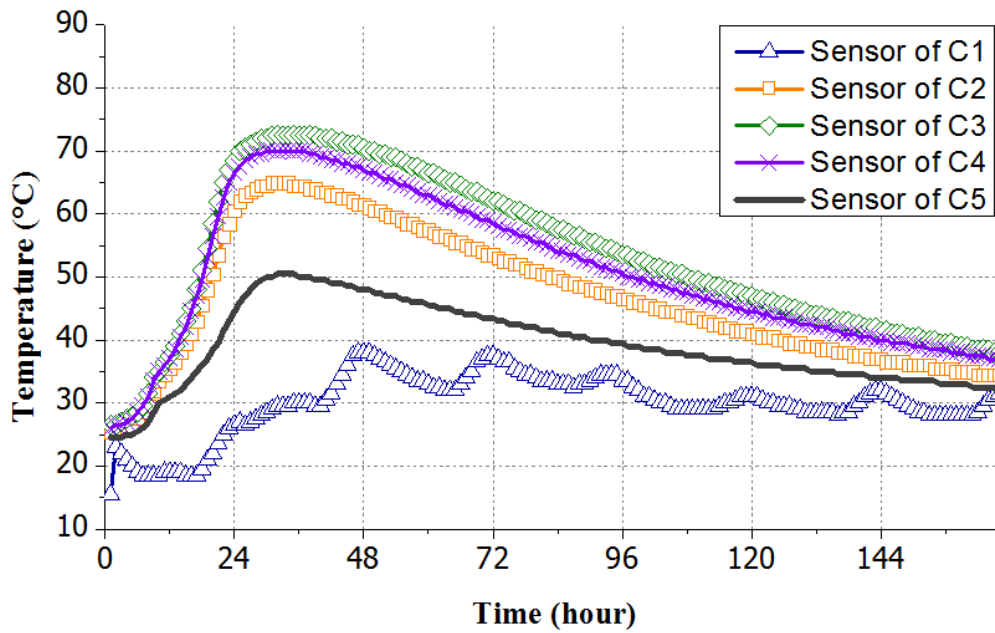


Figure 6-2. Measured temperatures in drilled shaft 1 along the center line under wet soil.

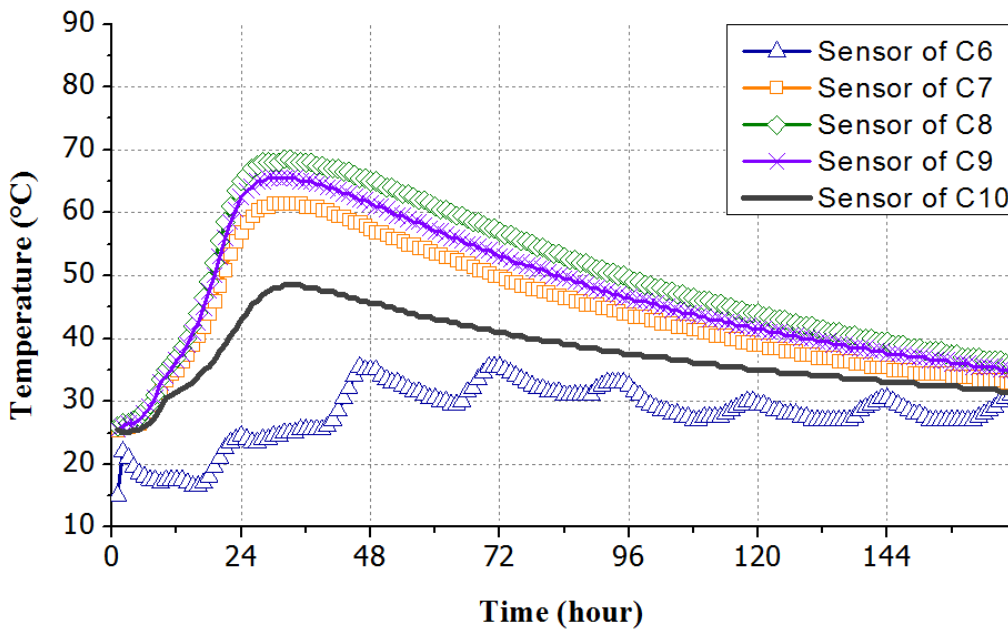


Figure 6-3. Measured temperatures in drilled shaft 1 along the middle line under wet soil,

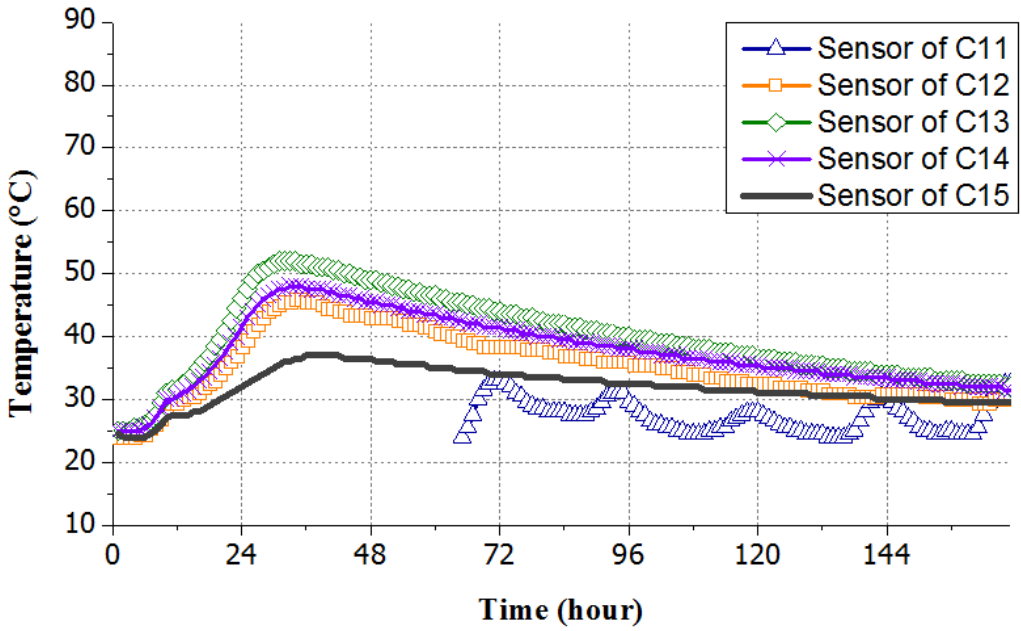


Figure 6-4. Measured temperatures in drilled shaft 1 along the edge line under wet soil.

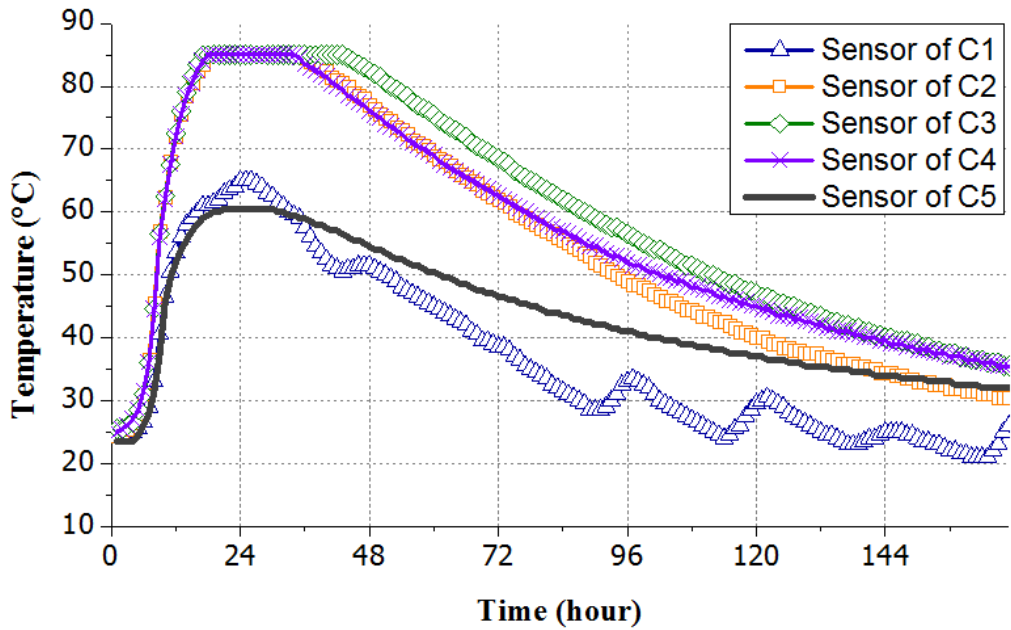


Figure 6-5. Measured temperatures in drilled shaft 2 along the center line under wet soil.

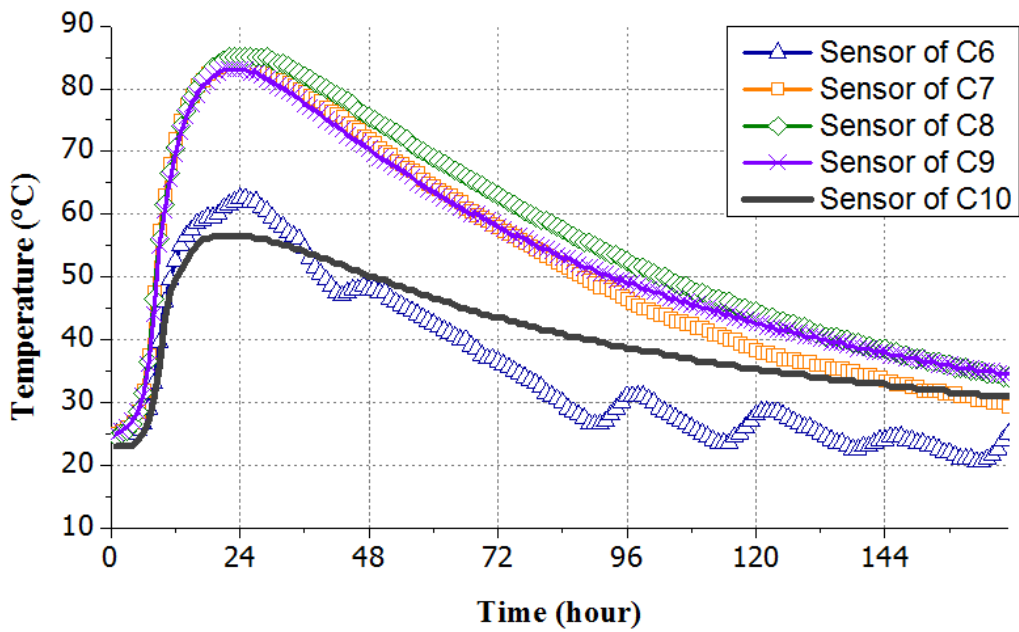


Figure 6-6. Measured temperatures in drilled shaft 2 along the middle line under wet soil.

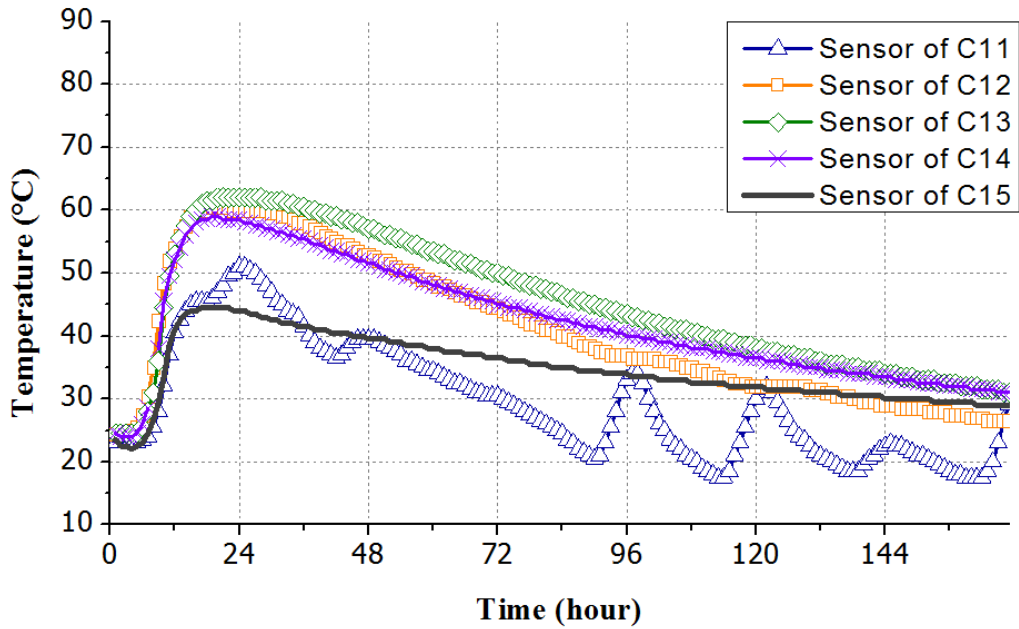


Figure 6-7. Measured temperatures in drilled shaft 2 under along the edge line wet soil.

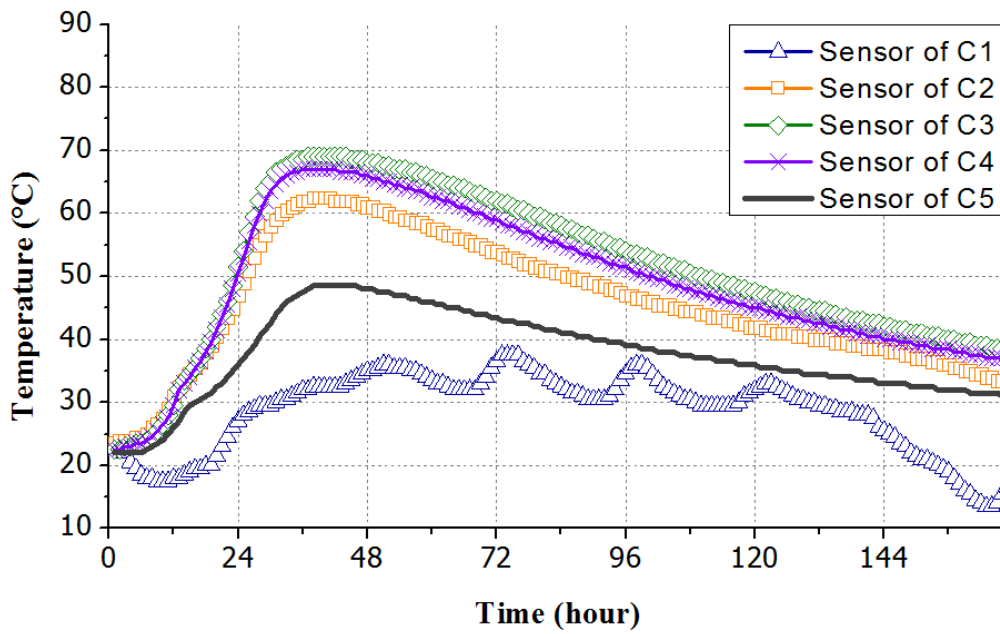


Figure 6-8. Measured temperatures in drilled shaft 3 along the center line under dry soil.

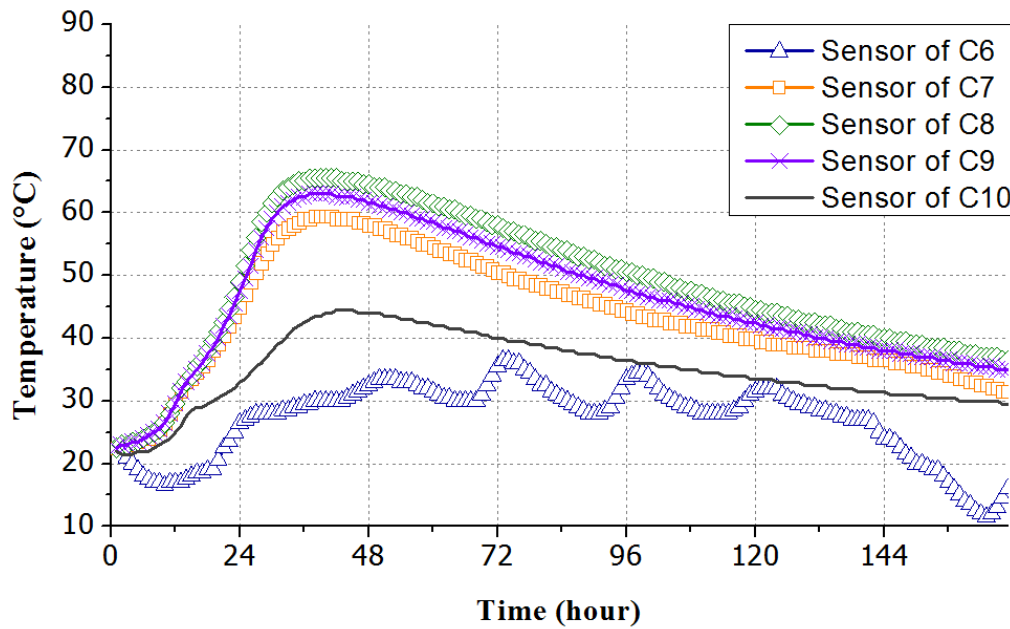


Figure 6-9. Measured temperatures in drilled shaft 3 along the middle line under dry soil.

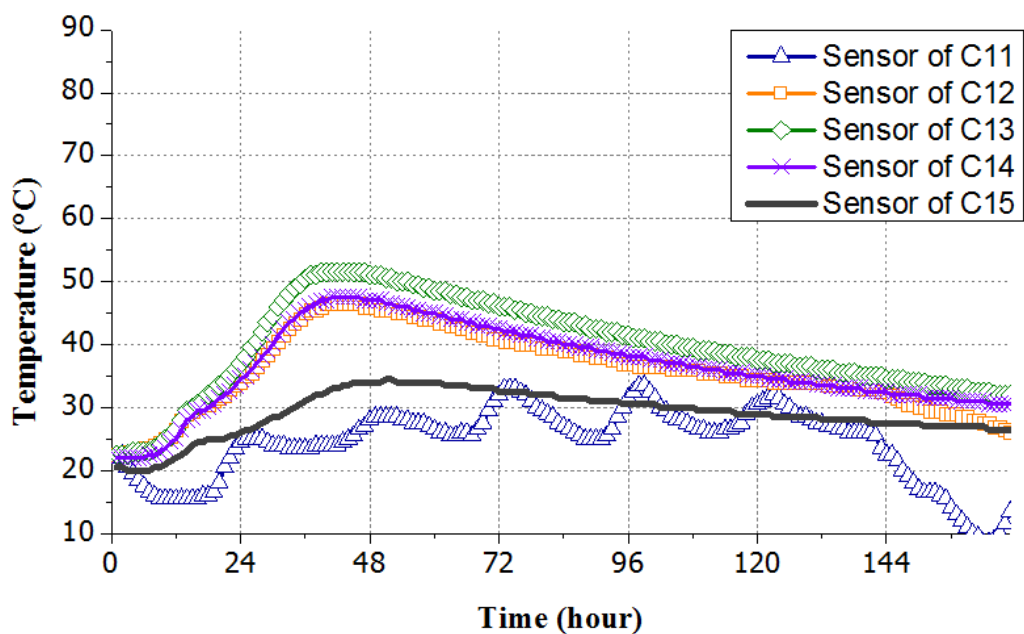


Figure 6-10. Measured temperatures in drilled shaft 3 along the edge line under dry soil.

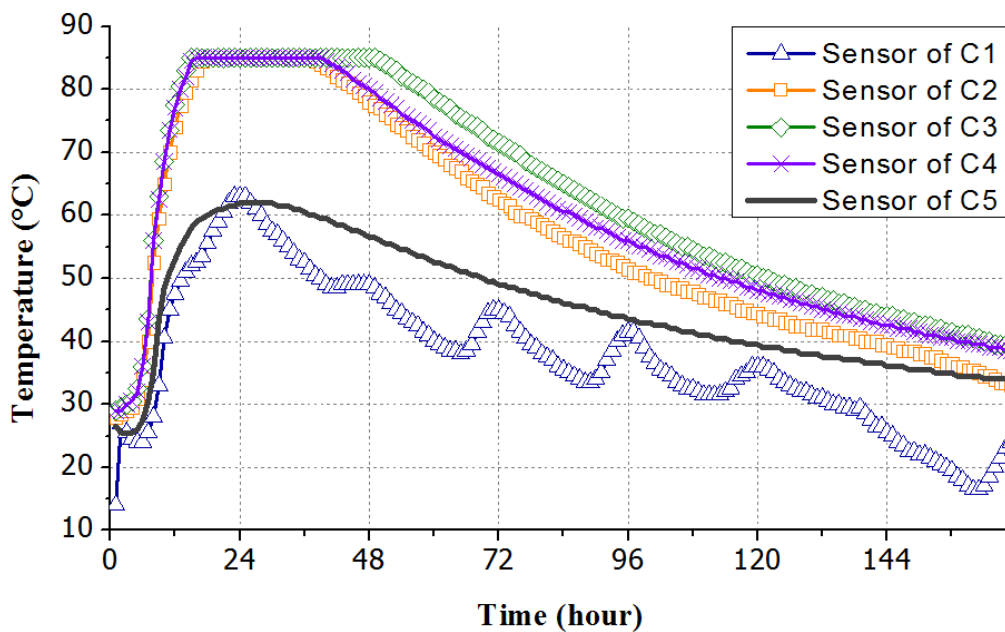


Figure 6-11. Measured temperatures in drilled shaft 4 along the center line under dry soil.

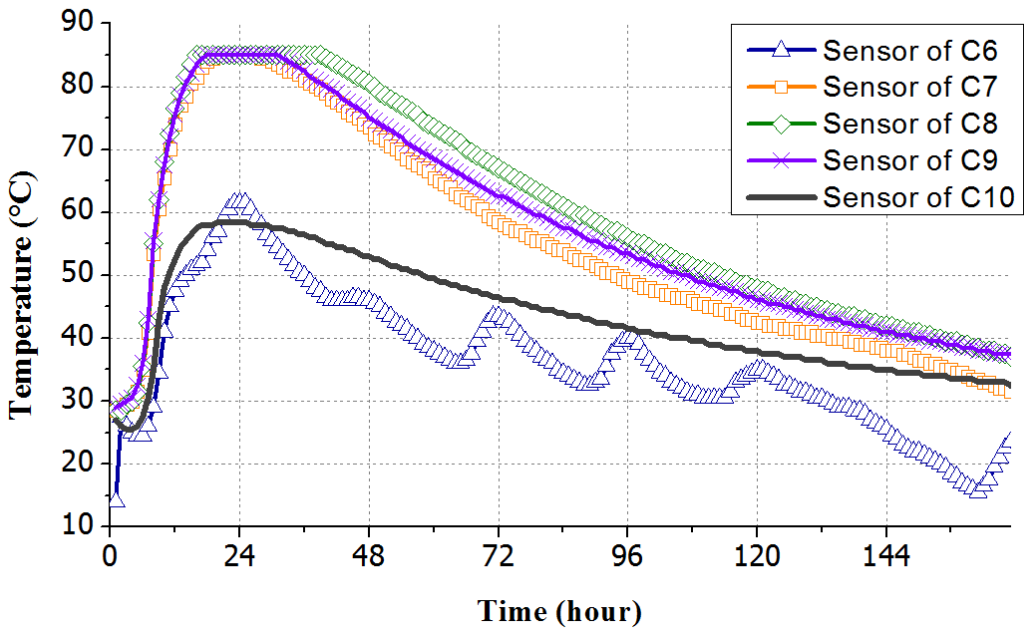


Figure 6-12. Measured temperatures in drilled shaft 4 along the middle line under dry soil.

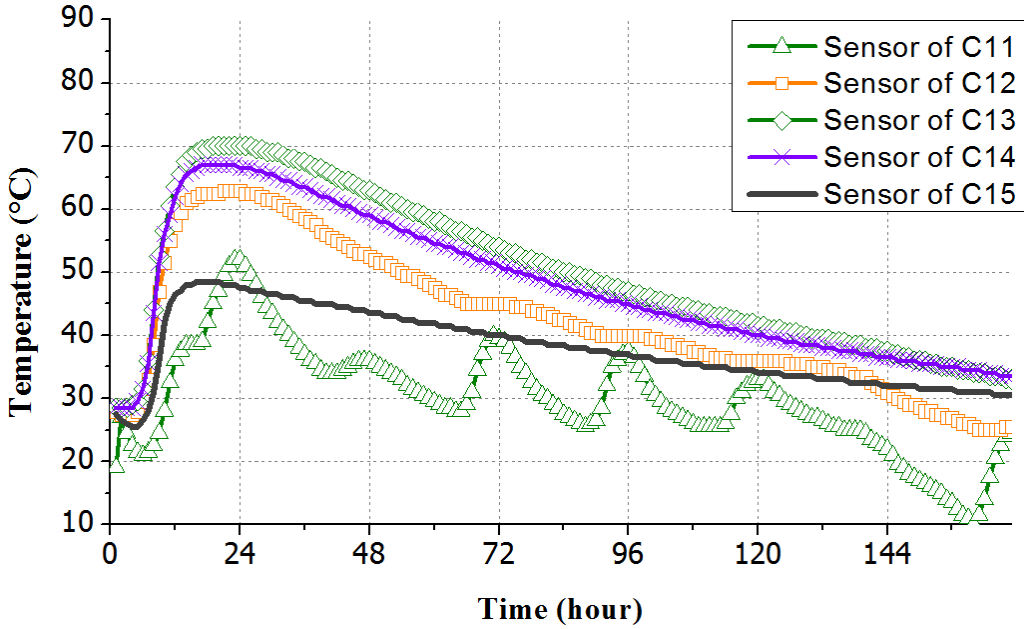


Figure 6-13. Measured temperatures in drilled shaft 4 along the edge line under dry soil.

Figure 6-14 presents the measured maximum temperatures at Sensor C3 after missing data for shafts 2 and 4 were imputed. Also shown on the figure are the computed maximum temperature differentials after missing data imputation.

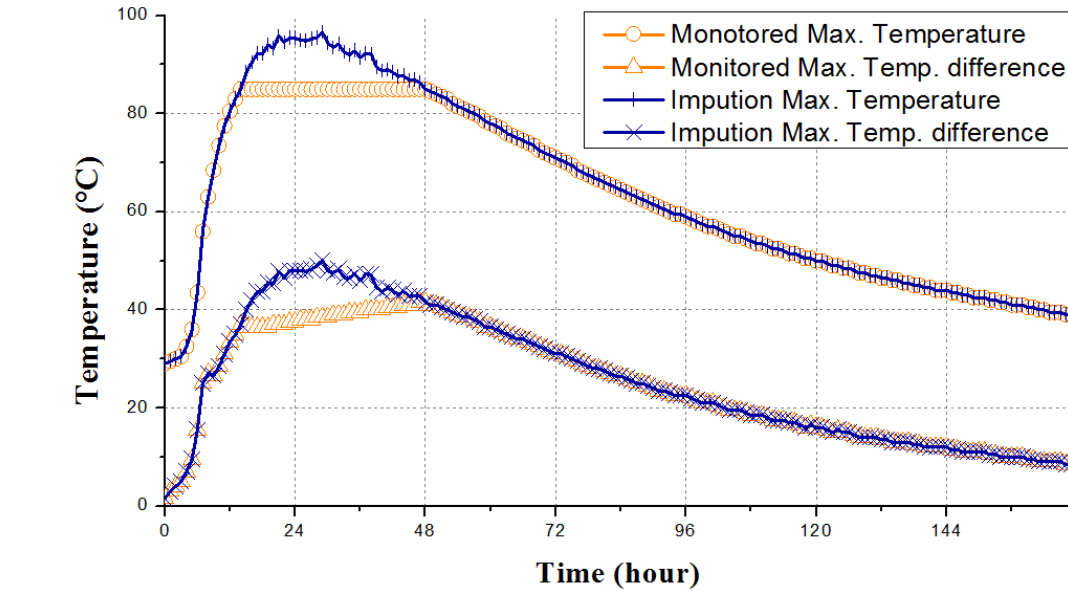
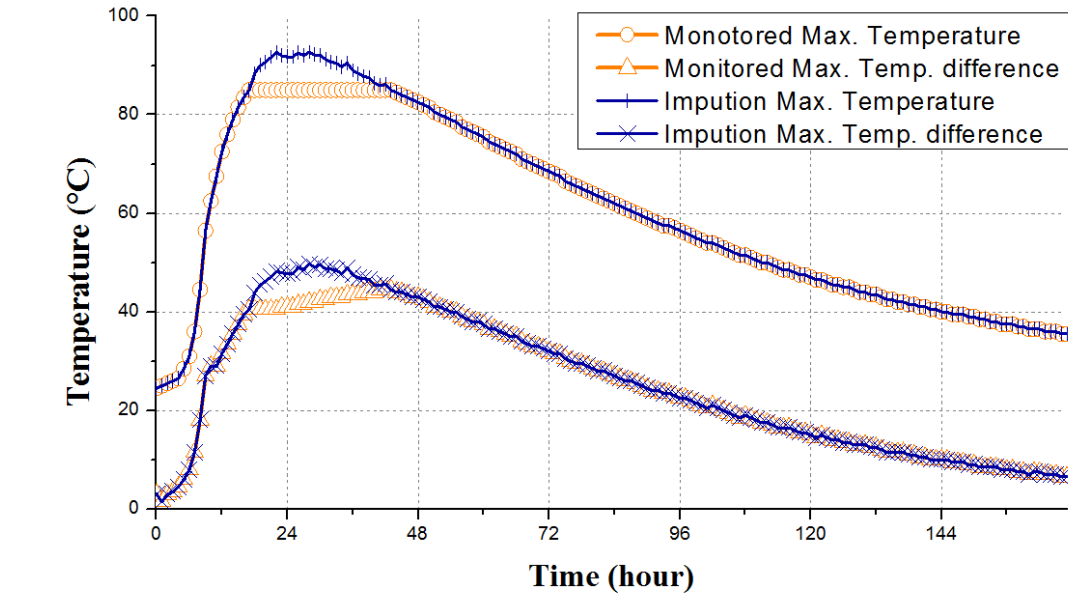
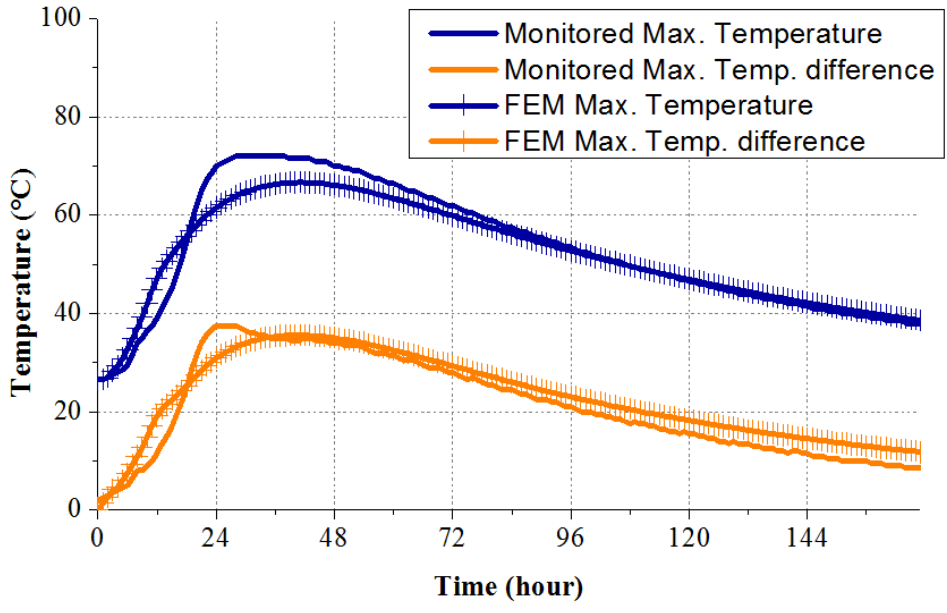
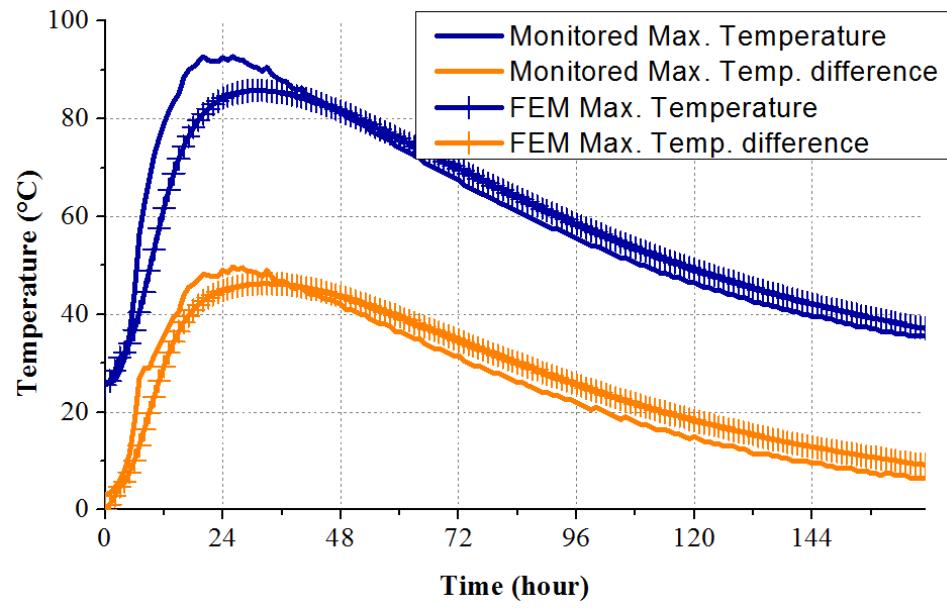


Figure 6-14. Maximum temperature and temperature differentials after missing data imputation for drilled shafts 2 and 4. A) drilled shaft 2 and B) drilled shaft 4.

After the estimated missing data were incorporated, the measured maximum temperatures and the maximum temperature differentials for the four drilled shafts are presented in Figure 6-15 to 6-16. It can be seen that the use of slag-cement concrete mix had substantially reduced the maximum temperature differential in the drilled shafts. However, the maximum temperature differentials in all four shafts exceeded the maximum allowable limit of 19.4 °C (35.0 °F) according to FDOT specifications for mass concrete. For shafts 1 and 3 (which used a slag-cement concrete mix and placed in wet and dry soils, respectively), the maximum measured temperature differentials were 37.5 °C (67.5 °F) and 38.0 °C (68.4 °F), respectively. For shafts 2 and 4 (which used a pure Portland cement concrete mix and placed in wet and dry soils, respectively), the maximum measured temperature differentials were 49.5 °C (89.1 °F) and 50.0 °C (90.0 °F), respectively. For shafts 2 and 4, the maximum allowable temperature of 82.2 °C (180.0 °F) according to FDOT specifications for mass concrete was also exceeded.

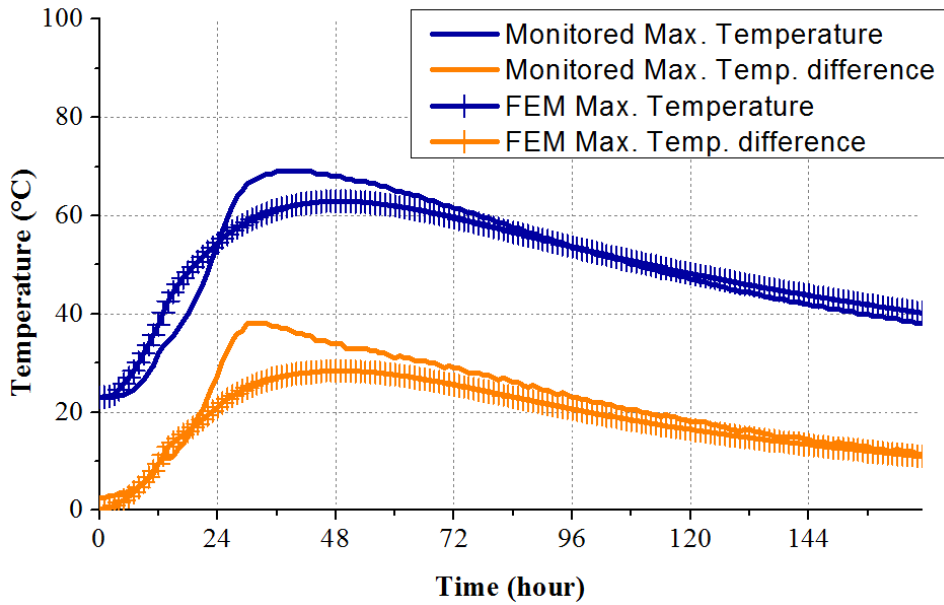


A

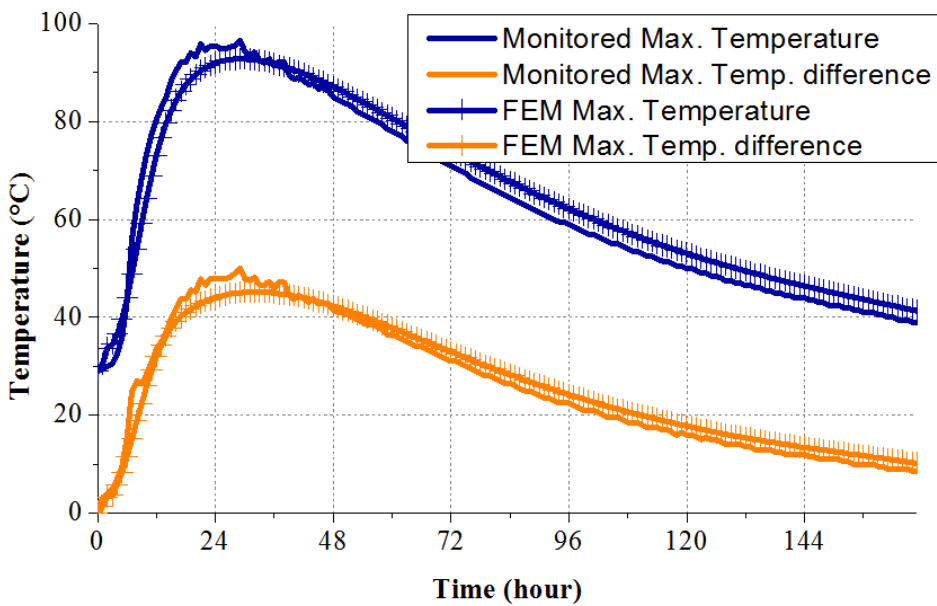


B

Figure 6-15. Measured and computed maximum temperature and temperature differentials in drilled shafts. A) drilled shaft 1 and B) drilled shaft 2.



A



B

Figure 6-16. Measured and computed maximum temperature and temperature differentials in drilled shafts. A) drilled shaft 3 and B) drilled shaft 4.

For the four shafts tested, there was no significant difference between effects of the wet soil and dry soil environment. This was due to the fact that there was no difference in the first 4 feet of soil, and the difference in moisture condition of the soil beyond 4 feet depth was not enough to cause any noticeable difference in the developed temperature in the shafts.

6.5 Thermal Analysis of the Four Drilled Shafts

6.5.1 Overview

Thermal analysis using the developed DIANA finite element model was performed to determine the temperature development of these four drilled shafts at early age, and the calculated temperatures were then compared with the measured ones to assess the validity of the developed finite element model. The detailed description of the developed finite element model for thermal analysis of drilled shafts has been presented in Chapter 5. This section presents the analysis of these four drilled shafts evaluated in the field study.

6.5.2 Finite Element Model for the Four Drilled Shafts

Figure 6-17 shows the finite element model for thermal analysis of the four drilled shafts. As described in detail in Chapter 5, the model made use of the axis-symmetry of the drilled shaft structure, and the 3-D model was reduced to a 2-D axis-symmetric model to reduce computational time without loss of accuracy. The drilled shaft was modeled as an axis-symmetric structure with a radius of 3 feet and length of 7 feet, and the drilled shaft was enclosed by the surrounding soil to a depth of 6 feet. The surrounding soil was modeled as two layers. The top soil layer had a depth of 4 feet, and the bottom soil layer was below the depth of 4 feet. The condition and properties of the surrounding soil are described in Section 6.3. For shafts #1 & #2, the top soil layer was modeled as having a moisture level close to 0.0 % and R-value/inch of 6.5, and the bottom soil layer was modeled as having a moisture content of around 16.0 % and R-value/inch of 0.89. For shafts #3 & #4, the top soil layer was also modeled as having a moisture level close to 0.0 % and R-value/inch of 6.5, but the bottom soil layer was modeled as having a moisture level of around 6.0 % and R-value/inch of 1.142.

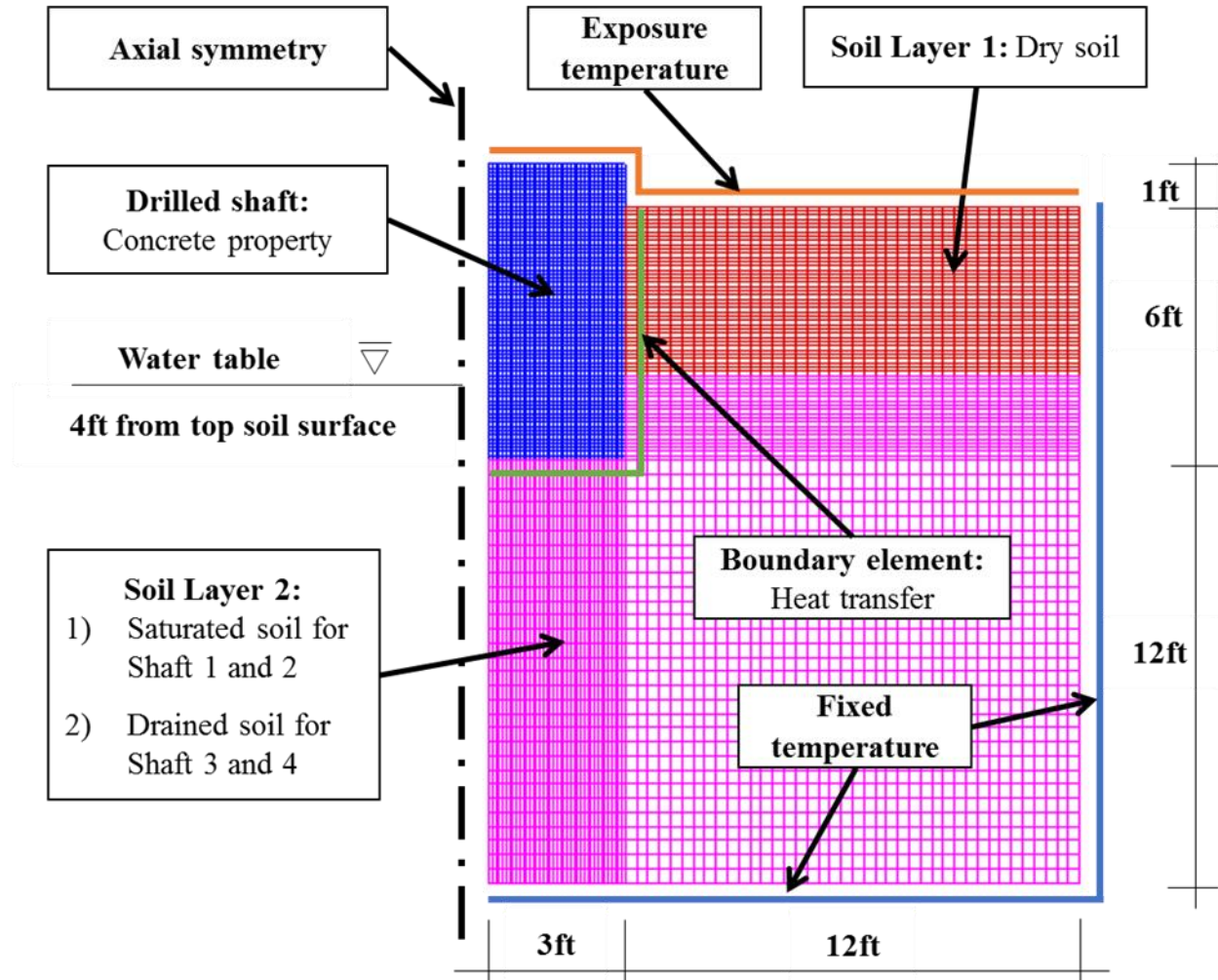


Figure 6-17. Axis-symmetric FE model for thermal analysis of the four drilled shafts.

6.5.3 Heat of Hydration and Thermal Properties of Concrete

Samples of the cementitious components of the drilled shaft concretes were collected and isothermal calorimetry tests were performed on them to obtain the heat of hydration data of these concretes, which are needed as inputs for the thermal analysis. The procedure for the isothermal calorimetry test and the analysis of the isothermal calorimetry test results are presented in Chapter 5. Figure 6-18 presents the adiabatic temperature rise data (using an initial temperature of 23.0 °C) for the four concrete mixes, which were calculated from the results of the isothermal calorimetry tests.

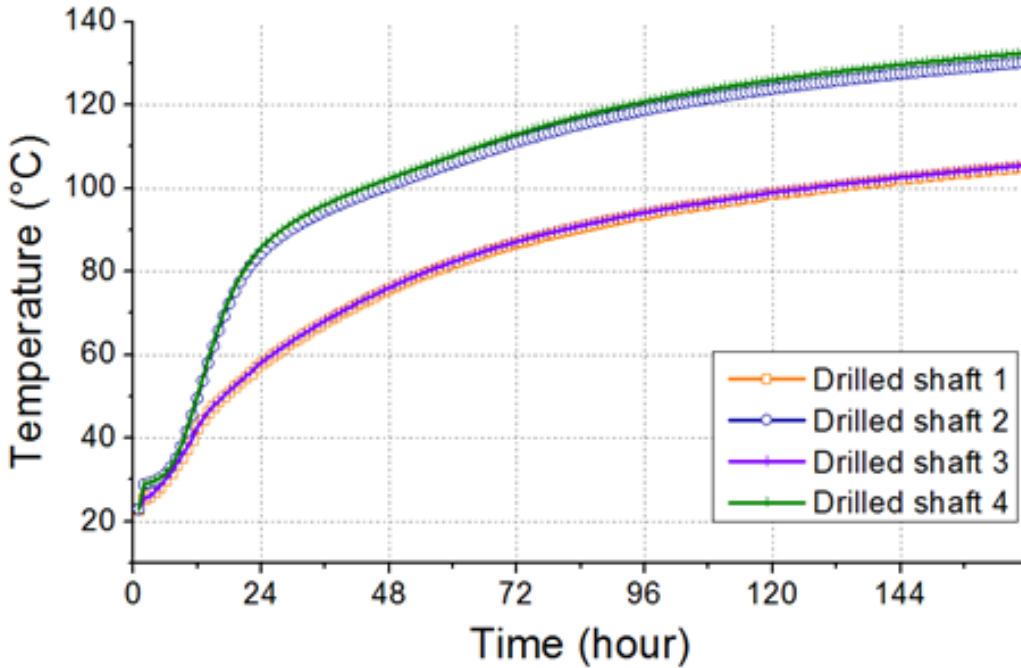


Figure 6-18. Adiabatic temperature rise data for the four drilled shaft concrete mixes.

Table 6-4 presents the specific heat, heat capacity, and thermal conductivity of the four drilled shaft concrete mixes. These properties were calculated from the properties of the components and their proportions in the concrete mixes. Table 6-4 presents also the initial temperatures of the concrete mixes at the time of placement, which were used as inputs for the thermal analysis.

Table 6-4. Thermal properties and initial temperatures of the four drilled shaft concretes.

Shaft No.	Specific Heat (J/g·°C)	Heat Capacity (J/m ³ ·°C)	Thermal Conductivity (J/m·s·°C)	Initial temperature (°C)
Drilled shaft 1	1.052	2,257,122	2.10	26.5
Drilled shaft 2	1.049	2,299,388	2.20	25.5
Drilled shaft 3	1.062	2,244,790	2.00	23.0
Drilled shaft 4	1.010	2,248,215	2.20	29.0

6.5.4 Results of Thermal Analysis of the Four Drilled Shafts

Thermal analysis, using the developed DIANA finite element model and the input parameters as described in the previous sections, was performed to determine the temperature development of these four drilled shafts at early age. The computed results were used to determine the maximum temperature and temperature differential for each of the four drilled shafts evaluated. The computed maximum temperatures and temperature differentials as obtained by the finite element thermal analysis are shown in Figure 4-5, along with the measured values. It can be seen that the computed temperatures matched fairly well with the measured temperature values. This indicates that the finite element thermal analysis model used in this study can make fairly accurate prediction of temperature development in concrete drilled shafts at early age.

6.6 Summary of Findings

Four concrete drilled shafts, which were 6 feet in diameter and 7 feet in length, were placed in a Florida soil to a depth of 6 feet to evaluate the temperature development in the concrete at early age subject to the effects of concrete mixes used and the moisture condition of the surrounding soil. The two concrete mixes used were a slag-cement concrete mix with a relatively low heat of hydration, and a pure Portland cement concrete mix with a high heat of hydration. The two soil conditions used were a dry condition and a wet condition.

The results of the study show that the use of slag-cement concrete mix had substantially reduced the maximum temperature differential in the drilled shafts. However, the maximum temperature differentials in all four shafts exceeded the maximum allowable limit of 19.4 °C (35.0 °F) according to FDOT specifications for mass concrete. For the two shafts which used a slag-cement concrete mix and placed in wet and dry soils, the maximum measured temperature differentials were 37.5 °C (67.5 °F) and 38.0 °C (68.4 °F), respectively. For the two shafts

which used a pure Portland cement concrete mix and placed in wet and dry soils, the maximum measured temperature differentials were 49.5 °C (89.1 °F) and 50.0 °C (90.0 °F), respectively. For the two shafts which used a pure cement concrete mix, the maximum allowable temperature of 82.2 °C (180.0 °F) according to FDOT specifications for mass concrete was also exceeded.

For the four shafts tested, there was no significant difference between effects of the wet soil and dry soil environment. This was due to the fact that there was no difference in the first 4 feet of soil, and the difference in moisture condition of the soil beyond 4 feet depth was not enough to cause any noticeable difference in the developed temperature in the shafts.

Thermal analysis using the developed DIANA finite element model was performed to determine the temperature development of these four drilled shafts at early age. The computed temperatures were found to match fairly well with the measured temperature values. This indicates that the finite element thermal analysis model used in this study can make fairly accurate prediction of temperature development in concrete drilled shafts at early age.

CHAPTER 7
LABORATORY STUDY ON STRENGTH DEVELOPMENT
OF TERNARY BLEND CONCRETE MIXES

7.1 Introduction

Based on past research (such as FDOT contract BD545-35), it has been determined that ternary blend concretes can provide a 100-year service life of structures in Florida. Since the ternary blends reduce Portland cement content and have usually only 30 to 40 % Portland cement, they also help to reduce initial heat generation, which may reduce the need for temperature control models for some structures that might typically require methods to control heat development.

The revised Section 346 of the 2016 FDOT Standard Specification for Road and Bridge Construction has included language to allow the ternary blends in all classes of concrete. However, the equations needed to assist in resolving low strength issues between the contractor and the Department as defined in Section 346-11 have been neglected. Thus, there was a need to study the strength development of ternary blend concretes so that equations for determining 28-day compressive strength from the strength of concrete cores that are older than 28 days can be developed.

To address this need, a laboratory study was conducted to evaluate the strength development of typical ternary blend concrete mixes in Florida in order to develop equations for estimating the 28-day compressive strength of this type of concrete from the compressive strength of cores taken after 28 days. The laboratory study had the following main objectives:

1. To develop equations for estimating the 28-day compressive strength from that obtained after 28 days for typical ternary blend concrete mixes used in Florida.
2. To develop equations for relating compressive strength to flexural strength, splitting tensile strength, and modulus of elasticity of typical ternary blend concrete mixes used in Florida.

7.2 Laboratory Testing Program

7.2.1 Design of Experiment

In this study six FDOT approved ternary blend mix designs were used to produce fourteen mix designs by changing cement type and aggregate source. Table 7-1 presents the Florida concrete class, cementitious materials, and aggregate source of the fourteen ternary blend mixes evaluated in this study.

Table 7-1. Classifications of ternary blend mixes evaluated.

Mix Design	Class	Type of Cement	Aggregate	RCM
Mix 1	IV	I/II	Miami Oolite	Slag & Fly Ash
Mix 2	II	I/II	Miami Oolite	Slag & Fly Ash
Mix 3	IV	I/II	Miami Oolite	Silica Fume & Fly Ash
Mix 4	V	I/II	Miami Oolite	Slag & Fly Ash
Mix 5	V	I/II	Miami Oolite	Silica Fume & Fly Ash
Mix 6	VI	I/II	Miami Oolite	Silica Fume & Fly Ash
Mix 7	IV	III	Miami Oolite	Slag & Fly Ash
Mix 8	IV	III	Miami Oolite	Silica Fume & Fly Ash
Mix 9	V	III	Miami Oolite	Slag & Fly Ash
Mix 10	V	III	Miami Oolite	Silica Fume & Fly Ash
Mix 11	IV	I/II	Brooksville	Slag & Fly Ash
Mix 12	IV	III	Brooksville	Slag & Fly Ash
Mix 13	V	I/II	Brooksville	Slag & Fly Ash
Mix 14	V	III	Brooksville	Slag & Fly Ash

Trial mixes were conducted for each mix design to achieve the workable proportions of mix ingredients after adjusting the water content and the admixtures dosages to satisfy the plastic properties requirements. After completing all trial mixes, production mixes of the required size were made.

Table 7-2 presents the proportions of mix ingredients used in the final production mixes for the fourteen concrete mixes evaluated in this study.

Table 7-2. Mix designs of ternary blend mixes evaluated.

Materials	Source	Mix 1	Mix 2	Mix 3	Mix 4	Mix 5
Coarse aggregate (lb./yd ³)	Miami Oolite	1629.0	1675.0	1650.0	1578.0	1743.0
Fine Aggregate (lb./ yd ³)	Silica sand	1110.0	1222.0	968.6	1038.0	906.0
Cement (lb./ yd ³)	Local source (I/II)	210.0	185.0	585.0	258.0	600.0
	Local source (III)	-	-	-	-	-
Fly ash (lb./ yd ³)	FDOT approved	70.0	61.5	175.0	86.0	185.0
Silica fume (lb./ yd ³)	FDOT approved	-	-	75.0	-	75.0
Slag (lb./ yd ³)	FDOT approved	420.0	369.0	-	516.0	-
Water (lb./ yd ³)	Local	284.0	257.0	292.0	287.0	267.0
AEA (oz./ yd ³)	FDOT approved	0.6	3.0	5.0	3.4	5.0
Type D Admix. (oz./ yd ³)	WRDA 60	46.3	24.6	33.0	55.0	60.0
Type F Admix. (oz./ yd ³)	ADVA 120	13.2	16.6	40.5	24.5	50.8

Table 7-2. Continued.

Materials	Source	Mix 6	Mix 7	Mix 8	Mix 9	Mix 10
Coarse aggregate (lb./yd ³)	Miami Oolite	1611.0	1629.0	1650.0	1578.0	1746.0
Fine Aggregate (lb./yd ³)	Silica sand	975.0	1110.0	967.0	1038.0	899.5
Cement (lb./yd ³)	Local source (I/II)	630.0	-	-	-	-
	Local source (III)	-	210.0	585.0	258.0	600.0
Fly ash (lb./yd ³)	FDOT approved	189.0	70.0	175.0	86.0	185.0
Silica fume (lb./yd ³)	FDOT approved	81.0	-	75.0	-	75.0
Slag (lb./yd ³)	FDOT approved	-	420.0	-	516.0	-
Water (lb./yd ³)	Local	281.0	284.0	292.0	287.0	267.0
AEA (oz./yd ³)	FDOT approved	3.0	0.7	9.0	3.4	15.0
Type D Admix. (oz./yd ³)	WRDA 60	63.0	28.0	26.6	55.0	60.0
Type F Admix. (oz./ yd ³)	ADVA 120	54.0	16.7	52.3	29.0	72.9

Table 7-2. Continued.

Materials	Source	Mix 11	Mix 12	Mix 13	Mix 14
Coarse aggregate (lb./yd ³)	Brooksville	1735.0	1735.0	1748.0	1748.0
Fine Aggregate (lb./yd ³)	Silica sand	1221.0	1221.0	1050.0	1050.0
Cement (lb./yd ³)	Local source (I/II)	210.0	-	258.0	-
	Local source (III)	-	210.0	-	258.0
Fly ash (lb./yd ³)	FDOT approved	70.0	70.0	86.0	86.0
Silica fume (lb./yd ³)	FDOT approved	-	-	-	-
Slag (lb./yd ³)	FDOT approved	420.0	420.0	516.0	516.0
Water (lb./yd ³)	Local	284.0	284.0	287.0	287.0
AEA (oz./yd ³)	FDOT approved	0.6	0.7	6.0	6.0
Type D Admix. (oz./yd ³)	WRDA 60	28.0	28.0	55.0	55.0
Type F Admix. (oz./yd ³)	ADVA 120	22.0	26.0	39.0	45.2

Concrete mix design preparation procedures as described in the ASTM C192 standard were followed in both trial and production mixes for all 14 concrete mix designs. The fresh concrete property tests on each batch of concrete are listed in Table 7-3. The mechanical property tests on the hardened concrete are listed in Table 7-4. All samples were demolded at 24 ± 4 hours after casting. Each specimen was labeled and placed in the standard moist curing room before the mechanical property tests. The test equipment and procedures used in this laboratory study are described in Appendix F.

Table 7-3. Fresh concrete property tests.

Test	Replicates
Slump (ASTM C143)	one measurement
Air content (ASTM C231)	one measurement
Unit weight (ASTM C138)	one measurement
Temperature (ASTM C1064)	one measurement

Table 7-4. Hardened concrete property tests.

Tests	Samples	Days of Testing
Compressive Strength (ASTM C39)	4" x 8" cylinder (3 replicates per curing age)	At 1, 3, 7, 28, 91, and 182 days
Modulus of Elasticity (ASTM C469)	4" x 8" cylinder (3 replicates per curing age)	At 7, 28, 91, and 182 days
Splitting Tensile Strength (ASTM C496)	4" x 8" cylinder (3 replicates per curing age)	At 7, 28, 91, and 182 days
Flexural Strength (ASTM C78)	4" x 4" x 14" beam (3 replicates per curing age)	At 7, 28, 91, and 182 days

7.2.2 Materials

This section presents the materials used for this research study. All the materials and mix designs used in this research are FDOT approved. In this research, five different cementitious materials were used in the 14 mix designs. The cementitious materials used are Type I/II cement, Type III cement, fly ash, slag and silica fume. Silica sand was used as fine aggregate. Miami Oolite aggregate and Brooksville aggregate were used as coarse aggregate.

7.2.2.1 Aggregates

7.2.2.1.1 Fine Aggregate

The fine aggregate used in all of the mix designs is a Georgia Silica Sand from plant GA397. The physical properties of fine aggregate were verified in the SMO labs and are shown in Table 7-5. The gradation of the fine aggregate is plotted in Figure 7-1.

Table 7-5. Physical properties of silica sand used.

Tests	Standard Test Method	Fine Aggregate*	Specification Limits
Materials Finer Than 75 μm	AASHTO T11	0.180 %	≤ 1.754 %
Fineness Modulus	AASHTO T27	2.35	not specified
Organic Impurities	AASHTO T21	1	≤ 3
SSD Specific Gravity	AASHTO T84	2.640	not specified
Apparent Specific Gravity	AASHTO T84	2.651	not specified
Bulk Specific Gravity	AASHTO T84	2.633	not specified
Absorption	AASHTO T84	0.30 %	not specified

(Note: * Tested at FDOT SMO)

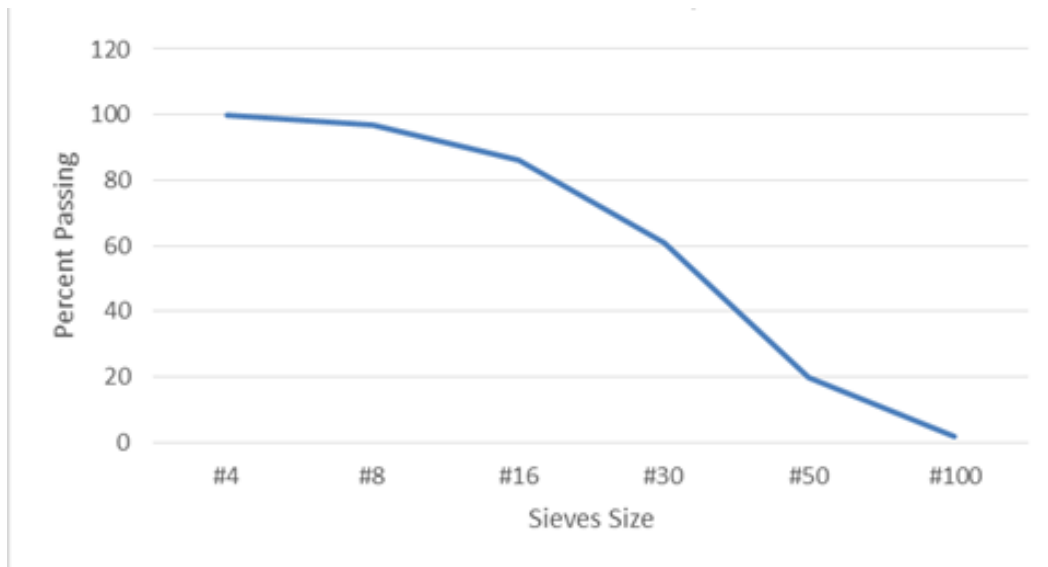


Figure 7-1. Gradation of silica sand.

Prior to using the silica sand, the sand was bagged and oven dried overnight (12 hours minimum) in order to eliminate moisture. After that, the silica sand bags were stored in a weather-controlled and dry environment to avoid any humidity that could affect the moisture content.

7.2.2.1.2 Coarse Aggregate

Two sources of limestone were used in this research. They are Miami Oolite and Brooksville limestones, which are the commonly used aggregate in the state of Florida. The coarse aggregate was stored outdoor in large permanent bins. Prior to using the aggregate, the aggregate was bagged and soaked in water for a minimum of 24 hours to ensure that the aggregate is saturated. The excess moisture was measured and considered in the water content of the concrete. The process of weighing the coarse aggregate is recommended to take place the day before mixing the concrete in order to avoid water draining out of the aggregates.

Miami Oolite

The Miami Oolite limestone was provided by SMO from mine number 87-090. The physical properties of the aggregate are shown in Table 7-6 and its gradation is plotted in Figure 7-2.

Table 7-6. Physical properties of Miami Oolite aggregate.

Tests	Standard Test Method	Coarse Aggregate*	Specification Limits
Materials Finer Than 75 μm	AASHTO T11	1.710 %	≤ 1.750 %
SSD Specific Gravity	AASHTO T85	2.434	not specified
Apparent Specific Gravity	AASHTO T85	2.556	not specified
Bulk Specific Gravity	AASHTO T85	2.356	not specified
Absorption	AASHTO T85	3.30 %	not specified

(Note: * Tested at FDOT SMO)

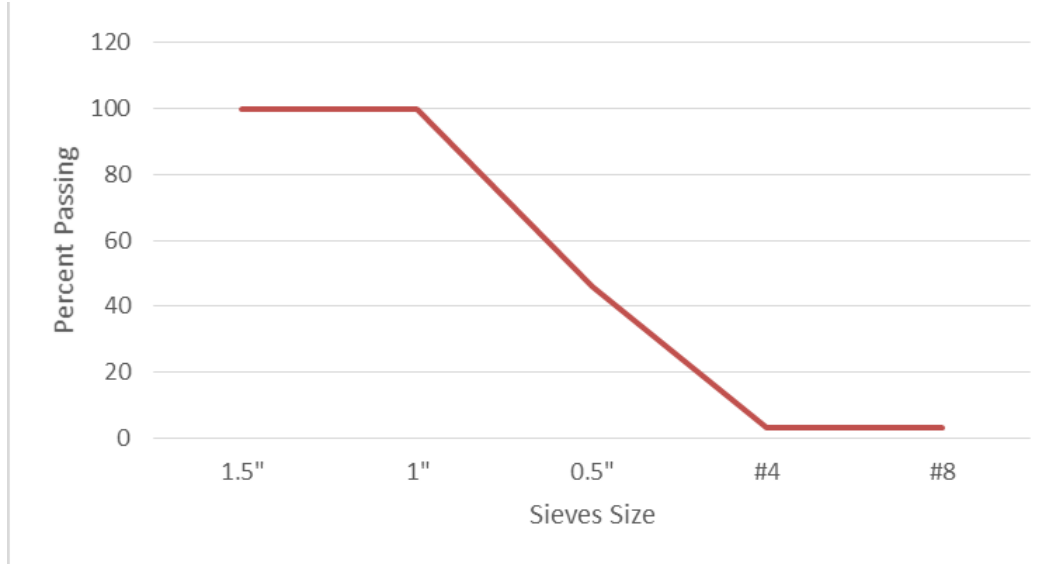


Figure 7-2. Gradation of Miami Oolite aggregate.

Brooksville Limestone

The Brooksville limestone aggregate was produced at mine 08-012. Its physical properties are shown in Table 7-7, and its gradation is shown in Figure 7-3.

Table 7-7. Brooksville aggregate physical properties.

Tests	Standard Test Method	Coarse Aggregate*	Specification Limits
Materials Finer Than 75 μm	AASHTO T11	3.510 %	≤ 3.750 %
SSD Specific Gravity	AASHTO T85	2.448	not specified
Apparent Specific Gravity	AASHTO T85	2.587	not specified
Bulk Specific Gravity	AASHTO T85	2.361	not specified
Absorption	AASHTO T85	3.70 %	not specified

(Note: * Tested at FDOT SMO)

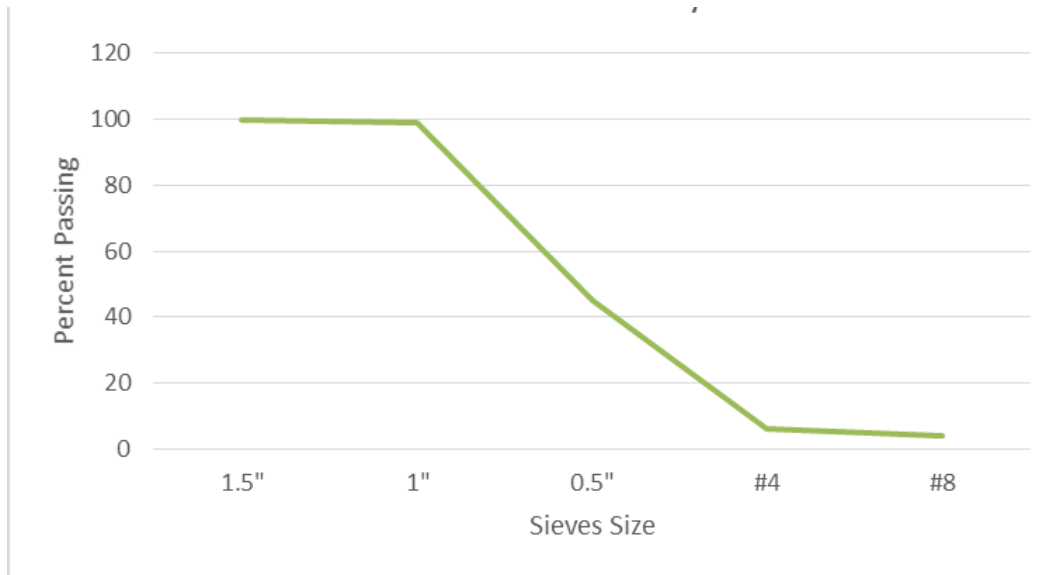


Figure 7-3. Gradation of Brooksville limestone aggregate.

7.2.2.2 Portland Cement

The Portland cement used in the laboratory testing were Type I/II and Type III cements provided by a local FDOT approved source. The cement met the requirement of AASHTO M85 standard specifications. The chemical and physical properties of Type I/II and Type III cements are shown in Tables 7-8 and 7-9.

Table 7-8. Chemical compositions of the cements used.

Item	Cement Type I/II	Cement Type III
Rapid Method, X-Ray (C 114)		
SiO ₂ (%)	19.6	19.7
Al ₂ O ₃ (%)	5.1 (6.0 max)	5.2
Fe ₂ O ₃ (%)	3.7 (6.0 max)	3.7
CaO (%)	64.0	63.5
MgO (%)	0.8 (6.0 max)	0.8 (6.0 max)
SO ₃ (%)	3.1 (3.0 max)	3.3 (3.5 max)
Loss on ignition (%)	2.6 (3.0 max)	1.9 (3.0 max)
Insoluble residue (%)	0.21 (0.75 max)	0.18 (0.75 max)
CO ₂ (%)	1.4	0.6
Limestone (%)	3.6 (5.0 max)	- (5.0 max)
CaCO ₃ in Limestone (%)	89.0 (70.0 min)	89.0 (70.0 min)
Adjusted Potential Phase Composition (C 150)		
C ₃ S (%)	56.0	56.0
C ₂ S (%)	14.0	14.0
C ₃ A (%)	7.0 (8.0 max)	7.0 (8.0 max)
C ₄ AF (%)	11.0	11.0
C ₃ S + 4.75 * C ₃ A (%)	91.0 (100.0 max)	91.0 (100.0 max)
ASTM C 150-12 and AASHTO M 85-12 Optional Chemical Requirements:		
NaEq (%)	0.46 (0.60 max)	0.39 (0.60 max)

Table 7-9. Physical properties of the cements used.

Item	Cement Type I/II	Cement Type III
Air content of mortar (%) (C 185)	5.0 (12.0 max)	5.0 (12.0 max)
Blaine Fineness (m ² /kg) (C 204)	378 (280-430 range)	595
-325 (%) (C 430)	96.70	99.61
Autoclave expansion (%) (C 151)	0.04 (0.08 max)	0.01 (0.08 max)
Time of setting (minutes)	115	82
Vicat Initial (C 191)	(45-375 range)	(45-375 range)
Mortar Bar Expansion (%) (C 1038)	0.002 (0.020 max)	0.007 (0.020 max)
Compressive strength (psi) (C 109)		
1 day	2370	3780 (1740 min)
3 day	3840 (1740 min)	4990 (3480 min)
7 day	5030 (2760 min)	5890
28 day	6590	7160

7.2.2.3 Fly Ash

The Fly Ash used in all of the mix designs in this project is a Class “F” fly ash, supplied by a local FDOT approved source and tested by TEC services. The fly ash met ASTM C618 and AASHTO M295-11 specifications. The chemical and physical properties of the fly ash are shown in Table 7-10.

Table 7-10. Fly ash chemical and physical properties.

Chemical Analysis	Results (%)	Specification (Class F)	
		ASTM C618-12a	AASHTO M295-11
SiO ₂	48.90	-	-
Al ₂ O ₃	20.20	-	-
Fe ₂ O ₃	17.14	-	-
SiO ₂ + Al ₂ O ₃ + Fe ₂ O ₃	86.20	70.00 % min.	70.00 % min.
CaO	5.10	-	-
MgO	0.90	-	-
Na ₂ O	0.82	-	-
K ₂ O	2.32	-	-
Na ₂ O + 0.658 K ₂ O	2.35	-	-
SO ₃	1.80	5.00 % max.	5.00 % max.
LOI	1.40	6.00 % max.	5.00 % max.
Moisture Content	0.16	3.00 % max.	3.00 % max.
Available Alkalies			
Na ₂ O as Available Alkalies	0.25	-	-
K ₂ O as Available Alkalies	0.64	-	-
Na ₂ O+0.658 K ₂ O as Available Alkalies	0.67	-	1.50 % max.

7.2.2.4 Ground Blast-Furnace Slag

The slag used in both trial and production concrete mixes was provided by a local FDOT approved source. The slag met ASTM C430, ASTM C204, ASMT C188 and ASTM C185 specifications, as shown in Table 7-11.

Table 7-11. Slag physical and chemical properties.

Slag Physical Properties			
Test		Composition	Limit
Fineness	Retained on 325 sieve (ASTM C430)	2.7 %	Max. 20.0 %
	Blaine (ASTM C204)	483 m ² /kg	
Specific Gravity (ASTM C188)		2.86	
Air Content (ASTM C185)		4.0 %	Max. 12.0 %
Slag Chemical Composition			
Sulfide Sulfur (S)		0.9 %	Max. 2.5 %
Sulfur Trioxide (SO ₃)		2.2 %	

7.2.2.5 Silica Fume

The Silica Fume was provided by a FDOT approved source and used in five mix designs in this project. The testing was conducted by Elkem Materials Inc. and the properties are shown in Table 7-12.

Table 7-12. Chemical composition of the silica fume used.

Test	Min.	Max.	Ave.
LOI (%)	1.96	3.97	3.96
H2O (%)	0.09	0.71	0.16
Oversize >45 μ (%)	1.07	1.49	1.48
SiO ₂ (%)	93.27	95.92	94.40
Pozz. Activity Index at 7 days (%)	115	154	135
Density (Mg/m ³) (SG)	1.88	2.16	1.95
Total Alkalies (%)	0.42	0.61	0.45
Chlo. (%)	0.04	0.10	0.05
SO ₃ (%)	0.19	0.30	0.24
Surface Area (m ² /g)	15.80	21.77	20.12

(Note: Conducted by Elkem Materials Inc. from Feb. 2010 to Aug. 2012.)

7.2.2.6 Admixtures

The three admixtures which were used in all of the fourteen concrete mix designs were air-entraining (AEA), retarding water reducer (Type D WRDA 60) and high-range water reducing (Type F ADVA 120) admixtures provided by a FDOT approved source.

AEA admixture is an aqueous solution of a complex mixture of organic acid salts. The specific gravity of the AEA is 1.02 ± 0.02 . AEA meets ASTM C260, AS1478, and AASHTO M154 specification for chemical admixtures.

ADVA 120 is considered Type F admixture, which is high-range water reducing admixture. The product is a non-reactive and inflammable liquid, but it could decompose producing carbon monoxide and carbon dioxide. ADVA 120 has a pH value of 5, which could cause skin irritation upon contact.

WRDA 60 is a Type D admixture, which is a water reducer and retarder. The product has a specific gravity of 1.1 at 20.0 °C (68.0 °F), and it is a non-reactive and inflammable liquid, but it could decompose producing carbon monoxide and carbon dioxide. WRDA 60 has a pH value of 6, which could cause skin irritation.

7.3 Test Results

7.3.1 Fresh Concrete Properties

The acceptable limits for the plastic properties were decided according to the concrete mix requirements, which included the slump and the air content. The slump range shall be 4-6 inch, and the air content shall be 3 ± 1 %.

The trial mixes were tested in order to insure that the production mixes would have satisfactory plastic properties. The plastic properties of production mixes were recorded as shown in Tables 7-13, 7-14, and 7-15.

Table 7-13. The plastic properties of slag and fly ash ternary blend concrete mixes containing Miami Oolite coarse aggregate.

Test	Mix 1 (W/C =0.41)	Mix 2 (W/C =0.42)	Mix 4 (W/C =0.33)	Mix 7 (W/C =0.41)	Mix 9 (W/C =0.33)
Air content (%)	4.0	3.7	2.3	2.0	1.6
Slump (in.)	6.00	4.75	4.00	4.75	4.00
Unit weight (lb./ft ³)	138.96	140.40	142.56	141.68	142.72
Temperature (°F)	74	76	74	75	74

Table 7-14. The plastic properties of silica fume and fly ash ternary blend concrete mixes containing Miami Oolite coarse aggregate.

Test	Mix 3 (W/C =0.35)	Mix 5 (W/C =0.31)	Mix 6 (W/C =0.31)	Mix 8 (W/C =0.35)	Mix 10 (W/C =0.31)
Air content (%)	3.5	2.1	2.7	2.1	4.0
Slump (in.)	4.25	4.50	4.00	4.00	4.00
Unit weight (lb./ft ³)	139.52	143.20	140.62	140.80	142.40
Temperature (°F)	76	77	77	77	78

Table 7-15. The plastic properties of slag and fly ash ternary concrete mixes containing Brooksville limestone aggregate.

Test	Mix 11 (W/C=0.41)	Mix 12 (W/C=0.41)	Mix 13 (W/C=0.33)	Mix 14 (W/C=0.33)
Air content (%)	2.2	2.0	3.5	3.1
Slump (in.)	4.00	4.00	5.50	6.00
Unit weight (lb./ft ³)	142.00	142.64	142.64	142.64
Temperature (°F)	75	76	72	73

7.3.2 Results of Hardened Concrete Tests

7.3.2.1 Compressive Strength

The compressive strength test results were recorded and plotted as a function of time in order to understand and predict strength gaining behavior in ternary blend concrete as shown in Tables 7-16, 7-17, 7-18, and 7-19. The 14 mix designs were divided into 4 categories according to the characteristics of the strength gaining factor ($f'(t)/f'(28)$) with respect to time.

The first category is slag and fly ash mixes with water binder ratio higher than 0.4 regardless of the type of cement, since the cement content is only $28 \pm 2\%$ of the total cementitious material. This category includes mixes 1, 2, 7, 11, and 12 as shown in Table 7-16, which are Class IV and below structural concrete.

Table 7-16. Compressive strength test results for slag and fly ash ternary blend concrete mixes with W/C higher than 0.4.

Testing age	Mix 1 (psi) W/C=0.41 fly ash =10% Slag = 60%	Mix 2 (psi) W/C =0.42 fly ash =10% Slag = 60%	Mix 7 (psi) W/C =0.41 fly ash =10% Slag = 60%	Mix 11 (psi) W/C =0.41 fly ash =10% Slag = 60%	Mix 12 (psi) W/C =0.41 fly ash =10% Slag = 60%
1 day	740	870	970	940	1,210
3 days	3,210	3,010	3,580	3,170	3,340
7 days	5,420	5,080	5,510	5,340	5,430
28 days	7,930	6,700	8,270	7,140	7,230
91 days	9,130	7,610	9,810	7,910	8,540
182 days	9,270	7,770	9,750	8,130	8,660

The second category is slag and fly ash mixes with water binder ratio lower than 0.4. This category includes mixes 4, 9, 13, and 14 as shown in Table 7-17, which are Class V and higher structural concrete.

Table 7-17. Compressive strength test results for slag and fly ash ternary blend concrete mixes with W/C lower than 0.4.

Testing age	Mix 4 (psi) W/C=0.33 fly ash =10% Slag = 60%	Mix 9 (psi) W/C=0.33 fly ash =10% Slag = 60%	Mix 13 (psi) W/C=0.33 fly ash =10% Slag = 60%	Mix 14 (psi) W/C=0.33 fly ash =10% Slag = 60%
1 day	1,270	1,580	970	1,340
3 days	5,050	4,640	5,020	4,860
7 days	7,650	6,890	6,820	6,640
28 days	9,820	9,900	8,540	7,980
91 days	10,630	11,110	9,070	9,080
182 days	10,690	11,300	9,540	9,400

The third category is silica fume and fly ash mixes containing Type I/II cement. This category includes mixes 3, 5, and 6 as shown in Table 7-18.

Table 7-18. Compressive strength test results for silica fume and fly ash ternary blend concrete mixes containing Type I/II Portland cement.

Testing age	Mix 3 (psi) W/C=0.35 fly ash =21% Silica fume = 9%	Mix 5 (psi) W/C=0.31 fly ash =22% Silica fume = 9%	Mix 6 (psi) W/C=0.31 fly ash =21% Silica fume = 9%
1 day	3,940	4,660	4,660
3 days	6,010	6,840	7,020
7 days	7,300	8,300	8,430
28 days	9,550	9,780	10,010
91 days	9,950	10,720	10,920
182 days	10,040	10,910	10,870

The fourth category is silica fume and fly ash mixes containing Type III cement. This category includes mixes 8 and 10 as shown in Table 7-19.

Table 7-19. Compressive strength test results for silica fume and fly ash ternary blend concrete mixes containing Type III Portland cement.

Testing age	Mix 8 (psi) W/C=0.35 fly ash =21% Silica fume = 9%	Mix 10(psi) W/C=0.31 fly ash =22% Silica fume = 9%
1 day	5,650	6,510
3 days	7,220	7,840
7 days	8,520	8,870
28 days	9,770	10,330
91 days	10,520	10,950
182 days	10,910	11,040

The difference in strength gaining is significant between most of the 14 mixes. This is due to the effect of water cement ratio and cementitious materials used. The difference was minimized by using the strength factor instead of the strength as shown in Figures 7-4 and 7-5.

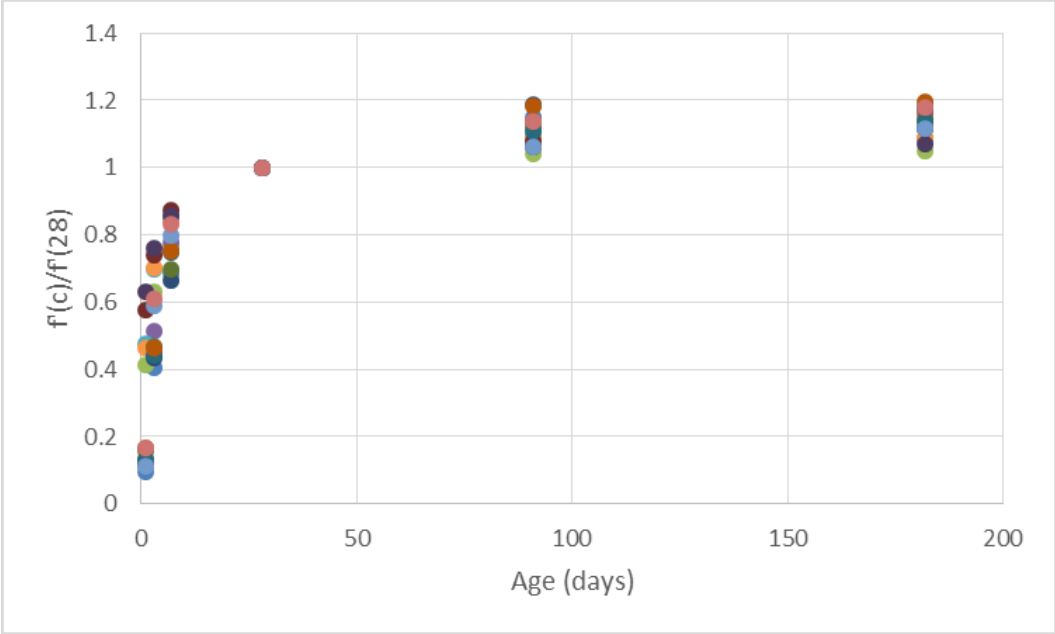


Figure 7-4. Strength factor versus age for all 14 concrete mixes.

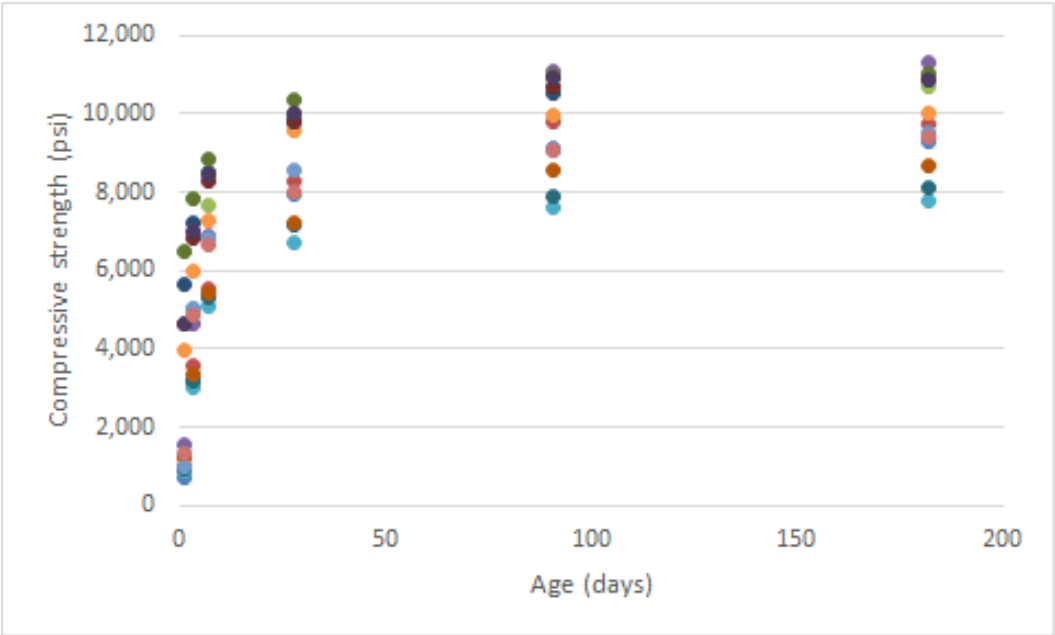


Figure 7-5. Compressive strength versus age for all 14 concrete mixes.

7.3.2.2 Splitting Tensile Strength

The splitting tensile strength test results were recorded and plotted as a function of time in order to understand its relationship between the splitting tensile and time for ternary blend concrete as shown in Figure 7-6.

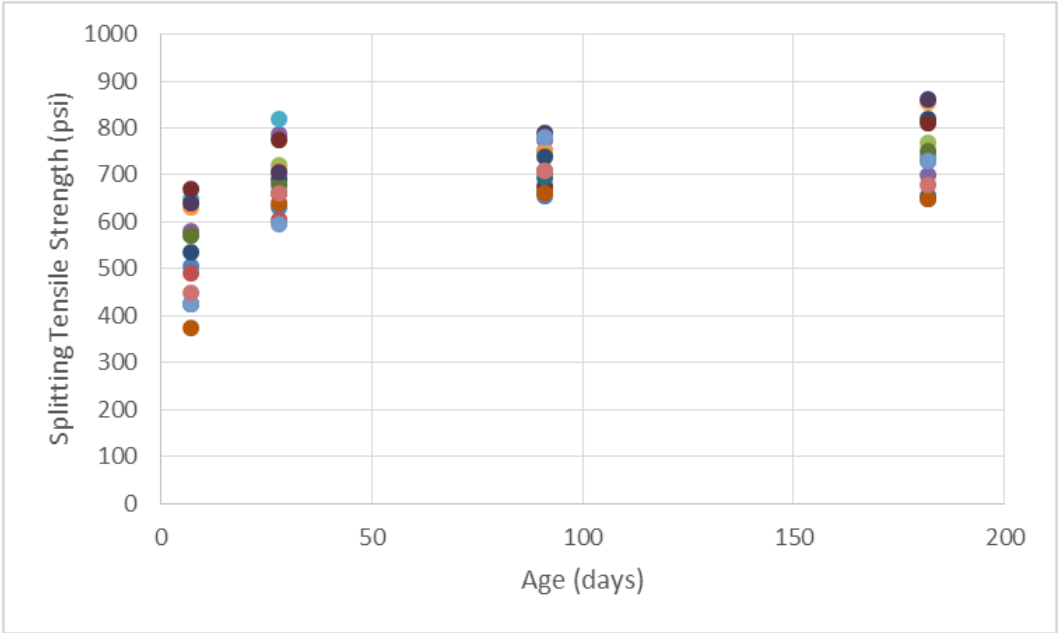


Figure 7-6. Splitting tensile strength versus age.

The first category is slag and fly ash mix designs with water cement ratio higher than 0.4 regardless of the type of cement, since the cement content is only $28 \pm 2\%$ of the total cementitious material. This category includes mixes 1, 2, 7, 11, and 12 as shown in Table 7-20. These mixes are Class IV and below structure concrete.

Table 7-20. Splitting tensile test results for slag and fly ash ternary blend concrete mixes with W/C higher than 0.4.

Testing age	Mix 1 (psi) W/C=0.41 fly ash =10% Slag = 60%	Mix 2 (psi) W/C=0.42 fly ash =10% Slag = 60%	Mix 7 (psi) W/C=0.41 fly ash =10% Slag = 60%	Mix 11 (psi) W/C=0.41 fly ash =10% Slag = 60%	Mix 12 (psi) W/C=0.41 fly ash =10% Slag = 60%
7 days	505	490	535	425	375
28 days	630	605	690	660	640
91 days	655	665	740	695	660
182 days	650	730	820	655	650

The second category is slag and fly ash mix designs with water cement ratio lower than 0.4. This category includes mixes 4, 9, 13, and 14 as shown in Table 7-21. These mixes are Class V and higher structure concrete.

Table 7-21. Splitting tensile test results for slag and fly ash ternary blend concrete mixes with W/C lower than 0.4.

Testing age	Mix 4 (psi) W/C=0.33 fly ash =10% Slag = 60%	Mix 9 (psi) W/C=0.33 fly ash =10% Slag = 60%	Mix 13 (psi) W/C=0.33 fly ash =10% Slag = 60%	Mix 14 (psi) W/C=0.33 fly ash =10% Slag = 60%
7 days	580	570	425	450
28 days	785	680	595	660
91 days	775	710	780	710
182 days	700	750	730	680

The third category is silica fume and fly ash mix designs containing Type I/II cement.

This category includes mixes 3, 5, and 6 as shown in Table 7-22.

Table 7-22. Splitting tensile test results for silica fume and fly ash ternary blend concrete mixes containing Type I/II Portland cement.

Testing age	Mix 3 (psi) W/C=0.35 fly ash =21% Silica fume = 9%	Mix 5 (psi) W/C=0.31 fly ash =22% Silica fume = 9%	Mix 6 (psi) W/C=0.31 fly ash =21% Silica fume = 9%
7 days	570	650	630
28 days	720	820	710
91 days	750	750	750
182 days	770	740	855

The fourth category is silica fume and fly ash mix designs containing Type III cement.

This category includes mixes 8 and 10 as shown in Table 7-23.

Table 7-23. Splitting tensile test results for silica fume and fly ash ternary blend concrete mixes containing Type III Portland cement.

Testing age	Mix 8 (psi) W/C=0.35 fly ash =21% Silica fume = 9%	Mix 10(psi) W/C=0.31 fly ash =22% Silica fume = 9%
7 days	670	640
28 days	775	705
91 days	675	790
182 days	810	860

7.3.2.3 Flexural Strength

The flexural strength test results were recorded and plotted as a function of time in order to understand its relationship with time as shown in Figure 7-7.

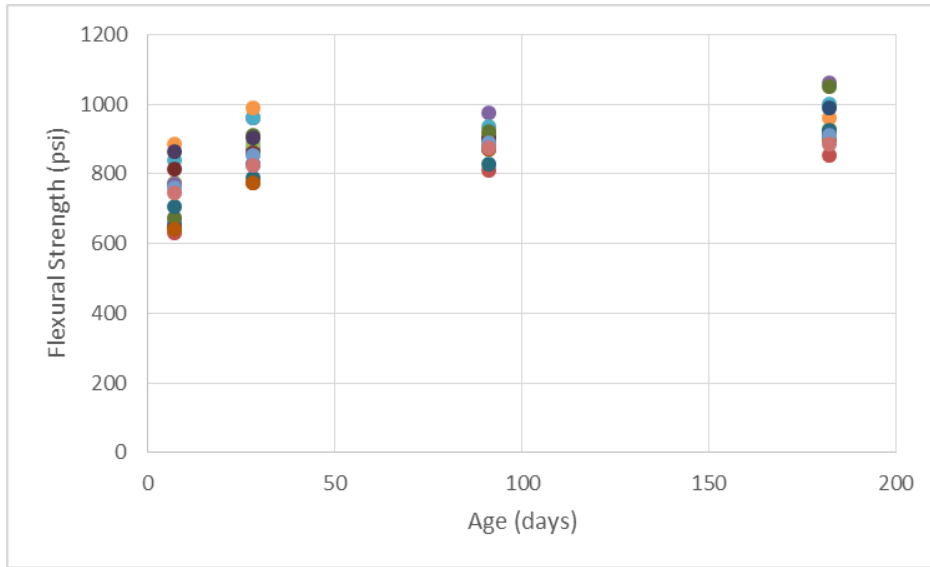


Figure 7-7. Flexural strength versus age.

The first category is slag and fly ash mix designs with water cement ratio higher than 0.4 regardless of the type of cement. This category includes mixes 1, 2, 7, 11, and 12 as shown in Table 7-24. These mixes are class IV and below structural concrete.

Table 7-24. Flexural strength test results for slag and fly ash ternary blend concrete mixes with W/C higher than 0.4.

Testing age	Mix 1 (psi) W/C=0.41 fly ash =10% Slag = 60%	Mix 2 (psi) W/C=0.42 fly ash =10% Slag = 60%	Mix 7 (psi) W/C=0.41 fly ash =10% Slag = 60%	Mix 11 (psi) W/C=0.41 fly ash =10% Slag = 60%	Mix 12 (psi) W/C=0.41 fly ash =10% Slag = 60%
7 days	660	630	650	705	640
28 days	870	775	830	790	775
91 days	885	810	900	830	870
182 days	915	855	990	925	895

The second category is slag and fly ash mix designs with water cement ratio lower than 0.4. This category includes mixes 4, 9, 13, and 14 as shown in Table 7-25. These mixes are class V and higher structural concrete.

Table 7-25. Flexural strength test results for slag and fly ash ternary blend concrete mixes with W/C lower than 0.4.

Testing age	Mix 4 (psi) W/C=0.33 fly ash =10% Slag = 60%	Mix 9 (psi) W/C=0.33 fly ash =10% Slag = 60%	Mix 13 (psi) W/C=0.33 fly ash =10% Slag = 60%	Mix 14 (psi) W/C=0.33 fly ash =10% Slag = 60%
7 days	770	675	760	745
28 days	960	910	855	825
91 days	975	920	890	875
182 days	1060	1050	910	885

The third category is silica fume and fly ash mix designs containing type I/II cement. This category includes mixes 3, 5, and 6 as shown in Table 7-26.

Table 7-26. Flexural strength test results for silica fume and fly ash ternary blend concrete mixes with W/C containing Type I/II Portland cement.

Testing age	Mix 3 (psi) W/C=0.35 fly ash =21% Silica fume = 9%	Mix 5 (psi) W/C=0.31 fly ash =22% Silica fume = 9%	Mix 6 (psi) W/C=0.31 fly ash =21% Silica fume = 9%
7 days	775	840	885
28 days	885	960	990
91 days	915	935	890
182 days	930	1000	960

The fourth category is silica fume and fly ash mix designs containing type III cement.

This category includes mixes 8 and 10 as shown in Table 7-27.

Table 7-27. Flexural strength test results for silica fume and fly ash ternary blend concrete mixes containing Types III Portland cement.

Testing age	Mix 8 (psi) W/C=0.35 fly ash =21% Silica fume = 9%	Mix 10(psi) W/C=0.31 fly ash =22% Silica fume = 9%
7 days	815	865
28 days	860	905
91 days	905	870
182 days	910	920

7.3.2.4 Modulus of Elasticity

The Modulus of Elasticity (MOE) test results were recorded and plotted as a function of time in order to understand its relationship with time, as shown in Figure 7-8.

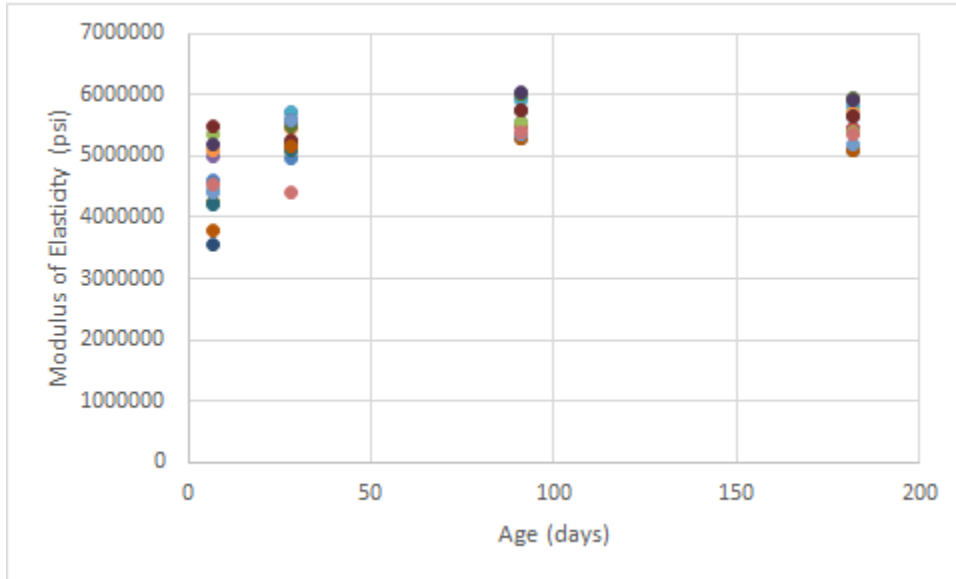


Figure 7-8. Modulus of elasticity versus age.

The first category is slag and fly ash mix designs with water cement ratio higher than 0.4 regardless of the type of cement. This category includes mixes 1, 2, 7, 11, and 12 as shown in Table 7-28.

Table 7-28. MOE test results for slag and fly ash ternary blend concrete mixes with W/C higher than 0.4.

Testing age	Mix 1 (psi) W/C=0.41 fly ash =10% Slag = 60%	Mix 2 (psi) W/C=0.42 fly ash =10% Slag = 60%	Mix 7 (psi) W/C=0.41 fly ash =10% Slag = 60%	Mix 11 (psi) W/C=0.41 fly ash =10% Slag = 60%	Mix 12 (psi) W/C=0.41 fly ash =10% Slag = 60%
7 days	4,600,000	4,250,000	3,550,000	4,200,000	3,800,000
28 days	5,050,000	5,100,000	5,200,000	5,100,000	5,150,000
91 days	5,550,000	5,500,000	5,750,000	5,300,000	5,300,000
182 days	5,450,000	5,450,000	5,650,000	5,100,000	5,100,000

The second category is slag and fly ash mix designs with water cement ratio lower than 0.4. This category includes mixes 4, 9, 13, and 14 as shown in Table 7-29.

Table 7-29. MOE test results for slag and fly ash ternary blend concrete mixes with W/C lower than 0.4.

Testing age	Mix 4 (psi) W/C=0.33 fly ash =10% Slag = 60%	Mix 9 (psi) W/C=0.33 fly ash =10% Slag = 60%	Mix 13 (psi) W/C=0.33 fly ash =10% Slag = 60%	Mix 14 (psi) W/C=0.33 fly ash =10% Slag = 60%
7 days	5,000,000	4,250,000	4,950,000	4,550,000
28 days	5,700,000	5,500,000	5,600,000	4,400,000
91 days	5,950,000	6,000,000	5,350,000	5,400,000
182 days	5,950,000	5,950,000	5,200,000	5,350,000

The third category is silica fume and fly ash mix designs containing Type I/II cement.

This category includes mixes 3, 5, and 6 as shown in Table 7-30.

Table 7-30. MOE test results for silica fume and fly ash ternary blend concrete mixes with W/C containing Type I/II Portland cement.

Testing age	Mix 3 (psi) W/C=0.35 fly ash =21% Silica fume = 9%	Mix 5 (psi) W/C=0.31 fly ash =22% Silica fume = 9%	Mix 6 (psi) W/C=0.31 fly ash =21% Silica fume = 9%
7 days	5,350,000	5,250,000	5,100,000
28 days	5,100,000	5,700,000	5,450,000
91 days	5,550,000	5,900,000	5,750,000
182 days	5,400,000	5,800,000	5,700,000

The fourth category is silica fume and fly ash mix designs containing Type III cement.

This category includes mixes 8 and 10 as shown in Table 7-31.

Table 7-31. MOE test results for silica fume and fly ash ternary blend concrete mixes with W/C containing Type III Portland cement.

Testing age	Mix 8 (psi) W/C=0.35 fly ash =21% Silica fume = 9%	Mix 10(psi) W/C=0.31 fly ash =22% Silica fume = 9%
7 days	5,500,000	5,200,000
28 days	5,250,000	5,600,000
91 days	5,750,000	6,050,000
182 days	5,650,000	5,900,000

7.4 Developed Prediction Equations

Statistical analyses were performed on the strength data to develop prediction equations for estimation of 28-day compressive strength of ternary blend concrete mixes from their compressive strength at other curing times. Statistical analyses were also performed to relate compressive strength of these mixes to their elastic modulus, splitting tensile strength, and flexural strength. These statistical analyses are presented in Appendix G. This section presents the summary of the results of these analyses.

Based on the strength gain characteristics of ternary blend mixes as evaluated by their strength gaining factor ($f'(t)/f'(28)$) in this laboratory study, the ternary blend mixes in Florida can be divided into four categories, and separate prediction equation can be used for each category of mix for estimation of 28-day compressive strength from compressive strength at other curing times. Table 7-32 presents the recommended prediction equations for estimating compressive strength at other curing times from compressive strength at 28 days. Table 7-33 presents the recommended prediction equations for estimating 28-day compressive strength from compressive strength at other curing times.

Table 7-32. Recommended equations for estimating compressive strength at other curing time from 28-day compressive strength.

Model	Category	Coefficient
$f'_c(t) = f'_c(28) \cdot A \cdot e^{-(B/t)^C}$	Fly ash & Slag (W/C > 0.4)	A = 1.25 B = 3.14 C = 0.72
	Fly ash & Slag (W/C < 0.4)	A = 1.14 B = 1.86 C = 0.90
	Fly ash & Silica fume Type I/II cement	A = 1.19 B = 0.92 C = 0.50
	Fly ash & Silica fume Type III cement	A = 1.16 B = 0.53 C = 0.47

Table 7-33. Recommended equations for estimating 28-day compressive strength from compressive strength at other curing time.

Model	Category	Coefficient
$f'_c(28) = f'_c(t) \cdot A \cdot e^{(B/t)^C}$	Fly ash & Slag (W/C > 0.4)	A = 0.80 B = 3.14 C = 0.72
	Fly ash & Slag (W/C < 0.4)	A = 0.88 B = 1.86 C = 0.90
	Fly ash & Silica fume Type I/II cement	A = 0.84 B = 0.92 C = 0.50
	Fly ash & Silica fume Type III cement	A = 0.86 B = 0.53 C = 0.47

Based on the test results from this laboratory study on ternary blend mixes, the following prediction equations were developed for relating compressive strength to other strength properties of ternary blend mixes in Florida:

For relating compressive strength (f'_c) to modulus of elasticity (E):

$$E = 81,000 \cdot (f'_c)^{0.46} \quad (7-1)$$

For relating compressive strength to splitting tensile strength (f_t):

$$f_t = 1.29 \cdot (f'_c)^{0.69} \quad (7-2)$$

For relating compressive strength (f'_c) to flexural strength (f_r):

$$f_r = 8.43 \cdot (f'_c)^{0.51} \quad (7-3)$$

Since the findings and developed prediction equations were based on a limited testing program on only 14 concrete mixes, it is recommended a more extensive testing program be conducted to verify and refine the developed equations.

CHAPTER 8 DEVELOPMENT OF USER-FRIENDLY SOFTWARE FOR THERMAL ANALYSIS OF MASS CONCRETE

8.1 Introduction

TNO DIANA computer software is a versatile finite-element program, which has been effectively used in thermal analysis of mass-concrete structures in this research project. While the DIANA software is a powerful tool for performing thermal analysis of mass-concrete structures, the users of this software need to have a good knowledge of finite-element method, and the commands and procedures of the DIANA software. There was a need to develop a user-friendly interface software, so that someone without extensive training in finite-element method or the DIANA software can also perform thermal analysis of typical mass-concrete structures in Florida. To meet this need, a user-friendly interface software, named DIFG (Diana Input File Generator), was developed for use in thermal analysis of (1) rectangular concrete footings and (2) cylindrical concrete drilled shafts. In the running of the DIFG software, a screen display as shown in Figure 8-1 would appear, and the user only needs to enter the needed information as shown on the screen. (Please note that the lines and words that are marked in red in this figure are not part of the screen display, but are added to explain the different information on the screen display.) With the provided input information, DIFG would then perform a thermal analysis using the DIANA software to determine the temperature development and distribution of the specified mass concrete at early age.

This chapter presents the functions and features of this developed software. The detailed users' manual for this software is presented in Appendix N.

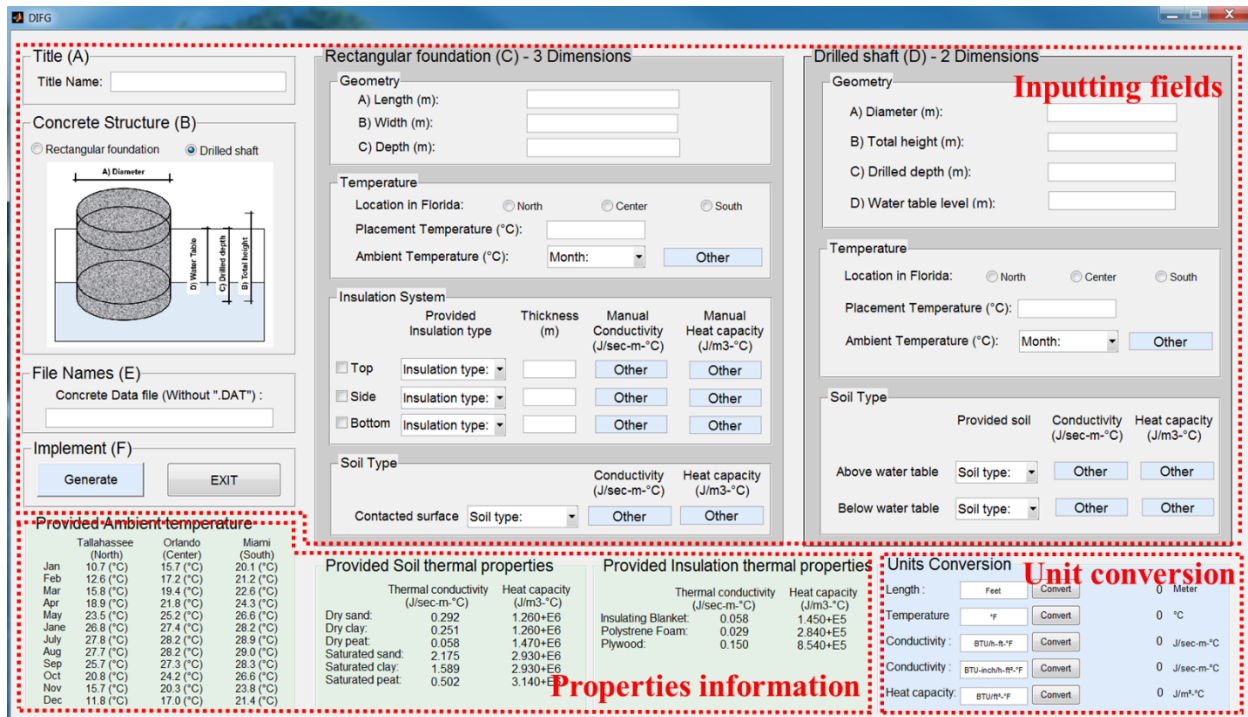


Figure 8-1. Screen display upon running of DIFG interface software.

8.2 Overview of DIFG

8.2.1 Three Main Steps in Thermal Analysis Using DIANA

In running the DIANA software to perform thermal analysis of mass concrete, the following three main steps usually need to be performed:

1. Pre-processing step – Information on the mass concrete are read in, and a finite-element geometric model for the mass concrete is then built.
2. Analysis step – Commands on how to analyze the geometric model are read in, and analysis is then performed. The results of the analysis are output to a result file with an extension of “.M72”.
3. Post-processing step – Commands are provided by the user on how to view and save the results of the analysis which are in the result file “*.V72”.

8.2.2 Main Functions of DIFG

The interface software, named DIFG (Diana Input File Generator), was developed to make the job of running thermal analysis of mass concrete using the DIANA software easier. It

is applicable to two types of concrete structures, namely (1) rectangular footing, and (2) cylindrical drilled shaft. In the running of the DIFG software, the user is prompted to provide information on (1) the dimensions of the mass concrete and insulation, (2) properties and condition of the concrete, soil, and insulation, and (3) initial concrete temperature and temperature of the environment. DIFG would then generate four input files, which are used to perform the thermal analysis and to present the results of the analysis using the DIANA software.

The four input files, which are generated by the DIFG in the intermediate steps, are as follows:

(1) Batch file (Run.bat) – This file contains commands which run (a) the pre-processing, (b) the analysis, and (c) the post-processing steps in the DIANA software automatically. (See an example file in Appendix I.)

(2) Pre-processing file (*.pre) – This file contains information on the structure to be analyzed. This information is used to build the geometric model in the pre-processing step. (See an example file in Appendix J).

(3) Command data file (*.dcf) – This file contains commands on how the geometric model is to be analyzed in the analysis step. (See an example file in Appendix K)

(4) Post-processing file (*.post) – This file contains commands on how the results from the analysis step are to be displayed in the post-processing step. (See an example file in Appendix L).

The user needs to provide a fifth input file, named “*.dat”, which contains information about the heat of hydration, thermal properties, and mechanical properties of the concrete used. This information is needed in the pre-processing step. (See an example file in Appendix M). The flow chart showing the main steps performed by DIFG is shown in Figure 8-2.

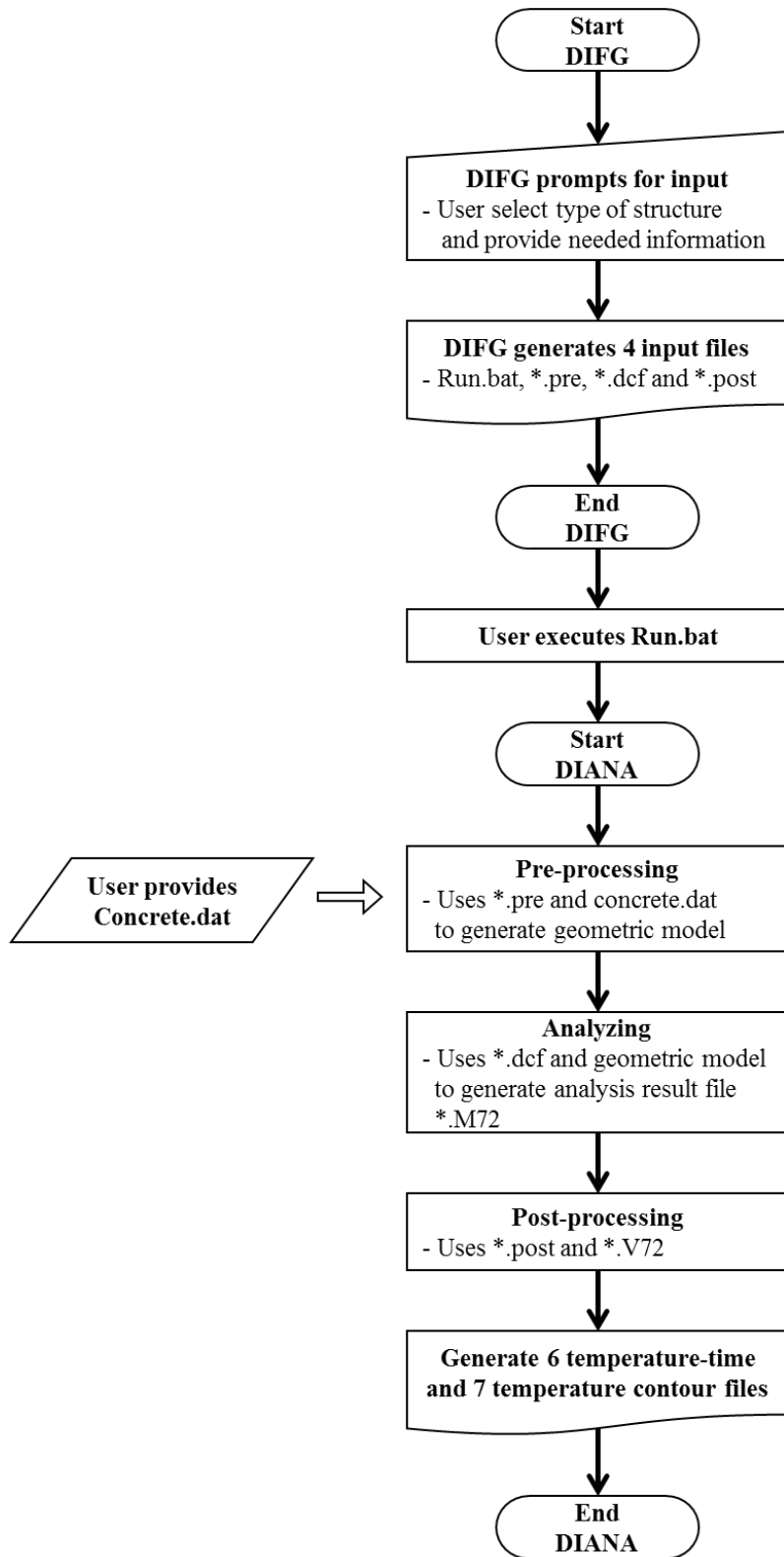


Figure 8-2. Flow chart showing main steps performed by DIFG and DIANA

8.3 Needed Inputs for Running of DIFG

8.3.1 Introduction

The developed software DIFG can be used to perform thermal analysis of either (1) rectangular concrete footings or (2) cylindrical concrete drilled shafts. This section describes the geometries of these two concrete structures, and the information that are needed as inputs to DIFG for each of these structures to be analyzed.

8.3.2 Needed information for Thermal Analysis of Rectangular Footing

The geometry of the rectangular footing that can be analyzed using DIFG is shown in Figure 8-3. As shown in the figure, the footing is placed on top of soil. The footing may have insulation on its top, bottom, and/or sides. The needed input information, which are entered manually by the user through the interface software DIFG, include the following:

- Length, width and depth of the footing (in meter).
- Insulation location (top, side, and bottom) system and thermal properties (conductivity and heat capacity) of insulation.
- Ambient temperature (in °C) of selected location in North, Center, and South Florida.
- Thermal properties (conductivity and heat capacity) of Soil.
- Initial concrete temperature (in °C).

The other needed information are the thermal properties and heat of hydration of the concrete used, and they are provided through a concrete data file named “*.dat”, which is specified by the user.

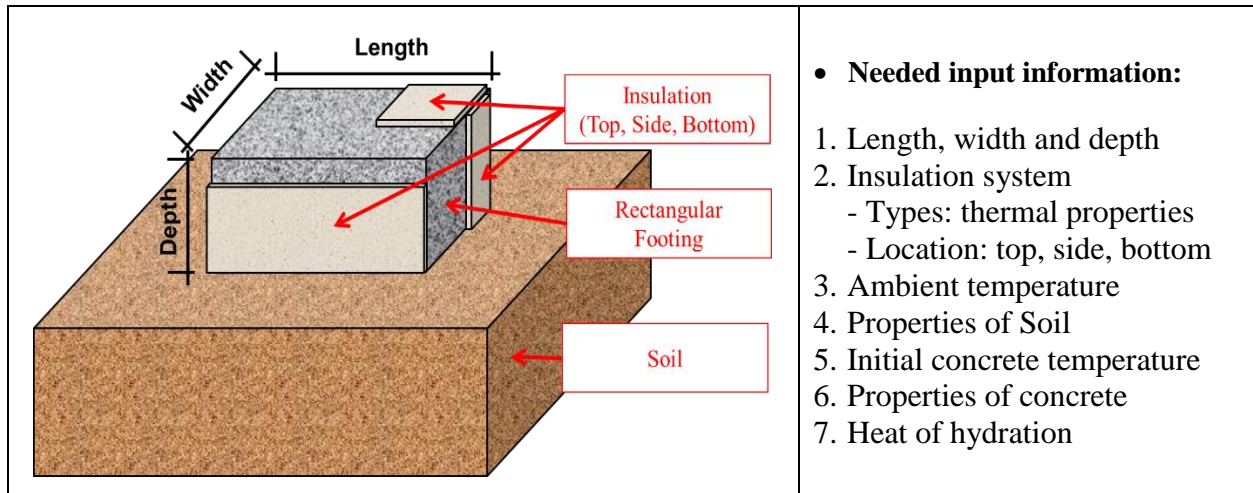


Figure 8-3. Geometry of the rectangular footing and needed inputs for thermal analysis

Figure 8-4 shows the different combinations of locations of insulation that can be used for rectangular footings. The user needs to specify the locations of insulations as well as the thermal properties of the insulation used.

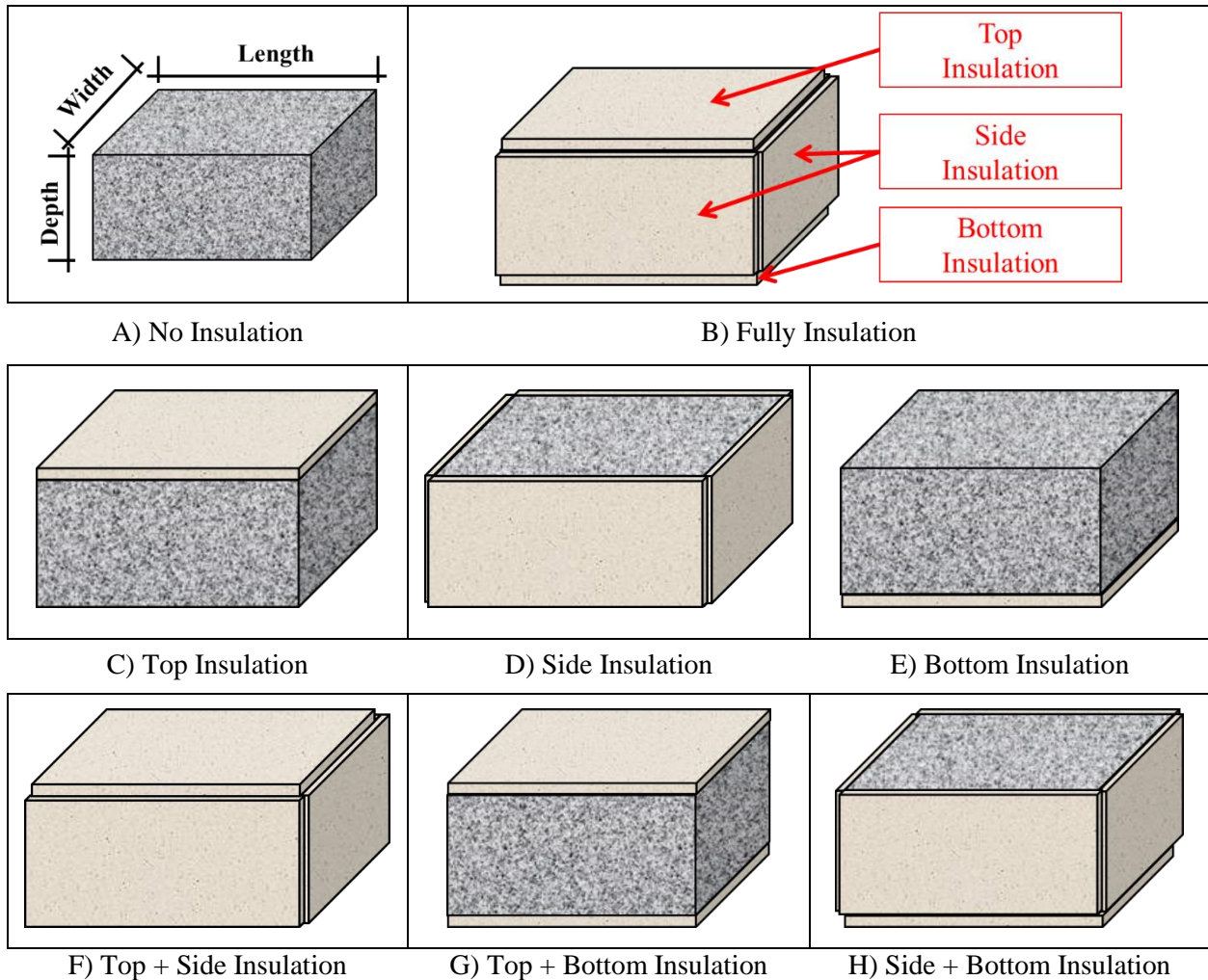


Figure 8-4. Various insulation for rectangular footing.

In the lower left corner of the interface screen as shown in Figure 8-1, some default values are provided for convenient use for (1) ambient temperature for different months of the year in Florida, (2) thermal properties of several types soil, and (3) thermal properties of several types of insulation materials.

The default ambient temperatures for the different months were obtained from the monthly average temperatures in Tallahassee (North Florida area), Orlando (Central Florida area), and Miami (South Florida area) from 1981 to 2010 as supplied by National Weather Service (2016). The monthly average ambient temperatures are presented in Table 8-1.

Table 8-1. Monthly mean ambient temperature (°C) in North, Central, and South Florida from 1981 to 2010.

	Jan	Feb	Mar	Apr	May	June	July	Aug	Sep	Oct	Nov	Dec
North Florida (Tallahassee)	10.7	12.6	15.8	18.9	23.5	26.8	27.8	27.7	25.7	20.8	15.7	11.8
Central Florida (Orlando)	15.7	17.2	19.4	21.8	25.2	27.4	28.2	28.2	27.3	24.2	20.3	17.0
South Florida (Miami)	20.1	21.2	22.6	24.3	26.6	28.2	28.9	29.0	28.3	26.6	23.8	21.4

The default thermal properties for various insulating materials and soils are obtained from references (Al-Homoud, 2005; Hillel, 1998). The default values of conductivity and heat capacity for various insulating materials and soils are shown in Table 8-2.

Table 8-2. Thermal properties of various insulating materials and soils

Conditions	Conductivity (J/s·m·°C)	Heat Capacity (J/m ³ ·°C)
Insulating Blanket	0.058	1.450×10 ⁵
Polystyrene Foam	0.029	2.840×10 ⁴
Plywood	0.150	8.540×10 ⁵
Dry sand	0.292	1.260×10 ⁶
Dry clay	0.251	1.260×10 ⁶
Dry peaty	0.058	1.470×10 ⁶
Saturated sand	2.175	2.930×10 ⁶
Saturated clay	1.589	2.930×10 ⁶
Saturated peaty	0.502	6.276×10 ⁶

The DIFG software uses the SI unit system, and all the inputs have to be in SI units. If needed, convenient conversions between U.S. customary units and SI units can be done by using the right lower corner of the interface screen as shown in Figure 8-1.

To model heat transfer through convection, a heat transfer coefficient of $30.0 \text{ W/m}^2 \cdot ^\circ\text{C}$ is used when the concrete is not insulated and is in direct contact with air. When there is an insulation between the concrete and air, a heat transfer coefficient of $3.0 \text{ W/m}^2 \cdot ^\circ\text{C}$ is used.

8.3.3 Needed information for Thermal Analysis of Drilled Shaft

The geometry of the cylindrical concrete drilled shaft that can be analyzed using DIFG is shown in Figure 8-5. As shown in the figure, most of the drilled shaft is placed under soil, and the water level in the soil needs to be known and properly specified. Unlike a rectangular footing which can have some insulation over it, a drilled shaft does not have insulation over it. The needed input information, which is entered manually by the user through the interface software DIFG, includes the following:

1. Diameter, total length, drilled depth and water table levels (in meter).
2. Ambient temperature (in $^\circ\text{C}$).
3. Thermal properties (conductivity and heat capacity) of dry soil above water level.
4. Thermal properties (conductivity and heat capacity) of wet soil below water level.
5. Initial concrete temperature (in $^\circ\text{C}$).

The other needed information is the thermal properties and heat of hydration of the concrete used, and they are provided through a concrete data file named “*.dat”, which is specified by the user.

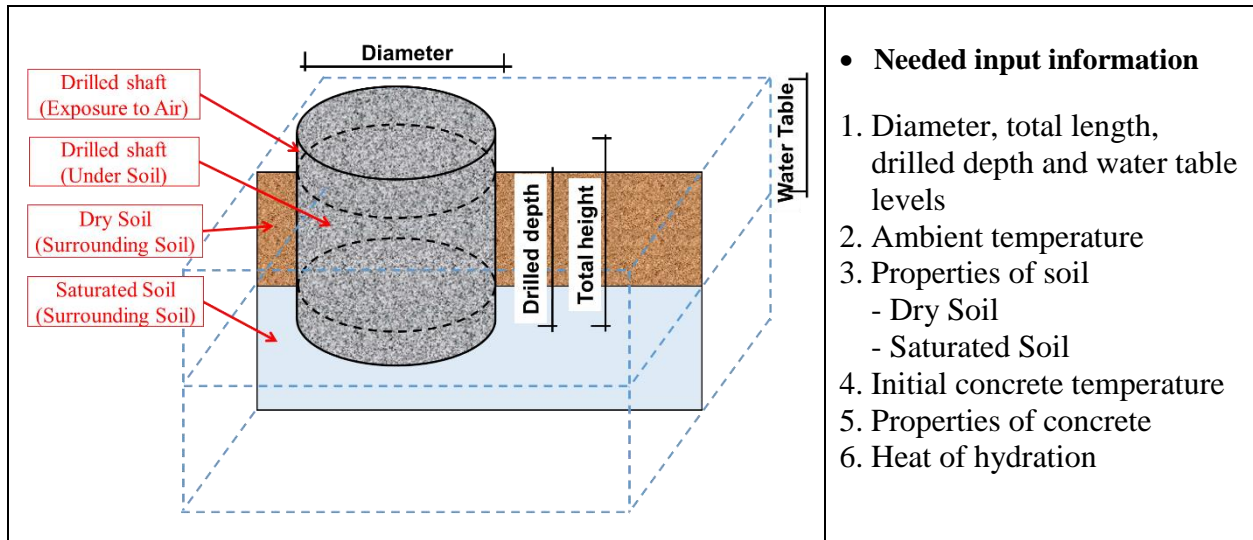


Figure 8-5. Geometry of the cylindrical drilled shaft and needed inputs for thermal analysis.

8.4 An Example of Thermal Analysis of a Drilled Shaft Using DIFG

8.4.1 Input Information for the Drilled Shaft TO BE Analyzed

Thermal analysis is to be performed on a cylindrical drilled shaft using DIFG. The following description presents the information on the drilled shaft which are to be entered through the DIFG interface software.

When the DIFG software is executed, a screen display as shown in Figure 8-6 will show up. (Please note that the lines and words that are displayed in red in this figure are not part of the screen display, but are added to indicate the different areas on the screen display.)

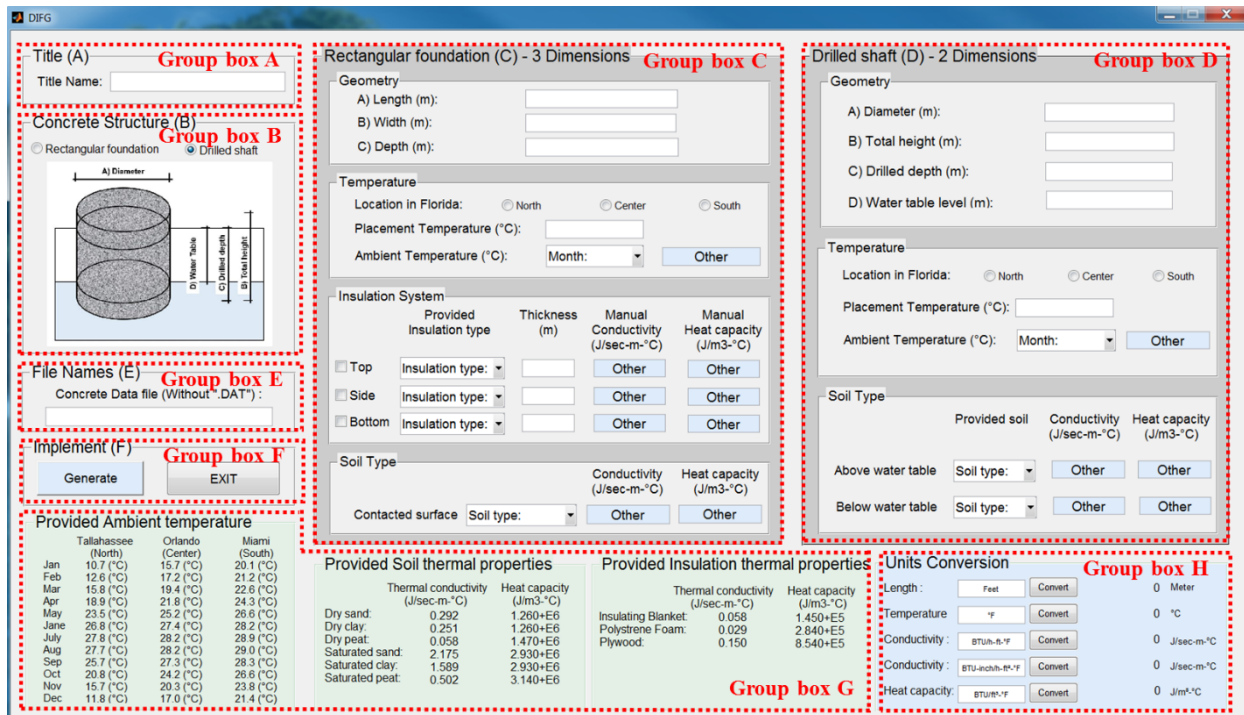


Figure 8-6. Grouping boxes in DIFG

- Step 1: Enter the title for this FE model. In this example, the title of “DS” is used in Group box A as shown in Figure 8-6.
(Note: This title will be used as the name of all saved files except the concrete data file.)
- Step 2: There are two options to select from – rectangular footing or drilled shaft. Select “Drilled shaft” in this example in Group box B.
- Step 3: Ignore the boxes in Group box C, since they deal with analysis of rectangular footing.
- Step 4: Enter a diameter of 1.8288 m, a height of 2.1336 m, a water table level of 1.2192 m and a drilled depth of 1.8288 m in the Geometry group in Group box D.
(Note: these numbers are the full dimensions of the drilled shaft. DIFG will generate a half-sized 2D model of the whole drilled shaft.)
- Step 5: In Temperature group, enter 26.0 (°C) for the placement temperature and click the “center” for location and choose the month of “January” for the ambient temperature in Group box D.
- Step 6: In Soil type group, choose the soil type of “Sand” for both above the water table and below the water table in Group box D.
(Note: The soil above the water table is considered as dry. On the other hand, the soil below the water table is considered as saturated.)

7. Step 7: Enter a name of concrete properties file. In this example, enter “concrete” without a file type of “dat” in Group box E. The concrete data file is presented in Appendix M.
8. Step 8: Click the button “Generate” in Group box F and the save window will appear to designate the directory for saving the batch file, the pre-processing file, the command file and the post-processing file. These files will be in the same folder with the concrete data file.
9. Step 9: After all the files have been saved, click the “Exit” button in Group box F to close the DIFG program.

8.4.2 Output Files from DIFG

Once the four input files have been generated by the DIFG software, they are ready to be used in the DIANA software for thermal analysis. When the user clicks the batch file named “RUN.bat”, all the steps in the thermal analysis will be performed automatically, including pre-processing, analysis and post-processing. The results of the analysis after post-processing are stored in thirteen (13) output files automatically.

There are six output files with extension of “PRT” and seven output files with extension of “PS”. The six PRT files have file names of “Cold1”, “Cold2”, “Cold3”, “Cold4”, “Cold5”, and “Hot”. They contain the calculated temperature-time history of the concrete at five possible coldest points and one hottest point in the concrete structure. Figure 8-7 shows the locations of these five coldest points and one hottest points for the rectangular footing and cylindrical drilled shafts. Figure 8-8 shows the content of file “Hot.PRT” from the analysis of the example drilled shaft.

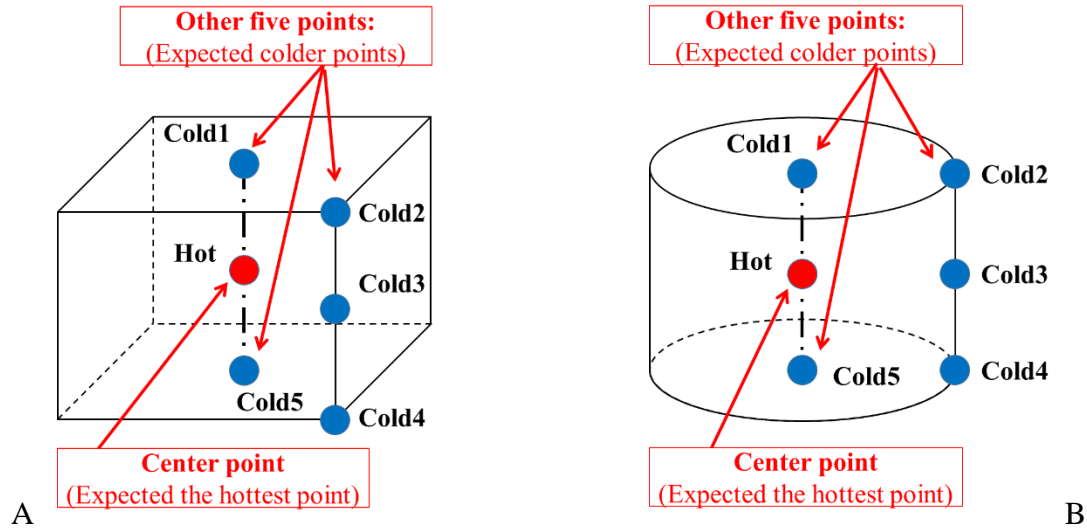


Figure 8-7. Locations of coldest and hottest points in rectangular footing and drilled shaft. A) rectangular footing and B) drilled shaft.

Point no.	X	Y
1,	.36E4,	20.6
2,	.72E4,	21.7
3,	.108E5,	22.6
4,	.144E5,	23.5
5,	.18E5,	24.7
6,	.216E5,	26
7,	.252E5,	27.4
8,	.288E5,	28.9
9,	.324E5,	30.4
10,	.36E5,	32
11,	.396E5,	33.8
12,	.432E5,	35.7
13,	.468E5,	37.7
14,	.504E5,	39.3
15,	.54E5,	40.7
16,	.576E5,	42
17,	.612E5,	43
18,	.648E5,	44
19,	.684E5,	44.9
20,	.72E5,	45.8
21,	.756E5,	46.6
22,	.792E5,	47.4
23,	.828E5,	48.1
24,	.864E5,	48.8

Figure 8-8. Content of Hot.PRT from analysis of example drilled shaft.

The seven output files with extension of “PS” have file names of “Day1”, “Day2”, “Day3”, “Day4”, “Day5”, “Day6, and “Day7”. They contain the temperature contour plots of the concrete structure at the end of the 1st, 2nd, 3rd, 4th, 5th, 6th, and 7th day after concrete placement. Figure 8-9 shows the temperature contour plot at 24 hours after concrete placement

as contained in the file “Day1.PS” from the analysis of the example drilled shaft. Figure 8-10 shows a close-up view of the same contour plot.

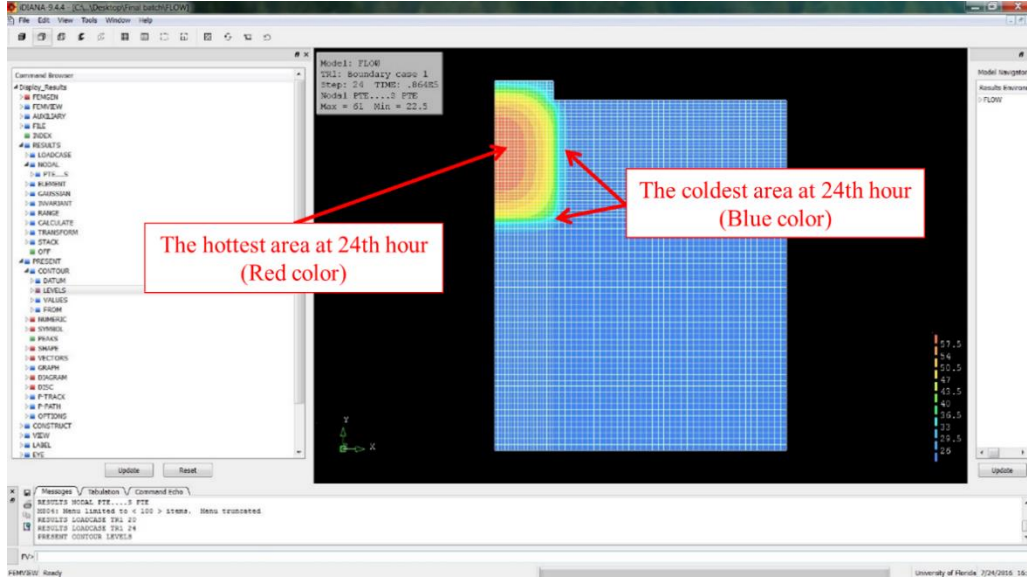


Figure 8-9. Temperature contour plot from Day1.PS.

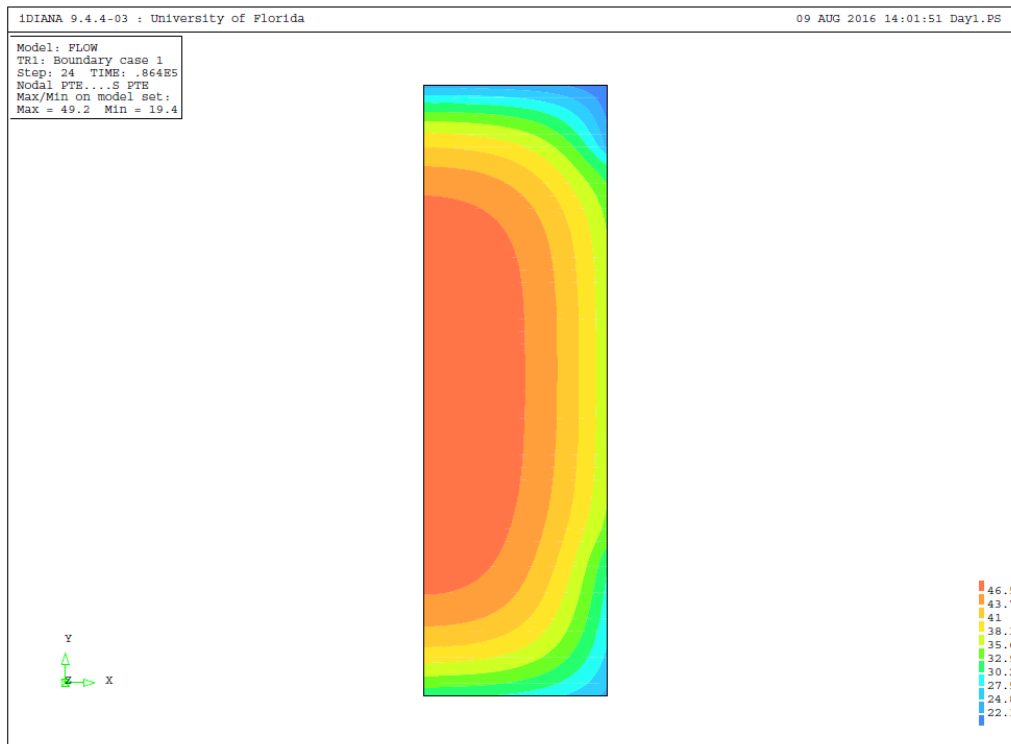


Figure 8-10. Close-up view of the temperature contour plot from Day1.PS.

CHAPTER 9
FINDINGS AND RECOMMENDATIONS

9.1 Summary of Work Accomplished and Main Findings

9.1.1 Development of Database of Rate of Heat Production of Cement Blends

Nine FDOT mix designs that are classified for use in mass concrete applications were identified. Samples of their cementitious components from these identified concrete mixes were tested for their heat of hydration with and without admixtures using the isothermal calorimetry chamber. Since the admixtures which were used in the concrete mixes in this testing program contained some retarders, the rate of hydration of the cement blend with admixtures was generally lower as compared with that of the corresponding cement blend without admixture. In order to be able to do a more conservative thermal analysis of mass concrete, the heat of hydration from the cement blends without admixture was used to develop the database of rate of heat production of cement blends for mass concrete. This database of adiabatic temperature rise tables can be used in the DIANA software for the modeling of mass concrete structures.

9.1.2 Thermal Analysis of Segmental Bridge Structures

Thermal analysis using the DIANA software were performed on typical segmental bridge pier segments used in Florida to evaluate their temperature development and distribution during construction. The main findings are as follows:

1. Classification of segmental bridge sections, as mass concrete structures, based on overall V/A ratio, is not adequate. Bridge sections with V/A ratios less than 1.0 feet could produce maximum temperature differentials which failed limits set by FDOT.
2. Local V/A ratio, which excludes extremities, is more appropriate in classifying and identifying segmental bridge sections as mass concrete structures.
3. Maximum temperatures and maximum temperature differentials of segmental bridge sections are greatly influenced by the heat of hydration of the cementitious materials used in the concrete.

4. Use of high-strength concrete in analysis produced the highest temperatures and temperature differentials.
5. Use of pozzolanic cementitious material replacement, in particular HVFA, greatly reduces the maximum temperature and maximum temperature differential in segmental bridge sections.

9.1.3 Determination of Thermal Properties of Soils in Different Moisture Conditions

A laboratory testing program was conducted to determine the R-values of several typical soils in Florida under varying moisture conditions. The test results show that moisture content is the main factor affecting the insulation property of soils. The R-value of soil decreases sharply as the moisture content increases. Variation in temperature has minimal effects on the R-value of soil.

9.1.4 Analytical Evaluation of Drilled Shafts

Finite element models using the DIANA software were developed to analyze the temperature development of drilled shaft under dry and wet conditions. The model developed was used to determine the effect the volume-to-surface area ratio of a drilled shaft, as well as the cementitious composition of the concrete mixture has on its thermal behavior. The temperature development of drilled shafts with centroid voids was also evaluated. The main findings are summarized as follows:

1. All concrete mixtures which were used in this study to model the thermal behavior of a drilled shaft with a diameter of over 4 feet produced maximum temperature differentials that exceeded the limit of 19.4 °C (35.0 °F) set by the FDOT.
2. For drilled shafts with diameters less than 6 feet, the maximum concrete temperature, and the maximum concrete temperature differential were not significantly affected by the depth of the drilled shaft.
3. The use of pozzolanic material as replacement for Portland cement reduced the maximum temperature and maximum temperature difference in the drilled shaft.
4. A shaft with centroid void is a viable alternative shaft design for controlling not only the maximum temperature but also the maximum temperature difference of mass concrete drilled shafts.

9.1.5 Field Evaluation of Drilled Shafts

Four concrete drilled shafts, which were 6 feet in diameter and 7 feet in length, were placed in a Florida soil to a depth of 6 feet to evaluate the temperature development in the concrete at early age subject to the effects of concrete mixes used and the moisture condition of the surrounding soil. The two concrete mixes used were a slag-cement concrete mix with a relatively low heat of hydration, and a pure Portland cement concrete mix with a high heat of hydration. The two soil conditions used were a dry condition and a wet condition.

The results of the study show that the use of slag-cement concrete mix had substantially reduced the maximum temperature differential in the drilled shafts. However, the maximum temperature differentials in all four shafts exceeded the maximum allowable limit of 19.4 °C (35.0 °F) according to FDOT specifications for mass concrete. For the two shafts which used a slag-cement concrete mix and placed in wet and dry soils, the maximum measured temperature differentials were 37.5 °C (67.5 °F) and 38.0 °C (68.4 °F), respectively. For the two shafts which used a pure Portland cement concrete mix and placed in wet and dry soils, the maximum measured temperature differentials were 49.5 °C (89.1 °F) and 50.0 °C (90.0 °F), respectively. For the two shafts which used a pure cement concrete mix, the maximum allowable temperature of 82.2 °C (180.0 °F) according to FDOT specifications for mass concrete was also exceeded.

For the four shafts tested, there was no significant difference between effects of the wet soil and dry soil environment. This was due to the fact that there was no difference in the first 4 feet of soil, and the difference in moisture condition of the soil beyond 4 feet depth was not enough to cause any noticeable difference in the developed temperature in the shafts.

Thermal analysis using the developed DIANA finite element model was performed to determine the temperature development of these four drilled shafts at early age. The computed temperatures were found to match fairly well with the measured temperature values. This

indicates that the finite element thermal analysis model used in this study can make fairly accurate prediction of temperature development in concrete drilled shafts at early age.

9.1.6 Laboratory Study on Strength Development of Ternary Blend Concrete Mixes

A laboratory testing program was conducted to study the strength development of ternary blend concrete mixes in Florida. Statistical analyses were performed to develop predictions which can be used for determining 28-day compressive strength from the strength of concrete that is older than 28 days. Based on the strength gain characteristics of ternary blend mixes as evaluated by their strength gaining factor ($f'(t)/f'(28)$) in this laboratory study, the ternary blend mixes in Florida can be divided into 4 categories and separate prediction equation can be used for each category of mix for estimation of 28-day compressive strength from compressive strength at other curing time. The recommended prediction equations for estimating 28-day compressive strength from compressive strength at other curing time are presented in Table 7-32 (in Chapter 7). Prediction equations were also developed for relating compressive strength to the elastic modulus, splitting tensile strength, and flexural strength of ternary blend mixes in Florida, and are presented in Equations 7-1, 7-2, and 7-3 (in Chapter 7).

9.1.7 Development of User-Friendly Interface Software for Mass Concrete Analysis

A user-friendly interface software, Diana Input File Generator (DIFG), was developed for use in thermal analysis of (1) rectangular concrete footings and (2) cylindrical concrete drilled shafts using the DIANA software. This developed interface software makes it possible for someone without extensive training in finite-element method or the DIANA software to perform thermal analysis of these two types of mass-concrete structures in Florida.

9.2 Recommendations

The following recommendations are made based on the findings from this study:

- (1) The database of adiabatic temperature rise tables which was developed in this study can be used in the DIANA software for the modeling of mass concrete structures. It is recommended that this database be expanded to include ternary blend mixes which are viable mix designs for mass concrete application.
- (2) Classification of segmental bridge sections should be based on local V/A ratio, which excludes extremities, when it is used to identify if a certain segmental bridge section is considered as a mass concrete structure. A thermal analysis should be performed if the LOCAL V/A ratio is very close to or exceeds 1.0 feet. A field study should be conducted to monitor the temperature development in segmental bridge sections during construction in order to validate the analytical results from the thermal analysis using the DIANA software.
- (3) Based on the results from laboratory testing program and literature review, the recommended thermal properties of various insulating materials and soils to be used in thermal analysis of mass concrete structures are presented in Table 8-2.
- (4) The results of thermal analysis indicate that a typical drilled shaft with a diameter of over 4 feet would have a maximum temperature differential that exceeded the limit of 19.4 °C (35.0 °F) set by the FDOT, and thus should be considered as mass concrete. However, the four drilled shafts placed in this study did not show any visible cracks in spite of the high temperatures differential, both calculated and measured. It is recommended that further investigation be undertaken to determine if the criterion for mass concrete could be relaxed for drilled shafts.

- (5) Prediction equations for estimating 28-day compressive strength from compressive strength at other curing time for ternary blend mixes were recommended. However, since the developed prediction equations were based on a limited testing program on only 14 concrete mixes, it is recommended a more extensive testing program be conducted to verify and refine the developed equations.
- (6) It is recommended that the developed interface software DIFG be used by FDOT personnel for quick thermal analysis of rectangular concrete footings and cylindrical concrete drilled shafts. After some period of evaluation of the software, further refinement and upgrade of the software can be done based on the needs of FDOT.

LIST OF REFERENCES

- ACI Committee 207. (2005). *Guide to mass concrete (207.1R-05)*. American Concrete Institute, Farmington Hills, MI.
- ACI Committee 207. (2007). *Report on thermal and volume change effects on cracking of mass concrete (207.2R-07)*. American Concrete Institute, Farmington Hills, MI.
- ACI Committee 225. (1999). *Guide to the selection and use of Hydraulic Cement (225R-99)*. American Concrete Institute, Farmington Hills, MI.
- ACI Committee 318. (2014). *Building Code Requirements for Reinforced Concrete (318R-14)*. American Concrete Institute, Farmington Hills, MI.
- ACI Committee 363. (2010). *Report on high-strength concrete (363R-10)*. American Concrete Institute, Farmington Hills, MI.
- Ahmad, S. H., and Shah, S. P. (1985). "Structural properties of high strength concrete and its implications for precast pre-stressed concrete." *PCI Journal*, 30(6), 92-119.
- Al-Homoud, M. S. (2005). "Performance characteristics and practical applications of common building thermal insulation materials." *Building and Environment*, 40(3), 353-366.
- ASTM C39/C39M. (2012). *Standard Testing Method for Compressive Strength of Cylindrical Concrete Specimens*. ASTM International, West Conshohocken, PA.
- ASTM C78/C78M. (2010). *Standard Test Method for Flexural Strength of Concrete (Using Simple Beam with Third-Point Loading)*. ASTM International, West Conshohocken, PA.
- ASTM C138/C138M. (2012). *Standard Test Method for Density (Unit Weight), Yield, and Air Content (Gravimetric) of Concrete*. ASTM International, West Conshohocken, PA.
- ASTM C143/C143M. (2010). *Standard Test Method for Slump of Hydraulic-Cement Concrete*. ASTM International, West Conshohocken, PA.
- ASTM C231/C231M. (2010). *Standard Test Method for Air Content of Freshly Mixed Concrete by the Pressure Method*. ASTM International, West Conshohocken, PA.
- ASTM C469/C469M. (2014). *Standard Test Method for Static Modulus of Elasticity and Poisson's Ratio of Concrete in Compression*. ASTM International, West Conshohocken, PA.
- ASTM C496/C496M. (2011). *Standard Test Method for Splitting Tensile Strength of Cylindrical Concrete Specimens*. ASTM International, West Conshohocken, PA.
- ASTM C989/C989M. (2014). *Standard Specification for Slag Cement for Use in Concrete and Mortars*. ASTM International, West Conshohocken, PA.

- ASTM C1064/C1064M. (2012). *Standard Test Method for Temperature of Freshly Mixed Hydraulic-Cement Concrete*. ASTM International, West Conshohocken, PA.
- ASTM C1702. (2015). *Standard Test Method for Measurement of Heat of Hydration of Hydraulic Cementitious Materials Using Isothermal Conduction Calorimetry*. ASTM International, West Conshohocken, PA.
- Bentz, D. P. (2009), "Influence of internal curing using lightweight aggregates on interfacial transition zone percolation and chloride ingress in mortars." *Cement and Concrete Composites*, 31(5), 285-289.
- Carino, N. J., and Lew, H. S. (1982). "Re-examination of the Relation between Splitting Tensile and Compressive Strength of Normal Weight Concrete." *Journal of American Concrete Institute*, 79(3), 214-219.
- CEB-FIP Model Code. (1993). *Final Draft*. CEB Bulletin D'Information, Lausanne Switzerland.
- Diana, T. (2011). *Finite Element Analysis User's Manual-Release 9.4.4*. TNO DIANA, Delft, Netherlands.
- Do, T. A. (2013). *Finite element modeling of behavior of mass concrete placed on soil*. Dissertation, University of Florida, Gainesville, FL.
- Engineering Toolbox (2014). *Specific Heats of Solids*. Retrieved from http://www.engineeringtoolbox.com/specific-heat-solids-d_154.html.
- Ferraro, C. C. (2009). *Determination of test methods for the prediction of the behavior of mass concrete*. Dissertation, University of Florida, Gainesville, FL.
- Florida Department of Transportation. (2016). *Standard specifications for road and bridge construction*. Florida Department of Transportation, Tallahassee, FL.
- Florida Department of Transportation. (2016). *Structures Design Guidelines*. Volume 1, Florida Department of Transportation, Tallahassee, FL.
- Gajda, J. (2007). "Mass Concrete for Buildings and Bridges." *Portland Cement Association*, Skokie, IL.
- Grace Concrete Products. (2011). *Darex AEA Air Entraining Admixture*. W. R. Grace, Columbia, MD.
- Grace Concrete Products. (2015). *Safety Data Sheet (SDS#60002) ADVA 120*. W. R. Grace, Columbia, MD.
- Grace Concrete Products. (2015). *Safety Data Sheet (SDS#60191) WRDA-60*. W. R. Grace, Columbia, MD.

- Hair, J. F., Black, W. C., Babin, B. J., and Anderson, R. E. (2009). *Multivariate data analysis*. Edition 6th, Pearson Prentice Hall, Upper Saddle River, NJ.
- Hakkinen, T. (1993). "The influence of slag content on the microstructure, permeability and mechanical properties of concrete." *Cement and Concrete Research*, 23(2), 407-421.
- Han-Seung, L., and Wang, X. (2016). "Evaluation of compressive strength development and carbonation depth of high volume slag-blended concrete." *Construction and Building Materials*, 124, 45-54.
- Hillel, D. (1998). *Environmental soil physics: Fundamentals, applications, and environmental considerations*. Edition 1st, Academic Press, Amherst, MA.
- Imbabi, M. S., Carrigan, C., and McKenna, S. (2012). "Trends and developments in green cement and concrete technology." *International Journal of Sustainable Built Environment*, 1(2), 194-216.
- Iravani, S. (1996). "Mechanical properties of high-performance concrete." *ACI Materials Journal*, 30(6), 416-426.
- Khan, M. I., and Siddique, R. (2011). "Utilization of silica fume in concrete: Review of durability properties." *Construction and Recycling*, 57, 30-35.
- Lawrence, A. M. (2009). *A finite element model for the prediction of thermal stresses in mass concrete*. Dissertation, University of Florida, Gainesville, Fl.
- Markandeya, A. (2014). *Determination of Internal Heat Generation Parameters for Mass Concrete Cementitious Systems*. Master of Science, University of Florida, Gainesville, Fl.
- Mehta, P. K. and Monteiro, P. J. M. (2014). *Concrete Microstructure, Properties, and Materials*. Edition 4th, McGraw-Hill, New York City, NY.
- National Weather Service. (2016). *Monthly Weather Summary in Tallahassee, Orlando and Miami*. Retrieved Aug 30, 2016 from <http://www.weather.gov>
- Nochaiya, T., Wongkeo, W., Chaipanich, A. (2010). "Utilization of fly ash with silica fume and properties of Portland cement-fly ash-silica fume concrete." *Fuel*, 89(3), 768-774.
- Oner, A., and Akyuz, S. (2007). "An experimental study on optimum usage of GGBS for the compressive strength of concrete." *Cement and Concrete Composites*, 29, 505-514.
- Plowman, J. M. (1956). "Maturity and the Strength of Concrete." *Magazine of Concrete Research*, 8(22), 13-22.
- Poole, J. L. (2007). *Modeling temperature sensitivity and heat evolution of concrete*. Dissertation, University of Texas at Austin, Austin, TX.

- Ramachandran, V.A. (1996). *Concrete Admixtures Handbook: Properties, Science, and Technology*. Edition 2nd, National Research Council, Ottawa, Canada.
- Rashid, M. A., Mansur, M. A., and Paramasivam, P. (2002). "Correlations between mechanical properties of high-strength concrete." *Journal of Material in Civil Engineering*, 14(3), 203-238.
- Rathan Raj, R., Perumal Pillai, E. B., and Santhakumar, A. R. (2013). "Evaluation and mix design for ternary blended high strength concrete." *Procedia Engineering*, 51, 65-74.
- Riding, K. A., Poole, J. L., Folliard, K. J., Juenger, M. C., and Schindler, A. K. (2012). "Modeling hydration of cementitious systems." *ACI Materials Journal*, 109(2), 225-234.
- Saridemir, M. (2013). "Effect of silica fume and ground pumice on compressive strength and modulus of elasticity of high strength concrete." *Construction and Building Materials*, 49, 484-489.
- Schindler, A. K., and Folliard, K. J. (2005). "Heat of hydration models for cementitious materials." *ACI Materials Journal*, 102(1), 24-33.
- Shannag, M. J. (2000). "High strength concrete containing natural pozzolan and silica fume." *Cement and Concrete Composites*, 22, 399-406.
- Thomas, M. D. A., Shehata, M. H., and Shashiprakash, S. G. (1999). "The Use of Fly Ash in Concrete: Classification by Composition." *Cement, Concrete, and Aggregates*, 21(2), 105-110.
- Tia, M., Yanjun, L., Boris, H., and Yu-Min, S. (2009). *Modulus of Elasticity, Creep and Shrinkage of Concrete – Phase II*. Florida Department of Transportation, Tallahassee, FL, Contract No: BD354.
- Tia, M., Ferraro, C., Lawrence, A., Smith, S., and Ochiai, F. (2010). *Development of Design Parameters for Mass Concrete using Finite Element Analysis*. Florida Department of Transportation, Tallahassee, FL, Contract No: BD545.
- Tia, M., Lawrence, A., Ferraro, C., Do, T. A., and Chen, Y. (2013). *Pilot Project for Maximum Heat of Mass Concrete*. Florida Department of Transportation, Tallahassee, FL, Contract No: BDK75-977-47.
- Triola, M. F. (1998). *Elementary Statistics*. Edition 7th, Addison Wesley Longman, Inc., Boston, IL.
- Wadsö, L. (2001). "Temperature changes within samples in heat conduction calorimeters." *Thermochimica Acta*, 366(2), 121-127.
- Wadsö, L. (2010). "Operational issues in isothermal calorimetry." *Cement and Concrete Research*, 40(7), 1129-1137.

Wetherill, Barrie. (1986). *Regression Analysis with Applications*. Chapman and Hall, London, United Kingdom.

Yazdani, N., and Mckinnie, S. B. (2004). *Time Dependent Compressive Strength and Modulus of Elasticity of Florida Concrete*. Florida Department of Transportation, Tallahassee, FL, Contract No: BD 221.

APPENDIX A
TYPICAL HIGH-STRENGTH CONCRETE DIANA INPUT FILE

CONDUC 2.2
CAPACI 2.675596E+06
ADIAB 0 23
3600 26.53418683
7200 27.07435325
10800 27.65247095
14400 28.43902563
18000 29.55789966
21600 31.07988297
25200 32.99514363
28800 35.24272363
32400 37.70660617
36000 40.27077444
39600 42.82314438
43200 45.3047244
46800 47.7017498
50400 50.04568275
54000 52.28539721
57600 54.39729653
61200 56.38531349
64800 58.26124641
68400 60.03296083
72000 61.70242314
75600 63.25193587
79200 64.68739816
82800 65.98521339
86400 67.14538154
90000 68.20723036
93600 69.15109598
97200 70.01630613
100800 70.80286082
104400 71.5304239
108000 72.19899538
111600 72.82823912
115200 73.41815513
118800 73.96874341
122400 74.49966782
126000 74.9912645
129600 75.50252504
133200 75.95479398
136800 76.40706293
140400 76.839668
144000 77.27227308

(Note: Explanations are in marked in red.)
Concrete conductivity
Heat Capacity concrete mixture
Adiabatic temperature Hours 0 -167

147600 77.68521429
151200 78.09815549
154800 78.49143283
158400 78.86504631
162000 79.23865978
165600 79.61227326
169200 79.98588673
172800 80.33983634
176400 80.69378595
180000 81.02807169
183600 81.36235743
187200 81.69664317
190800 82.03092891
194400 82.34555078
198000 82.66017265
201600 82.97479452
205200 83.2894164
208800 83.60403827
212400 83.91866014
216000 84.19395428
219600 84.50857615
223200 84.78387029
226800 85.09849217
230400 85.3737863
234000 85.64908044
237600 85.92437458
241200 86.19966872
244800 86.47496286
248400 86.750257
252000 87.02555114
255600 87.28118141
259200 87.53681168
262800 87.81210582
266400 88.04807222
270000 88.32336636
273600 88.55933277
277200 88.79529917
280800 89.07059331
284400 89.30655972
288000 89.54252612
291600 89.77849253
295200 90.01445893
298800 90.23076147
302400 90.44706401
306000 90.68303041
309600 90.91899681

313200 91.11563549
316800 91.35160189
320400 91.54824056
324000 91.78420697
327600 91.98084564
331200 92.17748431
334800 92.37412298
338400 92.61008938
342000 92.80672805
345600 93.00336672
349200 93.20000539
352800 93.39664406
356400 93.59328273
360000 93.78992141
363600 93.94723234
367200 94.14387101
370800 94.34050968
374400 94.53714835
378000 94.69445929
381600 94.89109796
385200 95.0484089
388800 95.24504757
392400 95.4023585
396000 95.59899717
399600 95.75630811
403200 95.95294678
406800 96.11025772
410400 96.26756865
414000 96.44454346
417600 96.62151826
421200 96.7788292
424800 96.93614013
428400 97.09345107
432000 97.25076201
435600 97.40807294
439200 97.56538388
442800 97.72269482
446400 97.88000575
450000 98.03731669
453600 98.19462763
457200 98.35193856
460800 98.5092495
464400 98.6272327
468000 98.78454364
471600 98.94185457
475200 99.09916551

478800 99.21714871
 482400 99.37445965
 486000 99.49244285
 489600 99.64975379
 493200 99.76773699
 496800 99.92504793
 500400 100.0430311
 504000 100.2003421
 507600 100.3183253
 511200 100.4756362
 514800 100.5936194
 518400 100.7116026
 522000 100.8689135
 525600 100.9868967
 529200 101.10488
 532800 101.2228632
 536400 101.3801741
 540000 101.4981573
 543600 101.6161405
 547200 101.7341237
 550800 101.8521069
 554400 101.989754
 558000 102.127401
 561600 102.2453842
 565200 102.3633674
 568800 102.4813506
 572400 102.5993338
 576000 102.717317
 579600 102.8353003
 583200 102.9532835
 586800 103.0516028
 590400 103.1499221
 594000 103.2679053
 597600 103.3858885
 601200 103.5038717
 604800 103.6218549

ARRHEN 4117.75

EQUAGE ARRTYP

TEMREF 23.0

YOUNG 2.523500E+10

POISON 2.000000E-01

DENSIT 2.2480000E+03

THERMX 9.160000E-06

FTTIME 0. 86400 172800 259200. 601200.

FTVALU 0. 1.25E+6 1.66E+6 1.93E+6 2.206E+6

MAXWEL 1

Arrhenius constant

Concrete reference Temperature

Young's Modulus

Poisson's Ratio

Density concrete

Thermal expansion coefficient

Tensile develop time 0 – 167 Hours

Tensile strength

APPENDIX B DEVELOPMENT of MIX DESIGN DATABASE 1.0

B.1 Introduction

The needed inputs to the finite element modeling of mass concrete include the properties of the cementitious materials used in the concrete mixes. Property files include both the thermal and structural material properties. Property files are text document files, which are used in finite element modeling of mass concrete to correctly model the temperature rise in a particular concrete mixture. Due to the large number of mix designs — and thus large number of property input files — an effective way to manage, organize and locate the desired property input files for use in finite element model applications is needed.

Establishing a database of this kind will allow the user to search and retrieve DIANA material input files more easily and efficiently. The proposed database has the potential to store hundreds of FDOT mix designs in an organized and efficient fashion — providing structure for the information and allowing it to be shared among different users and applications.

B.2 Overview of Database Applications

Database applications let users interact with information that are stored in databases. Program development tools like Microsoft's Visual Studio — software used in this report — provide support for relational database applications. Relational databases organize large sets of information into tables, which contain rows (records) and columns (fields). These tables can be manipulated by simple operations known as the relational calculus and thus be changed or edited when new information is available.

B.2.1 Types of Databases

Relational database servers vary in the way they store information and in the way they allow multiple users to access that information simultaneously. Visual Studio provides support for two types of relational database servers:

- **Remote Database Servers (RDS) as following:**
RDS's reside on a separate machine. Sometimes, the data from a remote database server do not even reside on a single machine, but are distributed over several servers. Although remote database servers vary in the way they store information, they provide a common logical interface to clients. This common interface is done through Structured Query Language (SQL).
- **Local Database (LD) as following:**
LDs reside on a local drive or on a local area network. They often have proprietary Application Programming Interfaces (APIs) for accessing the data. When they are shared by several users, they use file-based locking mechanisms.

Applications that use local databases are called single-tiered applications because the application and the database share a single file system. Applications that use remote database servers are called two-tiered applications or multi-tiered applications because the application and the database operate on independent systems (or tiers).

Local databases are faster than remote database servers because they reside on the same system as the database application. Also, local databases require less support than remote database servers. In addition, LDs are less expensive to operate because they do not require separately installed servers or expensive site licenses. As a result, a local database was chosen to be the most practical database server for this project.

B.3 Database Architecture

Database applications are built from user interface elements, components that represent database information (datasets), and components that connect these to each other and to the source of the database information. This section explains the general structure and the structural components of the material property database being developed.

B.3.1 General Structure

While there are many distinct ways to organize the components in a database application, the new database follows the general scheme illustrated in Figure B-1 below.

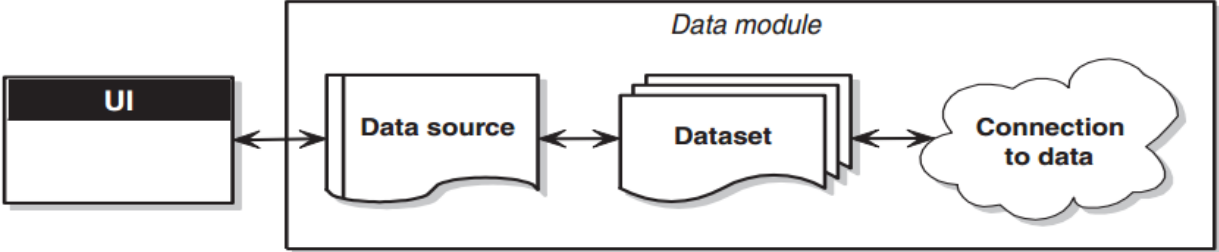


Figure B-1. Database architecture.

B.3.2 The User Interface (UI)

An isolated UI application will be used to manage, store, and manipulate data in the database. This has several advantages. By isolating the user interface from the components that represent the database information itself, we introduce a greater flexibility into the database design — changes to database information do not require reprogramming or rewriting of a new user interface, and changes to the user interface do not require reprogramming or rewriting the application that works with the database. In addition, this type of isolation allows development of common forms and files that can be shared between multiple applications, thereby providing a consistent user interface. Sharing forms and files also makes it possible for development of a shared application interface that can be accessed by multiple users at one time.

B.3.3 The Data Source and Dataset

Datasets are objects that contain data tables that temporarily store the data for use in the UI application. If the UI application requires working with data, it can load the data into a dataset, which provides the UI application with a local in-memory cache of the data to work with. One can work with the data in a dataset even if the application becomes disconnected from the database. The dataset maintains information about changes to its data, so updates can be tracked and sent back to the database when the UI application becomes reconnected. Datasets for this project are already integrated within the database program created by Visual Studio.

Mix designs within the database program are categorized by FDOT mix numbers and by mix property values found in the Deliverable of Subtask 1B report of the Maximum Heat of Mass Concrete – Phase 2 project.

The database includes the following information for each of the mixes:

- Water-to-cement ratio
- Unit weight
- Arrhenius constant
- Activation Energy
- Fly ash percentage
- Slag percentage
- Metakaolin (metaK) percentage
- Fine Aggregate (lb./yd³)
- Coarse aggregate (lb./yd³)
- Mix factor.

Tables B-1 and B-2 show the detailed property values for each of the mixes included within the database.

Table B-1. List of mixes included in this study.

MIX.	Cement (lb./ yd ³)	SCMs (lb./yd ³)			Fine Aggregate (lb./yd ³)	Coarse Aggregate (lb./yd ³)	W/B ratio	Unit Weight (lb./yd ³)
		Fly ash	Slag	Mk				
HVFA 1	365.00	365.00	-	-	1075.00	1770.00	0.30	140.60
HVFA 2	365.00	365.00	-	-	1079.50	1770.00	0.30	140.70
TB1	396.00	263.00	-	93.00	1125.00	1660.00	0.34	138.70
TB2	280.00	280.00	140.00	-	1058.00	1720.00	0.41	139.40
SB1	330.00	-	330.00	-	1062.00	1780.00	0.40	139.50
SB2	330.00	-	330.00	-	1103.00	1710.00	0.40	138.50
FB1	489.00	263.00	-	-	1082.00	1702.00	0.36	141.00
FB2	467.00	278.00	-	-	967.00	1778.00	0.37	139.40
FB3	455.00	245.00	-	-	1198.00	1600.00	0.38	139.40

Table B-2. Paste fractions of mixes tested in this study.

Mix	W/B ratio	Cement (g)	Fly Ash (g)	(%)	Slag (g)	(%)	Metakaolin (g)	Water (g)	Total (g)	% Material
07-0852 (SB1)	0.40	2.305	-	-	2.305	50%	-	1.863	6.473	71.2%
01-0550 (SB2)	0.40	2.305	-	-	2.305	50%	-	1.863	6.473	71.2%
03-1870 (FB1)	0.36	3.230	1.739	35%	-	-	-	1.789	6.759	73.5%
06-1202 (FB2)	0.37	3.059	1.821	37%	-	-	-	1.806	6.686	73.0%
01-1149 (TB1)	0.34	2.686	1.788	35%	-	-	0.633	1.737	6.844	74.6%
051526 (HVFA1)	0.3	2.804	2.804	50%	-	-	-	1.683	7.291	76.9%
061103 (HVFA2)	0.3	2.804	2.804	50%	-	-	-	1.683	7.291	76.9%
01-1099 (TB2)	0.41	1.827	0.913	20%	1.827	40%	-	1.872	6.439	70.9%
06-0531 (FB3)	0.38	3.114	1.677	35%	-	-	-	1.821	6.612	72.5%

B.4 Database Interface Program

The goal of the database is to easily categorize, identify, and select FDOT mix designs based on their thermal and mechanical properties. The database allows the user to navigate through the potential hundreds of mix designs within the FDOT catalogues. For this report, only the mass concrete mixes are displayed. This user-friendly database was developed using the Microsoft Visual Studio programming language and is designed to be used independently. The screen display for the interface is shown in Figure B-2.

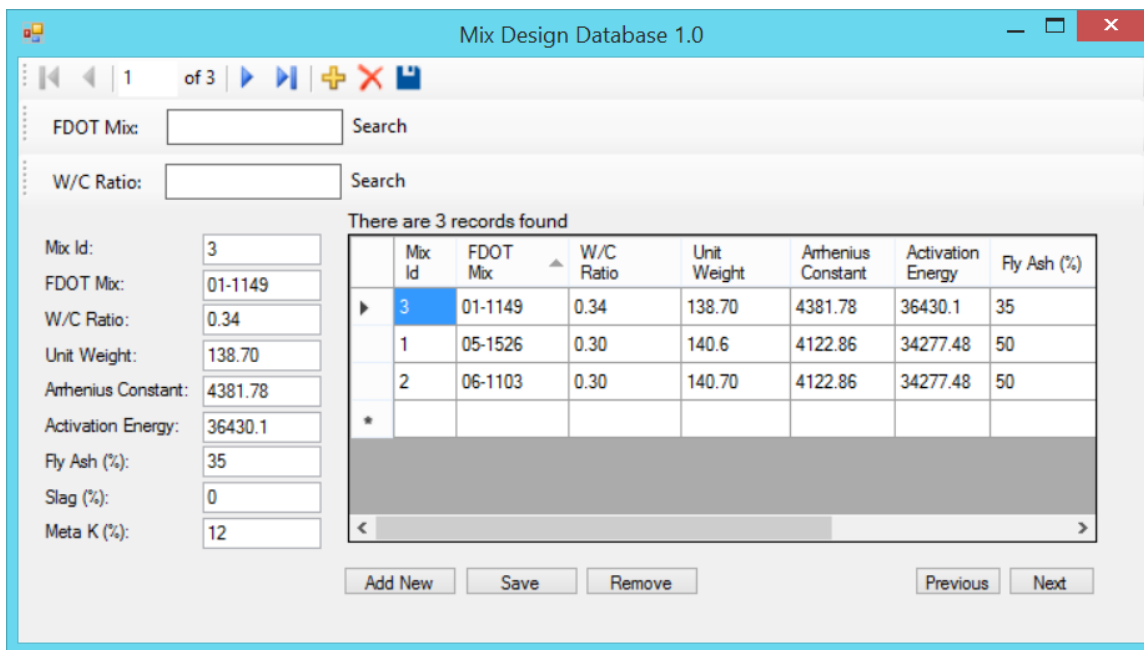


Figure B-2. Interface of database program for organizing FDOT mix designs.

Using the Mix Design Database (MDD) 1.0, any user can find, edit and add new mix design data in the database. Any mix design altered or added is automatically stored within the developed program. A user has the ability to search the database based on mix design's water-to-cement ratio values by typing them directly onto the search bar and pressing the button "search". A user can also search the database based on FDOT mix design numbers by typing them directly onto the search bar and pressing the button "search."

When a mix design is identified, MDD will isolate that particular mix design and show its properties both on the window (right side) and on the material property table (left side). This is illustrated in Figure B-3.

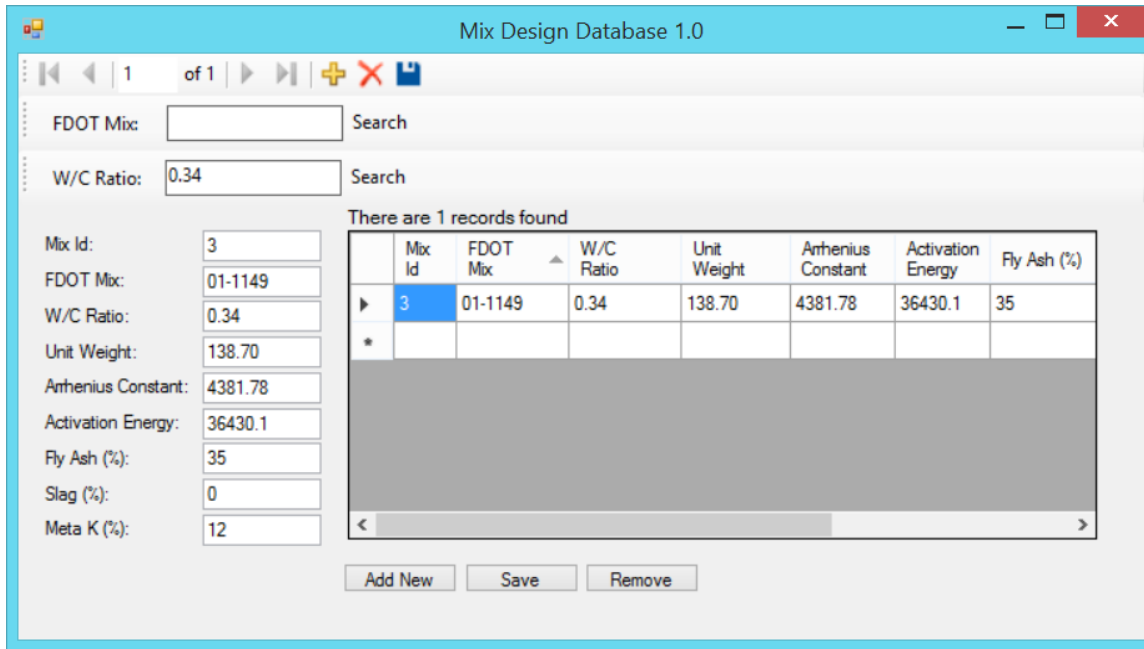


Figure B-3. Isolation of data for concrete mix design.

MDD will search the developed database for all mixes pertaining to the properties and present the mixes which meet the criteria to the user. If the user has typed in an incorrect property value or a property value of a mix not yet included in the database, a message will be shown on the screen by the software as shown in Figure B-4.

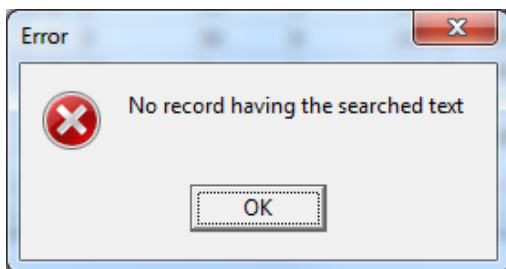


Figure B-4. Message indicating error in user entry or unavailability of data.

B.5 Example: How To Find a Mix Design Based on W/C Ratio

A mass concrete analysis is to be performed and analyzed using DIANA. The user would like to find the proper material information based on the following criteria:

- Water-to-cement ratio: 0.34

B.5.1 Step 1

Search by typing water-to-cement ratio onto search bar and pressing the button “Search”.

The Database Interface Program will automatically select and highlight all of the mixes which have the water-to-cement ratio of 0.34, as shown in Figure B-5.

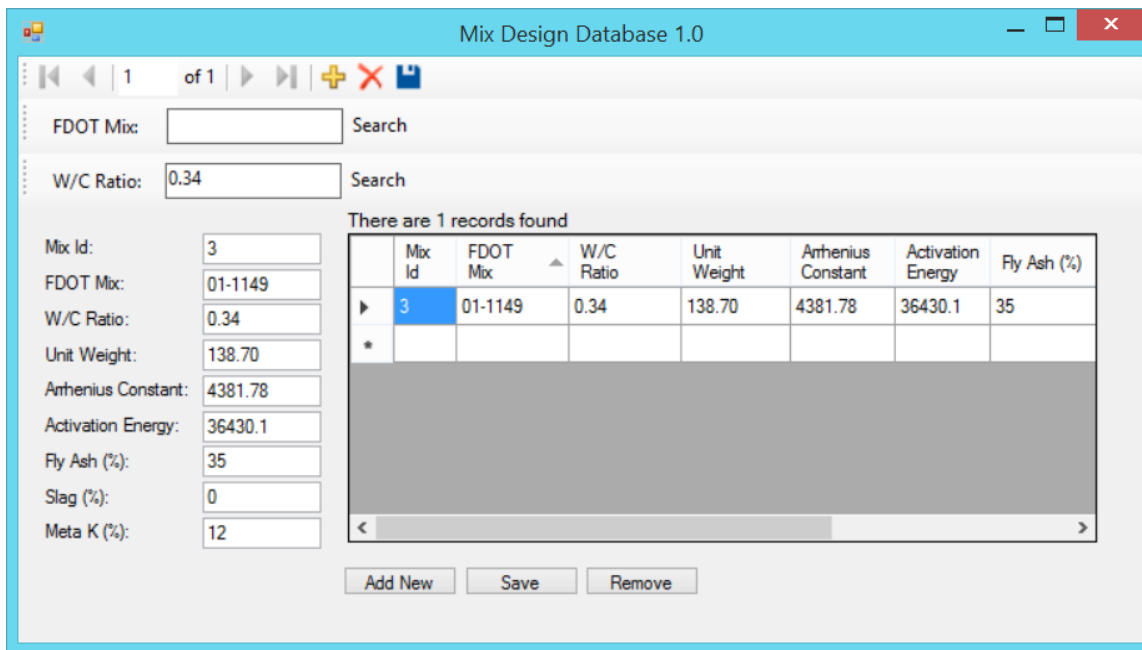


Figure B-5. Selection of data by W/C ratio.

B.5.2 Step 2

Select appropriate mix design. User can retrieve material property file for FDOT mix 01-1149, with W/C ratio of 0.34, to use for DIANA analysis.

B.6 Example: How To Find a Mix Design Based on Mix Number

A mass concrete analysis is to be performed and analyzed using DIANA. The user would like to find the proper material information based on the following criteria:

- FDOT Mix Number: 05-1526

B.6.1 Step 1

Search by typing the FDOT No onto search bar and pressing the button “Search”. The Database Interface Program will automatically select and isolate the mix which matches the Mix number searched. This is shown in Figure B-6.

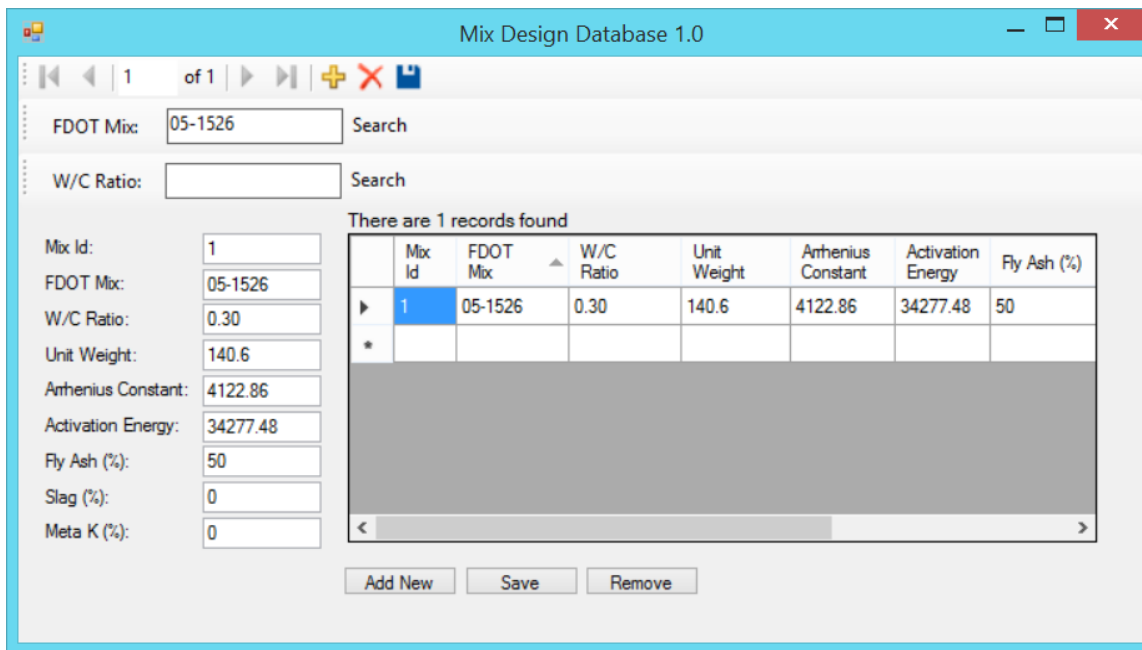


Figure B-6. Selection of data by mix number.

B.6.2 Step 2

Select appropriate mix design. User can retrieve material property file for FDOT mix 15-1526 to use for DIANA analysis.

B.7 Example: How To Change Mix Design Information

The following example shows how a user can edit the property value information listed on the database.

B.7.1 Step 1

Select or search for a mix within the MDD. The properties will be shown in the display window (right) and on the property table (left), as shown in Figure B-7.

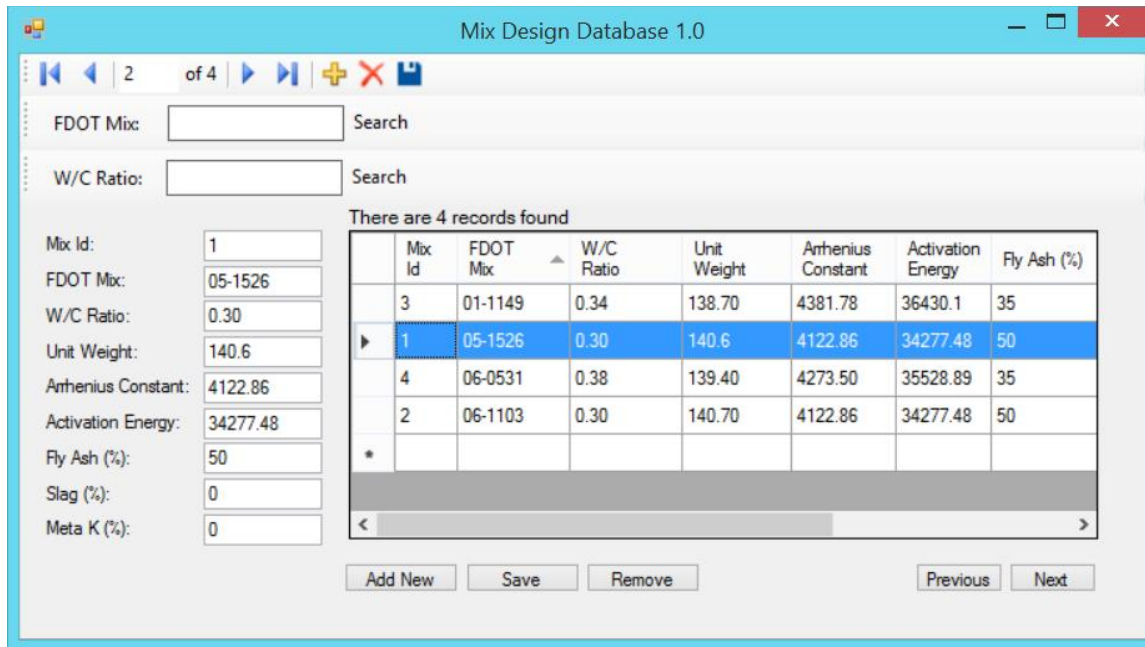


Figure B-7. Selection of a mix design to be edited.

B.7.2 Step 2

Click on the property table on the left and select the property to be edited. Double click on the property and change it to the desired value, as shown in Figure B-8.

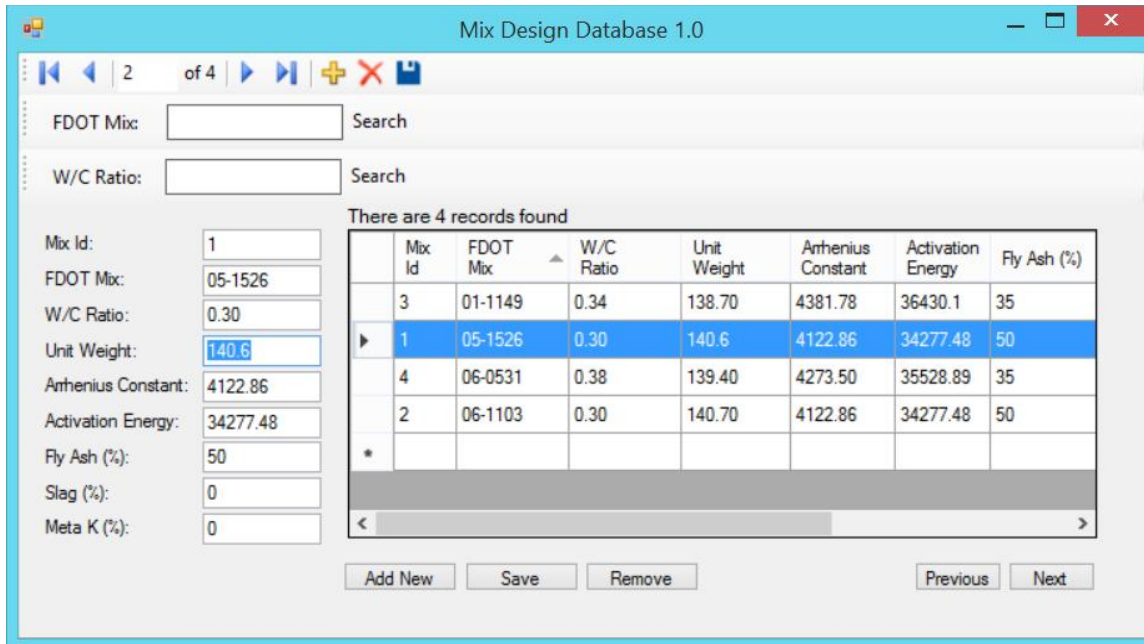


Figure B-8. Highlighting a property to be edited.

B.7.3 Step 3

Press the Save Button. All changes will be saved.

B.8 Example: How To Add New Mix Designs into the Database

This example shows the user how to add new mix design information and how to save it onto the database.

B.8.1 Step 1

Press “Add New” button at the bottom of the display screen of the Mix Design Database. A new row of information will be displayed on the table with a new Mix ID number, as shown in Figure B-9. Double click on the Mix Id to edit field and change to any value desired.

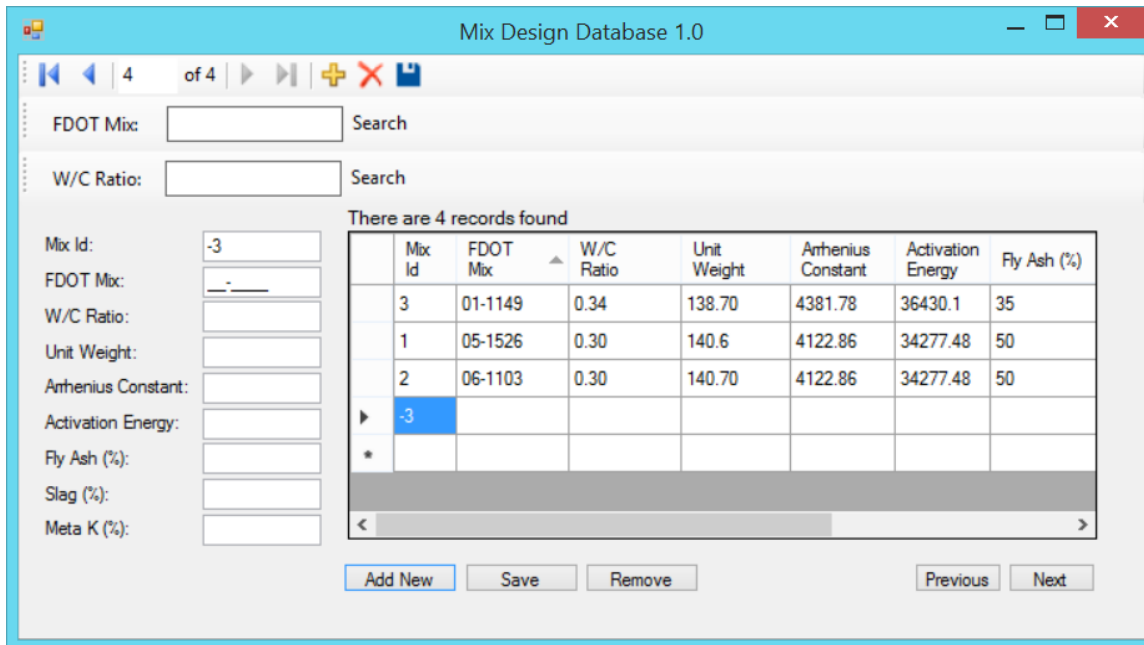


Figure B-9. Entering a new mix design entry (step 1).

B.8.2 Step 2

Enter the data for particular mix design into input table on the left, as shown in Figure B-10.

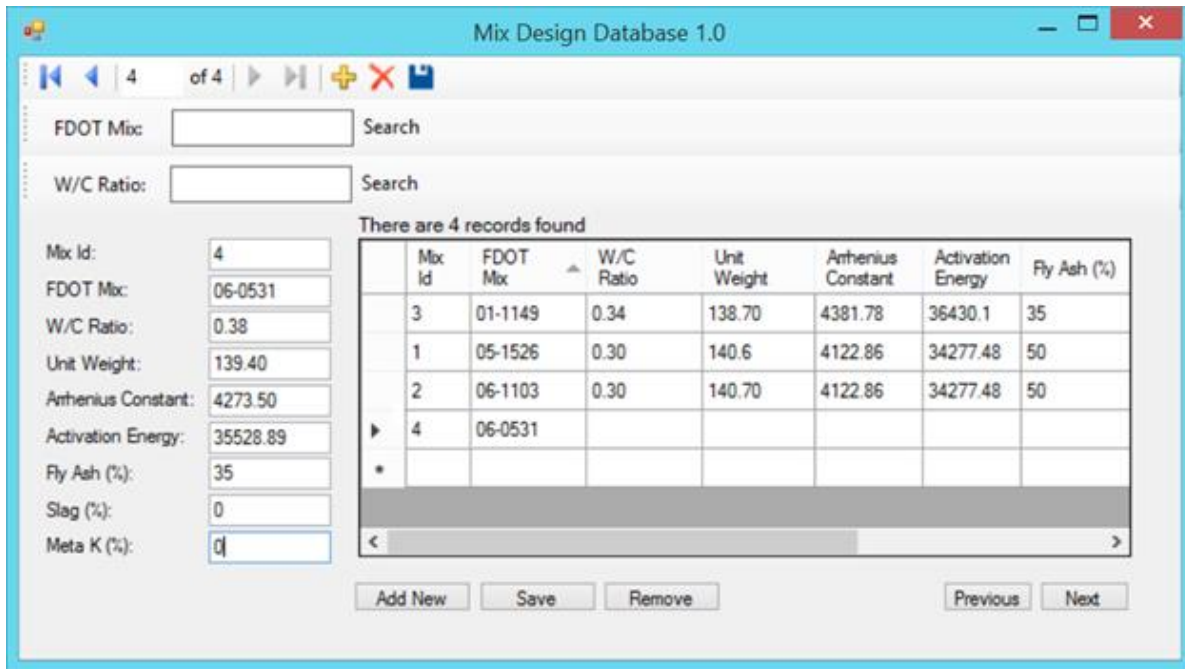


Figure B-10. Entering a new mix design entry (step 2).

B.8.3 Step 3

Press the Save Button. All changes on input table will be saved onto the database and shown on display chart.

APPENDIX C
CODES OF DATABASE MIX DESIGN DATABASE 1.0 FOR VISUAL STUDIO

Public Class Form1

Dim CCount As Integer = 0

Private Sub TableBindingNavigatorSaveItem_Click(sender As Object, e As EventArgs) Handles TableBindingNavigatorSaveItem.Click

Me.Validate()

Me.TableBindingSource.EndEdit()

Me.TableAdapterManager.UpdateAll(Me.ConMixesDataSet)

End Sub

Private Sub Form1_Load(sender As Object, e As EventArgs) Handles MyBase.Load
'TODO: This line of code loads data into the 'ConMixesDataSet.Table' table. You can
move, or remove it, as needed.

Me.TableTableAdapter.Fill(Me.ConMixesDataSet.Table)

Timer1.Start()

End Sub

Private Sub MetaK____TextBox_TextChanged(sender As Object, e As EventArgs) Handles MetaK____TextBox.TextChanged

End Sub

Private Sub MetaK____Label_Click(sender As Object, e As EventArgs)

End Sub

Private Sub Slag____TextBox_TextChanged(sender As Object, e As EventArgs) Handles Slag____TextBox.TextChanged

End Sub

Private Sub Slag____Label_Click(sender As Object, e As EventArgs)

End Sub

Private Sub Fly_Ash____TextBox_TextChanged(sender As Object, e As EventArgs) Handles Fly_Ash____TextBox.TextChanged

End Sub

Private Sub Fly_Ash____Label_Click(sender As Object, e As EventArgs)

End Sub

Private Sub Activation_EnergyTextBox_TextChanged(sender As Object, e As EventArgs)
Handles Activation_EnergyTextBox.TextChanged

End Sub

Private Sub Activation_EnergyLabel_Click(sender As Object, e As EventArgs)

End Sub

Private Sub Arrhenius_ConstantTextBox_TextChanged(sender As Object, e As EventArgs)
Handles Arrhenius_ConstantTextBox.TextChanged

End Sub

Private Sub Arrhenius_ConstantLabel_Click(sender As Object, e As EventArgs)

End Sub

Private Sub Unit_WeightTextBox_TextChanged(sender As Object, e As EventArgs) Handles
Unit_WeightTextBox.TextChanged

End Sub

Private Sub Unit_WeightLabel_Click(sender As Object, e As EventArgs)

End Sub

Private Sub W_C_RatioTextBox_TextChanged(sender As Object, e As EventArgs) Handles
W_C_RatioTextBox.TextChanged

End Sub

Private Sub W_C_RatioLabel_Click(sender As Object, e As EventArgs)

End Sub

Private Sub FDOT_MixTextBox_TextChanged(sender As Object, e As EventArgs)

End Sub

Private Sub FDOT_MixLabel_Click(sender As Object, e As EventArgs)

End Sub

```
Private Sub Mix_IdTextBox_TextChanged(sender As Object, e As EventArgs) Handles Mix_IdTextBox.TextChanged
```

```
End Sub
```

```
Private Sub Mix_IdLabel_Click(sender As Object, e As EventArgs)
```

```
End Sub
```

```
Private Sub Button1_Click(sender As Object, e As EventArgs) Handles Button1.Click  
Me.TableBindingSource.AddNew()
```

```
End Sub
```

```
Private Sub Button2_Click(sender As Object, e As EventArgs) Handles Button2.Click  
Try
```

```
Me.Validate()
```

```
Me.TableBindingSource.EndEdit()
```

```
Me.TableAdapterManager.UpdateAll(Me.ConMixesDataSet)
```

```
Catch ex As Exception
```

```
MessageBox.Show(ex.Message)
```

```
End Try
```

```
End Sub
```

```
Private Sub Button3_Click(sender As Object, e As EventArgs) Handles Button3.Click  
Me.TableBindingSource.RemoveCurrent()
```

```
End Sub
```

```
Private Sub Timer1_Tick(sender As Object, e As EventArgs) Handles Timer1.Tick  
COunt = TableBindingSource.Count
```

```
Label1.Text = "There are " & COunt & " records found"
```

```
If COunt > 1 And 2 Then
```

```
Button4.Visible = True
```

```
Button5.Visible = True
```

```
End If
```

```
If COunt <= 1 And 2 Then
```

```
Button4.Visible = False
```

```
Button5.Visible = False
```

```
End If
```

```
End Sub
```

```
Private Sub Button4_Click(sender As Object, e As EventArgs) Handles Button4.Click  
TableBindingSource.MoveNext()
```


End Sub

Private Sub Button5_Click(sender As Object, e As EventArgs) Handles Button5.Click
TableBindingSource.MovePrevious()

End Sub

Private Sub FDOTToolStripButton_Click(sender As Object, e As EventArgs)

End Sub

Private Sub FdotnewToolStripButton_Click(sender As Object, e As EventArgs)

End Sub

Private Sub FDOTMixToolStripButton_Click(sender As Object, e As EventArgs)

End Sub

Private Sub WtoCToolStripButton_Click(sender As Object, e As EventArgs)

End Sub

Private Sub MixToolStripButton_Click(sender As Object, e As EventArgs)

End Sub

Private Sub FDOTToolStripButton_Click_1(sender As Object, e As EventArgs)

End Sub

Private Sub FDOTToolStripButton_Click_2(sender As Object, e As EventArgs)

End Sub

Private Sub FDOTToolStripButton_Click_3(sender As Object, e As EventArgs)

End Sub

Private Sub FDOTMixToolStripButton_Click_1(sender As Object, e As EventArgs)

End Sub

Private Sub FdotToolStripButton_Click_4(sender As Object, e As EventArgs) Handles
FdotToolStripButton.Click

Try

Me.TableTableAdapter.Fdot(Me.ConMixesDataSet.Table, FdotToolStripTextBox.Text)

```
Catch ex As System.Exception
    System.Windows.Forms.MessageBox.Show(ex.Message)
End Try
```

```
End Sub
```

```
Private Sub WtocToolStripButton_Click_1(sender As Object, e As EventArgs) Handles
WtocToolStripButton.Click
```

```
    Try
        Me.TableTableAdapter.Wtoc(Me.ConMixesDataSet.Table, WtocToolStripTextBox.Text)
    Catch ex As System.Exception
        System.Windows.Forms.MessageBox.Show(ex.Message)
    End Try
```

```
End Sub
```

```
End Class
```

APPENDIX D
EQUIPMENT AND TEST PROCEDURE FOR EVALUATION OF INSULATION
PROPERTIES OF SOIL

D.1 Materials Tested

A laboratory testing program was developed to evaluate the insulation properties of several typical soils in Florida under various moisture and temperature conditions. For comparison purpose, the insulation properties of a lime rock, three Portland cement concretes, and an insulating mat material were also included in the testing program. The materials tested are presented in Table D-1.

Table D-1. Designation and origination of materials tested.

Material	Designation	Origination
Soil Sample 1	A-3	US 17 Nassau Co.
Soil Sample 2	A-7-5	US 17 Nassau Co.
Soil Sample 3	A-7-6	US 17 Nassau Co.
Soil Sample 4	A-2-4	US 17 Nassau Co.
Muck	77.59 % Organic content	US 17 Nassau Co.
Lime rock	-	Duval Co.
Concrete 1	Limestone, 57 stone	Lafayette Co.
Concrete 2	Limestone, 89 stone	Lafayette Co.
Concrete 3	Granite	Washington Co.
Insulation Mat	Polyethylene	FDOT SMO
Soil Sample 5	A-3	Alachua Co.
Soil Sample 6	A-3	Alachua Co.
Soil Sample 7	A-3	Alachua Co.
Soil Sample 8	A-3	Alachua Co.

Prior to conducting tests on the soil, muck, and lime rock samples, relevant analyses were conducted to determine the composition, group class, received moisture content, and particle size distribution. The standard tests performed to characterize these samples are shown in Table D-2. The results of these tests on the soil samples are summarized in Table D-3. The concrete samples also underwent analysis to determine such characteristics as strength and composition. The properties of the concrete samples are shown in Table D-4.

Table D-2. Standard tests used to characterize soil, muck, and lime rock samples.

Standard Designation	Test
ASTM C 136	Sieve Analysis
ASTM D 422	Particle-Size Analysis
ASTM D 2216	Moisture content
ASTM D 4318	Liquid Limit
ASTM D 4318	Plastic Limit

Table D-3. Properties of the soil samples,

Material	% Total Sand	% Silt	% Clay	% Passing									Material Passing #40		Group Class
				#8	#10	#16	#30	#40	#50	#60	#100	#200	LL	PL	
Sample 1	90	10	0	-	100	-	-	90.9	-	60.3	29.2	9.5	N.P.	N.P.	A-3
Sample 2	52	13	35	-	100	-	-	90.9	-	68.9	56.1	47.5	99	50	A-7-5
Sample 3	54	15	31	-	100	-	-	94	-	75.2	57.2	46	51	38	A-7-6
Sample 4	90	10	0	-	100	-	-	90.8	-	56.7	29.7	11.3	N.P.	N.P.	A-2-4
Sample 5	96	-	-	95.7	-	93.5	89.4	-	55.5	-	16.2	3.7	N.P.	N.P.	A-3
Sample 6	98	-	-	95.6	-	94.2	90.7	-	45.9	-	13.2	2.5	N.P.	N.P.	A-3
Sample 7	96	-	-	100	-	98.4	92.8	-	55.0	-	13.4	4.1	N.P.	N.P.	A-3
Sample 8	97	-	-	96.9	-	93.6	88.5	-	43.4	-	10.6	3.0	N.P.	N.P.	A-3

Table D-4. Properties and composition of concrete tested.

Sample	Compressive Strength at 28 days (psi)	Aggregate (lb./yd ³)	Sand (lb./yd ³)	Portland Cement (lb./yd ³)	Fly Ash (lb./yd ³)	Water (lb./yd ³)	Air Entrain. Admix.	Water Reducing Admixture
Concrete 1, #57	3500	725	1292	420	110	36	6 oz./yd ³	25.2 oz./ yd ³
Concrete 2, #89	3000	1625	1332	420	130	33	5 oz./ yd ³	50.4 oz./ yd ³
Concrete 3, Granite	4200	-	-	-	-	-	-	0 oz./ yd ³

D.2 Testing Equipment and Procedures

D.2.1 Thermal Properties Analyzer

The ASTM D5334-14 Standard Test Method for Determination of Thermal Conductivity of Soil and Soft Rock by Thermal Needle Probe Procedure was used to measure the insulation properties of these materials in units of R-value/inch. The KD2Pro thermal properties analyzer was used to measure the insulation properties of the test samples in accordance with this standard test method. The equipment comes with an assortment of probes to be used in different materials. The two probes used for this project are the TR1 probe and KS1 probe. The TR1 probe was used for all soil and concrete samples. The KS1 probe was used for the insulation mat

because it has a small probe and very little heat output. Figure D-1 shows the KD2Pro Thermal Properties Analyzer probes used in this study. The TR1 probe (used for soil and concrete) is pictured on the left and the KS1 probe (used for insulation mat) is depicted on the right. Figure D-2 shows the KD2Pro data recorder.



Figure D-1. KD2Pro thermal properties analyzer probes used.



Figure D-2. KD2Pro thermal properties analyzer data recorder.

According to the Operating Manual of the KD2Pro, when inserting the probe into cured concrete a lubricating compound needs to be placed on the probe to improve thermal conductivity between the probe and concrete. The Artic Silver compound was included in the KD2Pro kit and was used in this research to coat the TR1 probe. The Artic Silver thermal compound and the pilot pins are shown in Figure D-3.



Figure D-3. Artic Silver thermal compound and pilot pins used.

Before the wet concrete used in part of this study was allowed to cure, a pilot pin was inserted so that the probe would have a void to enter during testing of the cured product. To ease in both the insertion and removal of the pilot pin, the pin was coated in Vaseline oil prior to insertion in the wet concrete.

D.2.2 Temperature Control Box

The sample to be tested for its insulation properties was placed in a temperature-control box, so that the temperature of the test was controlled. The temperature-control box used in this study is an insulated 2 ft³ Coleman Cooler with a removable lid and a drain plug. The drain plug was completely removed to provide access for the testing equipment to enter/exit the box causing

the least amount of temperature fluctuations. Figure D-4 shows the Coleman cooler and the temperature control box. The drain plug on the bottom right of the cooler was removed and served as the opening where wires entered the unit.



Figure D-4. Temperature-control box used.

A Hunter 44100 A thermostat was used to control the turning on and off of a heating element (a 25-watt light bulb) inside the temperature-control box in order to control the temperature of the box. This standard household thermostat was chosen because unique programming properties were not needed. The thermostat, for the purposes of this study, was set to a one degree tolerance so as to better maintain a steady 35.0 °C (95.0 °F) within the temperature control box where its probe was placed. The thermostat remained external to the temperature control box so that temperature could be monitored throughout testing without disturbing the samples. The thermostat probe entered through the drain plug opening in the temperature control box.

The wiring going from the switched outlets on the temperature control unit to the porcelain light holder was a standard 14 gauge (AWG), stranded, insulated wire. A 12 gauge (AWG), stranded, copper conductor with ground, wire was used to power the temperature control unit circuit and was plugged into a 120 Volt outlet.

When the thermostat indicated that the temperature in the control box had dropped to 34.4 °C (94.0 °F), the thermostat would signal the relay to close the circuit thereby powering the red outlets used to turn on the light bulb. Once the unit reached 35.6 °C (96.0 °F), the thermostat would open the relay, breaking the circuit to the red outlets thereby turning off the light bulb. The 24V transformer converted the 120 V AC current into 24 V AC current because both the thermostat and relay required a 24 V power source. Figure D-5 shows the switched outlet, 24 V transformer, thermostat, and 24 V relay used. The red coloring on the left outlets designate them as switched outlets allowing them to turn on or off depending upon the input they receive from the thermostat, which is pictured on the far right in the figure.



Figure D-5. Switched outlet, transformer, thermostat, and relay used

Through experimenting with different heating elements, a 25-watt incandescent bulb was chosen to be the heating element utilized in the high temperature testing. The bulb was placed in a porcelain light fixture mounted to a gang box operated by the red outlet on the relay circuit.

Figure D-6 shows the porcelain light fixture used.



Figure D-6. Porcelain light fixture used.

In order to eliminate temperature fluctuations in the temperature-control box, all electronics and controllers were external to the temperature control unit so that data could be examined while testing was conducted. A half-inch hole located in the side of the unit allowed the necessary probes and sensors to enter with minimal heat transfer. The wires that entered through this hole were the TR1 probe, sensor for the KD2Pro, and the thermostat wire for the heating unit as well as a power cord that supplied 110 V power to the light bulb located inside the box. The temperature control circuit used 110 V power on the primary side of the transformer that reduced the voltage down to 24 V on the secondary winding. That 24 V power feed was the input to a Hunter 44100A thermostat. The temperature sensor on the thermostat

was routed through the half-inch opening in the box so as to continuously monitor the temperature within the unit. The thermostat then sent a small signal to pull in a 24 V relay that was used to complete a circuit for a switch outlet. This outlet was controlled by the thermostat. Plugged into this outlet was the 25-watt incandescent bulb that produced the heat to maintain a temperature of 35.0 °C (95.0 °F) within the temperature controlled testing unit. The setup is shown in Figure D-7.

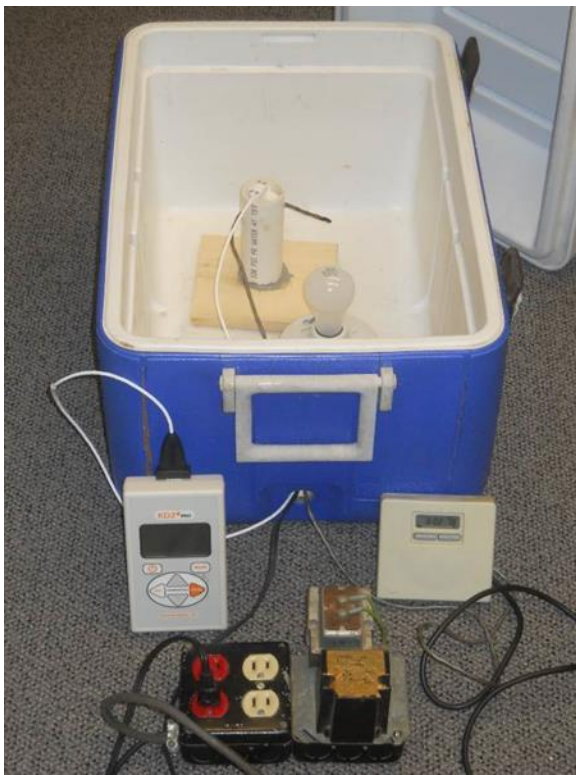


Figure D-7. Entire setup of the temperature control box.

D.2.3 Sample Container for Soil Samples

During both high and low temperature testing, the soil samples were placed in a 1.5 inch diameter PVC pipe affixed to a 5.5 inch X 6.5 inch wooden board. The PVC pipe was epoxied to the wood surface. The wood surface on the inside of the pipe was also coated with epoxy to prevent the wood from absorbing moisture from the samples placed inside. This size pipe was chosen based on the penetration depth and lateral spacing requirements set by the KD2Pro Thermal Properties Analyzer. Figure D-8 shows the PVC pipe which was epoxied to the wooden board.

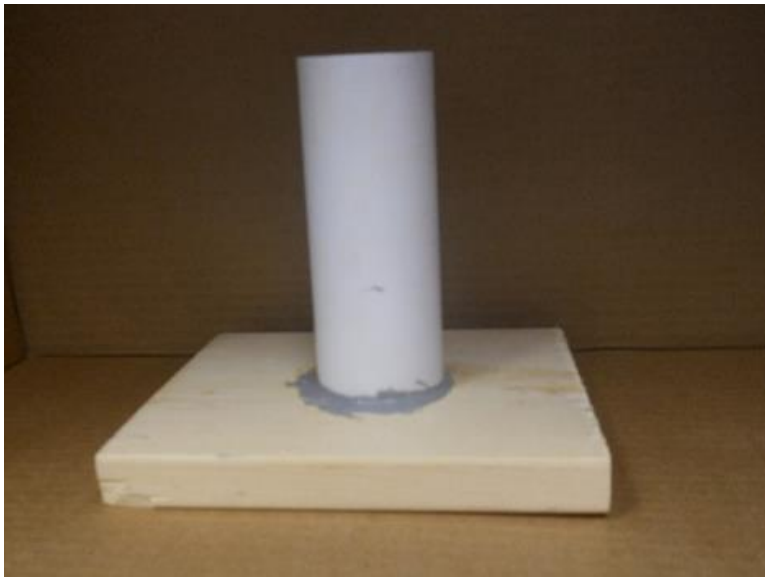


Figure D-8. PVC pipe epoxied to a wooden board.

The Operator's Manual of the Thermal Properties Analyzer covers good practices that should be followed during the testing procedure. The manual suggests that there must be at least 1.5 centimeters of material parallel to the probe in order to prevent error in measurement. The use of this sample holder allowed for full insertion of the probe while providing adequate material surrounding the probe as shown in Figure D-9.



Figure D-9. The PVC pipe with soil sample and TR1 probe in a 75° F testing condition.

D.2.4 Glass Jars for Holding Samples

Test samples were received in glass jars and were left in those jars at all times, except when that particular sample was undergoing testing. The glass jars ensured that the moisture content of the sample did not change due to absorption or evaporation. After a sample was tested, it was replaced into its jar. Figure D-10 shows a glass jar used to hold each sample before and after analysis.



Figure D-10. Glass jar used to hold soil sample.

D.2.5 Treatment of Test Samples

Each soil sample was tested under the following conditions of moisture and temperature: (1) in-situ moisture at 23.9 °C (75.0 °F), (2) in-situ moisture at 35.0 °C (95.0 °F), (3) 0 % moisture at 23.9 °C (75.0 °F), (4) 0 % moisture at 35.0 °C (95.0 °F), and (5) saturated moisture at 23.9 °C (75.0 °F). For testing at in-situ moisture condition, each test sample was placed in the PVC sample container for a four to five hour test. After the test, the soil sample was placed back into a sealed glass container. This ensured that very little change to the moisture condition of the soil occurred during the experiment. At the end of this portion of the experiment, the soil samples were taken to the Lake City Materials Lab where a moisture determination was made by drying the samples in a 110.0 °C (230.0 °F) oven for all samples except muck. The muck sample was dehydrated in a 60.0 °C (140.0 °F) oven to avoid organic burn off which would be likely to occur at 110.0 °C (230.0 °F). If muck's organic material were allowed to burn off in a 110.0 °C (230.0 °F) oven, weight of the sample would be reduced thereby obscuring what weight was due to material burn off and what weight was due to moisture burn off.

After being dehydrated in the ovens at the indicated temperatures overnight the samples were then reweighed and the moisture content in the in-situ condition was then able to be determined. The dehydrated samples were then resealed into glass jars to await further testing at 0 % moisture condition at 23.9 °C (75.0 °F) and 35.0 °C (95.0 °F).

Wet concrete for this study was obtained from the Anderson Materials Plant in Levy County, Florida and formed into 6 inch by 12 inch cylindrical samples. The samples were made in three lifts, each lift being rodded 25 times by a 5/8 inch diameter rod with the rodding penetrating into the previous layer each time. At that point, while the mix was still wet but consolidated into the cylinder form, a Vasoline coated pilot pin was inserted into the mix. The concrete was allowed to cure before the pilot pin was removed. The concrete was sufficiently

hard by that point to maintain shape, but was left in the plastic cylinder mold for the duration of testing. The concrete was allowed to cure for a minimum of one week prior to testing. Figure D-11 shows a concrete cylinder used in testing with the mold removed and pilot pin partially inserted to illustrate placement.

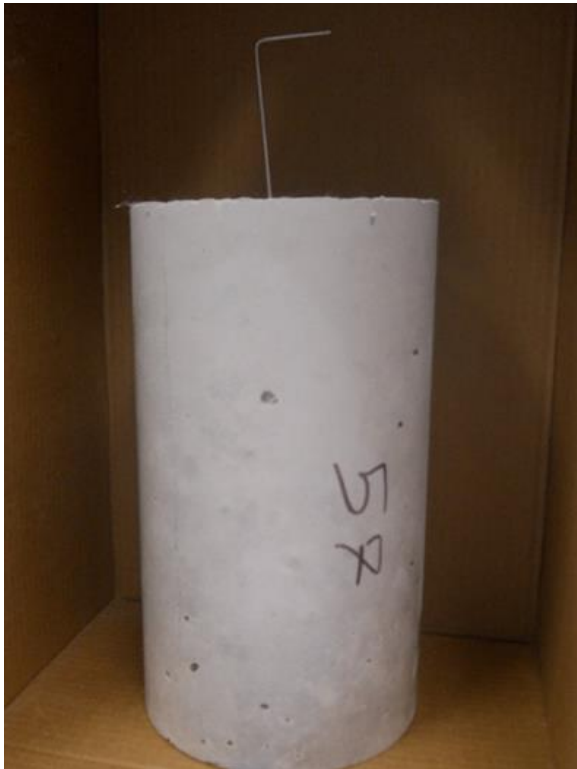


Figure D-11. A concrete cylinder used in testing with pilot pin partially inserted.

Artic Silver Five High Density Polysynthetic Silver Thermal Compound was placed for lubrication onto a 10 millimeter section of a 100 millimeter single meter probe inserted into the concrete sample via the void left by the pilot pin. It is critical that contact is made for the heating cycle of the probe to work properly and the compound allows for contact and complete insertion despite the small tolerances required. After the probe was fully inserted and the concrete allowed to acclimate to the testing temperature, testing was conducted.

The insulation mat material, as shown in Figure D-12, was acquired from the FDOT Materials Office and required no additional accommodations other than acclimation.



Figure D-12. Insulation mat material tested in the study.

All samples were kept at the steady-state temperature environment in the lab for a minimum of two days prior to testing in order to eliminate any temperature or moisture variations within the sample.

In order to reduce the possible thermal gradients within the temperature controlled box, the 25 watt incandescent bulb, which was used as the heating element within the temperature control box, was placed central to the box and the samples were placed half-way between the bulb and the inside surfaces of the unit, thereby decreasing the possibility of a thermal gradient from one side of the testing apparatus to the other side.

After the proper acclimation time, the TR1 probe was inserted into the prepared sample (taking approximately 30 seconds to complete) and a one-hour delay minimum was then incorporated to minimize the possible effects of heat transfer during insertion. Before any high temperature testing was performed on the sample, the unit had to reach a consistent cycling time,

indicating equilibrium within the temperature controlled unit. When there were several soil samples inside the unit, a consistent cycling time was determined to be reached when the 25 watt bulb would remain on for approximately two minutes and remain off for four minutes. A consistent cycling time for the concrete samples, due to the significant increase in thermal mass, was determined to be reached when the 25 watt bulb would turn on for approximately two minutes, but would remain off for fourteen minutes.

It was expressed as being very important inside the KD2Pro User Manual that the soil samples and the probe not be disturbed during testing. Any disturbance could increase error in the results by interfering with either the heating or measurement cycles of the probe. For high temperature testing at 35.0 °C (95.0 °F), this objective was easily achieved because the unit itself acted as a buffer from outside interferences. For the 23.9 °C (75.0 °F) testing, all samples were placed in a temperature-controlled location where they were exposed to neither fans, vibrations, nor other disturbances during the five-hour testing cycle.

D.2.6 Testing Procedures of the Thermal Properties Analyzer

The KD2Pro Thermal Properties Analyzer consists of a controller and various probes used in differing mediums. For soil samples and other materials not extremely granular, the TR1 probe, shown in Figure D-13 was used. The TR1 probe was also used for the concrete samples because a pilot pin was able to be inserted while the sample was still plastic.



Figure D-13. TR1 Probe used.

A KS1 probe, shown in Figure D-14, was used for measurements of the insulation mat material. The KS1 probe differs from the TR1 probe by providing a smaller amount of heat to the needle which helps to minimize errors that can come from excessive heat applied during the test.



Figure D-14. KS1 Probe used.

The KD2Pro controller has an auto-run feature enabling it to take successive tests of the sample automatically. The automatic feature allows for the necessary cool-off period required to prevent any thermal gradient from the heat pulse generated by the probe from affecting subsequent readings. Once the samples were prepared and the appropriate probe inserted, the KD2Pro was set to the auto-run mode and programmed to run a minimum of 20 testing cycles on each sample so that any errors in the data would be more noticeable. The KD2Pro Analyzer measures the reliability of the data by reporting an error measurement. As the User Manual states, a good data set will give error values below 0.01 R-value/inch. The exception to this is when testing materials with very low thermal conductivity (high insulation). When the insulation mat material was tested, contact was limited and air voids in the material allowed for movement of the air trapped within. According to the User Manual, when testing insulation material, the error reading is still considered acceptable if it is above 0.01 R-value/inch.

To increase accuracy, run-times were extended to the 10-minute maximum amount allowed by the KD2Pro. Sixty data measurements were taken by the KD2Pro during this 10-minute period followed by a 20-minute cool down period before the next testing cycle was run.

APPENDIX E
CONSTRUCTION AND INSTRUMENTATION OF DRILLED SHAFTS

E.1 Overview

In the field testing program on drilled shafts as presented in Chapter 6, a total of four concrete drilled shafts, which were 6 feet in diameter and 7 feet in length, were placed in a natural Florida soil (with an AASHTO classification of A-3) to a depth of 6 feet. Two of the drilled shafts (Shafts 1 & 2) were intended to be placed in a wet soil environment, while the other two shafts (Shafts 3 & 4) were intended to be placed in a dry soil environment. The Gainesville DOT Maintenance Yard was the area chosen to conduct the testing primarily because of its close proximity to the State Materials Office. The shafts were constructed from December 18th, 2015 through January 29th, 2016. Plastic properties of the fresh concrete were tested onsite for each shaft. They included air content, slump, temperature, and unit weight. Four-by-eight inch cylindrical concrete samples were taken and molded at the site for later strength testing. These samples were left to cure onsite for 24 hours before being removed and placed in a moist room to finish their curing. Each shaft was instrumented with temperature data loggers that recorded the temperature in the shaft, below the shaft, in the soil surrounding, and in the ambient air for a full seven days recorded at 30 minute increments.

The shafts were drilled under contract with Mammoth Constructors at six foot in diameter and seven foot in depth. After the hole was bored, a steel casing was installed and left in place until the placement of concrete. The site provided ample moisture as evident by the presence of the water table approximately four foot below grade. During work, de-watering was needed for the first two shafts poured in order to facilitate being able to work and install the loggers in the shaft. De-watering was provided for shafts three and four continuously for ten days as the intent was that they cure in a dry soil environment. Curing was allowed to take place

in open conditions. No attempt to mitigate shrinkage or thermally insulate the shafts was employed.

Detailed description of the construction and instrumentation of the four drilled shafts are given in the following sections.

E.2 Mix Designs of Concrete Used in Drilled Shafts

Two different mix designs were used in order to contrast the extremes of hydration heat generation. These mixes were developed by first using an approved FDOT mix design. This mix design was then altered in two main facets. First, the coarse aggregate used was limited to #89 stone. While this does not currently meet FDOT specifications for drilled shaft aggregate, it was selected to help mitigate the problems of entrapped voids that is a current concern with the current FDOT specification. It was of utmost importance for the temperature data loggers to be in complete contact with the concrete in order to accurately measure its temperature. Should this condition not be met, the variability in readings between shafts could be attributed not only to varying conditions but also to error in readings from the temperature sensors themselves. The second alteration in the mix designs was the amount of Portland cement. Both mixes had nearly the same cementitious quantity per yard, but Trial 1 replaced 70 % of the Portland cement with ground blast furnace slag. This “cold mix” was designed to delay hydration over a longer period thereby reducing extreme thermal gradients. Trial 2 was pure Type I/II cement thereby causing a rapid hydration and large subsequent thermal gradient. The different mixes and their proportions are shown in Table E-1.

Table E-1. Mix proportions of the concretes used.

Mix	Cement (lb./yd ³)	Slag (lb./yd ³)	89 Stone (lb./yd ³)	Sand (lb./yd ³)	Water (lb./yd ³)	All Entraining Admixture (oz./yd ³)	Water Reducing Admixture (oz./yd ³)	Target Slump (in.)	Target Air (%)	Unit Weight (lb. /ft ³)	W/C
Trial 1	282	658	1,200	1,72	383	0.20	65.8	8.5	4.5	133.2	0.41
Trial 2	940	0	1,200	1,238	383	0.20	65.8	8.5	2.3	139.3	0.41

The target slump for both mix designs was between 8 and 10 inches in order to mimic the requirements of FDOT specification 346. It is current FDOT procedure to check slump from the middle of the concrete. This is done by discharging approximately half of the mixer truck volume and then obtaining an appropriate amount to conduct the test onsite. In this case, two wheelbarrows were collected for sampling from each pour. The problem with this procedure is that half of the truck’s volume is already in use prior to determining any inherent problems with the mix’s plastic properties. The concrete deliveries for Shafts 1 and 2 were within the target range as can be seen in Table E-2. However, the delivery for Shaft 3 has a slump of 10.25 inches and was just outside the target range for slump. Since slump was close to the desired range and half of the truck had already been poured into the shaft, as per FDOT protocol, the decision was made to proceed with the pour. For Shaft 4, a change was made with respect to collecting the representative sample. This time, the sample was collected prior to any being placed within the shaft. The slump was determined to be 11.75 inches and the truck, as such, was rejected and sent back to the concrete supplier. A call was placed to the concrete supplier, Argos, in which they were instructed to send a stiff mix and water would be added onsite to reach the correct consistency. Upon arrival of the replacement truck, sampling was again conducted prior to placement. This time the slump was determined to be 6.5 inches and 20 gallons of water was added to achieve a slump of 8 inches.

The other plastic properties of the mixes were tested at the same time as the slump and are recorded in Table E-2. They did not play a role in the scope of this project.

Table E-2. Concrete plastic property test results for each shaft.

Mix	Cement (lb./yd ³)	Slag (lb./yd ³)	89 Stone (lb./yd ³)	Sand (lb./yd ³)	Water (lb./yd ³)	All Entrain- ing Admix. (oz./yd ³)	Water Reducin- g Admix. (oz./yd ³)	Actual Slump (in.)	Temp. (°F)	Target Air (%)	Unit Weight (lb./ft ³)	W/C
DS1	279	654	1,220	1,127	273	-	113.3	9.8	76	3.5	134	0.29
DS 2	942	-	1,217	1,299	274	0.32	112.6	9.5	76	4.0	136	0.29
DS 3	282	659	1,213	1,122	283	-	112.6	10.3	71	3.5	132	0.30
DS 4	959	-	1,220	1,299	233	0.21	112.6	8.0	82	2.7	138	0.24

E.3 Installation of Temperature Data Loggers

Important to this project was the monitoring of temperature development and distribution in the concrete shafts at early age of concrete. This temperature data were collected by the use of a self-powered thermistor from Command Center Corporation. This particular data logger has the ability to sample and record 2048 data points. Initially, the distance between the loggers and the soil and concrete boundary was laid out so that it maintained a 2 inch gap on the concrete side and a 2 inch gap on the soil side.

During construction, the 2 inch spacing proved to be unpractical and could not be maintained with the removal of the casing. With the movement of the casing from the crane and with the help of a backhoe the temperature data loggers in the soil were contacted by the concrete as the soil was displaced. It held its deformed shape while the concrete quickly flowed into the displaced soil area. For this reason, Shafts 2, 3, and 4 used a larger spacing of 4 inch offset into the concrete and 8 inch offset in the soil as shown in Figures E-1 and E-2.



Figure E-1. Four-inch spacing between data logger and casing inside shaft.



Figure E-2. Six-inch spacing between data logger in soil and casing.

In Shaft 1, the temperature loggers were attached with rebar ties and duct tape adhesive to a welded two dimensional steel frame constructed with #4 rebar as shown in Figure E-3.



Figure E-3. Temperature loggers attached to steel frame.

The shaft and surrounding soil was instrumented with 27 temperature data loggers and 1 was placed away from the shaft to record ambient air temperature. The concrete itself was instrumented from the center and radially outward in a two dimensional plane because the hydrating concrete was assumed to have a symmetrical thermal profile.

Because the temperature loggers were placed in such a way that occupied the center of the shaft, the trimming pipe had to be placed off center. This produced a lot of lateral force from the flowing concrete which showed that the #4 bars were not adequate in resisting this lateral load. Additional supports had to be installed while the concrete was being poured and then removed upon the finish of pouring. For Shafts 2, 3, and 4, a three-dimensional framework was used. This framework consisted of 27-inch squares tied to four vertical bars in each corner of the square. The temperature loggers were then tied to three foot pieces of #3 bar outside the shaft

and then the piece of #3 bar was brought in and tied to the frame. This improved layout that provides additional rigidity can be seen in Figure E-4.



Figure E-4. Layout for frame for temperature logger attachment for shafts 2 to 4.

E.4 Dewatering of Soil

Mammoth Constructors was contracted to install the shafts. To facilitate this, Mammoth used a drilling truck as seen in Figure E-5 to drill the hole approximately 72 inch in diameter and approximately 5 feet deep.



Figure E-5. Mammoth Constructor's drilling truck.

At that point, the drilling hit the natural water table. To avoid any cave-ins of the shaft wall and facilitate a safe work environment for the installation of the temperature loggers, a casing was installed with a crane truck, as seen in Figure E-6.



Figure E-6. Installation of casing.

The installation of the casing prevented the auger from being utilized further because the auger was larger than the diameter of the casing. When the shaft was approximately 5 feet deep, the 74 inch diameter auger was removed from the drilling truck and a baler head (Figure E-7) was placed on the drilling truck.



Figure E-7. Baler.

The baler was used to carefully remove an additional 18 inch of soil making the total depth of the shaft approximately 6 ½ feet below grade. As the baler removed the additional soil, the casing was driven with the aid of a backhoe (Figure E-8).



Figure E-8. Backhoe driving casing.

With the casing installed at the proper depth, work installing the data loggers could not commence because the natural water table was located approximately 4 feet below grade and thereby the bottom of the shaft was under 2 ½ feet of water as shown in Figure E-9.



Figure E-9. Water table inside casing.

The first two shafts only required the removal of water long enough to allow placement of the steel framework and thermistors. The shaft was also dewatered prior to concrete placement. A well point was driven in the middle of Shaft 1 for dewatering purposes and to gauge the sand-point's ability to dewater the sand on a long-term basis as this would be needed for Shafts 3 and 4. Because the well point was located in the middle of the shaft, the well point was removed just before pouring of concrete commenced. The well points themselves were 5 feet in length and 1.25 inches in diameter and were coupled to a 10 feet long and 1.25 inch diameter shaft as shown in Figure E-10.



Figure E-10. Well point.

This well point was placed so that the top of the well point was just below the bottom of the shaft. This well point adequately depressed the water table to remove all of the water from the bottom of the shaft, but could not remain in the shaft during pouring. Shafts 3 and 4 required a different well point design because the well points had to remain in place even while concrete was being placed. For Shafts 3 and 4, a well field was set-up (Figure E-11) with 2 well points on the outside of Shaft 3 and two well points on the outside of Shaft 4 and one common well point located between the two shafts.



Figure E-11. Well field.

The two well points on the outside of each shaft were piped in series to the common well point which was then connected to an engine driven diaphragm water pump (Figure E-12). The pump was outfitted with an 11-gallon tank in order to provide a means in which the pump could run continuously without refueling for a period of approximately 15 hours.



Figure E-12. Engine-driven diaphragm water pump.

These well points were set with the aid of the FDOT geotechnical drilling truck (Figure E-13) to a depth of 14 feet. This depth placed the top of the well point approximately 2 feet below the bottom of the shaft. From the results of dewatering Shafts 1 and 2, it was determined that in order to keep the bottom of the shaft dry the well points needed to be set deeper. Since Shafts 3 and 4 represented dry field conditions, the bottom of the shaft had to remain dry until curing of the concrete was significantly completed (day 10). Initial draw was 35 gallons per minute and tapered to approximately 20 gpm after 24 hours of dewatering.



Figure E-13. FDOT geotechnical drilling truck.

E.5 Pouring of Concrete

Now that the shafts have been dewatered and the instrumentation and framework have been placed, Mammoth Constructors assisted in pouring the concrete with the use of a tremie pipe suspended from the crane (Figure E-14).



Figure E-14. Tremie pipe.

The end of the tremie pipe was kept in the concrete the duration of the pour. The tremie pipe was in two sections. The entire unit was raised with the concrete until the lower section could be disconnected and then the upper section was used to bring the level of the concrete slightly above grade. At this point, the crane point disconnected from the tremie pipe and connected to a rigging beam that attached to the casing. The casing was removed by pulling vertical with the crane truck which was assisted with effort from the backhoe (Figure E-15). With the casing removed, a beauty ring or tub with leveling frame (Figure E-16) was then placed

into the concrete above the shaft. The beauty ring allowed concrete to be placed above grade while maintaining the correct shaft dimension.



Figure E-15. Removal of casing.



Figure E-16. Installation of beauty ring.

A transit was used to level the four corners of the beauty ring so that the instrumentation was covered with approximately 2 ½ inches of concrete. The beauty ring had a vertical seam that was bolted (Figure E-17) allowing it to remain in place while the concrete was curing and be unbolted for removal after concrete curing.



Figure E-17. Close-up of beauty ring.

APPENDIX F
TESTING EQUIPMENT AND PROCEDURES FOR STUDY ON TERNARY BLEND
CONCRETE MIXES

F.1 Fresh Concrete Tests (Plastic Properties)

F.1.1 Slump (ASTM C143/C143M-10a)

The slump test is conducted by placing and compacting by rodding a sample of freshly mixed concrete in a mold shaped as a cone. The mold is raised, and the concrete allowed to settle freely. The vertical distance between the original and displaced position of the center of the top surface of the concrete is measured and reported as the slump of the concrete.

The purpose of this test is to measure fresh concrete workability and consistency as shown in Figure F-1. The dimensions of the testing cone are shown in Figure F-2.

This test method is applicable to freshly mixed concrete having coarse aggregate size up to 1.5 inch. If the coarse aggregate is larger than 1.5 inch, the test method is applicable when it is performed on the fraction of concrete passing a 1.5 inch sieve, with the larger aggregate removed.



Figure F-1. Performing the slump test.

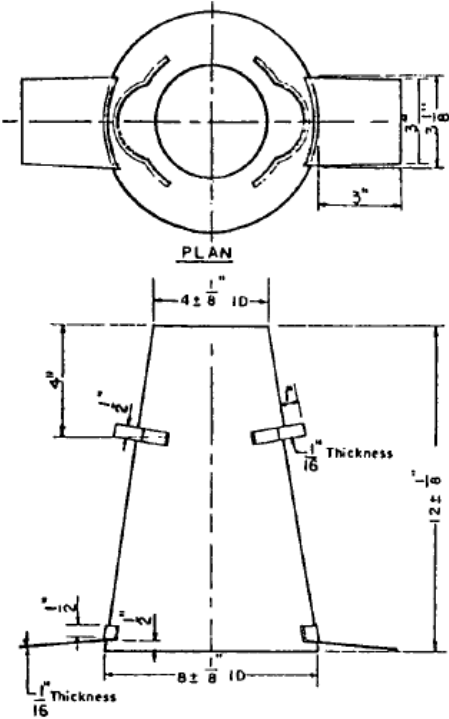


Figure F-2. Dimensions of the slump test mold.

F.1.2 Unit Weight (ASTM C138/C138M-12)

The unit weight test was run after the slump test was conducted and the results were accepted. The purpose of this test is to measure the density of the fresh concrete mix by dividing the weight of concrete sample by the volume of the container, which is 0.25 ft³ as shown in Figure F-3.



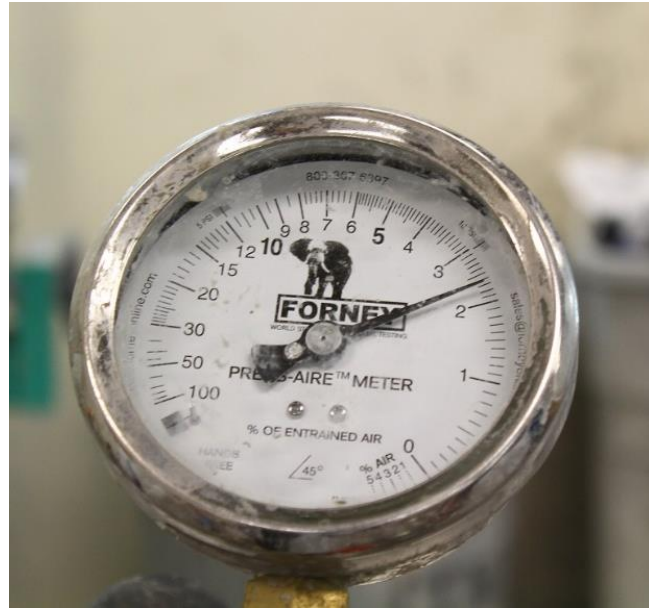
Figure F-3. Conducting unit weight test.

F.1.3 Air Content (ASTM C231/C231M-10)

The air content test was run after recording the unit weight, since the same apparatus was used for both tests as shown in Figures F-3 and F-4.

The purpose of this test is to determine the amount of air in the concrete sample as a percentage of the total volume. The total air content consists of entrained air in the cement paste and the entrapped air in the aggregate pores, which requires a correction factor to calculate the

precise air content when the pressure-air-meter is used. The correction factor is presented as a percentage that should be deducted from the gage reading to give the corrected air content. This test was run after conducting the slump test with an acceptable results.



A B

Figure F-4. Air content test. A) air content test apparatus and B) reading of air content.

F.1.4 Temperature of Freshly Mixed Hydraulic-Cement Concrete (ASTM C1064/C1064M-11)

The purpose of this test is to determine the temperature of freshly mixed concrete by using a thermometer as shown in Figure F-5. This test was run after the mixing of concrete is completed and the concrete was acceptable to record the concrete mix temperature while conducting other tests.



Figure F-5. Thermometer used in the temperature test.

F.2 Hardened Concrete Tests (Mechanical Properties)

F.2.1 Compressive Strength for 4" X 8" Cylindrical Concrete Specimens (ASTM C39/C39M)

The purpose of this test is to determine the compressive strength of cylindrical concrete specimens. The specimens were made and tested according to ASTM C192/C192M-07 standard. It is conducted by applying a compressive axial load to a concrete specimen at a rate which is within a prescribed range until failure occurs. The compressive strength of the specimen is calculated by dividing the maximum load attained during the test by the cross-sectional area of the specimen.

The testing machine met the testing requirements which include that the machine must be power-operated providing the load in a constant rate to avoid any shocks that could affect the test results. An automatic Forney testing machine was used as shown in Figure F-6.



Figure F-6. The Forney testing machine used for the compressive strength testing.

Specimens shall be excluded from the testing if any individual diameter of a cylinder differs from any other diameter of the same cylinder by more than 2 %. The ends of compression test specimens that are not plane within 0.002 inch shall be ground to meet that tolerance as shown in Figure F-7 and shall be kept moisturized until the test is completed.



Figure F-7. Grinding each side of the specimens and keeping the specimens moisturized until the test is completed.

The diameter used for calculating the cross-sectional area of the test specimen shall be determined to the nearest 0.01 inch by averaging two diameters measured at right angles to each other at about mid-height of the specimen, as shown in Figure F-8.



Figure F-8. Specimen measurement and alignment.

F.2.2 Modulus of Elasticity (MOE) (ASTM C469/C469M-10)

The purpose of this test is to obtain the modulus of elasticity. 4x8 cylindrical concrete specimens were used. MOE is the slope of a stress-strain curve, for the stress from 0 to 40 % of the ultimate concrete strength.

The specimens were treated, checked and measured using the same procedure which was used in the compressive strength test in accordance with ASTM C39/C39M. The testing was conducted using the same machine used for the compressive strength testing as shown in Figure F-9. The Forney software was used to plot and calculate the MOE.



Figure F-9. The Forney testing machine.

A compressometer was used to determine the strain, as shown in Figure F-10.



Figure F-10. The compressometer (electronic sensor connected to the Forney software).

The temperature and humidity of the test environment was controlled to avoid any effect on the test results. The MOE testing was done after conducting the compressive strength test for the same mix design and the same curing age to determine the ultimate compressive strength which was used in the MOE testing (the loading shall be from 0 to 40 % of the ultimate strength).

The compressometer was attached to the concrete specimen using an alignment object as shown in Figure F-10 to ensure that the compressometer was perfectly aligned with the concrete specimen. The attaching pins were placed on a smooth concrete surface and should avoid rough surface, holes, and air bubbles.

The MOE test results of duplicate cylinders should not depart by more than 5 % from the average. In case of multiple batches, the precision shall be ± 4.25 %, for MOE values within a range of 2.5×10^6 to 4×10^6 psi.

F.2.3 Splitting Tensile Strength Test (ASTM C496/C496M)

The splitting tensile strength test was performed on 4" x 8" concrete cylinder specimens in accordance with ASTM C496/C496M. This test method is conducted by applying a diametric compressive force along the concrete specimen at a rate that is within a prescribed range until failure occurs. This loading produces tensile stresses on the plane containing the applied load and relatively high compressive stresses in the area directly around the applied load. Thin plywood bearing strips, 1/8 inches thick, are used to distribute the load applied along the length of the cylinder, as shown in Figure F-11. Tensile failure occurs before compressive failure due to the areas of load application are in a state of tri-axial compression, thereby allowing them to withstand much higher compressive stresses than would be indicated by a uniaxial compressive strength test. A failed specimen after the splitting tensile strength test is shown in Figure F-12.

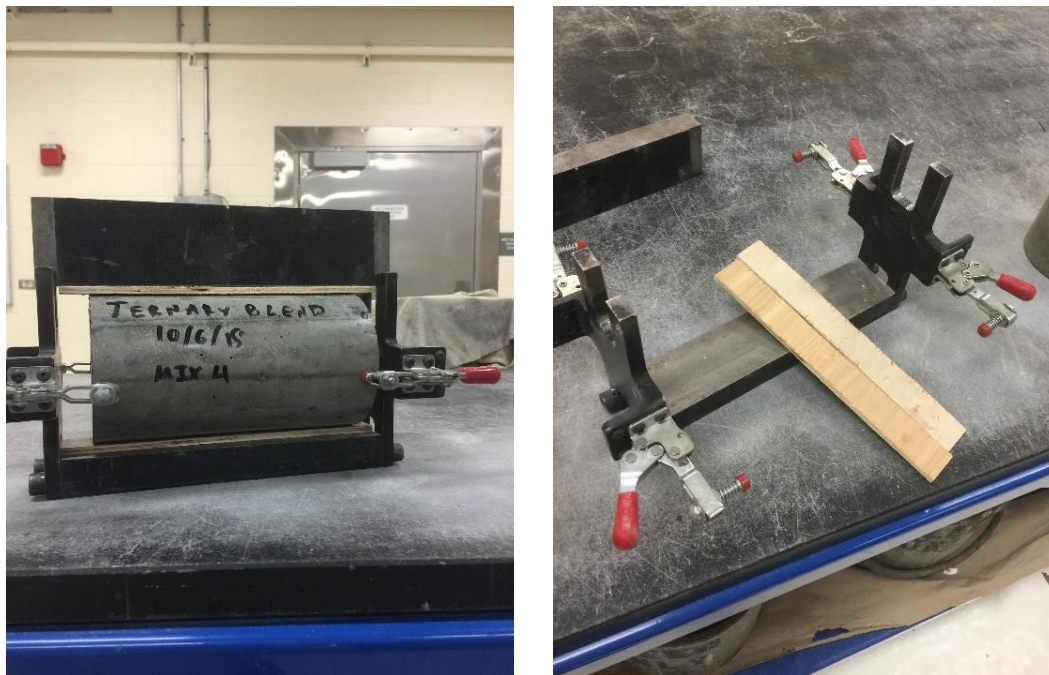


Figure F-11. The aligning jig for the splitting tensile strength test before and after placing the concrete specimen.



Figure F-12. Splitting tensile strength test specimen after conducting the test.

F.2.4 Flexural Strength of Concrete (ASTM C78/C78M)

The purpose of this test is to determine the flexural strength of concrete using a 4" x 4" x 14" simple beam with third-point loading, as shown in Figure F-13.

The testing took place after the moist-cured specimens were removed from the curing room. The test specimen was turned on its side with respect to its position as molded and centered on the support blocks.

Gaps in excess of 0.015 inch were eliminated only by grinding. The specimen was loaded continuously, without shock, and the load was applied at a constant rate to the breaking point. The load was applied at a rate that constantly increased the maximum stress on the tension face by 125 to 175 psi/min until rupture occurred.



Figure F-13. Testing machine for flexural strength test before and after installing concrete beam.

To determine the dimensions of the specimen cross section for use in calculating modulus of rupture, measurements were taken across one of the fractured faces after testing. Figure F-14 shows a fractured flexure beam specimen. The width and depth were measured with the specimen as oriented for testing. For each dimension, three measurements were taken (one at

each edge and one at the center). All measurements were taken to the nearest 0.05 inches. If the fracture occurs at a capped section, the cap thickness would be included in the measurement.



Figure F-14. A fractured flexure beam specimen.

APPENDIX G
STATISTICAL ANALYSIS OF DATA FROM TERNARY BLEND MIX STUDY

G.1 Analysis of Compressive Strength Data

G.1.1 Existing Models for Estimating Compressive Strength

A literature review was conducted to find existing models used for estimating concrete compressive strength as a function of time and 28 days compressive strength.

In 1956, Plowman proposed a model to predict concrete compressive strength as a factor of time, 28 days compressive strength and two variables as shown in Equation G-1 (Plowman, 1956). Plowman model has an infinite limit which makes it improper for predicting long term aged concrete.

$$f'_c(t) = [a + b \cdot \log(t)] \cdot f'_c(28) \quad (\text{G-1})$$

Where

$f'_c(t)$ is the compressive strength at time t in days,

$f'_c(28)$ is the compressive strength at 28 days,

t is time in days,

a and b are coefficients.

In the same year, Nykanen proposed a model for predicting concrete compressive strength by a function as shown in Equation G-2. The model has a finite limit but no setting age offset (Yazdani and Mckinnie, 2004).

$$f'_c(t) = f_{ult} \cdot (1 - e^{-k \cdot t}) \cdot f'_c(28) \quad (\text{G-2})$$

Where

f_{ult} is the concrete ultimate compressive strength,

k is coefficient.

Freiesleben proposed a model that has a finite limit and a sharp setting age offset, as shown in Equation G-3. The model is time dependent and has three coefficients. This model showed good results in predicting the compressive strength of concrete (Yazdani and Mckinnie, 2004).

$$f'_c(t) = a \cdot e^{-(b/t)^c} \cdot f'_c(28) \quad (G-3)$$

Where

a , b and c are coefficients.

CEB-FIP (French for European Committee for Concrete – International Federation for Prestressing) Model Code (CEB-FIP 1990) is a time dependent prediction model that has a finite limit and curved setting age offset, as shown in Equation G-4. The equation has only one coefficient.

$$f'_c(t) = f'_c(28) \cdot e^{a[1-\sqrt{28/t}]^1} \quad (G-4)$$

Where

a is a coefficient,

t_1 is the number of day.

ACI 209 uses a hyperbolic model that has two coefficients and time dependent, as shown in Equation G-5. The hyperbolic model has a finite limit and no setting age offset (Yazdani and Mckinnie, 2004).

$$f'_c(t) = \frac{t}{a + b \cdot t} \cdot f'_c(28) \quad (G-5)$$

Where

a and b are coefficients.

All of the above mentioned models have been used by researchers to predict the compressive strength of ordinary concrete.

G.1.2 Normalization of Data

Regression analysis was used to determine suitable models for predicting time-dependent concrete compressive strength. As a first step, compressive strength test results for all 14 mix designs and all curing ages were normalized by dividing each test result by the 28 days compressive strength test result for the same mix to produce a unit-less “strength factor” as shown in Table G-1. The purpose of normalizing the compressive strength test results is to minimize the difference between concrete mixes with different sources of aggregate which were used in this research and the difference between different classes of concrete.

Table G-1. The strength factor for all concrete mixes.

Time(days)	Strength Factor $f'_c(t)/f'_c(28)$					
	1	3	7	28	91	182
Mix 1	0.093	0.405	0.683	1.000	1.151	1.169
Mix 2	0.130	0.449	0.758	1.000	1.136	1.160
Mix 3	0.413	0.629	0.764	1.000	1.041	1.051
Mix 4	0.129	0.514	0.779	1.000	1.082	1.089
Mix 5	0.476	0.699	0.849	1.000	1.096	1.116
Mix 6	0.464	0.701	0.842	1.000	1.091	1.086
Mix 7	0.117	0.433	0.666	1.000	1.186	1.179
Mix 8	0.578	0.739	0.872	1.000	1.077	1.117
Mix 9	0.160	0.469	0.696	1.000	1.122	1.141
Mix 10	0.630	0.759	0.859	1.000	1.060	1.069
Mix 11	0.132	0.444	0.748	1.000	1.108	1.139
Mix 12	0.167	0.462	0.751	1.000	1.181	1.198
Mix 13	0.114	0.588	0.799	1.000	1.062	1.117
Mix 14	0.168	0.609	0.832	1.000	1.138	1.178

The normalization reduces the differences between the fourteen mixes as shown in Figures G-1 and G-2. Figures G-3, G-4, G-5, and G-6 show the strength factor versus curing time in days for each group.

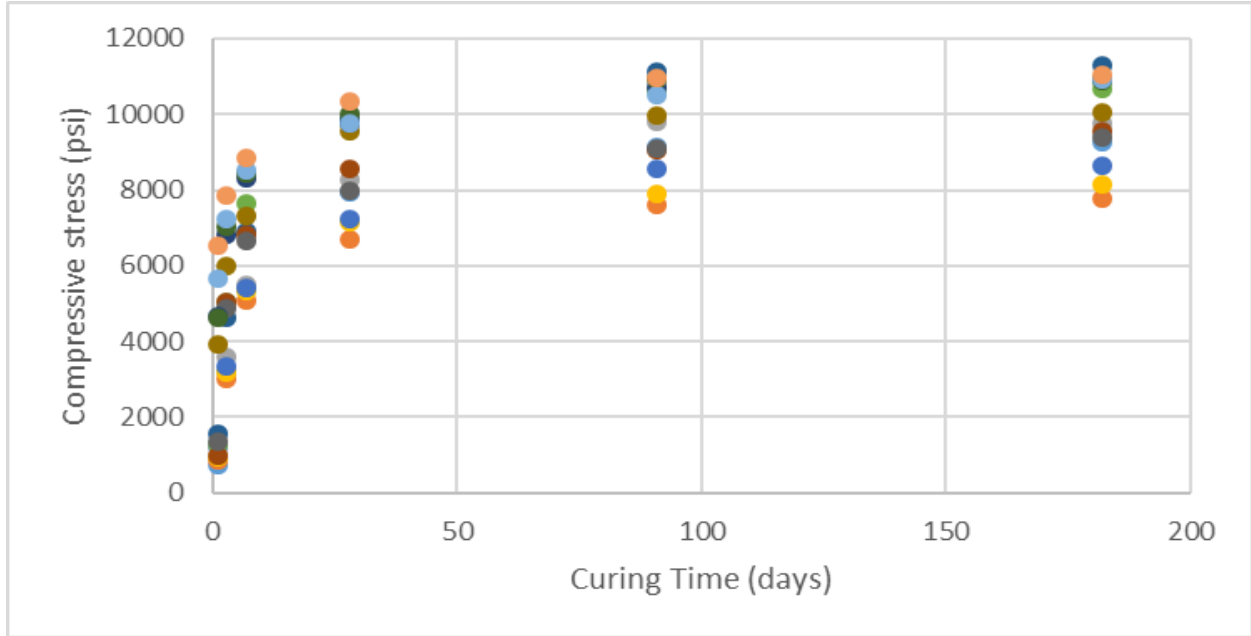


Figure G-1. The compressive strength test results before normalization.

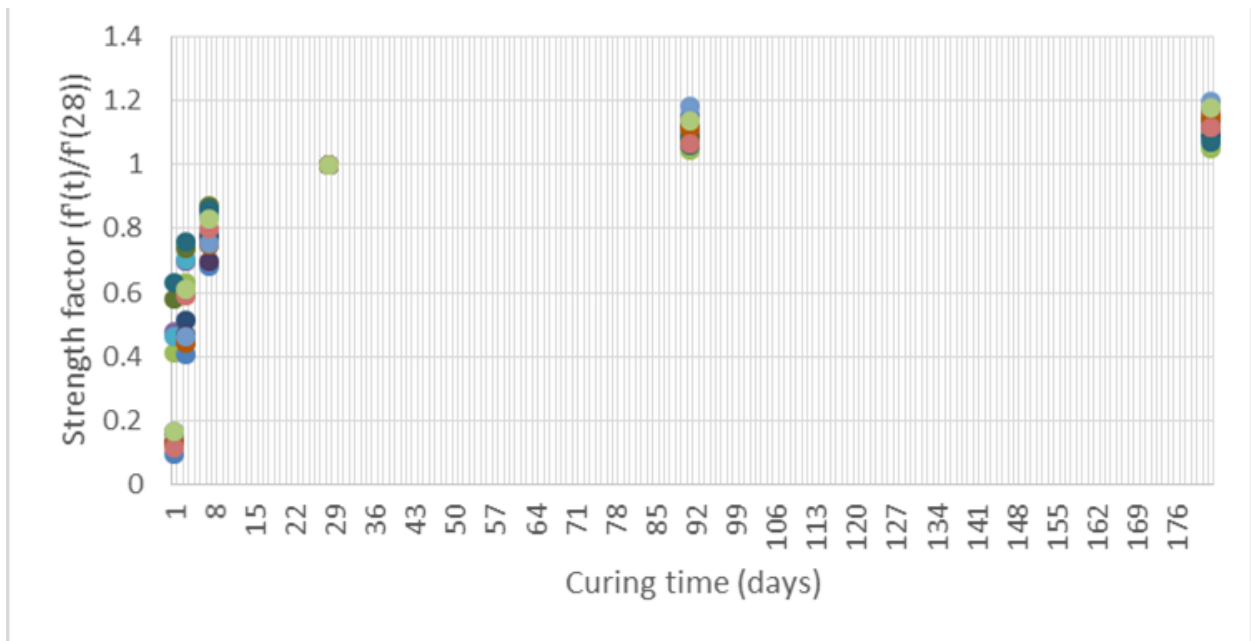


Figure G-2. The strength factor for all concrete mixes.

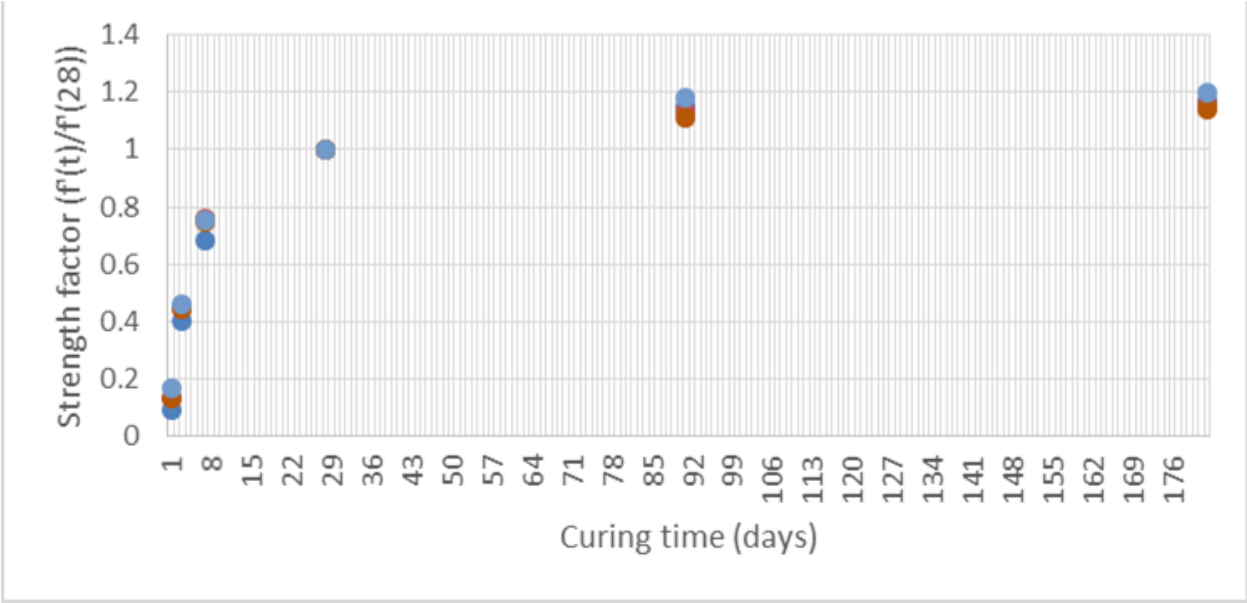


Figure G-3. The strength factors for slag and fly ash mixes with W/C more than 0.4.

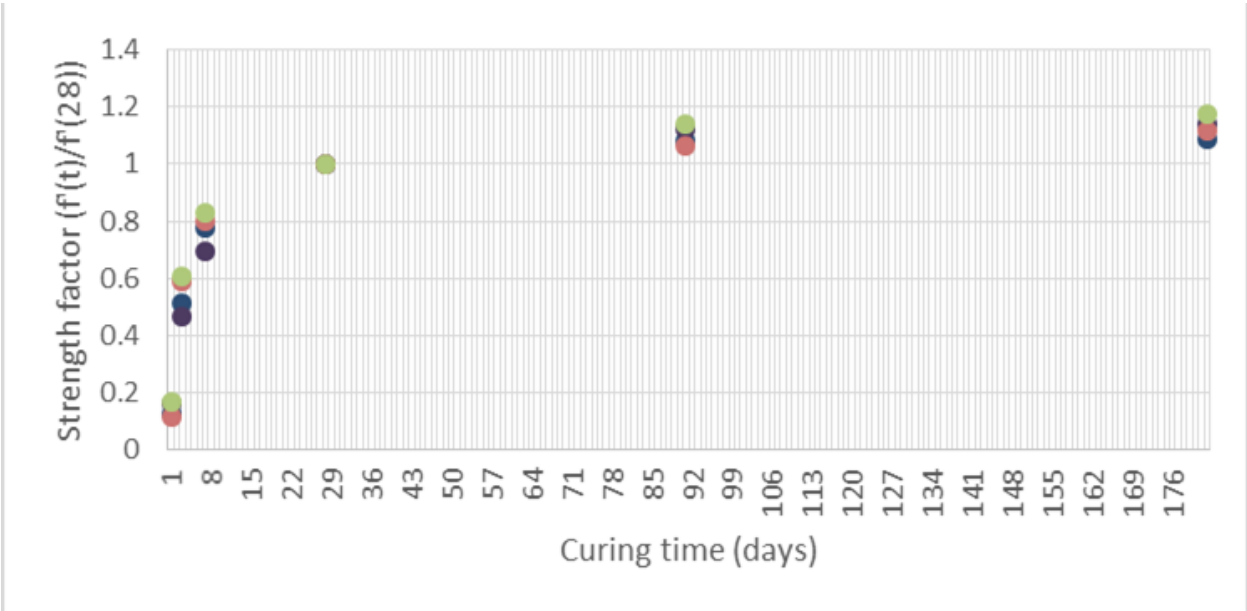


Figure G-4. The strength factors for slag and fly ash mixes with W/C less than 0.4.

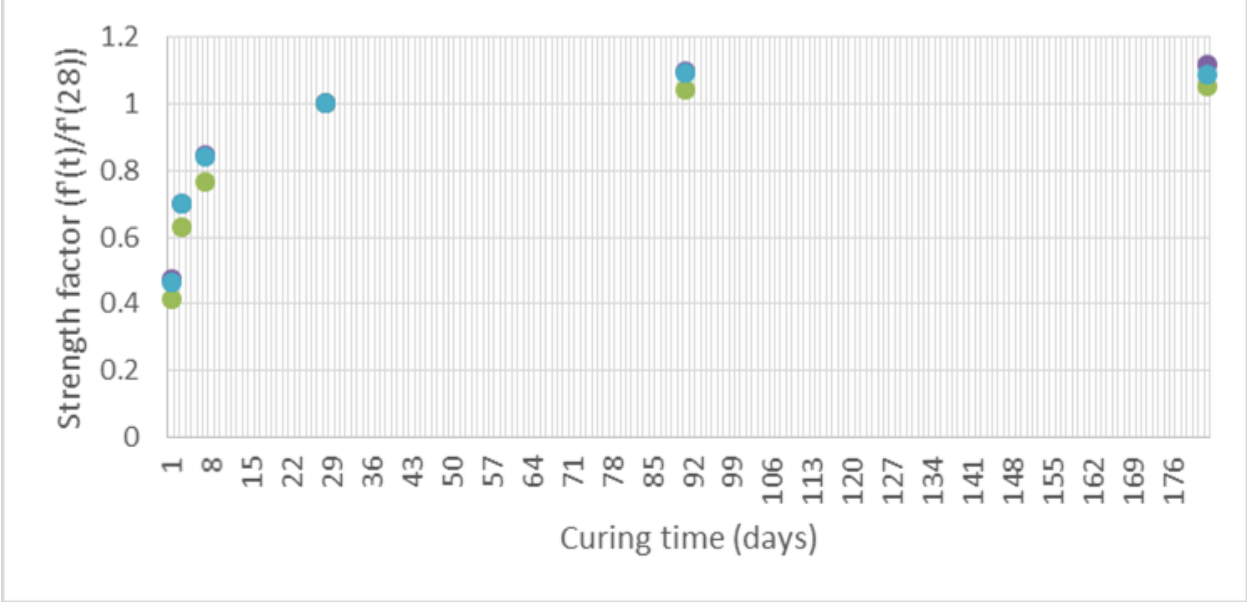


Figure G-5. The strength factors for silica fume, fly ash and Type I/II Portland cement mixes.

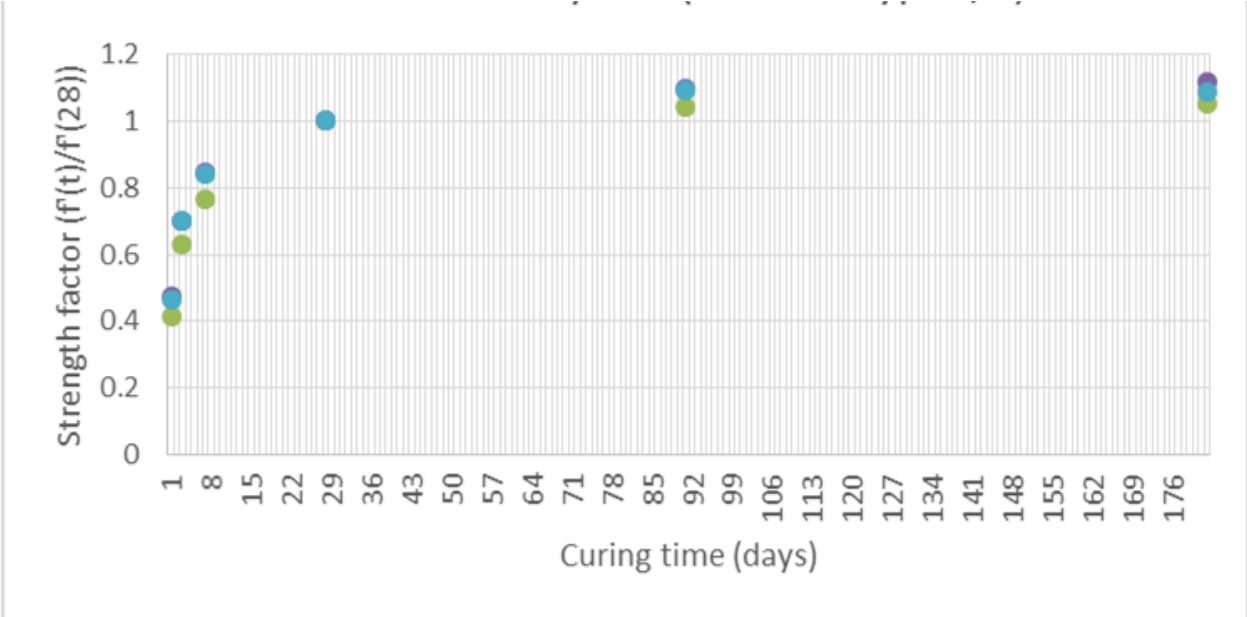


Figure G-6. The strength factors for silica fume, fly ash and Type III Portland cement mixes.

G.1.3 Accuracy Measures

The coefficient of determination, also referred as R^2 value, is the common statistical parameter used to measure the goodness of fit for a linear regression model to a set of data. This statistical test is not valid for nonlinear models (Wetherill, 1986). The strength of concrete versus age relationship is nonlinear, which make R^2 inapplicable in measuring the goodness of fit of the models. Therefore, the standard error of estimate (Se) was used to quantify the goodness of fit for the models evaluated. The equation for calculation of Se is shown in Equation G-6 (Triola, 1998):

$$S_e = \sqrt{\frac{\sum_{i=1}^n (y - y')^2}{n - 2}} \quad (\text{G-6})$$

Where

S_e is standard error of estimate,

y is the actual compressive strength of concrete,

y' is the predicted compressive strength of concrete,

n is the number of data points.

The standard error of estimate has the same unit as the estimated variable. If the estimated variable is the compressive strength, then the Se unit would be psi, and if the estimated variable is the strength factor, then the Se would be unit-less.

G.1.4 Results of Regression Analysis

Regression analysis was performed on the strength-ratio data sets in each of the four categories as described in Section 7.3.2 using two data sets, the first one includes the data in 1, 3, 7, 28, 91 and 182 days and the second one excludes the first day data.

Four models were chosen as candidates to be evaluated. They were the Freiesleben model, the CEB-FIP modified model, the Hyperbolic model, and the 2nd degree Hyperbolic model.

G.1.4.1 Freiesleben Model

The Freiesleben model was re-written in terms of the strength factor as shown in Equation G-7.

$$\left[\frac{f'_c(t)}{f'_c(28)} \right] = a \cdot e^{-(b/t)^c} \quad (\text{G-7})$$

By taking the logarithm of Equation G-7, the equation becomes as shown in Equation G-8.

$$\ln \left[\frac{f'_c(t)}{f'_c(28)} \right] = \ln a - (b/t)^c = \ln a - b^c \cdot (1/t)^c \quad (\text{G-8})$$

The above equation can be considered as a linear equation of the following form:

$$y = \alpha \cdot x + \beta \quad (\text{G-9})$$

where

$$y = \ln \left[\frac{f'_c(t)}{f'_c(28)} \right],$$

$$x = (1/t)^c,$$

α and β are coefficients.

Linear regression analysis was performed using equation (G-9) with different values of c. the value of c which gave the highest R² value was selected for use in the adopted regression equation. Figure G-7 shows a sample plot of this linearized equation.

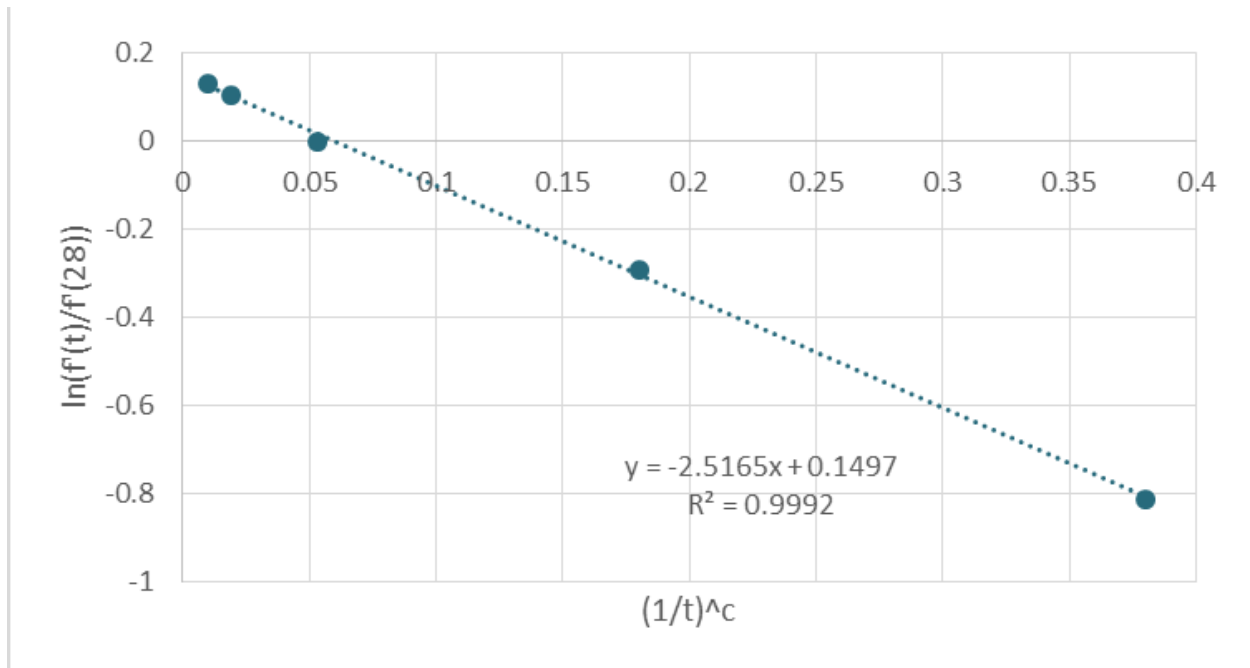


Figure G-7. Sample plot of linearized Freiesleben model.

Linearized regression analysis was performed on the strength factor data for the first group of mixes which were slag and fly ash mixes with W/C of more than 0.4. Similar analysis was also performed by excluding the first-day strength data. The two optimized linearized regression equations were as follows:

$$\ln\left[\frac{f'_c(t)}{f'_c(28)}\right] = 0.2231 - 2.279 \cdot \left(\frac{1}{t}\right)^{0.72} \quad (\text{G-10})$$

When first day data were excluded:

$$\ln\left[\frac{f'_c(t)}{f'_c(28)}\right] = 0.1989 - 2.369 \cdot \left(\frac{1}{t}\right)^{0.76} \quad (\text{G-11})$$

The above linearized equations were transformed back to the original Freiesleben equation as follows:

$$f'_c(t) = f'_c(28) \cdot 1.25 \cdot e^{-\left(\frac{3.14}{t}\right)^{0.72}} \quad (\text{G-12})$$

When first day data were excluded:

$$f'_c(t) = f'_c(28) \cdot 1.22 \cdot e^{-(3.11/t)^{0.76}} \quad (\text{G-13})$$

Table G-2 shows the actual strength of the concrete for this group of concrete and the corresponding predicted strengths using the two prediction equations. The standard error of the estimates for the strength and the strength factor using the two prediction equations are also shown in the table. Figure G-8 shows the comparison between the actual strength and the predicted strength using these two prediction equations.

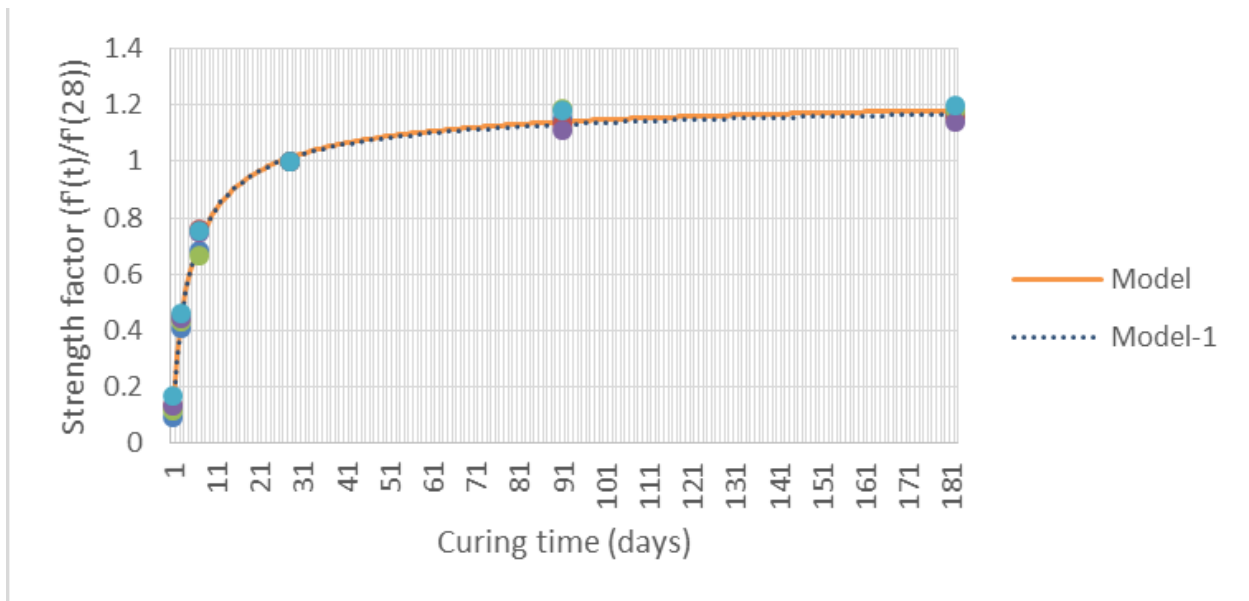


Figure G-8. Comparison between actual and predicted strength factors from Freiesleben model for slag and fly ash mixes with W/C more than 0.4

Table G-2. Comparison between the actual and Freiesleben model predicted compressive strength for slag and fly ash mixes with W/C more than 0.4.

	Time (days)	Mix 1(psi)	Mix 2(psi)	Mix 7(psi)	Mix 11(psi)	Mix 12(psi)
Actual strength	1	740	870	970	940	1,210
	3	3,210	3,010	3,580	3,170	3,340
	7	5,420	5,080	5,510	5,340	5,430
	28	7,930	6,700	8,270	7,140	7,230
	91	9,130	7,610	9,810	7,910	8,540
	182	9,270	7,770	9,750	8,130	8,660
	Time (days)	Mix 1'(psi)	Mix 2'(psi)	Mix 7'(psi)	Mix 11'(psi)	Mix 12'(psi)
Predicted strength	1	1,011	854	1,054	910	921
	3	3,515	2,969	3,665	3,164	3,204
	7	5,635	4,761	5,877	5,074	5,138
	28	8,034	6,788	8,378	7,233	7,325
	91	9,044	7,641	9,431	8,143	8,245
	182	9,364	7,912	9,765	8,431	8,537
	Time (days)	Mix 1'(psi)	Mix 2'(psi)	Mix 7'(psi)	Mix 11'(psi)	Mix 12'(psi)
Predicted strength without first day data	3	3,464	2,926	3,612	3,119	3,158
	7	5,644	4,768	5,886	5,082	5,146
	28	8,023	6,779	8,367	7,224	7,315
	91	8,969	7,578	9,353	8,075	8,177
	182	9,256	7,820	9,653	8,334	8,439
Strength	Se	212 (psi)				
	Se -1	217 (psi)				
Strength factor	Se	0.028				
	Se -1	0.029				

(Note: Se is the standard error of estimate and Se -1 is the standard error of estimate excluding the first day test results.)

Similar regression analysis using the Freiesleben model was performed on the strength factor data on the second group of mixes which were slag and fly ash mixes with W/C less than

0.4. The resulting two prediction equations are as follows:

$$\ln\left[\frac{f'_c(t)}{f'_c(28)}\right] = 0.1310 - 1.748 \cdot \left(\frac{1}{t}\right)^{0.90} \quad (\text{G-14})$$

When first day data were excluded:

$$\ln\left[\frac{f'_c(t)}{f'_c(28)}\right] = 0.1484 - 1.741 \cdot \left(\frac{1}{t}\right)^{0.72} \quad (\text{G-15})$$

The above linearized equations were transformed back to the original Freiesleben equation as follows:

$$f'_c(t) = f'_c(28) \cdot 1.14 \cdot e^{-\left(\frac{1.86}{t}\right)^{0.90}} \quad (\text{G-16})$$

When first day data were excluded:

$$f'_c(t) = f'_c(28) \cdot 1.16 \cdot e^{-\left(\frac{2.16}{t}\right)^{0.72}} \quad (\text{G-17})$$

Table G-3 shows the actual strength of the concrete for this group of concrete and the corresponding predicted strengths using the two prediction equations. The standard error of the estimates for the strength and the strength factor using the two prediction equations are also shown in the table. Figure G-9 shows the comparison between the actual strength and the predicted strength using these two prediction equations.

Table G-3. Comparison between the actual and Freiesleben model predicted compressive strength for slag and fly ash mixes with W/C less than 0.4.

		Time (days)	Mix 4(psi)	Mix 9(psi)	Mix 13(psi)	Mix 14(psi)
Actual strength	1		1,270	1,580	970	1,340
	3		5,050	4,640	5,020	4,860
	7		7,650	6,890	6,820	6,640
	28		9,820	9,900	8,540	7,980
	91		10,630	11,110	9,070	9,080
	182		10,690	11,300	9,540	9,400
		Time (days)	Mix 4'(psi)	Mix 9'(psi)	Mix 13'(psi)	Mix 14'(psi)
Predicted strength	1		1,411	1,423	1,227	1,147
	3		5,177	5,220	4,503	4,207
	7		7,808	7,872	6,790	6,345
	28		10,087	10,169	8,772	8,197
	91		10,791	10,879	9,384	8,769
	182		10,971	11,061	9,541	8,916
		Time (days)	Mix 4'(psi)	Mix 9'(psi)	Mix 13'(psi)	Mix 14'(psi)
Predicted strength without first day data	3		5,184	5,226	4,508	4,212
	7		7,432	7,493	6,463	6,039
	28		9,742	9,821	8,472	7,917
	91		10,663	10,750	9,273	8,665
	182		10,950	11,040	9,523	8,899
Slag & Fly ash (W/C < 0.4)						
Strength	Se		409 (psi)			
	Se -1		387 (psi)			
Strength factor	Se		0.045			
	Se -1		0.043			

(Note: Se is the standard error of estimate and Se -1 is the standard error of estimate excluding the first day test results.)

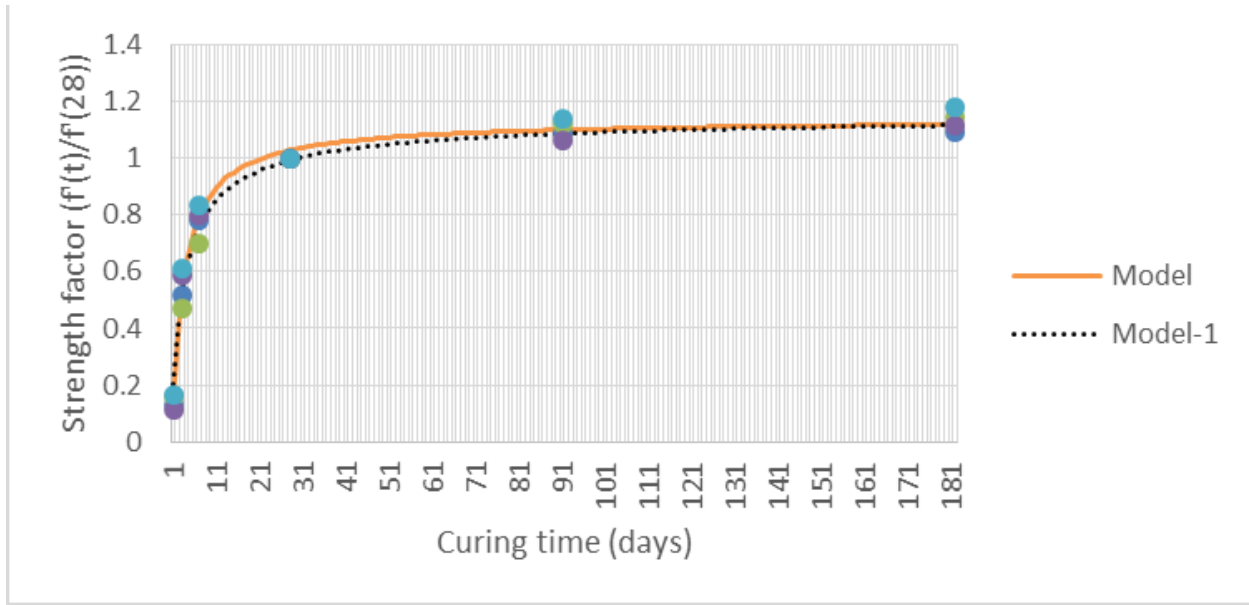


Figure G-9. Comparison between actual and predicted strength factors from Freiesleben model for slag and fly ash mixes with W/C less than 0.4.

Similar regression analysis using the Freiesleben model was performed on the strength factor data on the third group of mixes which were silica fume, fly ash and Type I/II Portland cement. The resulting two prediction equations are as follows:

$$\ln\left[\frac{f'_c(t)}{f'_c(28)}\right] = 0.1740 - 0.959 \cdot \left(\frac{1}{t}\right)^{0.50} \quad (\text{G-18})$$

When first day data were excluded:

$$\ln\left[\frac{f'_c(t)}{f'_c(28)}\right] = 0.1484 - 0.989 \cdot \left(\frac{1}{t}\right)^{0.55} \quad (\text{G-19})$$

The above linearized equations were transformed back to the original Freiesleben equation as follows:

$$f'_c(t) = f'_c(28) \cdot 1.19 \cdot e^{-(0.92/t)^{0.50}} \quad (\text{G-20})$$

When first day data were excluded:

$$f'_c(t) = f'_c(28) \cdot 1.16 \cdot e^{-(0.98/t)^{0.55}} \quad (\text{G-21})$$

Table G-4 shows the actual strength of the concrete for this group of concrete and the corresponding predicted strengths using the two prediction equations. The standard error of the estimates for the strength and the strength factor using the two prediction equations are also shown in the table. Figure G-10 shows the comparison between the actual strength and the predicted strength using these two prediction equations.

Table G-4. Comparison between the actual and Freiesleben model predicted compressive strength for silica fume, fly ash and Type I/II cement mixes.

	Time (days)	Mix 3(psi)	Mix 5(psi)	Mix 6(psi)
Actual strength	1	3,940	4,660	4,640
	3	6,010	6,840	7,020
	7	7,300	8,300	8,430
	28	9,550	9,780	10,010
	91	9,950	10,720	10,920
	182	10,040	10,910	10,870
<hr/>				
	Time (days)	Mix 3'(psi)	Mix 5'(psi)	Mix 6'(psi)
Predicted strength	1	4,334	4,439	4,543
	3	6,503	6,660	6,816
	7	7,875	8,065	8,254
	28	9,442	9,669	9,896
	91	10,236	10,482	10,729
	182	10,542	10,796	11,050
<hr/>				
	Time (days)	Mix 3'(psi)	Mix 5'(psi)	Mix 6'(psi)
Predicted strength without first day data	3	6,503	6,660	6,816
	7	7,875	8,065	8,254
	28	9,442	9,669	9,896
	91	10,236	10,482	10,729
	182	10,542	10,796	11,050
<hr/>				
S.F & F.A (cement type I/II)				
Strength	Se	309 (psi)		
	Se -1	302 (psi)		
Strength factor	Se	0.032		
	Se -1	0.031		

(Note: Se is the standard error of estimate and Se -1 is the standard error of estimate excluding the first day test results.)

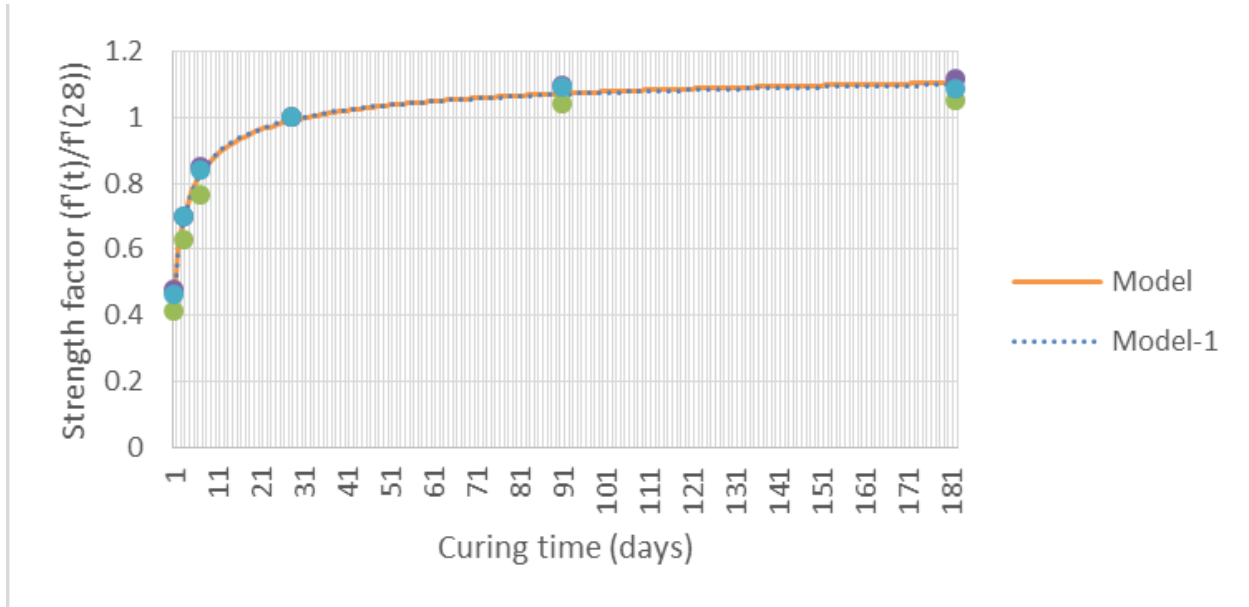


Figure G-10. Comparison between actual and predicted strength factors from Freiesleben model for silica fume, fly ash and Type I/II cement mixes.

Similar regression analysis using the Freiesleben model was performed on the strength factor data on the fourth group of mixes which were silica fume, fly ash and Type III Portland cement. The resulting two prediction equations are as follows:

$$\ln\left[\frac{f'_c(t)}{f'_c(28)}\right] = 0.2070 - 0.719 \cdot \left(\frac{1}{t}\right)^{0.35} \quad (\text{G-22})$$

When first day data were excluded:

$$\ln\left[\frac{f'_c(t)}{f'_c(28)}\right] = 0.1484 - 0.742 \cdot \left(\frac{1}{t}\right)^{0.47} \quad (\text{G-23})$$

The above linearized equations were transformed back to the original Freiesleben equation as follows:

$$f'_c(t) = f'_c(28) \cdot 1.23 \cdot e^{-(0.39/t)^{0.35}} \quad (\text{G-24})$$

When first day data were excluded:

$$f'_c(t) = f'_c(28) \cdot 1.16 \cdot e^{-(0.53/t)^{0.47}} \quad (\text{G-25})$$

The actual strength of the concrete for this group of concrete and the corresponding predicted strengths are shown in Table G-5 using the two prediction equations. The standard error of the estimates for the strength and the strength factor using the two prediction equations are also shown in the table. Figure G-11 shows the comparison between the actual strength and the predicted strength using these two prediction equations.

Table G-5. Comparison between the actual and Freiesleben model predicted compressive strength for silica fume, fly ash and Type III cement mixes.

	Time (days)	Mix 3(psi)	Mix 5(psi)
	Actual strength	1	3,940
3		6,010	6,840
7		7,300	8,300
28		9,550	9,780
91		9,950	10,720
182		10,040	10,910
<hr/>			
	Time (days)	Mix 3'(psi)	Mix 5'(psi)
	Predicted strength	1	4,334
3		6,503	6,660
7		7,875	8,065
28		9,442	9,669
91		10,236	10,482
182		10,542	10,796
<hr/>			
	Time (days)	Mix 3'(psi)	Mix 5'(psi)
	Predicted strength without first day data	3	6,503
7		7,875	8,065
28		9,442	9,669
91		10,236	10,482
182		10,542	10,796
<hr/>			
S.F & F.A (cement type III)			
Strength	Se	309 (psi)	
	Se -1	302 (psi)	
Strength factor	Se	0.032	
	Se -1	0.031	

(Note: Se is the standard error of estimate and Se -1 is the standard error of estimate excluding the first day test results.)

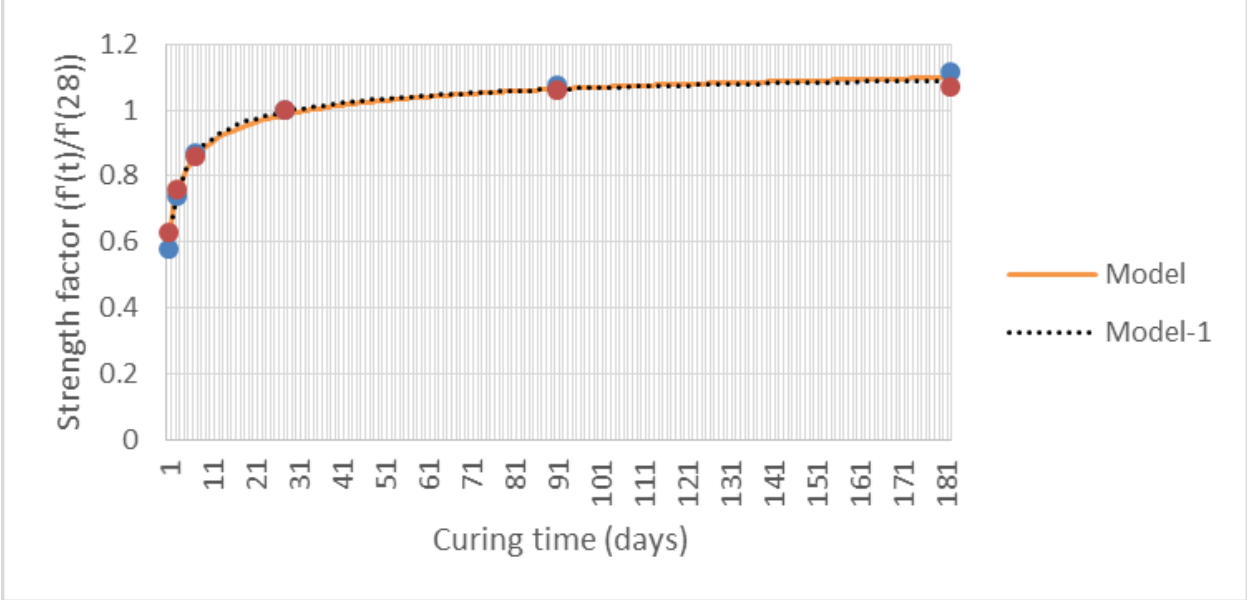


Figure G-11. Comparison between actual and predicted strength factors from Freiesleben model for silica fume, fly ash and Type III cement mixes.

G.1.4.2 Modified CEB-FIP Model

The CEB-FIP model was modified into the following form:

$$f'_c(t) = f'_c(28) \cdot e^{a[1-(28/t)^b]} \quad (\text{G-26})$$

Where

a and b are coefficients.

The above equation was re-written in terms of the strength factor as follows:

$$\frac{f'_c(t)}{f'_c(28)} = e^{a[1-(28/t)^b]} \quad (\text{G-27})$$

By taking the natural logarithm of the equation, the equation becomes the following:

$$\ln\left[\frac{f'_c(t)}{f'_c(28)}\right] = a\left(1 - \left(\frac{28}{t}\right)^b\right) \quad (\text{G-28})$$

The above equation can be considered as a linear equation in the following form:

$$y = \alpha \cdot x \quad (\text{G-29})$$

Where

$$y = \ln\left[\frac{f'_c(t)}{f'_c(28)}\right],$$

$$x = \left(1 - \left(\frac{28}{t}\right)^b\right),$$

a and b are coefficients.

Linear regression analysis was performed using equation (G-29) with different values of b. The value of b which gave the highest R² value was selected to be used in the adopted regression analysis. Figure G-12 shows a sample plot of this linearized equation.

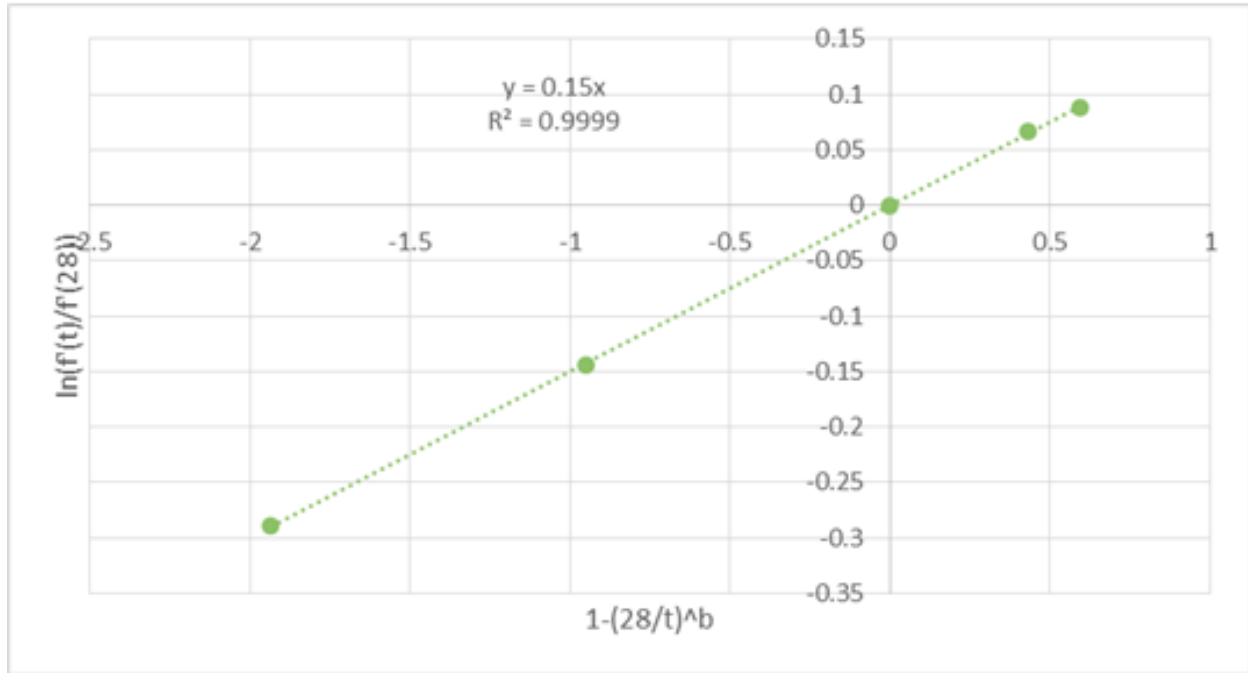


Figure G-12. Sample plot of linearized modified CEB-FIP model.

Linear regression analysis was performed on the strength factor data for the first group of mixes which were slag and fly ash mixes with W/C more than 0.4, with and without excluding the first day strength data. The two optimized linear regression equations obtained were as follows:

$$\ln\left[\frac{f'_c(t)}{f'_c(28)}\right] = 0.22 \cdot (1 - (28/t)^{0.70}) \quad (G-30)$$

When first-day data were excluded:

$$\ln\left[\frac{f'_c(t)}{f'_c(28)}\right] = 0.19 \cdot (1 - (28/t)^{0.75}) \quad (G-31)$$

The above linearized equations were transformed back to the original modified CEB-FIP model equation as follows:

$$f'_c(t) = e^{0.22 \cdot (1 - (28/t)^{0.70})} \cdot f'_c(28) \quad (G-32)$$

When first-day data were excluded:

$$f'_c(t) = e^{0.19 \cdot (1 - (28/t)^{0.75})} \cdot f'_c(28) \quad (G-33)$$

The comparison between the actual strength of the concrete for this group of concrete and the corresponding predicted strengths are shown in Table G-6 using the two prediction equations. Figure G-13 shows the comparison between the actual strength and the predicted strength using these two prediction equations

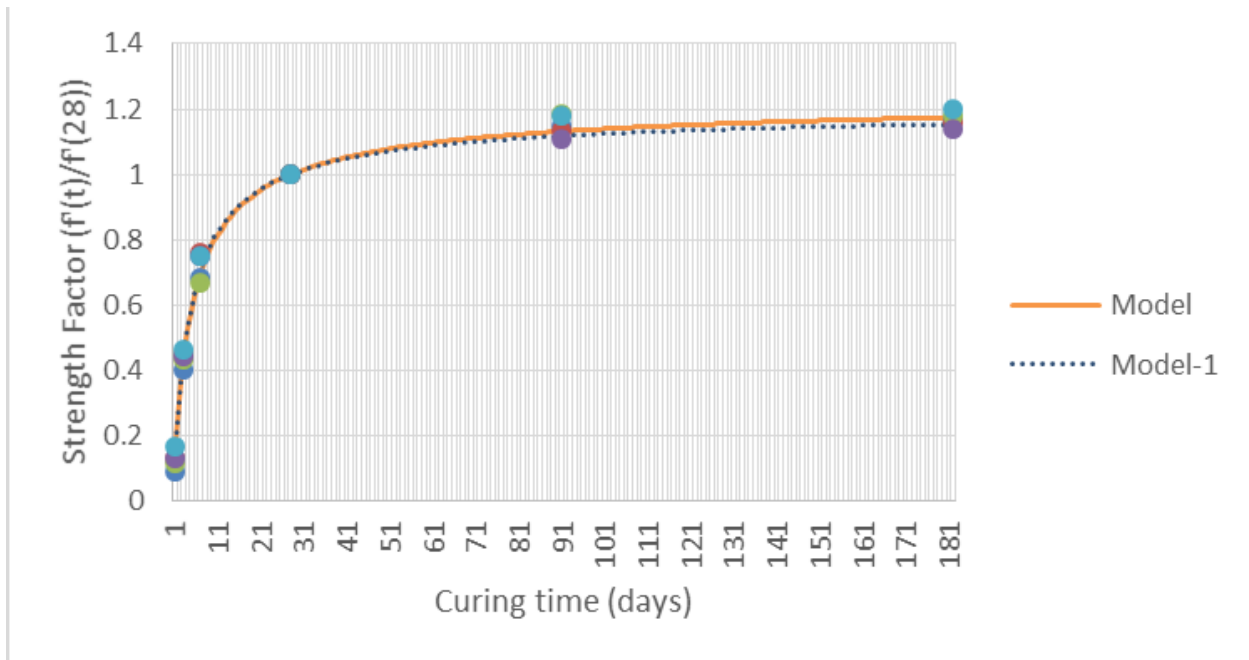


Figure G-13. Comparison between actual and predicted strength factors from modified CEB-FIP model for slag and fly ash mixes with W/C more than 0.4

Table G-6. Comparison between the actual and modified CEB-FIP model predicted compressive strength for slag and fly ash mixes with W/C more than 0.4.

	Time (days)	Mix 1(psi)	Mix 2(psi)	Mix 7(psi)	Mix 11(psi)	Mix 12(psi)
Actual strength	1	740	870	970	940	1,210
	3	3,210	3,010	3,580	3,170	3,340
	7	5,420	5,080	5,510	5,340	5,430
	28	7,930	6,700	8,270	7,140	7,230
	91	9,130	7,610	9,810	7,910	8,540
	182	9,270	7,770	9,750	8,130	8,660
	Time (days)	Mix 1'(psi)	Mix 2'(psi)	Mix 7'(psi)	Mix 11'(psi)	Mix 12'(psi)
Predicted strength	1	1,024	865	1,068	922	934
	3	3,456	2,920	3,604	3,111	3,151
	7	5,529	4,672	5,766	4,979	5,041
	28	7,930	6,700	8,270	7,140	7,230
	91	8,973	7,581	9,358	8,079	8,181
	182	9,312	7,868	9,711	8,384	8,490
	Time (days)	Mix 1'(psi)	Mix 2'(psi)	Mix 7'(psi)	Mix 11'(psi)	Mix 12'(psi)
Predicted strength without first day data	3	3,477	2,937	3,626	3,130	3,170
	7	5,603	4,734	5,843	5,045	5,108
	28	7,930	6,700	8,270	7,140	7,230
	91	8,865	7,490	9,246	7,982	8,083
	182	9,152	7,733	9,544	8,240	8,344
Strength	Se	221 (psi)				
	Se -1	242 (psi)				
Strength factor	Se	0.030				
	Se -1	0.033				

(Note: Se is the standard error of estimate and Se -1 is the standard error of estimate excluding the first day test results.)

Similar regression analysis using the modified CEB-FIP model was performed on the strength factor data on the second group of mixes which were slag and fly ash mixes with W/C less than 0.4. The resulting two prediction equations are as follows:

$$\ln\left[\frac{f'_c(t)}{f'_c(28)}\right] = 0.10 \cdot \left(1 - \left(\frac{28}{t}\right)^{0.90}\right) \quad (\text{G-34})$$

When first-day data were excluded:

$$\ln\left[\frac{f'_c(t)}{f'_c(28)}\right] = 0.15 \cdot \left(1 - \left(\frac{28}{t}\right)^{0.57}\right) \quad (\text{G-35})$$

The above linearized equations were transformed back to the original modified CEB-FIP model equation as follows:

$$f'_c(t) = e^{0.10 \cdot \left(1 - \left(\frac{28}{t}\right)^{0.90}\right)} \cdot f'_c(28) \quad (\text{G-36})$$

When first-day data were excluded:

$$f'_c(t) = e^{0.15 \cdot \left(1 - \left(\frac{28}{t}\right)^{0.57}\right)} \cdot f'_c(28) \quad (\text{G-37})$$

The comparison between the actual strength of the concrete for this group of concrete and the corresponding predicted strengths are shown in Table G-7 using the two prediction equations. Figure G-14 shows the comparison between the actual strength and the predicted strength using these two prediction equations.

Table G-7. Comparison between the actual and modified CEB-FIP model predicted compressive strength for slag and fly ash mixes with W/C less than 0.4.

		Time (days)	Mix 4(psi)	Mix 9(psi)	Mix 13(psi)	Mix 14(psi)
Actual strength		1	1,270	1,580	970	1,340
		3	5,050	4,640	5,020	4,860
		7	7,650	6,890	6,820	6,640
		28	9,820	9,900	8,540	7,980
		91	10,630	11,110	9,070	9,080
		182	10,690	11,300	9,540	9,400
		Time (days)	Mix 4'(psi)	Mix 9'(psi)	Mix 13'(psi)	Mix 14'(psi)
Predicted strength		1	1,459	1,471	1,269	1,186
		3	5,144	5,186	4,474	4,181
		7	7,661	7,724	6,663	6,226
		28	9,820	9,900	8,540	7,980
		91	10,484	10,569	9,117	8,519
		182	10,653	10,740	9,265	8,657
		Time (days)	Mix 4'(psi)	Mix 9'(psi)	Mix 13'(psi)	Mix 14'(psi)
Predicted strength without first day data		3	5,144	5,186	4,474	4,181
		7	7,661	7,724	6,663	6,226
		28	9,820	9,900	8,540	7,980
		91	10,484	10,569	9,117	8,519
		182	10,653	10,740	9,265	8,657
Strength	Se		443 (psi)			
	Se -1		377 (psi)			
Strength factor	Se		0.048			
	Se -1		0.041			

(Note: Se is the standard error of estimate and Se -1 is the standard error of estimate excluding the first day test results.)

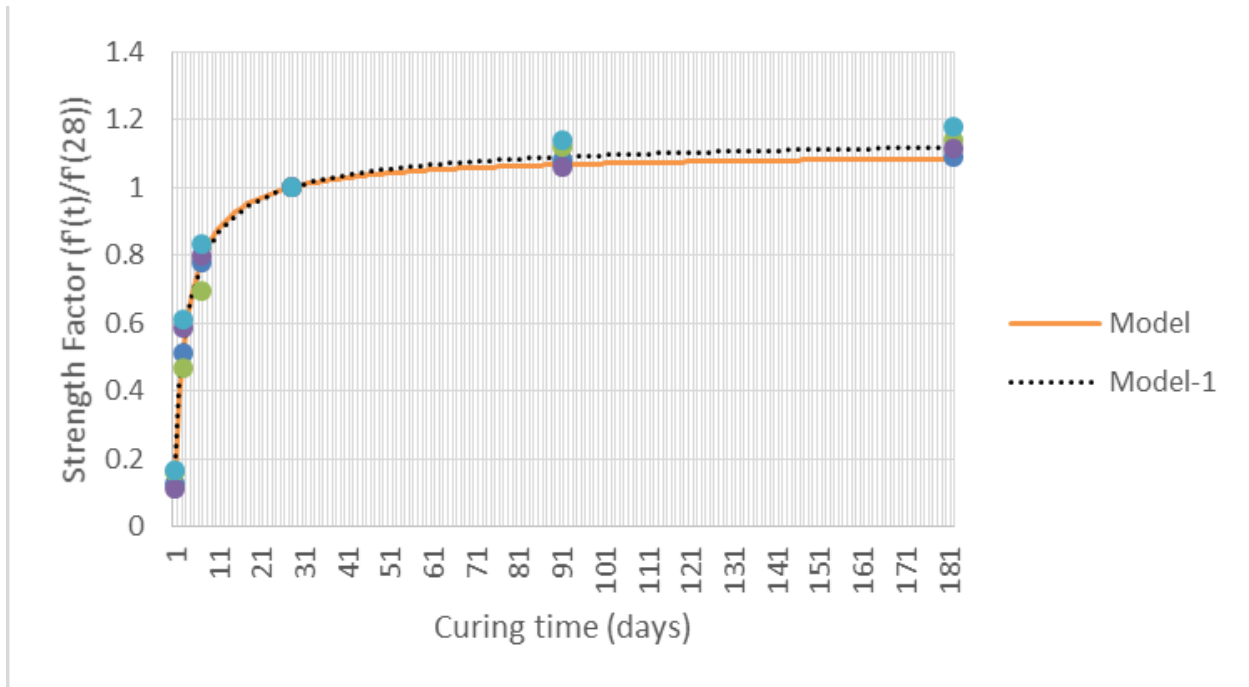


Figure G-14. Comparison between actual and predicted strength factors from modified CEB-FIP model for slag and fly ash mixes with W/C less than 0.4 modified.

Similar regression analysis using the modified CEB-FIP model was performed on the strength factor data on the third group of mixes which were silica fume, fly ash and type I/II Portland cement. The resulting two prediction equations are as follows:

$$\ln\left[\frac{f'_c(t)}{f'_c(28)}\right] = 0.18 \cdot \left(1 - \left(\frac{28}{t}\right)^{0.50}\right) + 0 \quad (\text{G-38})$$

When first-day data were excluded:

$$\ln\left[\frac{f'_c(t)}{f'_c(28)}\right] = 0.15 \cdot \left(1 - \left(\frac{28}{t}\right)^{0.57}\right) + 0 \quad (\text{G-39})$$

The above linearized equations were transformed back to the original modified CEB-FIP model equation as follows:

$$f'_c(t) = e^{0.18 \cdot (1 - (28/t)^{0.50})} \cdot f'_c(28) \quad (\text{G-40})$$

When first-day data were excluded:

$$f'_c(t) = e^{0.15 \cdot (1 - (28/t)^{0.57})} \cdot f'_c(28) \quad (\text{G-41})$$

Table G-8 shows the comparison between the actual strength of the concrete for this group of concrete and the corresponding predicted strengths using the two prediction equations. Figure G-15 shows the comparison between the actual strength and the predicted strength using these two prediction equations.

Table G-8. Comparison between the actual and modified CEB-FIP model predicted compressive strength for silica fume, fly ash and Type I/II cement mixes.

	Time (days)	Mix 3(psi)	Mix 5(psi)	Mix 6(psi)
Actual strength	1	3,940	4,660	4,640
	3	6,010	6,840	7,020
	7	7,300	8,300	8,430
	28	9,550	9,780	10,010
	91	9,950	10,720	10,920
	182	10,040	10,910	10,870
	Time (days)	Mix 3'(psi)	Mix 5'(psi)	Mix 6'(psi)
Predicted strength	1	4,411	4,517	4,623
	3	6,597	6,756	6,915
	7	7,977	8,169	8,361
	28	9,550	9,780	10,010
	91	10,347	10,596	10,845
	182	10,654	10,911	11,167
	Time (days)	Mix 3'(psi)	Mix 5'(psi)	Mix 6'(psi)
Predicted strength without first day data	3	6,597	6,756	6,915
	7	7,977	8,169	8,361
	28	9,550	9,780	10,010
	91	10,347	10,596	10,845
	182	10,654	10,911	11,167
Strength	Se	338 (psi)		
	Se -1	310 (psi)		
Strength factor	Se	0.035		
	Se -1	0.032		

(Note: Se is the standard error of estimate and Se -1 is the standard error of estimate excluding the first day test results.)

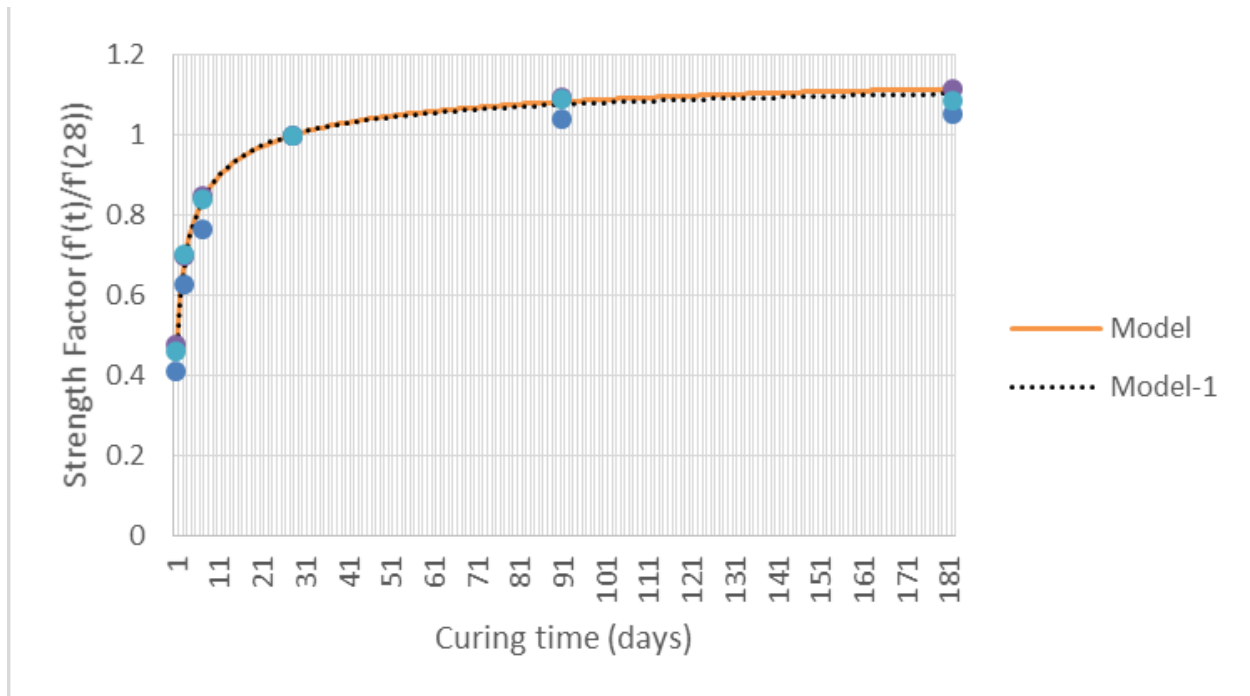


Figure G-15. Comparison between actual and predicted strength factors from modified CEB-FIP model for silica fume, fly ash and Type I/II cement mixes.

Similar regression analysis using the modified CEB-FIP model was performed on the strength factor data on the fourth group of mixes which were silica fume, fly ash and type III Portland cement. The resulting two prediction equations are as follows:

$$\ln\left[\frac{f'_c(t)}{f'_c(28)}\right] = 0.22 \cdot \left(1 - \left(\frac{28}{t}\right)^{0.35}\right) + 0 \quad (\text{G-42})$$

When first-day data were excluded:

$$\ln\left[\frac{f'_c(t)}{f'_c(28)}\right] = 0.16 \cdot \left(1 - \left(\frac{28}{t}\right)^{0.47}\right) + 0 \quad (\text{G-43})$$

The above linearized equations were transformed back to the original modified CEB-FIP model equation as follows:

$$f'_c(t) = e^{0.22 \cdot (1 - (28/t)^{0.35})} \cdot f'_c(28) \quad (\text{G-44})$$

When first-day data were excluded:

$$f'_c(t) = e^{0.16(1 - (28/t)^{0.47})} \cdot f'_c(28) \quad (\text{G-45})$$

Table G-9 shows the comparison between the actual strength of the concrete for this group of concrete and the corresponding predicted strengths using the two prediction equations. Figure G-16 shows the comparison between the actual strength and the predicted strength using these two prediction equations.

Table G-9. Comparison between the actual and modified CEB-FIP model predicted compressive strength for silica fume, fly ash and Type III cement mixes.

	Time	Mix 8(psi)	Mix 10(psi)
	(days)		
Actual strength	1	5,650	6,510
	3	7,220	7,840
	7	8,520	8,870
	28	9,770	10,330
	91	10,520	10,950
	182	10,910	11,040
<hr/>			
	Time	Mix 8'(psi)	Mix 10'(psi)
	(days)		
Predicted strength	1	6,008	6,353
	3	7,527	7,959
	7	8,516	9,004
	28	9,770	10,330
	91	10,524	11,127
	182	10,860	11,482
<hr/>			
	Time	Mix 8'(psi)	Mix 10'(psi)
	(days)		
Predicted strength without first day data	3	7,527	7,959
	7	8,516	9,004
	28	9,770	10,330
	91	10,524	11,127
	182	10,860	11,482
<hr/>			
Strength	Se	211 (psi)	
	Se -1	150 (psi)	
Strength factor	Se	0.021	
	Se -1	0.015	

(Note: Se is the standard error of estimate and Se -1 is the standard error of estimate excluding the first day test results.)

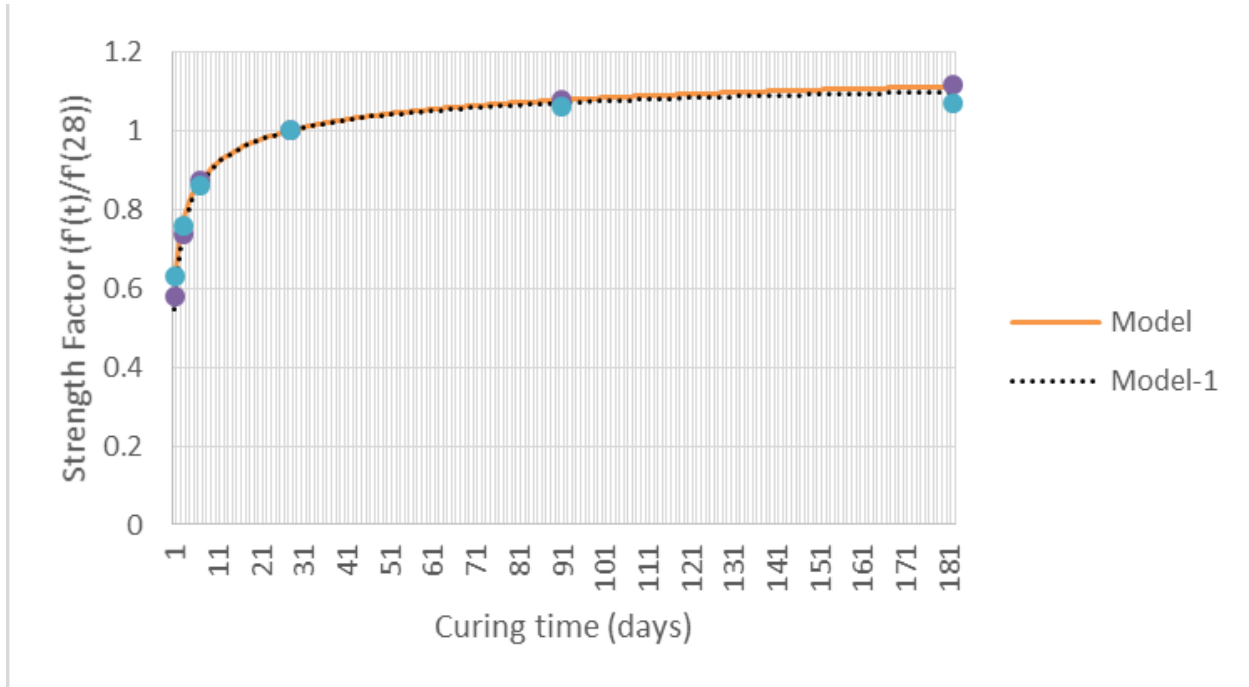


Figure G-16. Comparison between actual and predicted strength factors from modified CEB-FIP model for silica fume, fly ash and Type III cement mixes.

G.1.4.3 Modified Hyperbolic Model

The modified hyperbolic model was of the form shown in Equation G-46.

$$f'_c(t) = \frac{t^c}{a + b \cdot t^c} \cdot f'_c(28) \quad (\text{G-46})$$

It was re-written in terms of the strength factor as shown in Equation G-47.

$$\frac{f'_c(t)}{f'_c(28)} = \frac{t^c}{a + b \cdot t^c} \quad (\text{G-47})$$

By taking the reciprocal of Equation G-47, the equation becomes as follows:

$$\frac{f'_c(28)}{f'_c(t)} = \frac{a + b \cdot t^c}{t^c} = a \cdot \left(\frac{1}{t}\right)^c + b \quad (\text{G-48})$$

Equation G-48 can be considered as a linear equation in the following form:

$$y = \alpha \cdot x + b \quad (G-49)$$

Where

$$y = \frac{f'_c(28)}{f'_c(t)},$$

$$x = \left(\frac{1}{t}\right)^c,$$

a , b and c are coefficients.

Linear regression analysis was performed using Equation G-49 with different values of c . the value of c which gave the highest R^2 value was selected to be used in the adopted equation.

Figure G-17 shows the sample plot of this regression equation.

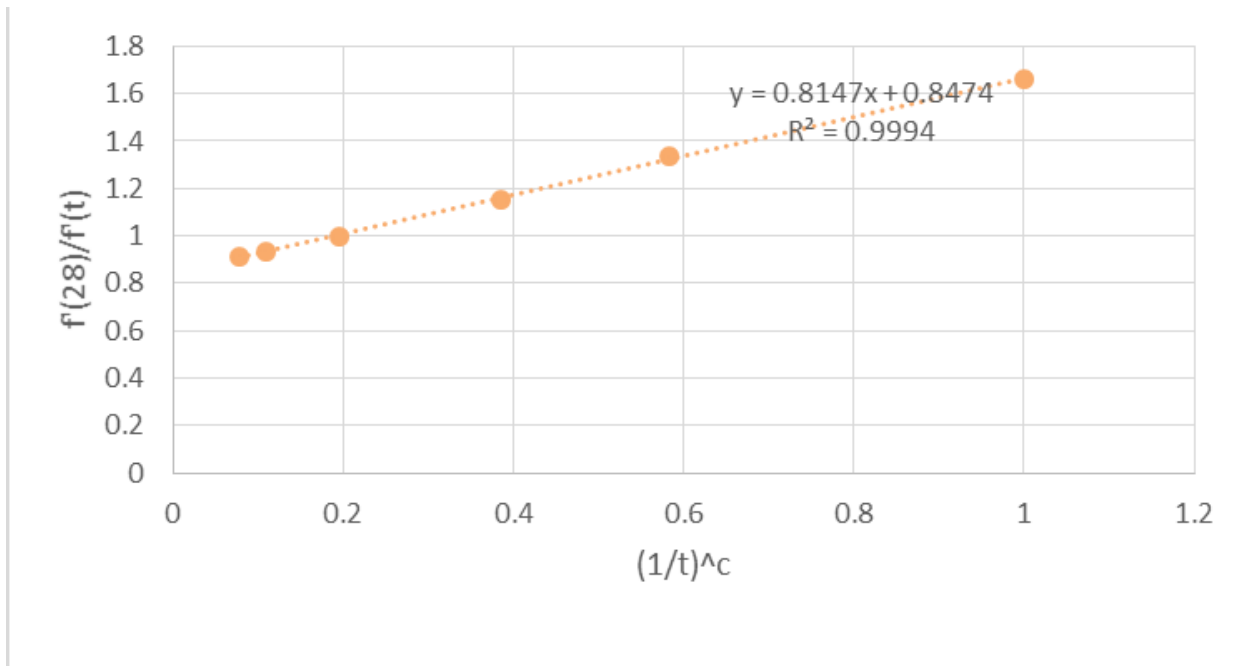


Figure G-17. Sample plot of linearized modified hyperbolic model.

Regression analysis was performed on the inverse of the strength factor data for the first group of mixes which were slag and fly ash mixes with W/C more than 0.4, with and without excluding the first day compressive strength data.

The two optimized regression equations are as shown in Equations G-50 and G-51.

$$\left[\frac{f'_c(28)}{f'_c(t)} \right] = 7.19 \cdot \left(\frac{1}{t} \right)^{1.50} + 0.91 \quad (\text{G-50})$$

When the first day data were excluded:

$$\left[\frac{f'_c(28)}{f'_c(t)} \right] = 5.05 \cdot \left(\frac{1}{t} \right)^{1.15} + 0.86 \quad (\text{G-51})$$

The above two regression equations were re-arranged to relate $f'(t)$ to $f'(28)$ as follows:

$$f'_c(t) = \frac{t^{1.5}}{0.91 \cdot t^{1.5} + 7.19} \cdot f'_c(28) \quad (\text{G-52})$$

When the first day compressive strength data were excluded:

$$f'_c(t) = \frac{t^{1.15}}{0.86 \cdot t^{1.15} + 5.05} \cdot f'_c(28) \quad (\text{G-53})$$

Table G-10 shows the comparison of the actual strength of the concrete for this group of concrete and the corresponding predicted strengths using the two prediction equations. The standard error of the estimates for the strength and the strength factor using the two prediction equations are also shown in the table. Figure G-18 shows the comparison between the actual strength and the predicted strength using these two prediction equations.

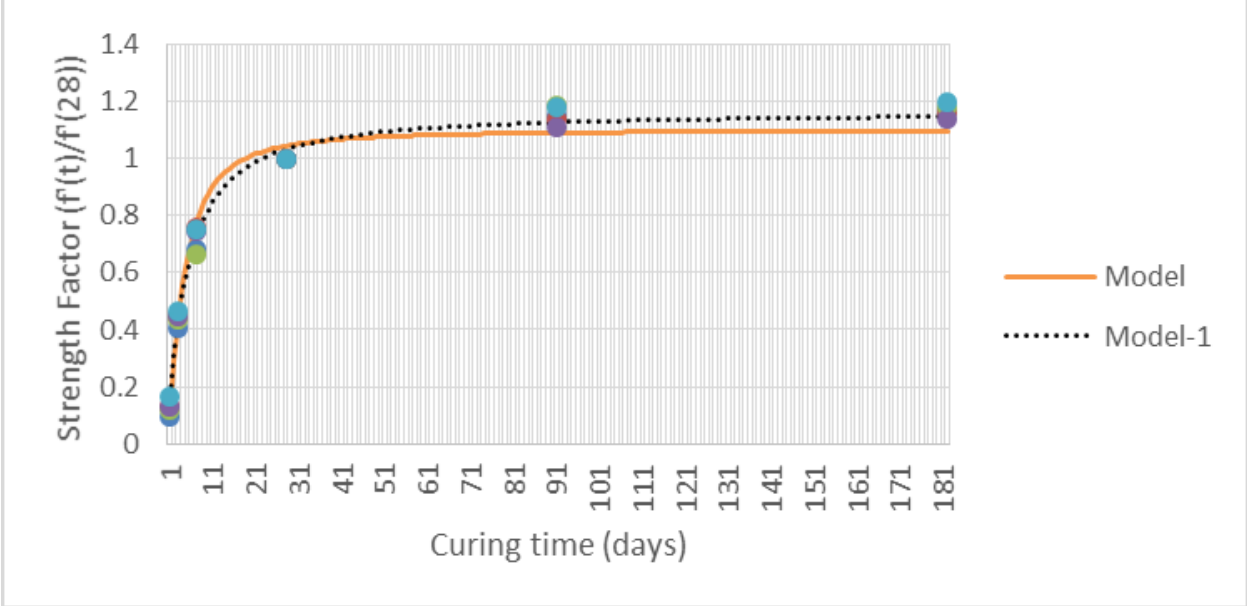


Figure G-18. Comparison between actual and predicted strength factors from modified hyperbolic model for slag and fly ash mixes with W/C more than 0.4.

Table G-10. Comparison between the actual and modified hyperbolic model predicted compressive strength for slag and fly ash mixes with W/C more than 0.4.

	Time (days)	Mix 1(psi)	Mix 2(psi)	Mix 7(psi)	Mix 11(psi)	Mix 12(psi)
Actual strength	1	740	870	970	940	1,210
	3	3,210	3,010	3,580	3,170	3,340
	7	5,420	5,080	5,510	5,340	5,430
	28	7,930	6,700	8,270	7,140	7,230
	91	9,130	7,610	9,810	7,910	8,540
	182	9,270	7,770	9,750	8,130	8,660
	Time (days)	Mix 1'(psi)	Mix 2'(psi)	Mix 7'(psi)	Mix 11'(psi)	Mix 12'(psi)
Predicted strength	1	979	827	1,021	881	893
	3	3,457	2,921	3,606	3,113	3,152
	7	6,108	5,161	6,370	5,500	5,569
	28	8,273	6,990	8,628	7,449	7,543
	91	8,636	7,296	9,006	7,775	7,873
	182	8,686	7,339	9,059	7,821	7,920
	Time (days)	Mix 1'(psi)	Mix 2'(psi)	Mix 7'(psi)	Mix 11'(psi)	Mix 12'(psi)
Predicted strength without first day data	3	3,467	2,929	3,615	3,121	3,161
	7	5,669	4,790	5,912	5,104	5,169
	28	8,180	6,911	8,531	7,365	7,458
	91	8,928	7,543	9,311	8,039	8,140
	182	9,087	7,677	9,476	8,181	8,285
Strength	Se	466 (psi)				
	Se -1	260 (psi)				
Strength factor	Se	0.063				
	Se -1	0.035				

(Note: Se is the standard error of estimate and Se -1 is the standard error of estimate excluding the first day test results.)

Similar regression analysis using the modified hyperbolic model was performed on the inverse of the strength factor data on the second group of mixes which were slag and fly ash mixes with W/C less than 0.4. The resulting two prediction equations are as follows:

$$\left[\frac{f'_c(28)}{f'_c(t)} \right] = 6.24 \cdot \left(\frac{1}{t} \right)^{1.70} + 0.95 \quad (\text{G-54})$$

When the first day compressive strength data were excluded:

$$\left[\frac{f'_c(28)}{f'_c(t)} \right] = 2.93 \cdot \left(\frac{1}{t} \right)^{1.00} + 0.88 \quad (\text{G-55})$$

The above two regression equations were re-arranged to relate $f'(t)$ to $f'(28)$ as follows:

$$f'_c(t) = \frac{t^{1.7}}{0.95 \cdot t^{1.7} + 6.24} \cdot f'_c(28) \quad (\text{G-56})$$

When the first day compressive strength data were excluded:

$$f'_c(t) = \frac{t^{1.0}}{0.88 \cdot t^{1.0} + 2.93} \cdot f'_c(28) \quad (\text{G-57})$$

Table G-11 shows the comparison of the actual strength of the concrete for this group of concrete and the corresponding predicted strengths using the two prediction equations. Figure G-19 shows the comparison between the actual strength and the predicted strength using these two prediction equations.

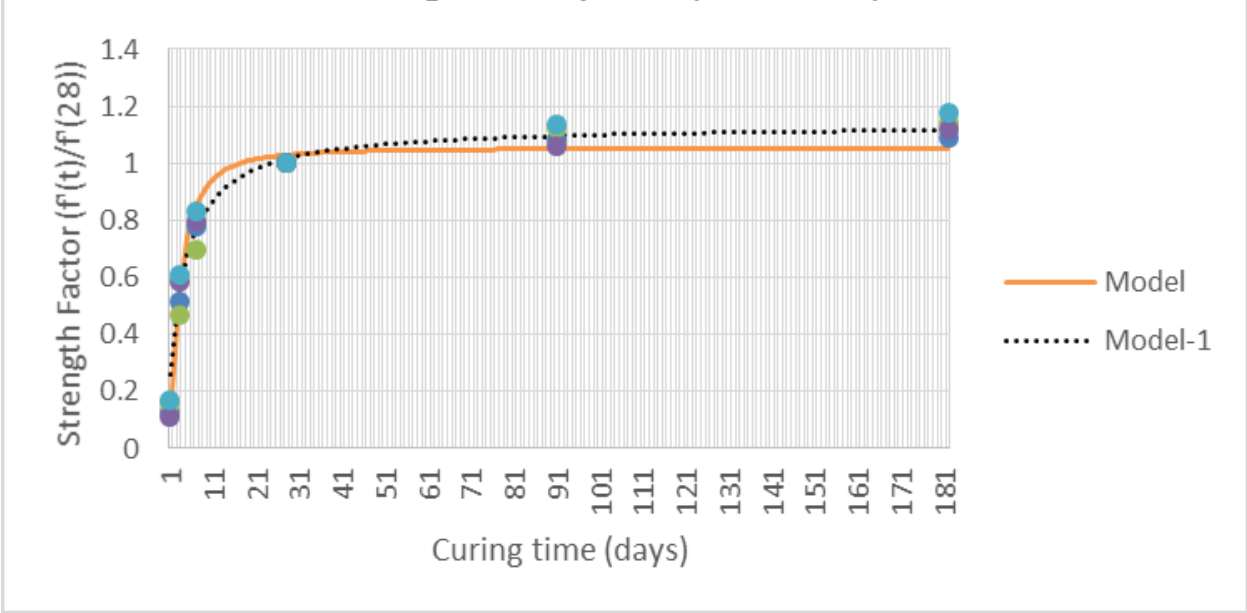


Figure G-19. Comparison between actual and predicted strength factors from modified hyperbolic model for slag and fly ash mixes with W/C less than 0.4.

Table G-11. Comparison between the actual and modified hyperbolic model predicted compressive strength for slag and fly ash mixes with W/C less than 0.4.

		Time (days)	Mix 4(psi)	Mix 9(psi)	Mix 13(psi)	Mix 14(psi)
Actual strength		1	1,270	1,580	970	1,340
		3	5,050	4,640	5,020	4,860
		7	7,650	6,890	6,820	6,640
		28	9,820	9,900	8,540	7,980
		91	1,0630	11,110	9,070	9,080
		182	1,0690	11,300	9,540	9,400
		Time (days)	Mix 4'(psi)	Mix 9'(psi)	Mix 13'(psi)	Mix 14'(psi)
Predicted strength		1	1,366	1,377	1,188	1,110
		3	5,131	5,172	4,462	4,169
		7	8,334	8,402	7,248	6,772
		28	10,107	10,189	8,789	8,213
		91	10,305	10,389	8,962	8,374
		182	10,327	10,411	8,981	8,392
		Time (days)	Mix 4'(psi)	Mix 9'(psi)	Mix 13'(psi)	Mix 14'(psi)
Predicted strength without first day data		3	5,289	5,332	4,600	4,298
		7	7,562	7,624	6,576	6,145
		28	9,973	10,054	8,673	8,104
		91	10,765	10,853	9,362	8,748
		182	10,959	11,048	9,530	8,905
Strength	Se		654 (psi)			
	Se -1		382 (psi)			
Strength factor	Se		0.072			
	Se -1		0.042			

(Note: Se is the standard error of estimate and Se -1 is the standard error of estimate excluding the first day test results.)

Similar regression analysis using the modified hyperbolic model was performed on the inverse of the strength factor data on the third group of mixes which were silica fume and fly ash mixes with Type I/II Portland cement. The resulting two prediction equations are as follows:

$$\left[\frac{f'_c(28)}{f'_c(t)} \right] = 1.34 \cdot \left(\frac{1}{t} \right)^{0.72} + 0.88 \quad (\text{G-58})$$

When the first day data were excluded:

$$\left[\frac{f'_c(28)}{f'_c(t)} \right] = 1.30 \cdot \left(\frac{1}{t} \right)^{0.70} + 0.88 \quad (\text{G-59})$$

The above two regression equations were transformed relate $f'_c(t)$ to $f'_c(28)$ as shown in Equations G-60 and G-61.

$$f'_c(t) = \frac{t^{0.72}}{0.88 \cdot t^{0.72} + 1.34} \cdot f'_c(28) \quad (\text{G-60})$$

When the first day data were excluded:

$$f'_c(t) = \frac{t^{0.70}}{0.88 \cdot t^{0.70} + 1.30} \cdot f'_c(28) \quad (\text{G-61})$$

Table G-12 shows the comparison between the actual strength of the concrete for this group of concrete and the corresponding predicted strengths using the two prediction equations. Figure G-20 shows the comparison between the actual strength and the predicted strength using these two prediction equations.

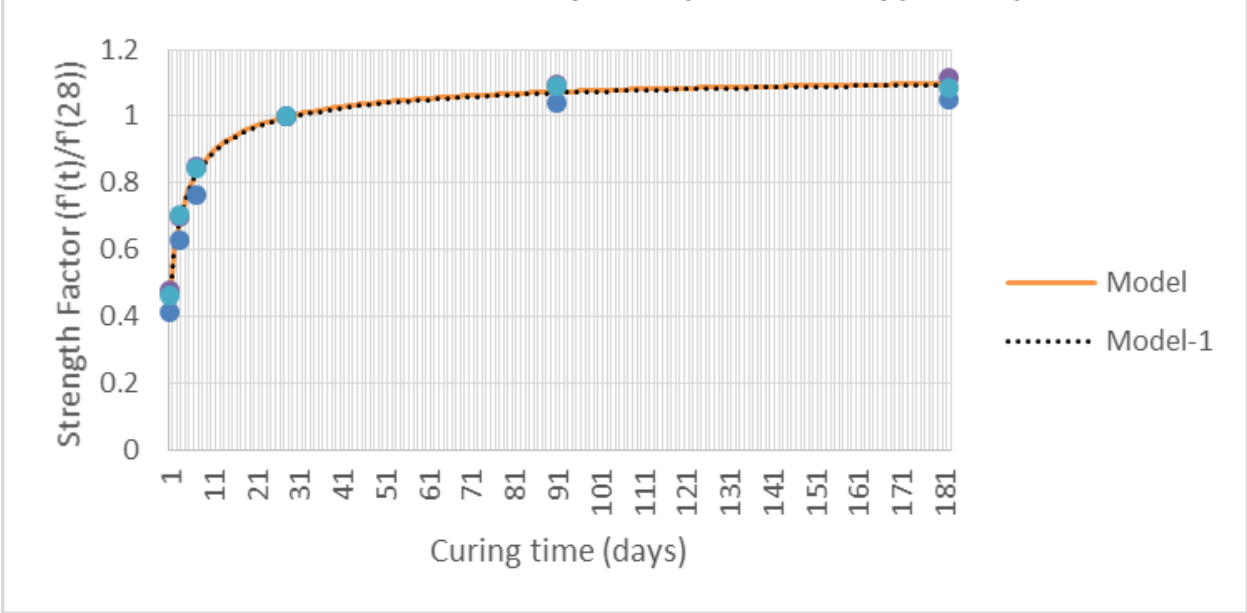


Figure G-20. Comparison between actual and predicted strength factors from modified hyperbolic model for silica fume, fly ash and Type I/II cement mixes.

Table G-12. Comparison between the actual and modified hyperbolic model predicted compressive strength for silica fume, fly ash and Type I/II cement mixes.

	Time (days)	Mix 3(psi)	Mix 5(psi)	Mix 6(psi)
Actual strength	1	3,940	4,660	4,640
	3	6,010	6,840	7,020
	7	7,300	8,300	8,430
	28	9,550	9,780	10,010
	91	9,950	10,720	10,920
	182	10,040	10,910	10,870
	Time (days)	Mix 3'(psi)	Mix 5'(psi)	Mix 6'(psi)
Predicted strength	1	4,302	4,405	4,509
	3	6,420	6,575	6,729
	7	7,892	8,082	8,272
	28	9,534	9,764	9,993
	91	10,246	10,493	10,740
	182	10,476	10,728	10,981
	Time (days)	Mix 3'(psi)	Mix 5'(psi)	Mix 6'(psi)
Predicted strength without first day data	3	6,442	6,597	6,752
	7	7,873	8,063	8,253
	28	9,492	9,720	9,949
	91	10,211	10,457	10,703
	182	10,448	10,700	10,951
Strength	Se	298 (psi)		
	Se -1	297 (psi)		
Strength factor	Se	0.031		
	Se -1	0.031		

(Note: Se is the standard error of estimate and Se -1 is the standard error of estimate excluding the first day test results.)

Similar regression analysis using the modified hyperbolic model was performed on the inverse of the strength factor data on the fourth group of mixes which were silica fume and fly ash mixes with Type III Portland cement. The resulting two prediction equations are as shown in Equations G-62 and G-63.

$$\left[\frac{f'_c(28)}{f'_c(t)} \right] = 0.81 \cdot \left(\frac{1}{t} \right)^{0.49} + 0.85 \quad (\text{G-62})$$

When the first day data were excluded:

$$\left[\frac{f'_c(28)}{f'_c(t)} \right] = 0.88 \cdot \left(\frac{1}{t} \right)^{0.58} + 0.87 \quad (\text{G-63})$$

The above two regression equations were reformed to rebate $f'_c(t)$ to $f'_c(28)$ as shown in Equations G-64 and G-65.

$$f'_c(t) = \frac{t^{0.49}}{0.85 \cdot t^{0.49} + 0.81} \cdot f'_c(28) \quad (\text{G-64})$$

When the first day data were excluded:

$$f'_c(t) = \frac{t^{0.58}}{0.87 \cdot t^{0.58} + 0.88} \cdot f'_c(28) \quad (\text{G-65})$$

Table G-13 shows the comparison between the actual strength of the concrete for this group of concrete and the corresponding predicted strengths using the two prediction equations. Figure G-21 shows the comparison between the actual strength and the predicted strength using these two prediction equations.

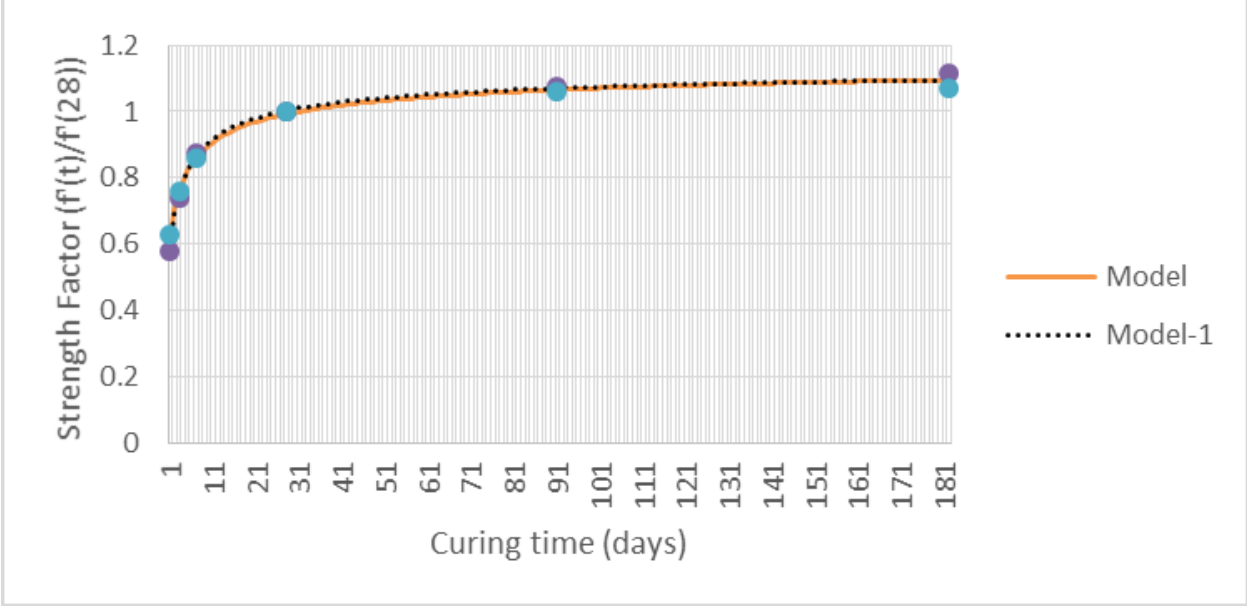


Figure G-21. Comparison between actual and predicted strength factors from modified hyperbolic model for silica fume, fly ash and Type III cement mixes.

Table G-13. Comparison between the actual and modified hyperbolic model predicted compressive strength for silica fume, fly ash and Type III cement mixes.

	Time (days)	Mix 8(psi)	Mix 10(psi)
	Actual strength	1	5,650
3		7,220	7,840
7		8,520	8,870
28		9,770	10,330
91		10,520	10,950
182		10,910	11,040
	Time (days)	Mix 8'(psi)	Mix 10'(psi)
	Predicted strength	1	5,886
3		7,386	7,809
7		8,407	8,889
28		9,690	10,245
91		10,407	11,003
182		10,698	11,311
	Time (days)	Mix 8'(psi)	Mix 10'(psi)
	Predicted strength without first day data	3	7,317
7		8,461	8,946
28		9,796	10,357
91		10,457	11,056
182		10,701	11,314
Strength	Se	154 (psi)	
	Se -1	144 (psi)	
Strength factor	Se	0.015	
	Se -1	0.014	

(Note: Se is the standard error of estimate and Se -1 is the standard error of estimate excluding the first day test results.)

G.1.4.4 Second Degree Hyperbolic Model,

The second degree hyperbolic model was of the form shown in Equation G-66.

$$f'_c(t) = \frac{t^2}{a \cdot t^2 + b \cdot t + c} \cdot f'_c(28) \quad (\text{G-66})$$

It was re-written in terms of the strength factor as shown in Equation G-67.

$$\frac{f'_c(t)}{f'_c(28)} = \frac{t^2}{a \cdot t^2 + b \cdot t + c} \quad (\text{G-67})$$

By taking the reciprocal of equation G-67, the equation becomes as follows:

$$\frac{f'_c(28)}{f'_c(t)} = \frac{a \cdot t^2 + b \cdot t + c}{t^2} = a + b \cdot \left(\frac{1}{t}\right)^1 + c \cdot \left(\frac{1}{t}\right)^2 \quad (\text{G-68})$$

Equation G-68 can be considered as a linear equation in the following form:

$$y = a + b \cdot x + c \cdot x^2 \quad (\text{G-69})$$

Where

$$y = \frac{f'_c(28)}{f'_c(t)},$$

$$x = \left(\frac{1}{t}\right),$$

a , b and c are coefficients.

Second degree regression analysis was performed using equation G-69 to obtain the best-fit equation. The regression analysis was performed on the inverse of the strength factor data for the first group of mixes which were slag and fly ash mixes with W/C more than 0.4, with and without excluding the first day compressive strength data.

The two optimized regression equations are as shown in Equations G-70 and G-71.

$$[f'_c(28)/f'_c(t)] = 0.86 + 2.88(1/t) + 4.36(1/t)^2 \quad (\text{G-70})$$

When the first-day data were excluded:

$$[f'_c(28)/f'_c(t)] = 0.84 + 3.57(1/t) + 2.25(1/t)^2 \quad (\text{G-71})$$

The above two regression equations were re-arranged to relate $f'_c(t)$ to $f'_c(28)$ as shown in Equations G-72 and G-73.

$$f'_c(t) = \frac{t^2}{0.86 \cdot t^2 + 2.88 \cdot t + 4.36} \cdot f'_c(28) \quad (\text{G-72})$$

When the first-day data were excluded:

$$f'_c(t) = \frac{t^2}{0.84 \cdot t^2 + 3.57 \cdot t + 2.25} \cdot f'_c(28) \quad (\text{G-73})$$

Table G-14 shows the comparison between the actual strength of the concrete for this group of concrete and the corresponding predicted strengths using the two prediction equations. The standard error of the estimates for the strength and the strength factor using the two prediction equations are also shown in the table. Figure G-22 shows the comparison between the actual strength and the predicted strength using these two prediction equations.

Table G-14. Comparison between the actual and 2nd degree hyperbolic predicted compressive strength for slag and fly ash mixes with W/C more than 0.4.

	Time (days)	Mix 1(psi)	Mix 2(psi)	Mix 7(psi)	Mix 11(psi)	Mix 12(psi)
Actual strength	1	740	870	970	940	1,210
	3	3,210	3,010	3,580	3,170	3,340
	7	5,420	5,080	5,510	5,340	5,430
	28	7,930	6,700	8,270	7,140	7,230
	91	9,130	7,610	9,810	7,910	8,540
	182	9,270	7,770	9,750	8,130	8,660
	Time (days)	Mix 1'(psi)	Mix 2'(psi)	Mix 7'(psi)	Mix 11'(psi)	Mix 12'(psi)
Predicted strength	1	979	827	1,021	881	893
	3	3,441	2,907	3,589	3,098	3,137
	7	5,829	4,925	6,079	5,248	5,315
	28	8,189	6,918	8,540	7,373	7,466
	91	8,888	7,510	9,269	8,003	8,104
	182	9,053	7,649	9,441	8,151	8,254
	Time (days)	Mix 1'(psi)	Mix 2'(psi)	Mix 7'(psi)	Mix 11'(psi)	Mix 12'(psi)
Predicted strength without first day data	3	3,478	2,939	3,627	3,132	3,171
	7	5,681	4,800	5,924	5,115	5,179
	28	8,172	6,905	8,523	7,358	7,451
	91	9,016	7,618	9,403	8,118	8,221
	182	9,224	7,794	9,620	8,305	8,410
Strength	Se	282 (psi)				
	Se -1	232 (psi)				
Strength factor	Se	0.038				
	Se -1	0.031				

(Note: Se is the standard error of estimate and Se -1 is the standard error of estimate excluding the first day test results.)

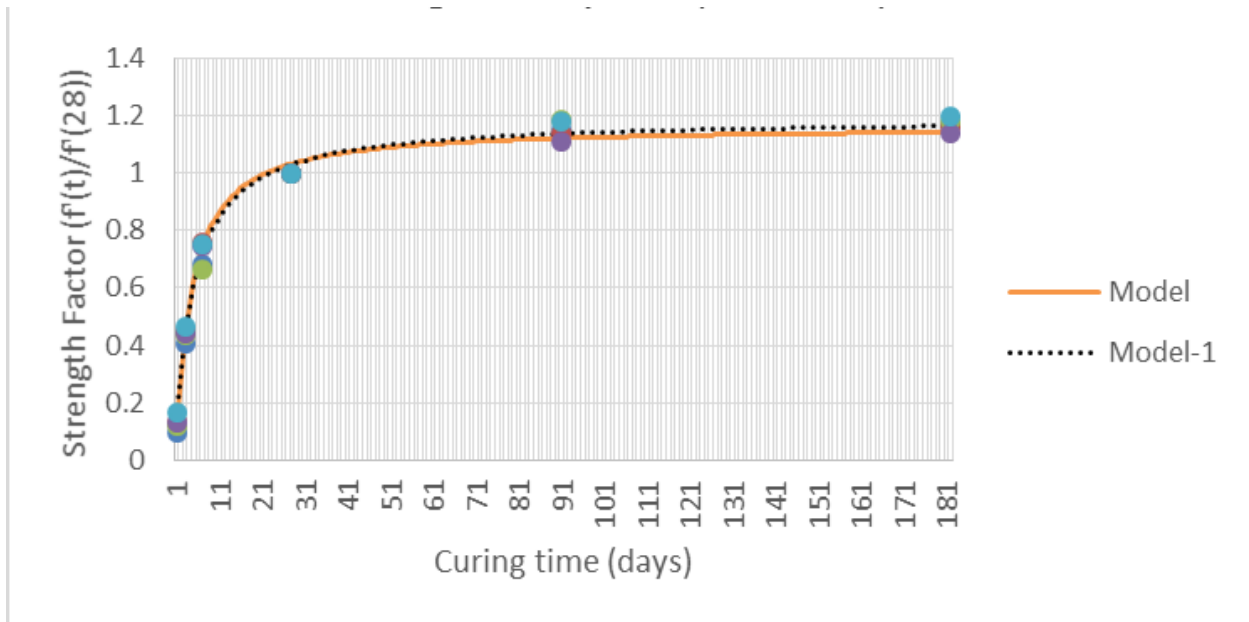


Figure G-22. Comparison between actual and predicted strength factors from 2nd degree hyperbolic model for slag and fly ash mixes with W/C more than 0.4.

Similar regression analysis using the 2nd degree hyperbolic model was performed on the inverse of the strength factor data on the second group of mixes which were slag and fly ash mixes with W/C less than 0.4. The resulting two prediction equations are as shown in Equations G-74 and G-75.

$$f'_c(t) = \frac{t^2}{0.92 \cdot t^2 + 1.30 \cdot t + 4.96} \cdot f'_c(28) \quad (\text{G-74})$$

When the first day data were excluded:

$$f'_c(t) = \frac{t^2}{0.88 \cdot t^2 + 2.69 \cdot t - 0.09} \cdot f'_c(28) \quad (\text{G-75})$$

Table G-15 shows the comparison between the actual strength of the concrete for this group of concrete and the corresponding predicted strengths using the two prediction equations. The standard error of the estimates for the strength and the strength factor using the two prediction equations are also shown in the table. Figure G-23 shows the comparison between the actual strength and the predicted strength using these two prediction equations.

Table G-15. Comparison between the actual and 2nd degree hyperbolic predicted compressive strength for slag and fly ash mixes with W/C less than 0.4.

		Time (days)	Mix 4(psi)	Mix 9(psi)	Mix 13(psi)	Mix 14(psi)
Actual strength		1	1,270	1,580	970	1,340
		3	5,050	4,640	5,020	4,860
		7	7,650	6,890	6,820	6,640
		28	9,820	9,900	8,540	7,980
		91	10,630	11,110	9,070	9,080
		182	10,690	11,300	9,540	9,400
		Time (days)	Mix 4'(psi)	Mix 9'(psi)	Mix 13'(psi)	Mix 14'(psi)
Predicted strength		1	1,368	1,379	1,189	1,111
		3	5,156	5,198	4,484	4,190
		7	8,136	8,203	7,076	6,612
		28	10,095	10,177	8,779	8,204
		91	10,504	10,590	9,135	8,536
		182	10,590	10,676	9,210	8,606
		Time (days)	Mix 4'(psi)	Mix 9'(psi)	Mix 13'(psi)	Mix 14'(psi)
Predicted strength without first day data		3	5,558	5,604	4,834	4,517
		7	7,779	7,842	6,765	6,321
		28	10,062	10,144	8,750	8,177
		91	10,797	10,885	9,389	8,774
		182	10,975	11,064	9,544	8,918
Strength	Se		531 (psi)			
	Se -1		422 (psi)			
Strength factor	Se		0.059			
	Se -1		0.047			

(Note: Se is the standard error of estimate and Se -1 is the standard error of estimate excluding the first day test results.)

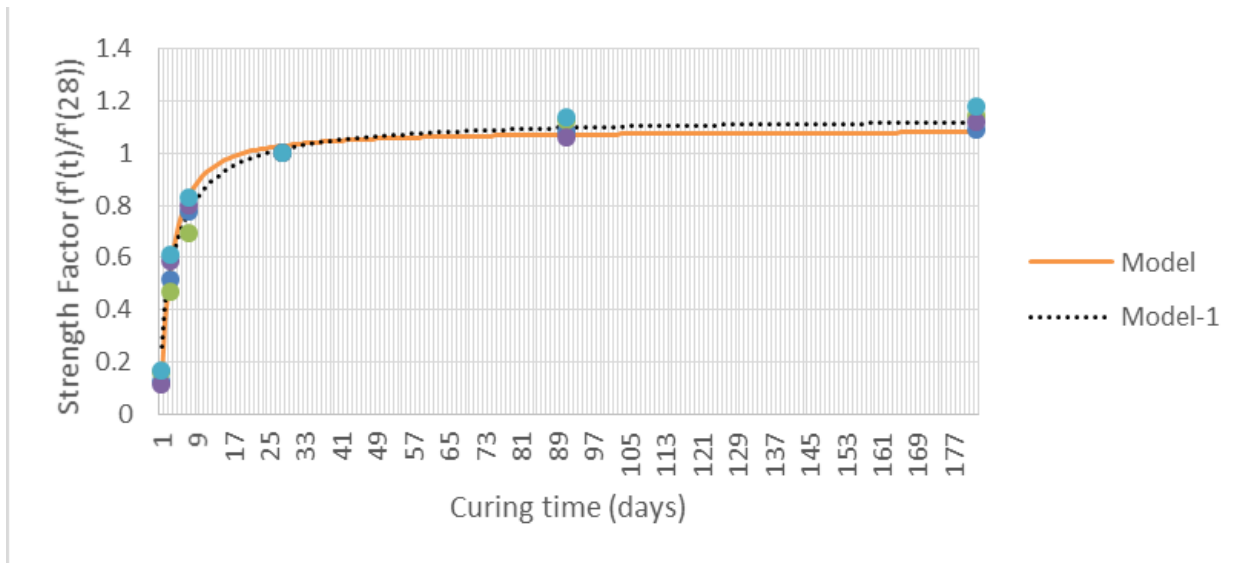


Figure G-23. Comparison between actual and predicted strength factors from 2nd degree hyperbolic model for slag and fly ash mixes with W/C less than 0.4

Similar regression analysis using the 2nd degree hyperbolic model was performed on the inverse of the strength factor data on the third group of mixes which were silica fume and fly ash mixes with Type I/II Portland cement. The resulting two prediction equations are as shown in Equations G-76 and G-77.

$$f'_c(t) = \frac{t^2}{0.92 \cdot t^2 + 1.95 \cdot t - 0.65} \cdot f'_c(28) \quad (\text{G-76})$$

$$f'_c(t) = \frac{t^2}{0.91 \cdot t^2 + 2.62 \cdot t - 2.67} \cdot f'_c(28) \quad (\text{G-77})$$

Table G-16 shows the comparison between the actual strength of the concrete for this group of concrete and the corresponding predicted strengths using the two prediction equations. The standard error of the estimates for the strength and the strength factor using the two prediction equations are also shown in the table. Figure G-24 shows the comparison between the actual strength and the predicted strength using these two prediction equations.

Table G-16. Comparison between the actual and 2nd degree hyperbolic predicted compressive strength for silica fume, fly ash, and type I/II cement mixes.

	Time (days)	Mix 3(psi)	Mix 5(psi)	Mix 6(psi)
Actual strength	1	3,940	4,660	4,640
	3	6,010	6,840	7,020
	7	7,300	8,300	8,430
	28	9,550	9,780	10,010
	91	9,950	10,720	10,920
	182	10,040	10,910	10,870
	Time (days)	Mix 3'(psi)	Mix 5'(psi)	Mix 6'(psi)
Predicted strength	1	4,302	4,405	4,509
	3	6,376	6,530	6,683
	7	8,057	8,251	8,445
	28	9,658	9,891	10,123
	91	10,145	10,389	10,634
	182	10,261	10,508	10,755
	Time (days)	Mix 3'(psi)	Mix 5'(psi)	Mix 6'(psi)
Predicted strength without first day data	3	6,424	6,578	6,733
	7	7,766	7,953	8,140
	28	9,548	9,778	10,008
	91	10,176	10,421	10,666
	182	10,332	10,581	10,830
Strength	Se	329 (psi)		
	Se -1	297 (psi)		
Strength factor	Se	0.034		
	Se -1	0.031		

(Note: Se is the standard error of estimate and Se -1 is the standard error of estimate excluding the first day test results.)

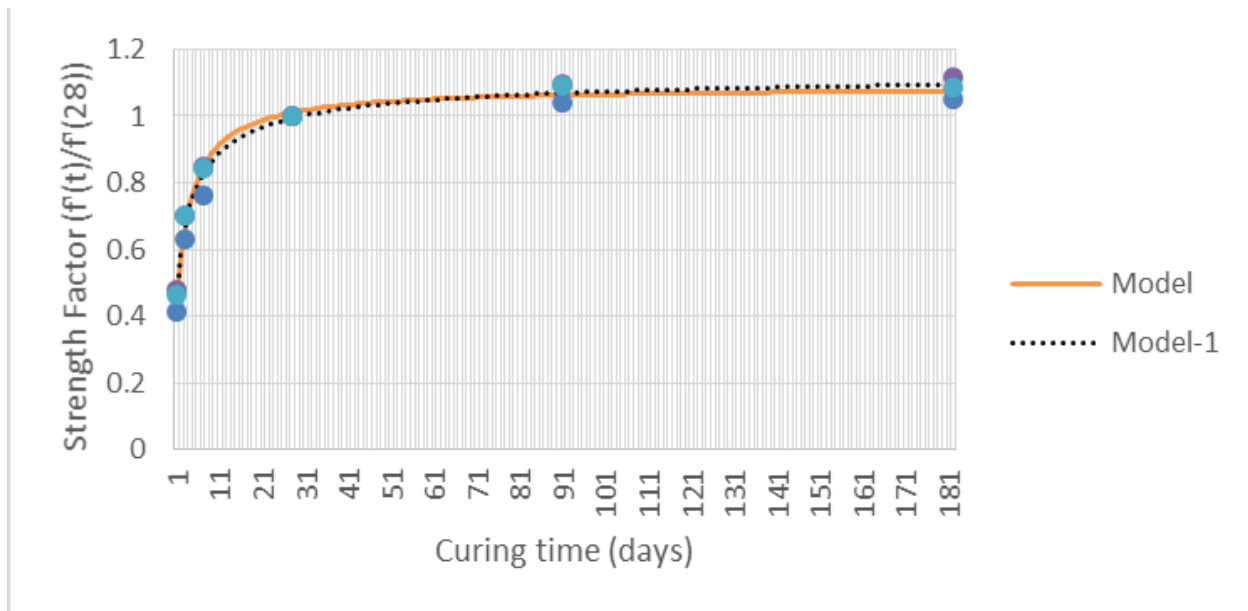


Figure G-24. Comparison between actual and predicted strength factors from 2nd degree hyperbolic model for silica fume, fly ash and Type I/II cement mixes

Similar regression analysis using the modified hyperbolic model was performed on the inverse of the strength factor data on the fourth group of mixes which were silica fume and fly ash mixes with Type III Portland cement. The resulting two prediction equations are as shown in Equations G-78 and G-79.

$$f'_c(t) = \frac{t^2}{0.93 \cdot t^2 + 1.54 \cdot t - 0.81} \cdot f'_c(28) \quad (\text{G-78})$$

$$f'_c(t) = \frac{t^2}{0.91 \cdot t^2 + 2.07 \cdot t - 2.44} \cdot f'_c(28) \quad (\text{G-79})$$

Table G-17 shows the comparison between the actual strength of the concrete for this group of concrete and the corresponding predicted strength using the two prediction equations. The standard error of the estimates for the strength and the strength factor using the two prediction equations are also shown in the table. Figure G-25 shows the comparison between the actual strength and the predicted strength using these two prediction equations.

Table G-17. Comparison between the actual and 2nd degree hyperbolic predicted compressive strength for silica fume, fly ash, and Type III cement mixes.

	Time (days)	Mix 8(psi)	Mix 10(psi)
	Actual strength	1	5,650
3		7,220	7,840
7		8,520	8,870
28		9,770	10,330
91		10,520	10,950
182		10,910	11,040
<hr/>			
	Time (days)	Mix 8'(psi)	Mix 10'(psi)
	Predicted strength	1	5,886
3		7,219	7,633
7		8,620	9,114
28		9,929	10,498
91		10,319	10,910
182		10,411	11,008
<hr/>			
	Time (days)	Mix 8'(psi)	Mix 10'(psi)
	Predicted strength without first day data	3	7,352
7		8,452	8,937
28		9,961	10,532
91		10,478	11,078
182		10,605	11,212
<hr/>			
Strength	Se	239 (psi)	
	Se -1	177 (psi)	
Strength factor	Se	0.023	
	Se -1	0.017	

(Note: Se is the standard error of estimate and Se -1 is the standard error of estimate excluding the first day test results.)

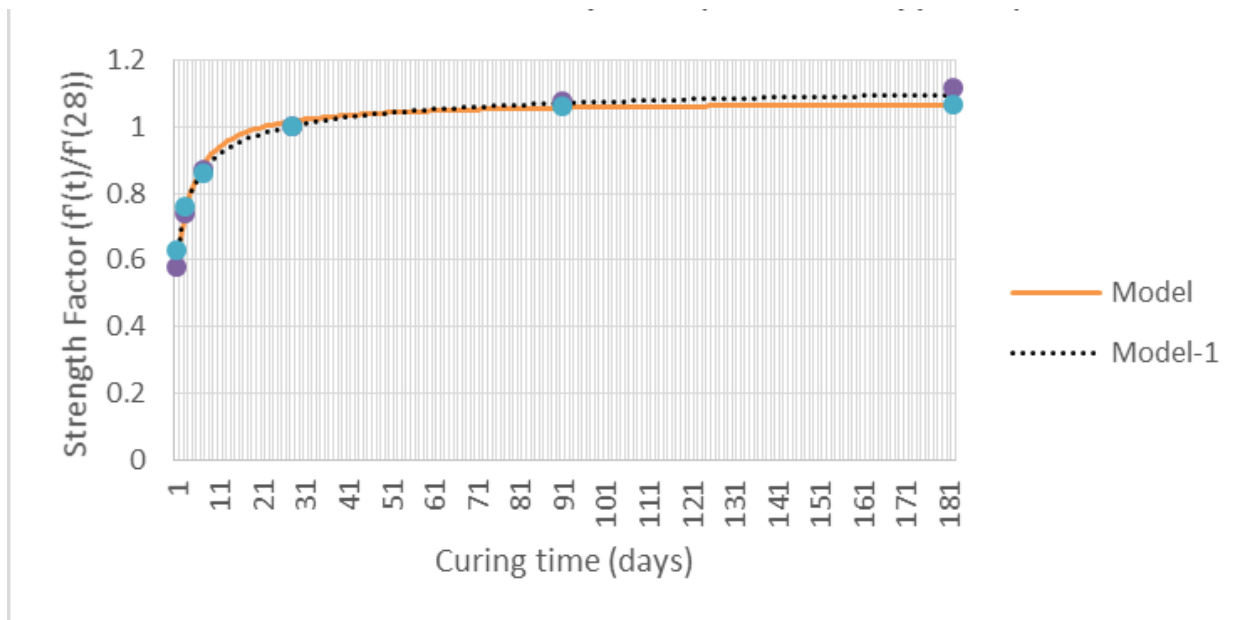


Figure G-25. Comparison between actual and predicted strength factors from 2nd degree hyperbolic model for silica fume, fly ash and Type III cement mixes.

G.1.5 Comparison of Standard Error of Estimate for All Models

Table G-18 presents the comparison of standard error of estimate for all four statistical models evaluated and for the four groups of concrete mixes. For each of the four statistical models evaluated, two options were considered, namely (1) including the first-day compressive strength data and (2) excluding the first-day compressive strength data. Only the option with lower standard error of estimate is presented. For each concrete group, the model with the lowest standard error of estimate is highlighted with a shaded box.

It can also be noted that the standard error of estimate of the Freiesleben model is the lowest for the first group of concrete and very close to the lowest value in the other three groups of concrete mixes. In order to reduce the complexity of the prediction equations, it is recommended that the developed prediction equations from the Freiesleben model be used for all four groups of concrete mixes. In this way, all the prediction equations will have the same form but with only slightly different coefficients.

Table G-18. Comparison of standard error of estimate for all models.

		Freiesleben	CEB-FIP	Hyperbolic	2nd Degree Hyperbolic
Standard Error of Estimate	SL & FA (W/C >0.4)	212 psi (0.028)* (1st day data included)	221 psi (0.030) (1st day data included)	260 psi (0.035) (1st day data excluded)	232 psi (0.031) (1st day data excluded)
	SL & FA (W/C <0.4)	387 psi (0.043) (1st day data excluded)	377 psi (0.041) (1st day data excluded)	382 psi (0.042) (1st day data excluded)	422 psi (0.047) (1st day data excluded)
	SF & FA (Type I/II cement)	302 psi (0.031) (1st day data excluded)	310 psi (0.032) (1st day data excluded)	297 psi (0.031) (1st day data excluded)	297 psi (0.031) (1st day data excluded)
	SF & FA (Type III cement)	146 psi (0.015) (1st day data excluded)	150 psi (0.015) (1st day data excluded)	144 psi (0.014) (1st day data excluded)	177 psi (0.017) (1st day data excluded)

(Note: * Errors of estimate in terms of strength factor are in (). SL=slag. FA=fly ash. SF=silica fume.).

The recommended prediction equations are as follows:

For slag and fly ash ternary blend mixes (W/C >0.4):

$$f'_c(t) = f'_c(28) \cdot 1.25 \cdot e^{-(3.14/t)^{0.72}} \quad (\text{G-80})$$

$$f'_c(28) = f'_c(t) \cdot 0.8 \cdot e^{(3.14/t)^{0.72}} \quad (\text{G-81})$$

For slag and fly ash ternary blend mixes (W/C <0.4):

$$f'_c(t) = f'_c(28) \cdot 1.16 \cdot e^{-(2.16/t)^{0.72}} \quad (\text{G-82})$$

$$f'_c(28) = f'_c(t) \cdot 0.86 \cdot e^{(2.16/t)^{0.72}} \quad (\text{G-83})$$

For silica fume and fly ash ternary blend mixes with Type I/II cement:

$$f'_c(t) = f'_c(28) \cdot 1.16 \cdot e^{-(0.98/t)^{0.55}} \quad (\text{G-84})$$

$$f'_c(28) = f'_c(t) \cdot 0.86 \cdot e^{(0.98/t)^{0.55}} \quad (\text{G-85})$$

For silica fume and fly ash ternary blend mixes with Type III cement:

$$f'_c(t) = f'_c(28) \cdot 1.16 \cdot e^{-(0.53/t)^{0.47}} \quad (\text{G-86})$$

$$f'_c(28) = f'_c(t) \cdot 0.86 \cdot e^{(0.53/t)^{0.47}} \quad (\text{G-87})$$

G.2 Analysis of Modulus of Elasticity Data

The compressive strength is related to the modulus of elasticity in a non-linear relationship as shown in the plot of experimental test results in Figure G-26, which shows that the rate of increase in the modulus of elasticity is much lower than that in the compressive strength.

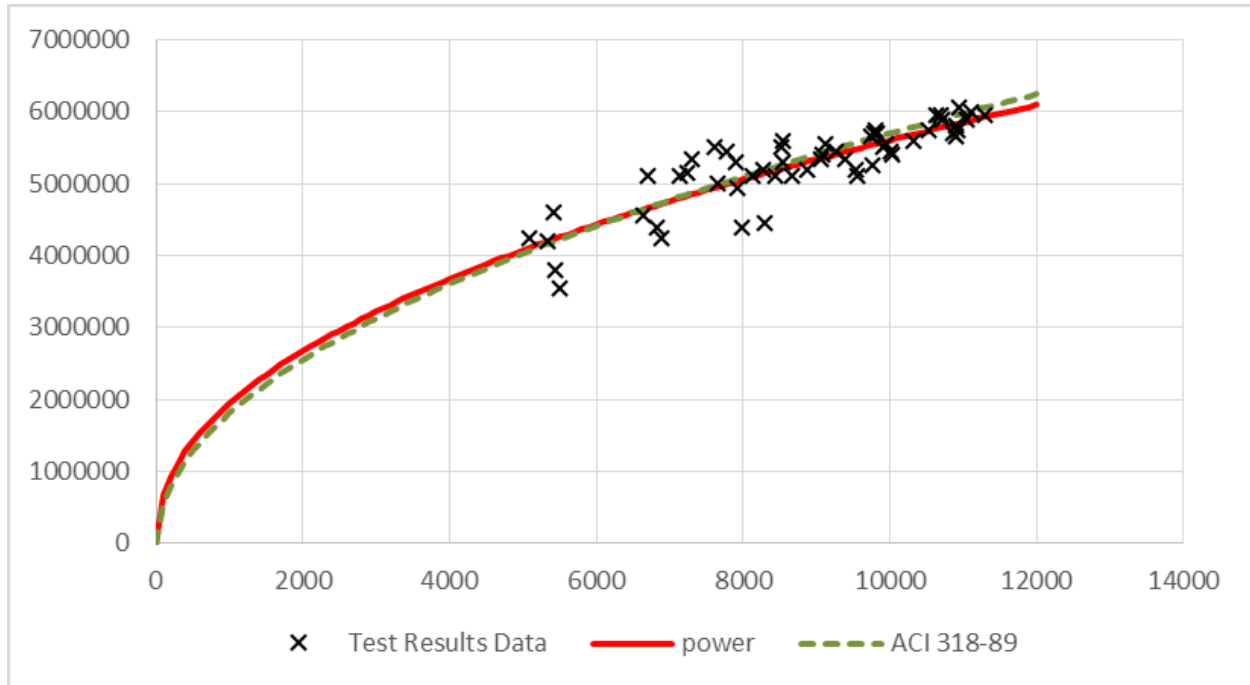


Figure G-26. Plot of MOE versus compressive strength.

CEB-FIP, ACI 318 and Iravani (1996) recommended a model shown in Equation G-88 to define the relationship between the compressive strength and the modulus of elasticity (E).

$$E = A \cdot \sqrt{f'_c} \quad (\text{G-88})$$

Where

E is the Modulus of Elasticity,

A is a coefficient.

Ahmad and Shah (1985) and Rashid et al. (2002) modified the model by replacing the square root with a variable power term as shown in Equation G-89.

$$E = A \cdot (f'_c)^B \quad (\text{G-89})$$

Where

A and B are coefficients.

Results of regression analysis using these two models are presented in Table G-19. The standard error of estimate for these two models are also shown in this table.

Table G-19. Results of regression analysis relating MOE to compressive strength.

Model	Equation	Coefficients	Standard Error of Estimate (psi)
ACI	$E = A \cdot \sqrt{f'_c}$	A = 56,500	270,833
Modified ACI	$E = A \cdot (f'_c)^B$	A = 81,000 B = 0.46	266,540

The results of regression analysis as presented in Table G-19 indicate that the modified ACI model expressed in Equation G-89 has a lower standard error of estimate, and the developed prediction equation is as follows:

$$E = 81,000 \cdot (f'_c)^{0.46} \quad (\text{G-90})$$

G.3 Analysis of Flexural Strength Data

The plot of flexural strength versus compressive strength from the experimental results are presented in Figure G-27. Regression analysis was performed to relate compressive strength to flexural strength (f_r) of the ternary blend mixes using the ACI and the modified ACI equations, as presented in Equations G-91 and G-92, respectively. The results of the regression analysis are presented in Table G-20.

ACI Model:

$$f_r = A \cdot \sqrt{f'_c} \quad (\text{G-91})$$

Where

f_r is the flexural strength,
 A is a coefficient.

Modified ACI Model:

$$f_r = A \cdot (f'_c)^B \quad (\text{G-92})$$

Where

f_r is the flexural strength,
 A and B are coefficients.

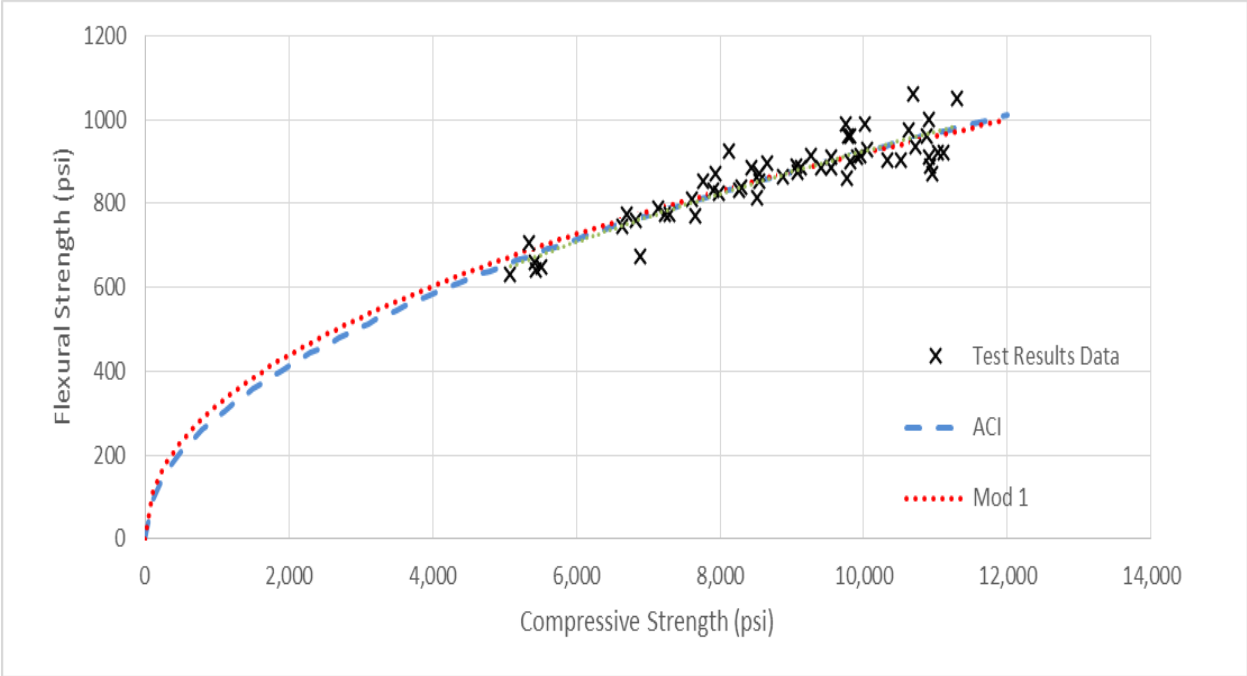


Figure G-27. Plot of flexural strength versus compressive strength.

Table G-20. Results of regression analysis relating flexural strength to compressive strength.

Model	Equation	Coefficients	Standard Error of Estimate (psi)
ACI	$f_r = A \cdot \sqrt{f'_c}$	A = 9.23	42.14
Modified ACI	$f_r = A \cdot (f'_c)^B$	A = 8.43 B = 0.51	42.11

The results of regression analysis using these two models as presented in Table 3-39 indicate that the modified ACI model as expressed in Equation G-93 has a lower standard error of estimate and the prediction equation is as follows:

$$f_r = 9.23 \cdot \sqrt{f'_c} \tag{G-93}$$

G.4 Analysis of Splitting Tensile Strength Data

The plot of splitting tensile strength versus compressive strength from the experimental results are presented in Figure G-28. Regression analysis was performed to relate compressive strength to splitting tensile strength (f_t) of the ternary blend mixes using the ACI and the modified ACI (Carino and Lew, 1982) models, as presented in equations G-94 and G-95, respectively. The results of the regression analysis are presented in Table G-21.

ACI model:

$$f_t = A \cdot \sqrt{f'_c} \quad (\text{G-94})$$

Carino and Lew model:

$$f_t = A \cdot (f'_c)^B \quad (\text{G-95})$$

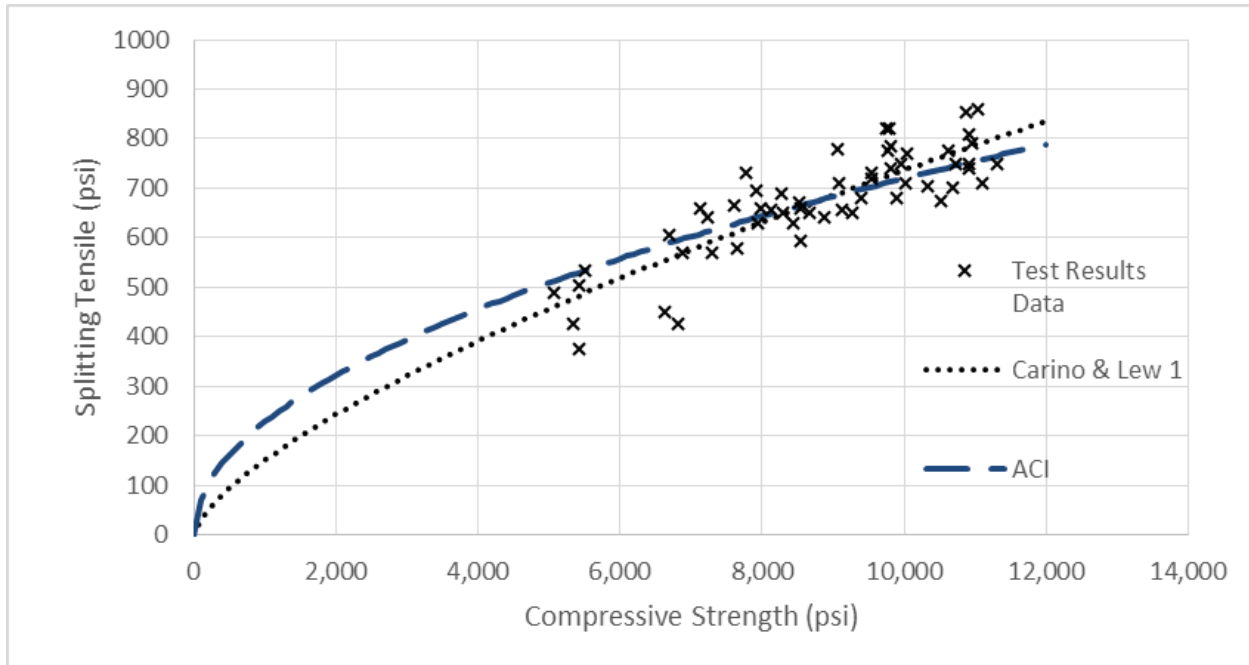


Figure G-28. Plot of splitting tensile strength versus compressive strength.

Table G-21. Results of regression analysis relating splitting tensile strength to compressive strength.

Model	Equation	Coefficients	Standard Error of Estimate
ACI	$f_t = A \cdot \sqrt{f'_c}$	A = 7.20	61.43
Carino & Lew	$f_t = A \cdot (f'_c)^B$	A = 1.29 B = 0.69	56.70

The results of regression analysis are shown in Table G-21. The Carino and Lew (1982) model as presented in Equation G-95, gave a lower standard error of estimate and the developed prediction equation is as follows:

$$f_t = 1.29 \cdot (f'_c)^{0.69} \quad (G-96)$$

APPENDIX H
STRENGTH DATA FROM TERNARY BLEND MIX STUDY

H.1 Compressive Strength Data.

Table H-1. Compressive strength data of mix 1.

Identifier	Age (days)	Sample	Max. Load (lb.)	Max. Stress (psi)	Ave. Stress (psi)
Mix 1	1	A	9,750	770	740
		B	9,110	720	
		C	9,150	720	
	3	A	40,322	3,180	3,210
		B	40,116	3,180	
		C	41,433	3,280	
	7	A	65,263	5,110	5,420
		B	70,615	5,560	
		C	71,052	5,600	
	28	A	101,819	8,060	7,930
		B	100,813	7,940	
		C	98,466	7,800	
	91	A	117,611	9,310	9,130
		B	111,455	8,780	
		C	117,524	9,310	
182	A	114,351	9,050	9,270	
	B	120,608	9,550		
	C	116,455	9,220		

Table H-2. Compressive strength data of mix 2.

Identifier	Age (days)	Sample	Max. Load (lb.)	Max. Stress (psi)	Ave. Stress (psi)
Mix 2	1	A	10,276	810	870
		B	11,458	910	
		C	11,362	900	
	3	A	37,320	2,950	3,010
		B	39,450	3,110	
		C	37,650	2,980	
	7	A	65,849	5,210	5,080
		B	63,270	5,010	
		C	63,521	5,030	
	28	A	84,747	6,710	6,700
		B	83,432	6,610	
		C	85,866	6,770	
	91	A	97,043	7,680	7,610
		B	97,051	7,650	
		C	94,827	7,510	
182	A	100,321	8,030	7,770	
	B	94,195	7,420		
	C	99,297	7,860		

Table H-3. Compressive strength data of mix 3.

Identifier	Age (days)	Sample	Max. Load (lb.)	Max. Stress (psi)	Ave. Stress (psi)
Mix 3	1	A	50,513	3,980	3,940
		B	49,397	3,910	
		C	50,051	3,940	
	3	A	76,232	6,040	6,010
		B	74,348	5,890	
		C	77,121	6,110	
	7	A	94,767	7,500	7,300
		B	92,251	7,300	
		C	89,668	7,100	
	28	A	115,780	9,170	9,550
		B	126,571	9,970	
		C	120,154	9,510	
	91	A	128,451	10,120	9,950
		B	131,823	10,330	
		C	118,547	9,390	
182	A	127,512	10,100	10,040	
	B	124,789	9,880		
	C	128,631	10,140		

Table H-4. Compressive strength data of mix 4.

Identifier	Age (days)	Sample	Max. Load (lb.)	Max. Stress (psi)	Ave. Stress (psi)
Mix 4	1	A	17,045	1,350	1,270
		B	14,863	1,180	
		C	16,070	1,270	
	3	A	63,133	4,980	5,050
		B	64,955	5,140	
		C	63,626	5,040	
	7	A	98,856	7,830	7,650
		B	97,724	7,740	
		C	93,462	7,370	
	28	A	125,481	9,890	9,820
		B	122,590	9,710	
		C	125,143	9,860	
	91	A	134,483	10,600	10,630
		B	137,248	10,870	
		C	132,176	10,420	
182	A	133,486	10,520	10,690	
	B	137,548	10,890		
		C	134,496	10,650	

Table H-5. Compressive strength data of mix 5.

Identifier	Age (days)	Sample	Max. Load (lb.)	Max. Stress (psi)	Ave. Stress (psi)
Mix 5	1	A	61,015	4,810	4,660
		B	57,464	4,550	
		C	58,229	4,610	
	3	A	86,639	6,860	6,840
		B	87,007	6,860	
		C	86,252	6,800	
	7	A	107,767	8,530	8,300
		B	101,937	8,070	
		C	105,369	8,300	
	28	A	129,126	10,220	9,780
		B	124,668	9,870	
		C	116,937	9,260	
	91	A	133,535	10,570	10,720
		B	132,912	10,520	
		C	140,534	11,070	
182	A	129,729	10,270	10,900	
	B	144,841	11,470		
	C	139,220	10,970		

Table H-6. Compressive strength data of mix 6.

Identifier	Age (days)	Sample	Max. Load (lb.)	Max. Stress (psi)	Ave. Stress (psi)
Mix 6	1	A	58,730	4,630	4,640
		B	58,657	4,620	
		C	59,102	4,660	
	3	A	89,291	7,070	7,020
		B	87,863	6,960	
		C	88,778	7,030	
	7	A	106,166	8,410	8,430
		B	106,745	8,450	
		C	106,395	8,420	
	28	A	119,883	9,490	10,010
		B	127,035	10,010	
		C	132,905	10,520	
	91	A	135,707	10,740	10,920
		B	141,437	11,150	
		C	138,017	10,880	
182	A	130,599	10,340	10,870	
	B	137,643	10,900		
	C	143,706	11,380		

Table H-7. Compressive strength data of mix 7.

Identifier	Age (days)	Sample	Max. Load (lb.)	Max. Stress (psi)	Ave. Stress (psi)
Mix 7	1	A	13,620	1,070	970
		B	13,470	1,070	
		C	9,810	780	
	3	A	45,155	3,560	3,580
		B	45,617	3,610	
		C	45,376	3,580	
	7	A	70,773	5,600	5,510
		B	70,400	5,570	
		C	68,023	5,360	
	28	A	103,283	8,140	8,270
		B	104,524	8,320	
		C	105,446	8,350	
	91	A	125,128	9,910	9,810
		B	120,177	9,520	
		C	126,444	10,010	
182	A	120,498	9,540	9,750	
	B	123,501	9,780		
	C	125,264	9,920		

Table H-8. Compressive strength data of mix 8.

Identifier	Age (days)	Sample	Max. Load (lb.)	Max. Stress (psi)	Ave. Stress (psi)
Mix 8	1	A	71,130	5,630	5,650
		B	71,553	5,670	
		C	-	-	
	3	A	89,800	7,080	7,220
		B	91,785	7,270	
		C	92,740	7,310	
	7	A	107,611	8,520	8,520
		B	106,522	8,390	
		C	109,406	8,660	
	28	A	127,172	10,070	9,770
		B	121,765	9,640	
		C	121,365	9,610	
	91	A	133,328	10,560	10,520
		B	132,245	10,420	
		C	133,560	10,570	
182	A	140,138	11,040	10,910	
	B	139,670	11,060		
	C	134,161	10,620		

Table H-9. Compressive strength data of mix 9.

Identifier	Age (days)	Sample	Max. Load (lb.)	Max. Stress (psi)	Ave. Stress (psi)
Mix 9	1	A	21,354	1,680	1,580
		B	18,637	1,480	
		C	19,853	1,570	
	3	A	58,019	4,570	4,640
		B	59,710	4,710	
		C	58,935	4,640	
	7	A	86,612	6,830	6,890
		B	86,079	6,820	
		C	88,976	7,010	
	28	A	118,582	9,390	9,900
		B	128,778	10,200	
		C	127,598	10,100	
	91	A	143,933	11,280	1,110
		B	138,400	10,960	
		C	140,551	11,080	
182	A	146,879	11,570	11,300	
	B	140,593	11,080		
	C	141,972	11,240		

Table H-10. Compressive strength data of mix 10.

Identifier	Age (days)	Sample	Max. Load (lb.)	Max. Stress (psi)	Ave. Stress (psi)
Mix 10	1	A	81,141	6,390	6,510
		B	82,112	6,500	
		C	84,308	6,640	
	3	A	99,042	7,800	7,840
		B	102,238	8,060	
		C	96,685	7,660	
	7	A	109,024	8,590	8,870
		B	111,349	8,770	
		C	116,928	9,260	
	28	A	129,080	10,170	10,330
		B	128,555	10,180	
		C	135,048	10,640	
	91	A	142,027	11,250	10,950
		B	136,093	10,720	
		C	138,178	10,890	
182	A	144,240	11,370	11,040	
	B	135,767	10,700		
	C	140,041	11,040		

Table H-11. Compressive strength data of mix 11.

Identifier	Age (days)	Sample	Max. Load (lb.)	Max. Stress (psi)	Ave. Stress (psi)
Mix 11	1	A	11,985	950	940
		B	11,448	910	
		C	12,103	960	
	3	A	40,319	3,210	3,170
		B	39,630	3,170	
		C	39,511	3,140	
	7	A	66,624	5,300	5,340
		B	67,757	5,360	
		C	67,831	5,370	
	28	A	91,167	7,250	7,140
		B	91,644	7,260	
		C	87,446	6,920	
	91	A	98,760	7,860	7,910
		B	95,123	7,570	
		C	104,820	8,300	
182	A	101,060	8,040	8,130	
	B	102,510	8,160		
		C	102,935	8,190	

Table H-12. Compressive strength data of mix 12.

Identifier	Age (days)	Sample	Max. Load (lb.)	Max. Stress (psi)	Ave. Stress (psi)
Mix 12	1	A	15,176	1,210	1,210
		B	15,249	1,210	
		C	15,277	1,220	
	3	A	41,057	3,360	3,340
		B	42,929	3,400	
		C	42,258	3,250	
	7	A	67,964	5,410	5,430
		B	68,618	5,430	
		C	68,584	5,460	
	28	A	94,584	7,490	7,230
		B	84,348	6,710	
		C	94,160	7,490	
	91	A	109,660	8,720	8,540
		B	107,930	8,550	
		C	105,414	8,350	
182	A	110,847	8,780	8,660	
	B	107,522	8,550		
	C	108,558	8,640		

Table H-13. Compressive strength data of mix 13.

Identifier	Age (days)	Sample	Max. Load (lb.)	Max. Stress (psi)	Ave. Stress (psi)
Mix 13	1	A	12,429	980	970
		B	12,235	970	
		C	11,992	950	
	3	A	63,859	5,060	5,020
		B	63,245	5,010	
		C	63,114	5,000	
	7	A	88,567	7,010	6,820
		B	81,307	6,440	
		C	88,376	7,000	
	28	A	110,013	8,670	8,540
		B	107,747	8,570	
		C	105,481	8,390	
	91	A	121,823	9,650	9,070
		B	109,164	8,640	
		C	113,182	8,920	
182	A	116,114	9,240	9,540	
	B	120,093	9,510		
	C	124,079	9,870		

Table H-14. Compressive strength data of mix 14.

Identifier	Age (days)	Sample	Max. Load (lb.)	Max. Stress (psi)	Ave. Stress (psi)
Mix 14	1	A	16,856	1,330	1,340
		B	16,951	1,340	
		C	16,956	1,340	
	3	A	61,916	4,900	4,860
		B	61,937	4,900	
		C	60,521	4,770	
	7	A	80,184	6,350	6,640
		B	86,495	6,850	
		C	84,994	6,730	
	28	A	95,895	7,590	7,980
		B	102,464	8,070	
		C	104,557	8,280	
	91	A	112,792	8,930	9,080
		B	113,293	8,970	
		C	118,111	9,350	
182	A	120,880	9,570	9,400	
	B	122,334	9,690		
	C	112,989	8,950		

H.2 Modulus of Elasticity Data

Table H-15. Modulus of elasticity data of mix 1.

Identifier	Age (days)	Sample	MOE (psi) x10 ³	Ave. MOE (psi) x10 ³
Mix 1	7	A	4,650	4,600
		B	4,750	
		C	4,400	
	28	A	5,250	5,050
		B	4,900	
		C	5,050	
	91	A	5,600	5,550
		B	5,450	
		C	5,650	
	182	A	5,450	5,450
		B	5,450	
		C	5,450	

Table H-16. Modulus of elasticity data of mix 2.

Identifier	Age (days)	Sample	MOE (psi) x10 ³	Ave. MOE (psi) x10 ³
Mix 2	7	A	4,100	4,250
		B	4,200	
		C	4,450	
	28	A	5,150	5,100
		B	5,100	
		C	5,050	
	91	A	5,400	5,500
		B	5,500	
		C	5,600	
	182	A	5,550	5,450
		B	5,350	
		C	5,450	

Table H-17. Modulus of elasticity data of mix 3.

Identifier	Age (days)	Sample	MOE (psi) x10 ³	Ave. MOE (psi) x10 ³
Mix 3	7	A	5,450	5,350
		B	5,300	
		C	5,250	
	28	A	5,100	5,100
		B	5,100	
		C	5,150	
	91	A	5,500	5,550
		B	5,600	
		C	5,550	
	182	A	5,450	5,400
		B	5,400	
		C	5,350	

Table H-18. Modulus of elasticity data of mix 4.

Identifier	Age (days)	Sample	MOE (psi) x10 ³	Ave. MOE (psi) x10 ³
Mix 4	7	A	5,000	5,000
		B	5,050	
		C	4,950	
	28	A	5,800	5,700
		B	5,450	
		C	5,800	
	91	A	6,000	5,950
		B	5,900	
		C	5,950	
	182	A	5,950	5,950
		B	6,000	
		C	5,850	

Table H-19. Modulus of elasticity data of mix 5.

Identifier	Age (days)	Sample	MOE (psi) x10 ³	Ave. MOE (psi) x10 ³
Mix 5	7	A	5,150	5,250
		B	5,250	
		C	5,300	
	28	A	5,550	5,700
		B	5,750	
		C	5,750	
	91	A	5,900	5,900
		B	5,900	
		C	5,900	
	182	A	5,900	5,800
		B	5,800	
		C	5,750	

Table H-20. Modulus of elasticity data of mix 6.

Identifier	Age (days)	Sample	MOE (psi) x10 ³	Ave. MOE (psi) x10 ³
Mix 6	7	A	5,100	5,100
		B	5,100	
		C	5,100	
	28	A	5,200	5,450
		B	5,500	
		C	5,650	
	91	A	5,750	5,750
		B	5,800	
		C	5,700	
	182	A	5,700	5,700
		B	5,650	
		C	5,750	

Table H-21. Modulus of elasticity data of mix 7.

Identifier	Age (days)	Sample	MOE (psi) x10 ³	Ave. MOE (psi) x10 ³
Mix 7	7	A	3,700	3,550
		B	4,000	
		C	3,000	
	28	A	5,250	5,200
		B	5,350	
		C	5,050	
	91	A	5,700	5,750
		B	5,850	
		C	5,650	
	182	A	5,750	5,650
		B	5,550	
		C	5,650	

Table H-22. Modulus of elasticity data of mix 8.

Identifier	Age (days)	Sample	MOE (psi) x10 ³	Ave. MOE (psi) x10 ³
Mix 8	7	A	5,850	5,500
		B	5,550	
		C	5,150	
	28	A	4,950	5,250
		B	5,250	
		C	5,600	
	91	A	5,700	5,750
		B	5,750	
		C	5,800	
	182	A	5,600	5,650
		B	5,750	
		C	5,650	

Table H-23. Modulus of elasticity data of mix 9.

Identifier	Age (days)	Sample	MOE (psi) x10 ³	Ave. MOE (psi) x10 ³
Mix 9	7	A	4,250	4,250
		B	4,300	
		C	4,150	
	28	A	5,550	5,500
		B	5,400	
		C	5,550	
	91	A	5,950	6,000
		B	6,050	
		C	6,000	
	182	A	5,900	5,950
		B	5,950	
		C	5,950	

Table H-24. Modulus of elasticity data of mix 10.

Identifier	Age (days)	Sample	MOE (psi) x10 ³	Ave. MOE (psi) x10 ³
Mix 10	7	A	5,450	5,200
		B	5,250	
		C	4,850	
	28	A	5,300	5,600
		B	5,750	
		C	5,750	
	91	A	6,150	6,050
		B	5,900	
		C	6,050	
	182	A	5,950	5,900
		B	5,900	
		C	5,800	

Table H-25. Modulus of elasticity data of mix 11.

Identifier	Age (days)	Sample	MOE (psi) x10 ³	Ave. MOE (psi) x10 ³
Mix 11	7	A	4,200	4,200
		B	4,200	
		C	4,200	
	28	A	5,100	5,100
		B	5,200	
		C	5,000	
	91	A	5,200	5,300
		B	5,250	
		C	5,450	
	182	A	5,100	5,100
		B	5,100	
		C	5,100	

Table H-26. Modulus of elasticity data of mix 12.

Identifier	Age (days)	Sample	MOE (psi) x10 ³	Ave. MOE (psi) x10 ³
Mix 12	7	A	3,900	3,800
		B	3,700	
		C	3,800	
	28	A	4,950	5,150
		B	5,250	
		C	5,250	
	91	A	5,400	5,300
		B	5,250	
		C	5,300	
	182	A	5,050	5,100
		B	5,250	
		C	4,950	

Table H-27. Modulus of elasticity data of mix 13.

Identifier	Age (days)	Sample	MOE (psi) x10 ³	Ave. MOE (psi) x10 ³
Mix 13	7	A	4,800	4,950
		B	4,750	
		C	5,250	
	28	A	5,800	5,600
		B	5,350	
		C	5,600	
	91	A	5,200	5,350
		B	5,400	
		C	5,400	
	182	A	5,200	5,200
		B	5,150	
		C	5,250	

Table H-28. Modulus of elasticity data of mix 14.

Identifier	Age (days)	Sample	MOE (psi) x10 ³	Ave. MOE (psi) x10 ³
Mix 14	7	A	4,600	4,550
		B	4,500	
		C	4,600	
	28	A	3,950	4,400
		B	4,850	
		C	4,350	
	91	A	5,400	5,400
		B	5,350	
		C	5,400	
	182	A	5,350	5,350
		B	5,300	
		C	5,350	

H.3 Splitting Tensile Strength Data

Table H-29. Splitting tensile strength data of mix 1.

Identifier	Age (days)	Sample	Max. Load (lb.)	Max. Stress (psi)	Ave. Stress (psi)
Mix 1	7	A	21,200	440	505
		B	27,720	585	
		C	23,860	495	
	28	A	33,990	705	630
		B	31,680	660	
		C	25,210	525	
	91	A	33,820	705	655
		B	29,050	600	
		C	39,760	830	
	182	A	33,000	680	650
		B	30,540	625	
			C	25,740	530

Table H-30. Splitting tensile strength data of mix 2.

Identifier	Age (days)	Sample	Max. Load (lb.)	Max. Stress (psi)	Ave. Stress (psi)
Mix 2	7	A	24,470	500	490
		B	24,710	520	
		C	20,970	440	
	28	A	29,460	610	605
		B	27,890	580	
		C	28,230	590	
	91	A	32,760	680	665
		B	32,100	670	
		C	30,870	640	
	182	A	34,024	700	730
		B	36,788	770	
			C	34,899	725

Table H-31. Splitting tensile strength data of mix 3.

Identifier	Age (days)	Sample	Max. Load (lb.)	Max. Stress (psi)	Ave. Stress (psi)
Mix 3	7	A	29,140	600	570
		B	26,330	545	
		C	27,590	570	
	28	A	36,650	750	720
		B	29,950	615	
		C	38,140	795	
	91	A	36,650	775	750
		B	42,730	880	
		C	34,820	725	
	182	A	35,750	740	770
		B	38,740	805	
			C	37,170	760

Table H-32. Splitting tensile strength data of mix 4.

Identifier	Age (days)	Sample	Max. Load (lb.)	Max. Stress (psi)	Ave. Stress (psi)
Mix 4	7	A	28,150	575	580
		B	28,650	595	
		C	27,990	575	
	28	A	39,820	820	785
		B	35,420	735	
		C	38,180	800	
	91	A	37,150	770	775
		B	38,910	805	
		C	36,290	750	
	182	A	35,290	725	700
		B	33,390	695	
			C	32,900	685

Table H-33. Splitting tensile strength data of mix 5.

Identifier	Age (days)	Sample	Max. Load (lb.)	Max. Stress (psi)	Ave. Stress (psi)
Mix 5	7	A	31,020	645	650
		B	32,150	665	
		C	28,050	570	
	28	A	39,100	805	820
		B	38,580	795	
		C	41,580	855	
	91	A	40,170	835	750
		B	34,900	730	
		C	33,180	685	
	182	A	34,690	720	740
		B	36,150	755	
			C	36,340	740

Table H-34. Splitting tensile strength data of mix 6.

Identifier	Age (days)	Sample	Max. Load (lb.)	Max. Stress (psi)	Ave. Stress (psi)
Mix 6	7	A	27,740	570	630
		B	34,390	715	
		C	29,340	610	
	28	A	25,490	525	710
		B	28,600	595	
		C	34,340	710	
	91	A	32,890	690	750
		B	40,220	830	
		C	35,210	730	
	182	A	45,159	935	855
		B	38,169	775	
			C	28,044	580

Table H-35. Splitting tensile strength data of mix 7.

Identifier	Age (days)	Sample	Max. Load (lb.)	Max. Stress (psi)	Ave. Stress (psi)
Mix 7	7	A	24,710	515	535
		B	27,510	580	
		C	24,400	510	
	28	A	34,360	705	690
		B	37,720	775	
		C	28,700	585	
	91	A	37,730	775	740
		B	36,230	750	
		C	33,340	690	
	182	A	29,740	605	820
		B	41,100	830	
			C	39,600	805

Table H-36. Splitting tensile strength data of mix 8.

Identifier	Age (days)	Sample	Max. Load (lb.)	Max. Stress (psi)	Ave. Stress (psi)
Mix 8	7	A	36,140	750	670
		B	31,130	650	
		C	30,150	615	
	28	A	37,600	775	775
		B	23,350	475	
		C	19,160	390	
	91	A	34,540	695	675
		B	31,780	655	
		C	26,820	555	
	182	A	39,630	820	810
		B	40,450	835	
			C	37,700	775

Table H-37. Splitting tensile strength data of mix 9.

Identifier	Age (days)	Sample	Max. Load (lb.)	Max. Stress (psi)	Ave. Stress (psi)
Mix 9	7	A	27,580	570	570
		B	27,150	560	
		C	28,090	585	
	28	A	34,430	710	680
		B	33,510	695	
		C	30,430	630	
	91	A	25,620	530	710
		B	46,110	965	
		C	30,320	630	
	182	A	38,210	785	750
		B	35,290	720	
		C	36,450	745	

Table H-38. Splitting tensile strength data of mix 10.

Identifier	Age (days)	Sample	Max. Load (lb.)	Max. Stress (psi)	Ave. Stress (psi)
Mix 10	7	A	29,500	600	640
		B	40,700	830	
		C	33,020	675	
	28	A	36,150	750	705
		B	32,660	685	
		C	32,630	680	
	91	A	43,780	915	790
		B	37,540	795	
		C	31,050	650	
	182	A	42,781	865	860
		B	41,481	855	
		C	41,378	855	

Table H-39. Splitting tensile strength data of mix 11.

Identifier	Age (days)	Sample	Max. Load (lb.)	Max. Stress (psi)	Ave. Stress (psi)
Mix 11	7	A	19,390	395	425
		B	21,410	440	
		C	21,670	445	
	28	A	30,890	640	660
		B	33,210	690	
		C	31,090	645	
	91	A	34,300	720	695
		B	27,330	575	
		C	31,690	665	
	182	A	34,870	695	655
		B	30,090	620	
			C	31,330	650

Table H-40. Splitting tensile strength data of mix 12.

Identifier	Age (days)	Sample	Max. Load (lb.)	Max. Stress (psi)	Ave. Stress (psi)
Mix 12	7	A	18,500	385	375
		B	17,420	360	
		C	18,100	375	
	28	A	32,440	675	640
		B	30,580	635	
		C	29,670	615	
	91	A	37,600	785	660
		B	29,040	595	
		C	35,050	730	
	182	A	29,110	600	650
		B	35,340	730	
			C	30,150	615

Table H-41. Splitting tensile strength data of mix 13.

Identifier	Age (days)	Sample	Max. Load (lb.)	Max. Stress (psi)	Ave. Stress (psi)
Mix 13	7	A	21,660	445	425
		B	19,060	395	
		C	21,220	440	
	28	A	27,540	570	595
		B	30,170	620	
		C	29,070	605	
	91	A	38,620	800	780
		B	36,200	750	
		C	38,140	790	
	182	A	34,460	725	730
		B	33,120	700	
			C	36,860	760

Table H-42. Splitting tensile strength data of mix 14.

Identifier	Age (days)	Sample	Max. Load (lb.)	Max. Stress (psi)	Ave. Stress (psi)
Mix 14	7	A	21,480	445	450
		B	30,400	630	
		C	21,470	450	
	28	A	35,270	735	660
		B	30,170	620	
		C	30,390	625	
	91	A	35,730	740	710
		B	32,440	670	
		C	34,880	715	
	182	A	32,910	665	680
		B	28,330	585	
			C	34,020	700

H.4 Flexural Strength Data

Table H-43. Flexural strength data of mix 1.

Identifier	Age (days)	Sample	Max. Load (lb.)	Max. Stress (psi)	Ave. Stress (psi)
Mix 1	7	A	3,830	700	660
		B	3,580	670	
		C	3,200	600	
	28	A	4,720	885	870
		B	4,800	890	
		C	4,450	835	
	91	A	4,680	865	885
		B	4,580	860	
		C	4,950	930	
	182	A	5,120	950	915
		B	4,790	900	
		C	4,760	895	

Table H-44. Flexural strength data of mix 2.

Identifier	Age (days)	Sample	Max. Load (lb.)	Max. Stress (psi)	Ave. Stress (psi)
Mix 2	7	A	3,540	655	630
		B	3,320	615	
		C	3,490	625	
	28	A	4,490	790	775
		B	4,220	790	
		C	4,080	745	
	91	A	4,320	790	810
		B	4,830	860	
		C	4,290	785	
	182	A	4,900	895	855
		B	4,740	865	
		C	4,630	855	

Table H-45. Flexural strength data of mix 3.

Identifier	Age (days)	Sample	Max. Load (lb.)	Max. Stress (psi)	Ave. Stress (psi)
Mix 3	7	A	4,170	765	775
		B	4,540	800	
		C	4,020	755	
	28	A	4,800	880	885
		B	4,860	900	
		C	4,800	880	
	91	A	4,890	895	915
		B	4,890	895	
		C	5,070	950	
	182	A	4,730	865	930
		B	5,070	940	
			C	5,190	975

Table H-46. Flexural strength data of mix 4.

Identifier	Age (days)	Sample	Max. Load (lb.)	Max. Stress (psi)	Ave. Stress (psi)
Mix 4	7	A	4,050	750	770
		B	4,040	730	
		C	4,500	835	
	28	A	5,390	985	960
		B	4,320	790	
		C	5,130	940	
	91	A	5,290	970	975
		B	5,450	995	
		C	5,230	955	
	182	A	6,190	1,130	1,060
		B	5,300	980	
			C	5,740	1,065

Table H-47. Flexural strength data of mix 5.

Identifier	Age (days)	Sample	Max. Load (lb.)	Max. Stress (psi)	Ave. Stress (psi)
Mix 5	7	A	4,640	840	840
		B	4,360	820	
		C	4,650	860	
	28	A	5,210	965	960
		B	5,110	945	
		C	5,510	970	
	91	A	5,150	920	935
		B	5,240	935	
		C	5,170	945	
	182	A	5,410	1,000	1,000
		B	5,270	975	
		C	5,540	1,025	

Table H-48. Flexural strength data of mix 6.

Identifier	Age (days)	Sample	Max. Load (lb.)	Max. Stress (psi)	Ave. Stress (psi)
Mix 6	7	A	5,310	970	885
		B	4,690	830	
		C	4,720	855	
	28	A	5,170	925	990
		B	5,650	1,010	
		C	5,830	1,030	
	91	A	5,380	915	890
		B	4,790	855	
		C	4,980	890	
	182	A	5,510	1,010	960
		B	4,820	870	
		C	5,430	995	

Table H-49. Flexural strength data of mix 7.

Identifier	Age (days)	Sample	Max. Load (lb.)	Max. Stress (psi)	Ave. Stress (psi)
Mix 7	7	A	3,540	655	650
		B	3,720	655	
		C	3,510	640	
	28	A	4,640	870	830
		B	4,410	805	
		C	4,540	820	
	91	A	4,960	930	900
		B	5,130	925	
		C	4,490	840	
	182	A	4,950	930	990
		B	5,260	985	
			C	5,600	1,050

Table H-50. Flexural strength data of mix 8.

Identifier	Age (days)	Sample	Max. Load (lb.)	Max. Stress (psi)	Ave. Stress (psi)
Mix 8	7	A	4,640	840	815
		B	4,310	810	
		C	4,320	800	
	28	A	4,660	875	860
		B	4,480	830	
		C	4,770	895	
	91	A	5,350	955	905
		B	4,970	885	
		C	4,770	870	
	182	A	4,850	900	910
		B	4,910	920	
			C	4,810	900

Table H-51. Flexural strength data of mix 9.

Identifier	Age (days)	Sample	Max. Load (lb.)	Max. Stress (psi)	Ave. Stress (psi)
Mix 9	7	A	3,520	630	675
		B	3,890	720	
		C	3,660	680	
	28	A	4,860	900	910
		B	4,940	890	
		C	5,090	945	
	91	A	4,650	830	920
		B	5,140	915	
		C	5,430	1,020	
	182	A	5,940	1,085	1,050
		B	5,290	970	
			C	5,840	1,095

Table H-52. Flexural strength data of mix 10.

Identifier	Age (days)	Sample	Max. Load (lb.)	Max. Stress (psi)	Ave. Stress (psi)
Mix 10	7	A	4,590	830	865
		B	5,260	940	
		C	4,530	830	
	28	A	4,880	870	905
		B	5,050	890	
		C	5,410	955	
	91	A	5,420	945	870
		B	4,990	840	
		C	5,020	875	
	182	A	4,640	850	920
		B	5,140	965	
			C	5,050	935

Table H-53. Flexural strength data of mix 11.

Identifier	Age (days)	Sample	Max. Load (lb.)	Max. Stress (psi)	Ave. Stress (psi)
Mix 11	7	A	3,870	725	705
		B	3,720	700	
		C	3,720	690	
	28	A	4,330	775	790
		B	4,160	760	
		C	4,450	835	
	91	A	4,420	800	830
		B	4,480	820	
		C	4,830	865	
	182	A	5,160	945	925
		B	5,060	960	
			C	4,640	870

Table H-54. Flexural strength data of mix 12.

Identifier	Age (days)	Sample	Max. Load (lb.)	Max. Stress (psi)	Ave. Stress (psi)
Mix 12	7	A	3,530	645	640
		B	3,620	655	
		C	3,500	625	
	28	A	4,290	755	775
		B	4,180	745	
		C	4,640	830	
	91	A	5,020	905	870
		B	4,720	865	
		C	4,560	845	
	182	A	4,640	860	895
		B	4,980	920	
			C	4,960	905

Table H-55. Flexural strength data of mix 13.

Identifier	Age (days)	Sample	Max. Load (lb.)	Max. Stress (psi)	Ave. Stress (psi)
Mix 13	7	A	3,940	740	760
		B	3,950	730	
		C	4,390	805	
	28	A	4,960	885	855
		B	4,390	815	
		C	4,860	865	
	91	A	5,120	925	890
		B	4,660	850	
		C	5,040	900	
	182	A	4,990	925	910
		B	4,930	925	
			C	4,700	880

Table H-56. Flexural strength data of mix 14.

Identifier	Age (days)	Sample	Max. Load (lb.)	Max. Stress (psi)	Ave. Stress (psi)
Mix 14	7	A	3,800	705	745
		B	4,200	770	
		C	4,120	765	
	28	A	4,310	790	825
		B	4,550	820	
		C	4,760	870	
	91	A	5,050	910	875
		B	4,640	850	
		C	4,670	865	
	182	A	4,970	920	885
		B	4,390	825	
			C	4,860	910

APPENDIX I
DIFG BATCH FILE

rem === Diana Environment Setup ===
call "C:\Program Files\Diana 9.4.4\dialogin.bat"

Open DIANA software

rem === Preprocessing ===

Run pre-processing

set FGVSTR=.

copy ds.pre fgvstr.str

idiana -alpha

del fgvstr.str

rem === analysis ===

Run analysis

diana ds

rem === Postprocessing ===

Run post-processing

copy ds.post fgvstr.str

idiana -alpha

del fgvstr.str

APPENDIX J
DIFG PRE-PROCESSING FILE

FEMGEN DS

PROPERTY FE-PROG DIANA HTSTAG_AX

Generated Staggered Model

yes

UTILITY SETUP UNITS LENGTH METER

Unit setting

UTILITY SETUP UNITS MASS KILOGRAM

UTILITY SETUP UNITS FORCE NEWTON

UTILITY SETUP UNITS TIME SECOND

UTILITY SETUP UNITS TEMPERATURE CELSIUS

CONSTRUCT SPACE TOLERANCE OFF

Geometry of structure

GEOMETRY POINT COORD P1 0.0000E+00 0.0000E+00 0.0000E+00

GEOMETRY POINT COORD P2 9.1440E-01 0.0000E+00 0.0000E+00

GEOMETRY POINT COORD P3 0.0000E+00 6.0960E-01 0.0000E+00

GEOMETRY POINT COORD P4 9.1440E-01 6.0960E-01 0.0000E+00

GEOMETRY POINT COORD P5 0.0000E+00 1.8288E+00 0.0000E+00

GEOMETRY POINT COORD P6 9.1440E-01 1.8288E+00 0.0000E+00

GEOMETRY POINT COORD P7 0.0000E+00 2.1336E+00 0.0000E+00

GEOMETRY POINT COORD P8 9.1440E-01 2.1336E+00 0.0000E+00

GEOMETRY POINT COORD P9 0.0000E+00 -3.6576E+00 0.0000E+00

GEOMETRY POINT COORD P10 9.1440E-01 -3.6576E+00 0.0000E+00

GEOMETRY POINT COORD P11 2.7432E+00 -3.6576E+00 0.0000E+00

GEOMETRY POINT COORD P12 2.7432E+00 0.0000E+00 0.0000E+00

GEOMETRY POINT COORD P13 2.7432E+00 6.0960E-01 0.0000E+00

GEOMETRY POINT COORD P14 2.7432E+00 1.8288E+00 0.0000E+00

GEOMETRY SURFACE 4POINTS P8 P7 P5 P6

GEOMETRY SURFACE 4POINTS P6 P5 P3 P4

GEOMETRY SURFACE 4POINTS P4 P3 P1 P2

GEOMETRY SURFACE 4POINTS P2 P1 P9 P10

GEOMETRY SURFACE 4POINTS P12 P2 P10 P11

GEOMETRY SURFACE 4POINTS P13 P4 P2 P12

GEOMETRY SURFACE 4POINTS P14 P6 P4 P13

CONSTRUCT SET X1 APPEND LINES L1 L3 L6 L9 L12

CONSTRUCT SET X2 APPEND LINES L14 L15 L17 L19

CONSTRUCT SET Y1 APPEND LINES L2 L4

CONSTRUCT SET Y2 APPEND LINES L5 L7 L20

CONSTRUCT SET Y3 APPEND LINES L8 L10 L18

CONSTRUCT SET Y4 APPEND LINES L11 L13 L16

MESHING DIVISION LINE X1 36
MESHING DIVISION LINE X2 80
MESHING DIVISION LINE Y1 10
MESHING DIVISION LINE Y2 56
MESHING DIVISION LINE Y3 28
MESHING DIVISION LINE Y4 30

Meshing divisions

CONSTRUCT SET Conc APPEND SURFACES S1 S2 S3
CONSTRUCT SET SoTop APPEND SURFACES S7
CONSTRUCT SET SoBottom APPEND SURFACES S4 S5 S6
MESHING TYPE Conc qu8 cq16a
MESHING GENERATE Conc
MESHING TYPE SoTop qu8 cq16a
MESHING TYPE SoBottom qu8 cq16a

CONSTRUCT SET OPEN Abounda
GEOMETRY LINE STRAIGHT P7 P8 50
GEOMETRY LINE STRAIGHT P6 P8 10
GEOMETRY LINE STRAIGHT P6 P14 30
CONSTRUCT SET CLOSE
CONSTRUCT SET OPEN Sbounda1
GEOMETRY LINE STRAIGHT P1 P2 50
CONSTRUCT SET CLOSE
CONSTRUCT SET OPEN Sbounda2
GEOMETRY LINE STRAIGHT P2 P4 28
CONSTRUCT SET CLOSE
CONSTRUCT SET OPEN Sbounda3
GEOMETRY LINE STRAIGHT P4 P6 56
CONSTRUCT SET CLOSE
CONSTRUCT SET SoilFix APPEND LINES L12 L15 L16 L18 L20
MESHING DIVISION FACTOR Abounda 0.5
MESHING DIVISION FACTOR Sbounda1 0.5
MESHING DIVISION FACTOR Sbounda2 0.5
MESHING DIVISION FACTOR Sbounda3 0.5

MESHING TYPES Abounda be2 b2aht
MESHING TYPES Sbounda1 be2 b2aht
MESHING TYPES Sbounda2 be2 b2aht

MESHING TYPES Sbounda3 be2 b2aht
MESHING GENERATE MESHING MERGE ALL 0.001

Each material properties

PROPERTY MATERIAL ConMAT EXTERNAL EXTERNAL "concrete.dat"
PROPERTY MATERIAL SoilBO FLOW BOUNDARY CONVECTI 3.00E+00 0
PROPERTY MATERIAL AirBO FLOW BOUNDARY CONVECTI 3.00E+01 0
PROPERTY MATERIAL SoilMAT1 FLOW ISOTROP 2.920E-01 1.260E+06
PROPERTY MATERIAL SoilMAT2 FLOW ISOTROP 2.175E+00 2.930E+06
PROPERTY ATTACH Conc ConMAT
PROPERTY ATTACH SoTop SoilMAT1
PROPERTY ATTACH SoBottom SoilMAT2
PROPERTY ATTACH Abounda AirBO
PROPERTY ATTACH Sbounda1 SoilBO
PROPERTY ATTACH Sbounda2 SoilBO
PROPERTY ATTACH Sbounda3 SoilBO

PROPERTY LOADS EXTTEMP 1 Sbounda1 2.00E+01
PROPERTY LOADS EXTTEMP 2 Sbounda2 2.00E+01
PROPERTY LOADS EXTTEMP 3 Sbounda3 2.00E+01
PROPERTY LOADS EXTTEMP 4 Abounda 1.57E+01
PROPERTY LOADS FIXTEMP 5 SoilFix 2.00E+01

Temperature loading condition

CONSTRUCT TCURVE TCDUM LIST 0 1 601200 1
PROPERTY ATTACH LOADCASE 1 TCDUM
PROPERTY ATTACH LOADCASE 2 TCDUM
PROPERTY ATTACH LOADCASE 3 TCDUM
PROPERTY ATTACH LOADCASE 4 TCDUM
PROPERTY ATTACH LOADCASE 5 TCDUM

Setting the time 601200 second

CONSTRUCT SET CONSX APPEND LINES L2 L5 L8
PROPERTY BOUNDARY CONSTRAINT CONSX X

PROPERTY INITIAL INITEMP Conc 2.60E+01
PROPERTY INITIAL INITEMP SoTop 2.00E+01
PROPERTY INITIAL INITEMP SoBottom 2.00E+01
UTILITY WRITE DIANA DS.dat

Initial temperature

yes
stop
yes
no

APPENDIX K DIFG COMMAND FILE

In this appendix, the analysis commands for the standard staggered analysis are presented. The standard staggered analysis is one in which the thermal flow analysis is coupled with the structural analysis. The temperatures calculated in the thermal analysis are automatically converted to input for the structural analysis (If user wants to analysis the structure analysis).

```
*FILOS
INITIA Initiate Analysis
*INPUT
*HEATTR Analysis Type Thermal
BEGIN INITIA
BEGIN NONLIN
EQUAGE Calculate Equivalent Age
HYDRAT DGRINI=0.01
END NONLIN
TEMPER INPUT FIELD=1
END INITIA
BEGIN EXECUT
BEGIN NONLIN
HYDRAT ITERAT
BEGIN ITERAT
CONVER TEMPER TOLCON=0.01
MAXITE=30 Maximum No. of Iterations
END ITERAT
END NONLIN
SIZES 3600.0(167) Magnitude & No. Time Steps
END EXECUT
BEGIN OUTPUT FEMVIE FILE="FLOW" File to print to output
EQUAGE TOTAL INTPNT
TEMPER
REACTI TOTAL INTPNT
END OUTPUT
*END
```

APPENDIX L
POST-PROCESSING FILE

FEMVIEW FLOW *1ST day contour view of the thermal profile*
VIEW MESH CONC
EYE FRAME
RESULTS LOADCASE TR1 24
RESULTS NODAL PTE....S PTE
PRESENT CONTOUR LEVELS
UTILITY SETUP PLOTTER FORMAT POSTSCRIPT COLOUR
DRAWING SAVE PLOTFILE Day1.PS
Yes

VIEW MESH CONC *2nd day contour view of the thermal profile*
EYE FRAME
RESULTS LOADCASE TR1 48
RESULTS NODAL PTE....S PTE
PRESENT CONTOUR LEVELS
UTILITY SETUP PLOTTER FORMAT POSTSCRIPT COLOUR
DRAWING SAVE PLOTFILE Day2.PS
Yes

VIEW MESH CONC *3rd day contour view of the thermal profile*
EYE FRAME
RESULTS LOADCASE TR1 72
RESULTS NODAL PTE....S PTE
PRESENT CONTOUR LEVELS
UTILITY SETUP PLOTTER FORMAT POSTSCRIPT COLOUR
DRAWING SAVE PLOTFILE Day3.PS
Yes

VIEW MESH CONC *4th day contour view of the thermal profile*
EYE FRAME
RESULTS LOADCASE TR1 96
RESULTS NODAL PTE....S PTE
PRESENT CONTOUR LEVELS
UTILITY SETUP PLOTTER FORMAT POSTSCRIPT COLOUR
DRAWING SAVE PLOTFILE Day4.PS
Yes

VIEW MESH CONC *5th day contour view of the thermal profile*
EYE FRAME
RESULTS LOADCASE TR1 120
RESULTS NODAL PTE....S PTE
PRESENT CONTOUR LEVELS
UTILITY SETUP PLOTTER FORMAT POSTSCRPT COLOUR
DRAWING SAVE PLOTFILE Day5.PS
Yes

VIEW MESH CONC *6th day contour view of the thermal profile*
EYE FRAME
RESULTS LOADCASE TR1 144
RESULTS NODAL PTE....S PTE
PRESENT CONTOUR LEVELS
UTILITY SETUP PLOTTER FORMAT POSTSCRPT COLOUR
DRAWING SAVE PLOTFILE Day6.PS
Yes

VIEW MESH CONC *7th day contour view of the thermal profile*
EYE FRAME
RESULTS LOADCASE TR1 167
RESULTS NODAL PTE....S PTE
PRESENT CONTOUR LEVELS
UTILITY SETUP PLOTTER FORMAT POSTSCRPT COLOUR
DRAWING SAVE PLOTFILE Day7.PS
yes

RESULTS LOADCASE ALL
RESULTS NODAL PTE....S PTE
UTILITY TABULATE PRINTFILE OPEN HOT *Tabulate of the hottest point*
PRESENT GRAPH NODE 26
UTILITY TABULATE PRINTFILE CLOSE
UTILITY TABULATE PRINTFILE OPEN COLD1 *Tabulate of one of the coldest point*
PRESENT GRAPH NODE 1
UTILITY TABULATE PRINTFILE CLOSE
UTILITY TABULATE PRINTFILE OPEN COLD2 *Tabulate of one of the coldest point*
PRESENT GRAPH NODE 801
UTILITY TABULATE PRINTFILE CLOSE
UTILITY TABULATE PRINTFILE OPEN COLD3 *Tabulate of one of the coldest point*
PRESENT GRAPH NODE 1269

UTILITY TABULATE PRINTFILE CLOSE
UTILITY TABULATE PRINTFILE OPEN COLD4
PRESENT GRAPH NODE 1294
UTILITY TABULATE PRINTFILE CLOSE
UTILITY TABULATE PRINTFILE OPEN COLD5
PRESENT GRAPH NODE 826
UTILITY TABULATE PRINTFILE CLOSE

Tabulate of one of the coldest point

Tabulate of one of the coldest point

STOP
yes

APPENDIX M
CONCRETE.DAT FILE

(Note: Explanations are in marked in red.)

CONDUC 2.2

Concrete conductivity

CAPACI 2.453380E+06

Heat Capacity concrete mixture

ADIAB 0 23.0

Adiabatic temperature Hours 0 -167

3600 25.36

7200 26.06

10800 27.07

14400 28.40

— Lines skipped —

590400 104.06

594000 104.15

597600 104.28

601200 104.30

ARRHEN 4873.6

Arrhenius constant

EQUAGE ARRTYP

TEMREF 23.0

Concrete reference Temperature

YOUNG 2.7721E+10

Young's Modulus

POISON 2.100000E-01

Poisson's Ratio

DENSIT 2.130444E+03

Density concrete

THERMX 1.11E-05

Thermal expansion coefficient

FTTIME 0. 86400. 259200. 432000. 601200.

Tensile develop time 0 – 167 Hours

FTVALU 0. 1.09E+6 2.43E+6 2.83E+6 3.02E+6

Tensile strength

MAXWEL 1

,1

TIME 0. 86400. 172800. 259200. 601200.

Young's Modulus develop time 0-167 Hours

YOUNG 12587.E+6 12587.E+6 12712.E+6 12985.E+6 19009.E+6

Young's Modulus

APPENDIX N
USER MANUAL FOR DIFG FOR THERMAL ANALYSIS OF MASS CONCRETE

N.1 Introduction

TNO DIANA computer software has been effectively used in thermal analysis of mass-concrete structures in this research project conducted by the University of Florida (UF) for the Florida Department of Transportation (FDOT). While the DIANA software is a powerful tool for performing thermal analysis of mass-concrete structures, the users of this software need to have a good knowledge of finite-element method, and the commands and procedures of the DIANA software. To facilitate the use of DIANA, a user-friendly interface software, named DIFG (Diana Input File Generator), was developed for use in thermal analysis of (1) rectangular concrete footings and (2) cylindrical concrete drilled shafts. Chapter 8 presents the functions and features of this developed software. This appendix presents a user manual for DIFG.

Figure N-1 shows the sequence of the user's seven main steps involved in the use of DIFG and DIANA in performing a thermal analysis on either a rectangular footing or a cylindrical drilled shaft. These seven main steps are as follows:

1. Install Matlab Compiler Runtime (MCR) software so that the DIFG executable file will run on the computer.
2. Open and run the DIFG software.
3. Input data through the DIFG interface software.
4. Save the output files from DIFG and close the DIFG software.
5. Pre-set all the necessary files before running the DIANA software.
6. Open and run the DIANA software.
7. Read and store the output files from the thermal analysis by DIANA.

Section N.2 presents the step-by-step instructions for the use of DIFG and DIANA for thermal analysis of a rectangular footing as an example. Section N.3 presents the step-by-step instructions for the use of DIFG and DIANA for thermal analysis of a cylindrical drilled shaft as an example. The same seven main steps are used in referencing the steps to be taken by the user.

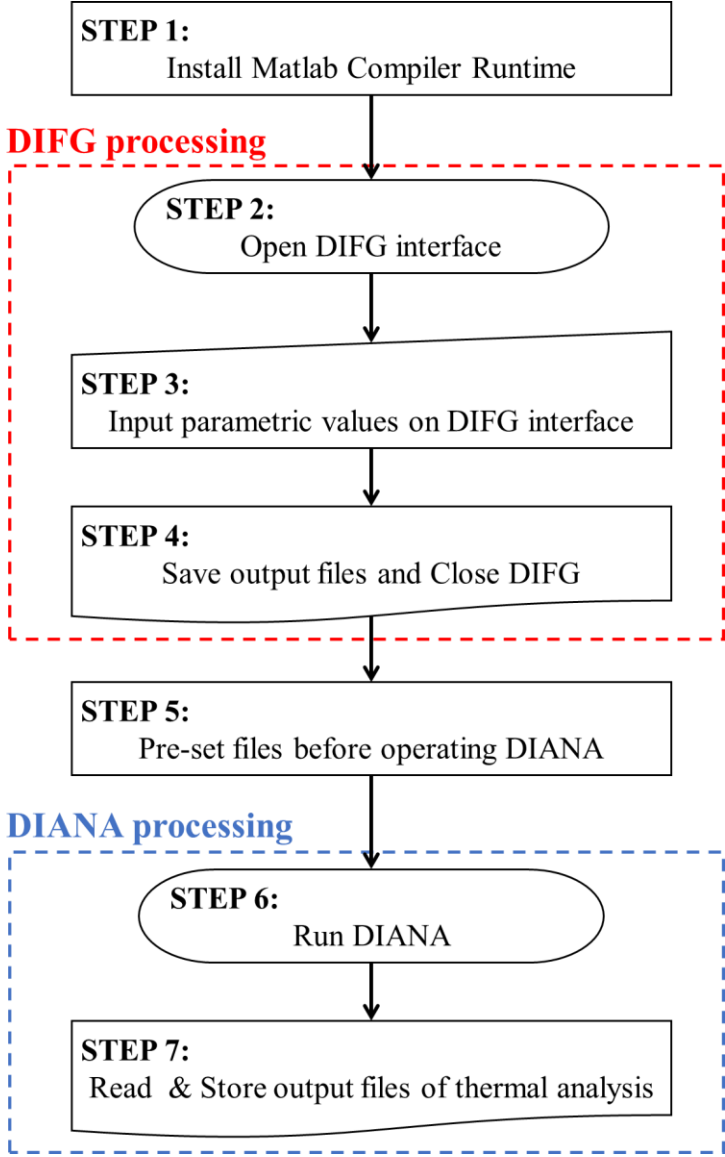


Figure N-1. Main steps in the use of DIFG and DIANA in performing a thermal analysis.

N.2 Running DIFG and DIANA for Thermal Analysis of a Rectangular Footing

N.2.1 STEP 1: Installing Matlab Compiler Runtime

The user-friendly software named “DIANA Input File Generator” (DIFG) was developed using the Matlab program. In order to run the executable DIFG file without the Matlab software, the user can install a free Matlab Compiler Runtime (MCR) software. The following two computer files are provided by the University of Florida to FDOT as deliverables of the project:

- **DIFG.EXE**: This is executable file to run the DIFG program.
- **MCR_R2013a_win64_installer**: This is free share program originally provided by Matlab software company.

Figure N-2 shows the display of these two file names as seen on the computer screen. If the MCR software has not been installed yet, the user should click “MCR_R2013a_win64_installer” to install it. The screen is displayed as shown in Figure N-3 will appear after the MCR installer is click. (Please note that the lines and words that are marked in red in this and other figures are not part of the screen display, but are added to explain the different information on the screen display.)



Name	Date modified	Type	Size
 DIFG	8/23/2016 1:10 PM	Application	7,154 KB
 MCR_R2013a_win64_installer	6/14/2016 9:36 AM	Application	423,910 KB

Figure N-2. Provided files for running DIFG software.

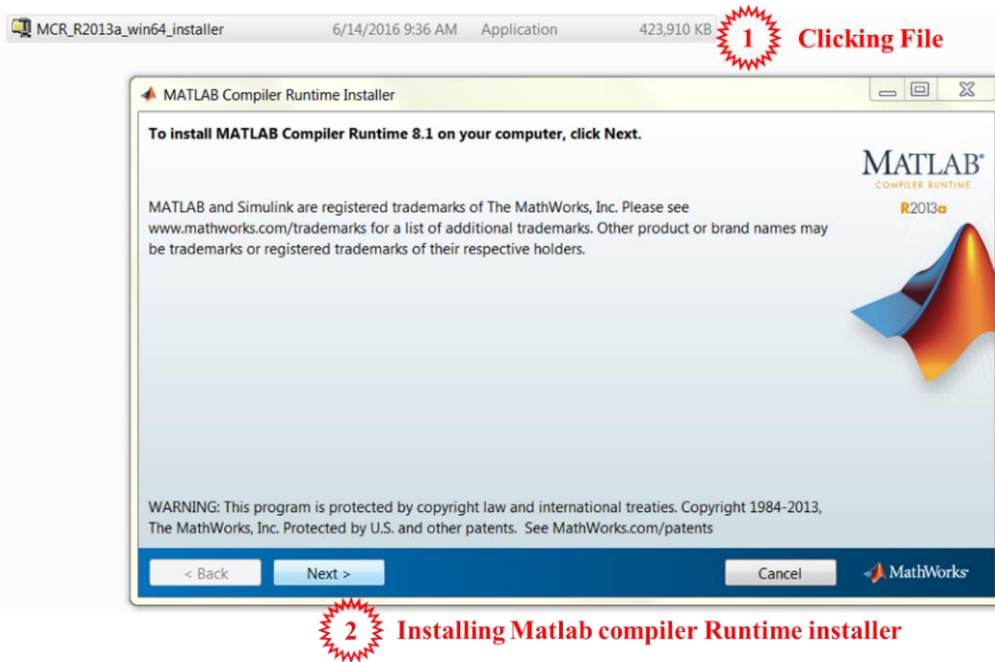


Figure N-3. Running of MCR_R2013a_win64_installer.

N.2.2 STEP 2: Opening DIANA Input File Generator (DIFG)

Before starting DIFG, it is recommended to set up the specific directory where all output files will be saved. The way to set the designated directory is to create the folder and to save the file “DIFG.EXE” in that folder, as shown in Figure N-4 (The directory named “Rectangular foundation testing” for this demonstration).

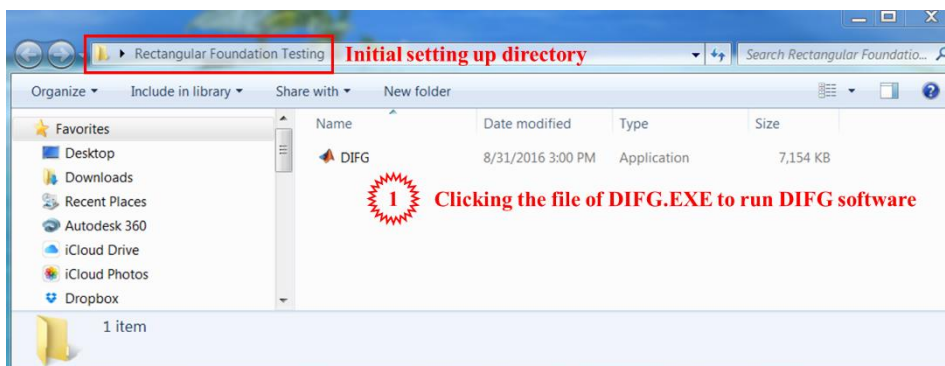


Figure N-4. Creating the folder and saving DIFG.EXE in it.

Click “DIFG.EXE” to open the software. The interface screen of DIFG will appear soon as shown in Figure N-5.

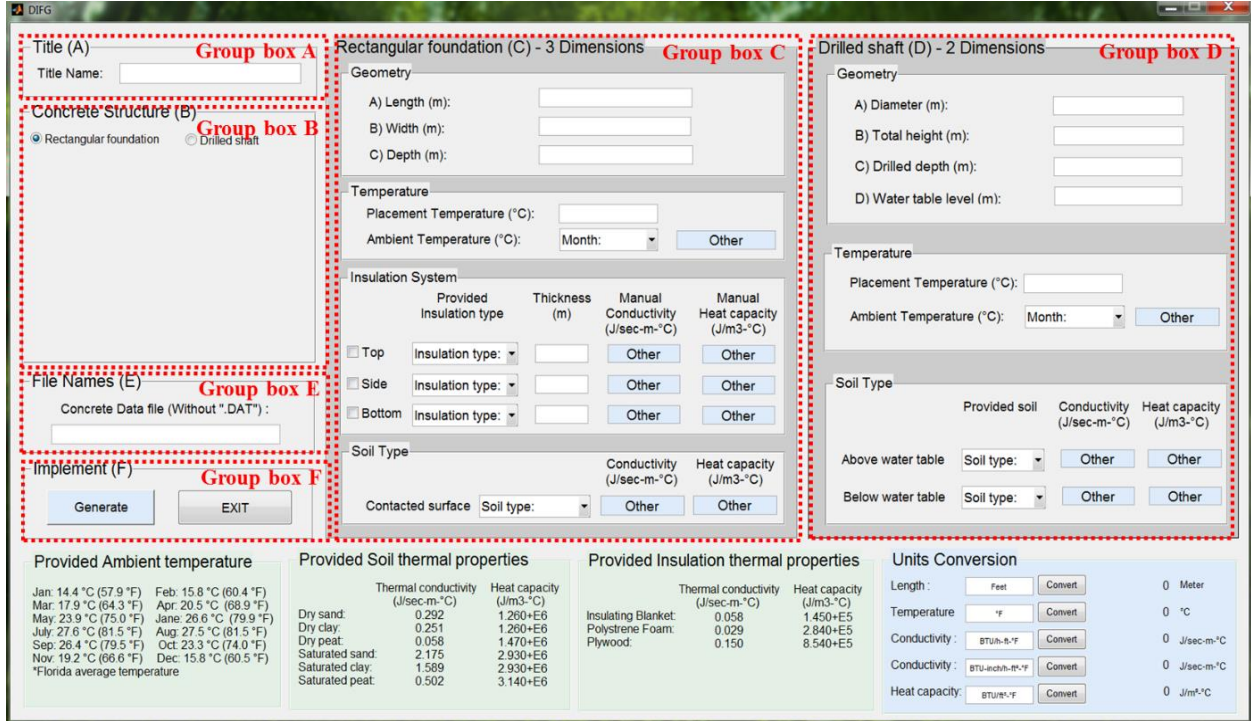


Figure N-5. Screen display upon running of DIFG interface software.

N.2.3 STEP 3: Inputting Parametric Values on DIFG Interface

In order to generate DIANA input files for analyzing a rectangular foundation, Group box A, B, C, E and F (Not including Group box D) should be entered as in the following steps.

Firstly, the field of Title Name is entered as “rectangular” in the Group box (A) as shown in Figure N-6.

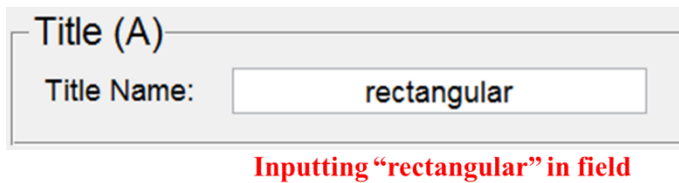


Figure N-6. Inputting title name for analysis.

The DIFG has two choices for structures, which are rectangular foundation and cylindrical drilled shaft. In order to analyze a rectangular foundation, the user clicks the round button of “Rectangular foundation” in Group box (B)” as illustrated in Figure N-7. When the structure type of “Rectangular foundation” is selected, the figure of a rectangular geometry will appear, as shown in Figure N-7. The figure will also indicate the side dimensions of the rectangular foundation. Besides, it will activate the Group box (C)”, while Group box (D)” will be deactivated.

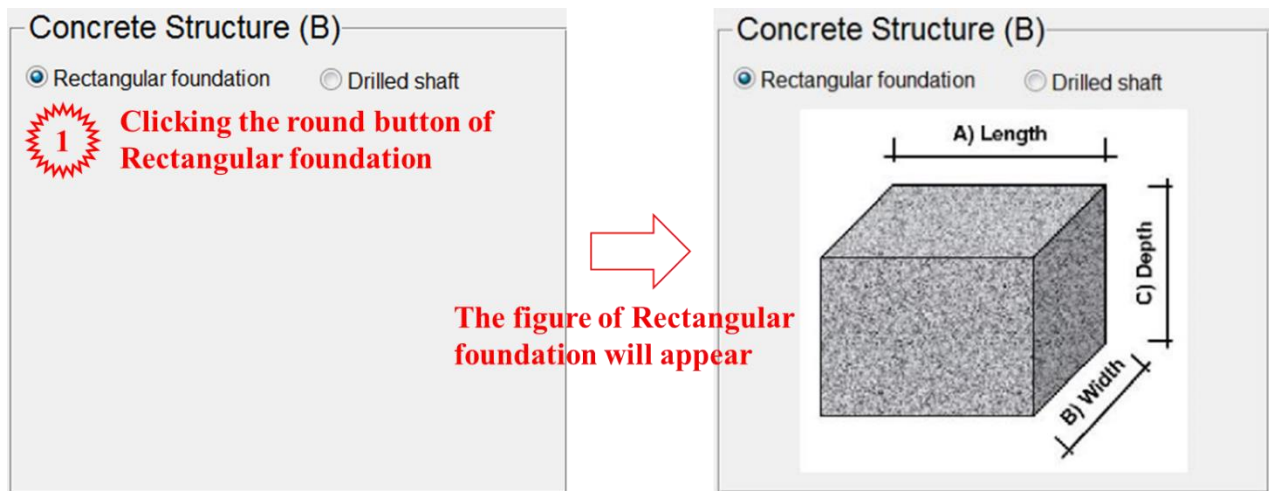


Figure N-7. Structure selection of rectangular foundation.

The next step is inputting the parametric values — geometry dimensions, temperature, insulation combination and soil type — in Group box (C) as shown in Figure N-8.

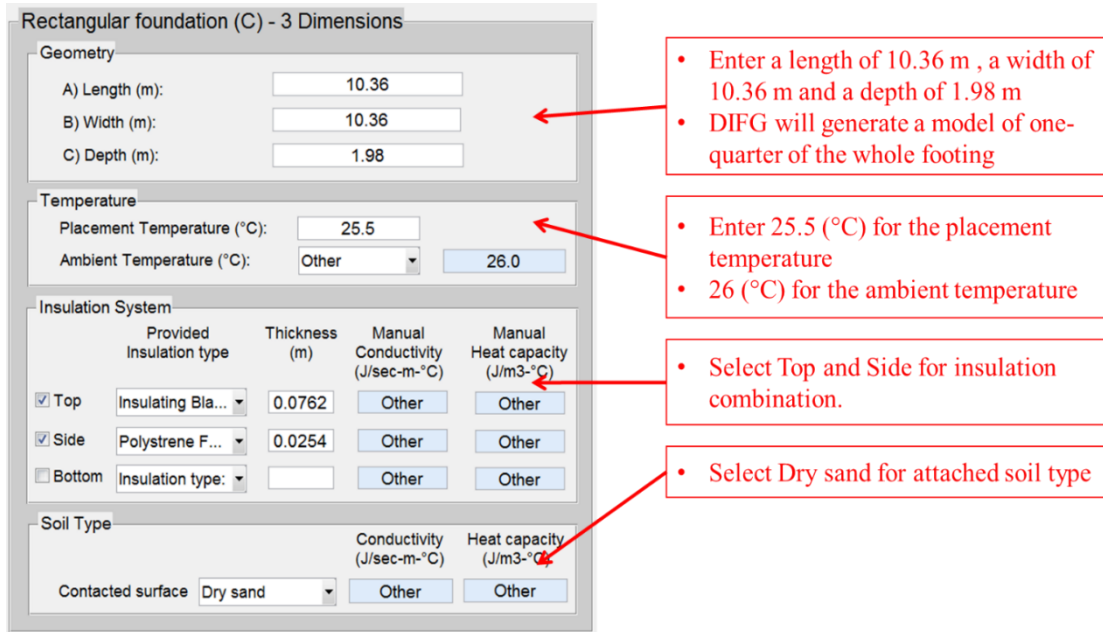
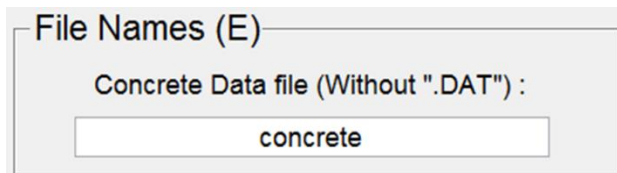


Figure N-8. Inputting parametric values for Rectangular foundation.

In the next step, the user must input the name of concrete data file in Group box (E), as shown in Figure N-9. In this group box, these file names have the extension of “*.DAT”, but the file name should be entered without “.DAT”. The file name entered should match with actual name of the data file in the directory. The pre-created concrete property input file must include the thermal and mechanical properties of the concrete. The concrete data file used in this example is shown in Appendix I.



Inputting “concrete” in field

Figure N-9. Inputting the name of concrete data file.

N.2.4 STEP 4: Saving Output Files and Closing DIFG

After all parameter values are determined and entered through the DIFG interface, the final step is that the user has to click the button of “Generate”, as shown in Figure N-10, in order for DIFG to generate four different input files. These four generated files include a batch file, pre-processing file, command file, and post-processing file. These four files will be generated one-by-one sequentially. When each generated file appears, the user should click the “save” button to save the file in the specified folder, as shown in Figure N-11. When all the files have been generated and saved, the user can click the “Exit” button to close the DIFG software.

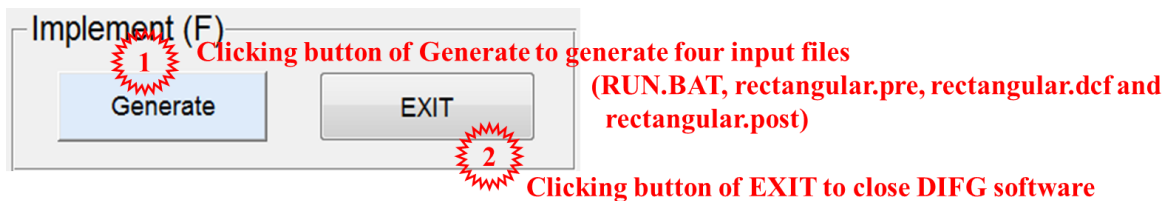
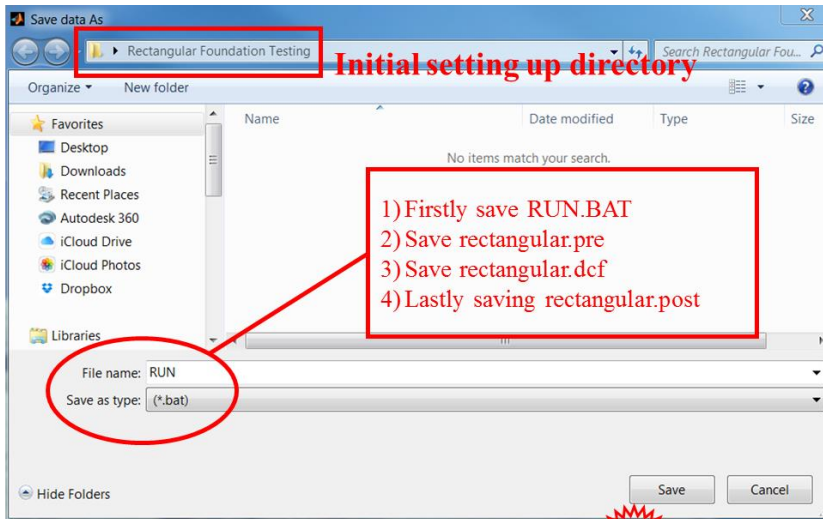


Figure N-10. Generating four input files and closing DIFG software.



Clicking for saving files

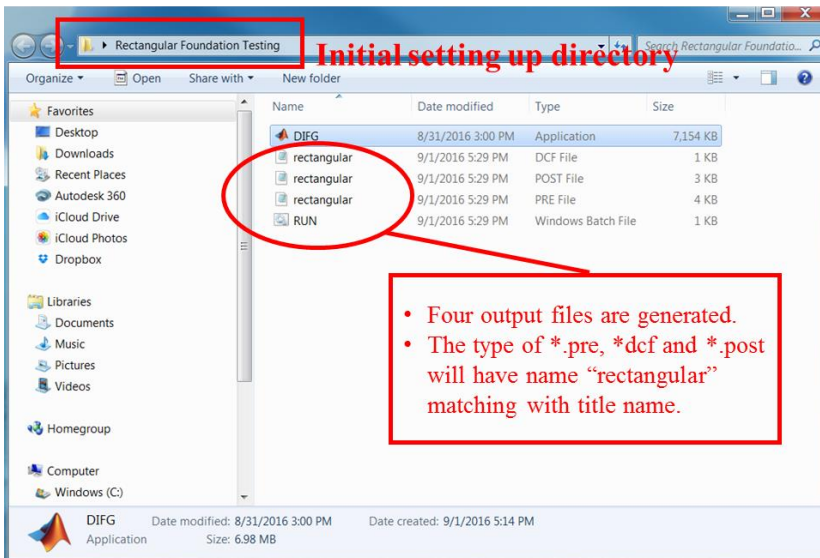



Figure N-11. Saving the generated input files in initial setting directory.

N.2.5 STEP 5: Pre-Setting before Operating DIANA

When the files are generated by DIFG as shown in Figure N-11, they are ready to be used in DIANA for thermal analysis. Once the user clicks the batch file of “RUN.BAT”, all the steps are going to execute automatically, including pre-processing, analysis, and post-processing. After the batch file of “RUN.BAT” is clicked, thermal analysis starts and the results files are saved automatically. However, before clicking the batch file, it is necessary to set up one important thing as follows:

- iDIANA should be set in the initial directory as the same folder where all files have been saved in advance as shown in Figure N-12. This program can be opened by clicking this icon ( Diana) among the programs in the user’s computer. (Note: Directory: iDIANA → Tool → Options In iDIANA program)

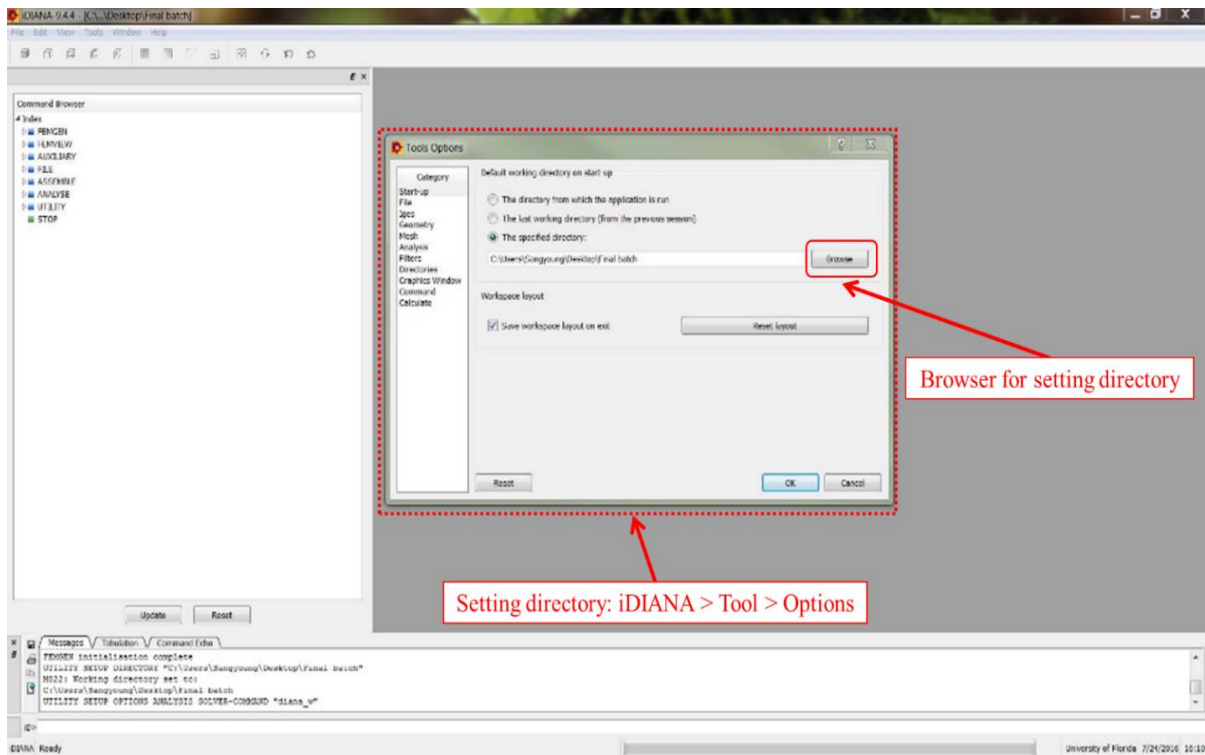


Figure N-12. Setting iDIANA in the initial directory where all files are located.

N.2.6 STEP 6: Running DIANA Automatically

After setting iDIANA in the initial directory as the same folder where all files have been saved in advance, the user can click the file of “RUN.BAT” as shown in Figure N-13 in order to run DIANA for analyzing the thermal behavior of the rectangular foundation. Once DIANA starts to run, a screen display as shown in Figure N-14 will appear initially. It will be followed by a screen display as shown in Figure N-15 when it is performing the pre-processing step. It will then be followed by a screen display as shown in Figure N-16 when it is performing the analyzing step, and a screen display as shown in Figure N-17 when it is performing the post-processing step.

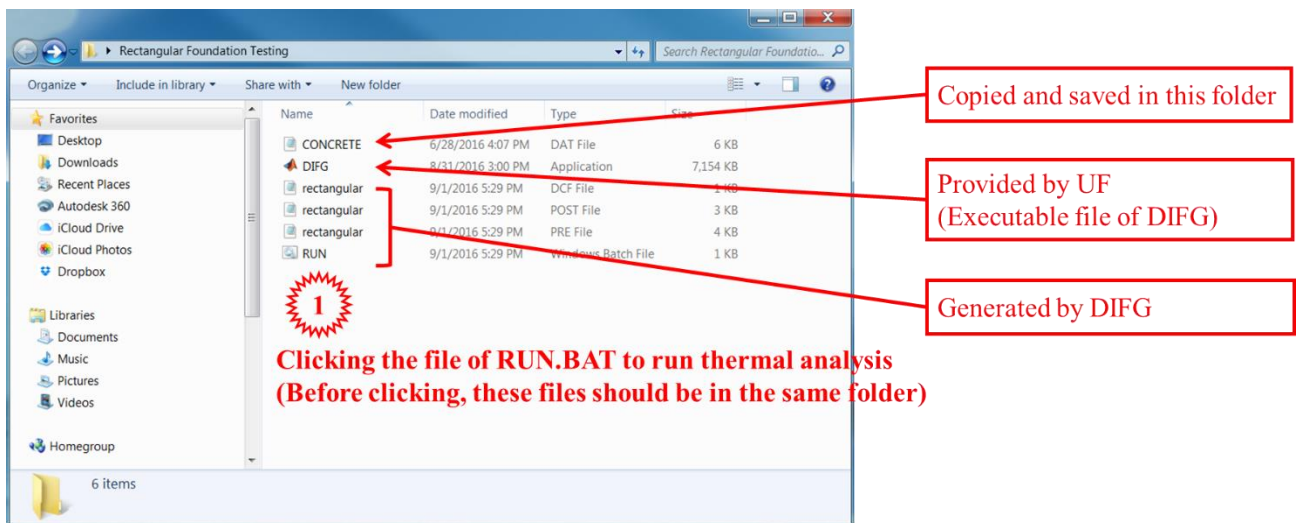


Figure N-13. All needed files for running thermal analysis using DIANA.

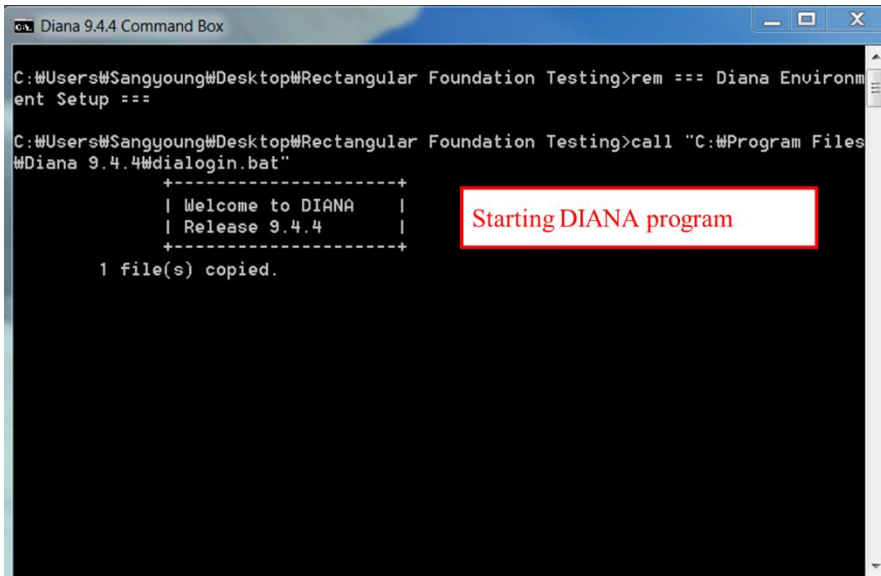


Figure N-14. Starting DIANA initially.

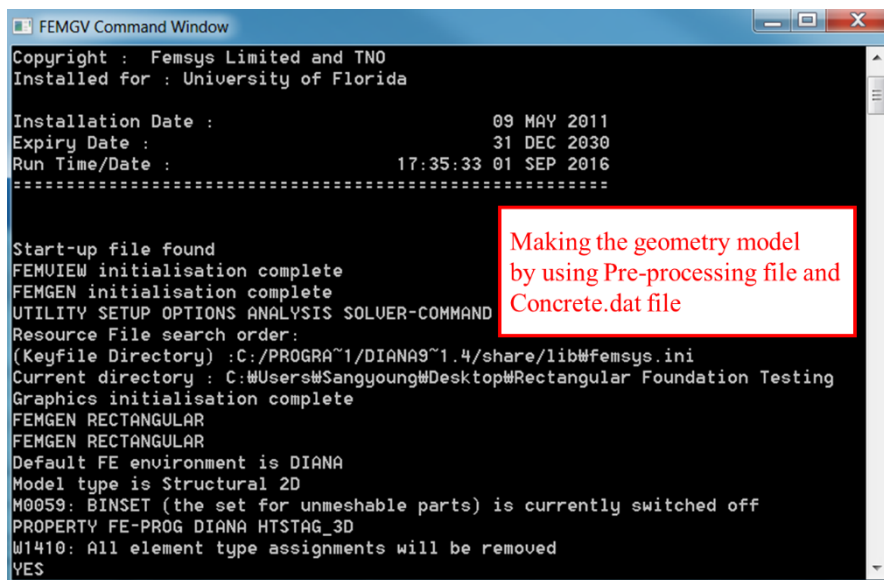


Figure N-15. Starting DIANA for pre-processing.

```

Diana 9.4.4 Command Box
C:\Users\Sangyoung\Desktop\Rectangular Foundation Testing>rem === Diana Environment Setup ===
C:\Users\Sangyoung\Desktop\Rectangular Foundation Testing>call "C:\Program Files\Diana 9.4.4\dialogin.bat"
+-----+
| Welcome to DIANA |
| Release 9.4.4    |
+-----+
1 file(s) copied.
diana: working directory is C:\Users\Sangyoung\Desktop\Rectangular Foundation Testing
diana: input file is rectangular.dat
diana: command file is rectangular.dcf
diana: output file is rectangular.out
diana: filios file is diana.ff

```

Starting thermal Analysis by using command file

Figure N-16. Starting DIANA for analyzing.

```

FEMGV Command Window
Installation Date : 09 MAY 2011
Expiry Date : 31 DEC 2030
Run Time/Date : 17:43:58 01 SEP 2016
=====
Start-up file found
FEMUIEW initialisation complete
FEMGEN initialisation complete
UTILITY SETUP OPTIONS ANALYSIS SOLVER-COMMAND "diana_w"
Resource File search order:
(Keyfile Directory) :C:/PROGRA~1/DIANA9~1.4/share/lib#femsys.ini
Current directory : C:\Users\Sangyoung\Desktop\Rectangular Foundation Testing
Graphics initialisation complete
FEMUIEW FLOW
FEMUIEW FLOW
M019: Loadcase < TR1 > step < 1 > selected
UIEW MESH CONC
EYE FRAME
EYE ROTATE TO 30 45 45
UIEW OPTIONS EDGES OUTLINE
RESULTS LOADCASE TR1 24
RESULTS NODAL PTE...$ PTE
PRESENT CONTOUR LEVELS

```

Making output files (LRT, PS) by using Post-processing file

Figure N-17. Starting DIANA for post-processing.

N.2.7 STEP 7: Reading the Output Files from DIANA Post-Processing

The results of the analysis after post-processing by DIANA are stored in thirteen (13) output files automatically. There are six output files with extension of “PRT” and seven output files with extension of “PS”. The six PRT files have file names of “Cold1”, “Cold2”, “Cold3”, “Cold4”, “Cold5”, and “Hot”. They contain the calculated temperature-time history of the concrete at five possible coldest points and one hottest point in the concrete structure. The locations of these five coldest points and one hottest points for the rectangular footing are shown in Figure N-18.

The seven output files with extension of “PS” have file names of “Day1”, “Day2”, “Day3”, “Day4”, “Day5”, “Day6, and “Day7”. They contain the temperature contour plots of the concrete structure at the end of the 1st, 2nd, 3rd, 4th, 5th, 6th, and 7th day after concrete placement.

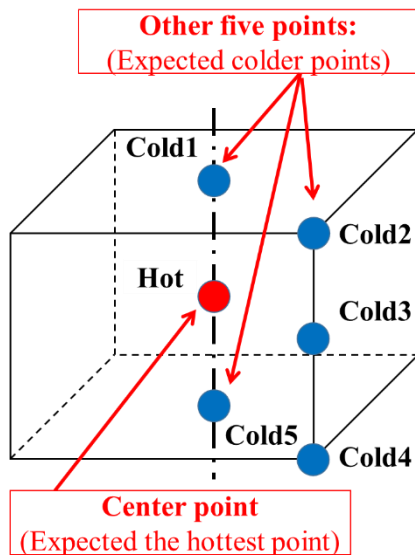


Figure N-18. Locations of coldest and hottest points in rectangular footing.

Figure N-19 presents the screen display showing all the thirteen output files from post-processing by DIANA. The contents of the six PRT files “Cold1”, “Cold2”, “Cold3”, “Cold4”, “Cold5”, and “Hot” are shown in Figures N-20. The temperature contour plots from the seven PS files “Day1”, “Day2”, “Day3”, “Day4”, “Day5”, “Day6, and “Day7” are shown in Figures N-21.

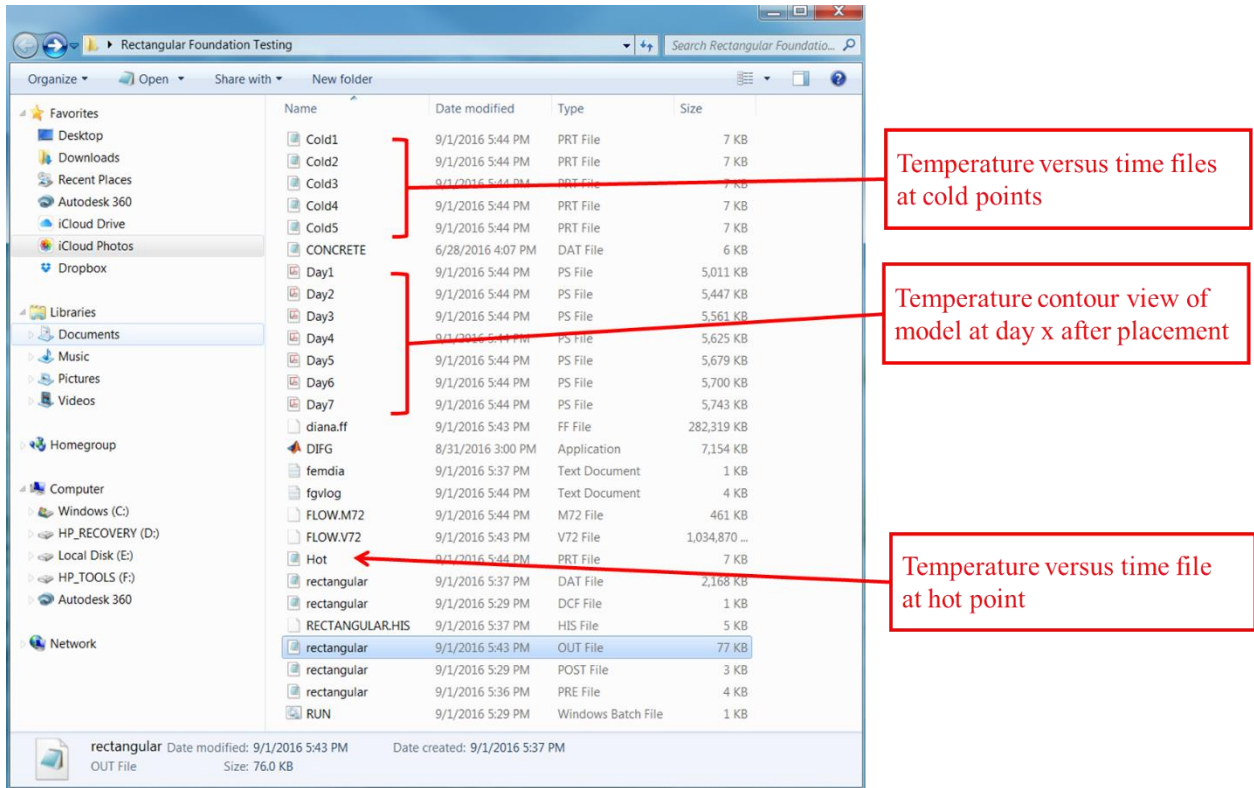


Figure N-19. Screen display showing all output files from DIANA.

Model: FLOW
Nodal PTE....S PTE

Graph begins

Point no.	X	Y
1,	.36E4,	26.7
2,	.72E4,	27.7
3,	.108E5,	29
4,	.144E5,	30.6
5,	.18E5,	32.4
6,	.216E5,	34.4
7,	.252E5,	36.5
8,	.288E5,	38.7
9,	.324E5,	41.3
10,	.36E5,	43.9
11,	.396E5,	45.9
12,	.432E5,	47.6
13,	.468E5,	49
14,	.504E5,	50.3
15,	.54E5,	51.6
16,	.576E5,	52.8
17,	.612E5,	54
18,	.648E5,	55.1
19,	.684E5,	56.3
20,	.72E5,	57.6
- Line Skipped -		
165,	.594E6,	81.7
166,	.598E6,	81.6
167,	.601E6,	81.5

Increment Time (hours)

Irrelevant Data (DIANA internal Information)

Temperature at corresponding time

A

Model: FLOW Nodal PTE....S PTE	Model: FLOW Nodal PTE....S PTE
Graph begins	Graph begins
Point no. X Y	Point no. X Y
1, .36E4, 26.9	1, .36E4, 27
2, .72E4, 27.8	2, .72E4, 27.8
3, .108E5, 28.8	3, .108E5, 28.7
4, .144E5, 30.2	4, .144E5, 29.8
5, .18E5, 31.8	5, .18E5, 31
6, .216E5, 33.4	6, .216E5, 32.1
7, .252E5, 35.1	7, .252E5, 33.2
8, .288E5, 36.8	8, .288E5, 34.3
9, .324E5, 38.8	9, .324E5, 35.5
10, .36E5, 40.8	10, .36E5, 36.7
11, .396E5, 42.4	11, .396E5, 37.7
12, .432E5, 43.6	12, .432E5, 38.3
13, .468E5, 44.6	13, .468E5, 38.7
14, .504E5, 45.4	14, .504E5, 39
15, .54E5, 46.2	15, .54E5, 39.1
16, .576E5, 46.9	16, .576E5, 39.2
17, .612E5, 47.5	17, .612E5, 39.3
18, .648E5, 48.2	18, .648E5, 39.4
19, .684E5, 48.8	19, .684E5, 39.5
20, .72E5, 49.4	20, .72E5, 39.6
- Line Skipped -	
165, .594E6, 59.2	165, .594E6, 33.2
166, .598E6, 59.2	166, .598E6, 33.1
167, .601E6, 59.1	167, .601E6, 33.1

B.

C

Figure N-20. Content of tabulation from analysis of example rectangular footings. A) Hot.PRT, B) Cold1.PRT, C) Cold2.PRT, D) Cold3.PRT, E) Cold4.PRT, and F) Cold5.PRT.

```

; Model: FLOW
; Nodal PTE....S PTE
;
; Graph begins
; Point no.          X          Y
;
1,      .36E4,      27.1
2,      .72E4,      28
3,      .108E5,     29
4,      .144E5,     30.3
5,      .18E5,      31.6
6,      .216E5,     33
7,      .252E5,     34.4
8,      .288E5,     35.8
9,      .324E5,     37.3
10,     .36E5,      38.9
11,     .396E5,     40.2
12,     .432E5,     41
13,     .468E5,     41.7
14,     .504E5,     42.1
15,     .54E5,      42.5
16,     .576E5,     42.9
17,     .612E5,     43.2
18,     .648E5,     43.5
19,     .684E5,     43.7
20,     .72E5,      44

- Line Skipped -

165,    .594E6,     37.7
166,    .598E6,     37.6
167,    .601E6,     37.6

```

D

```

; Model: FLOW
; Nodal PTE....S PTE
;
; Graph begins
; Point no.          X          Y
;
1,      .36E4,      26.3
2,      .72E4,      26.6
3,      .108E5,     27
4,      .144E5,     27.5
5,      .18E5,      28
6,      .216E5,     28.5
7,      .252E5,     29
8,      .288E5,     29.5
9,      .324E5,     30
10,     .36E5,      30.5
11,     .396E5,     31
12,     .432E5,     31.5
13,     .468E5,     31.7
14,     .504E5,     31.9
15,     .54E5,      32
16,     .576E5,     32
17,     .612E5,     32
18,     .648E5,     32
19,     .684E5,     32
20,     .72E5,      32

- Line Skipped -

165,    .594E6,     29.3
166,    .598E6,     29.3
167,    .601E6,     29.2

```

E

```

; Model: FLOW
; Nodal PTE....S PTE
;
; Graph begins
; Point no.          X          Y
;
1,      .36E4,      26.1
2,      .72E4,      26.7
3,      .108E5,     27.5
4,      .144E5,     28.4
5,      .18E5,      29.5
6,      .216E5,     30.7
7,      .252E5,     32
8,      .288E5,     33.2
9,      .324E5,     34.6
10,     .36E5,      36.1
11,     .396E5,     37.6
12,     .432E5,     38.8
13,     .468E5,     39.7
14,     .504E5,     40.6
15,     .54E5,      41.2
16,     .576E5,     41.9
17,     .612E5,     42.4
18,     .648E5,     43
19,     .684E5,     43.5
20,     .72E5,      44

- Line Skipped -

165,    .594E6,     55.9
166,    .598E6,     55.8
167,    .601E6,     55.8

```

F.

Figure N-20. Continued.

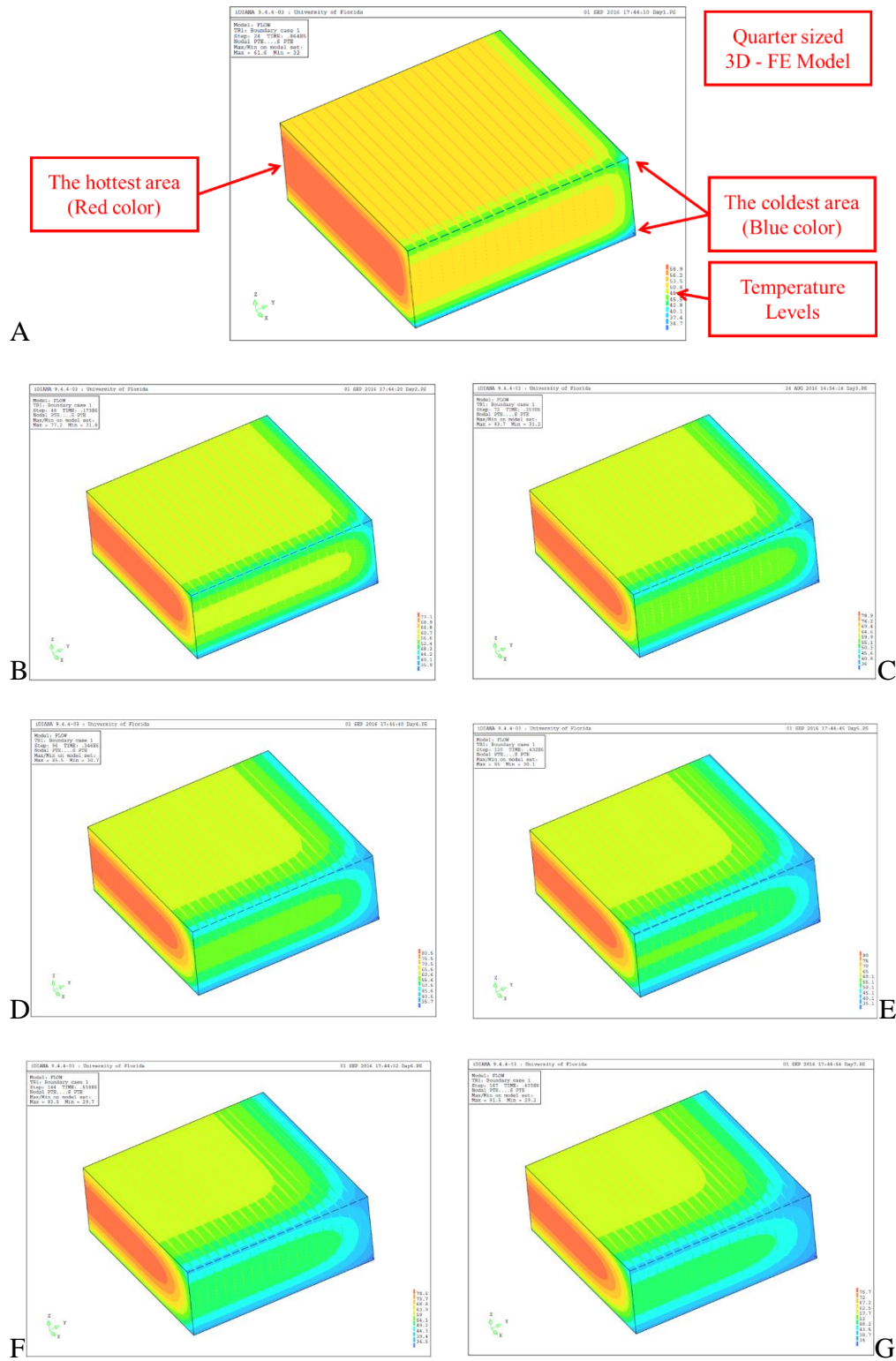


Figure N-21. Temperature contour view. A) day 1 after placement, B) day 2 after placement, C) day 3 after placement, D) day 4 after placement, E) day 5 after placement, F) day 6 after placement, and G) day 7 after placement.

N.3 Thermal Analysis of Drilled Shaft

N.3.1 STEP 1: Installing Matlab-Language Operating File

If the user already installed “MCR_R2013a_win64_installer” or installed Matlab program, it is possible to skip Step1 and go to Step 2 directly. Otherwise, it is required to see Step 1 in Chapter 2 for installing “MCR_R2013a_win64_installer”. Please note that the lines and words that are marked in red in this figure as following below are not part of the screen display, but are added to explain the different information on the screen display.

N.3.2 STEP 2: Opening DIANA Input File Generator (DIFG)

Before starting DIFG, it is recommended to set up the specific directory where all output files will be saved. The way to set the designated directory is to create the folder and to save the file “DIFG.EXE” in that folder, as shown in Figure N-22 (The directory named “Drilled shaft testing” for this demonstration).

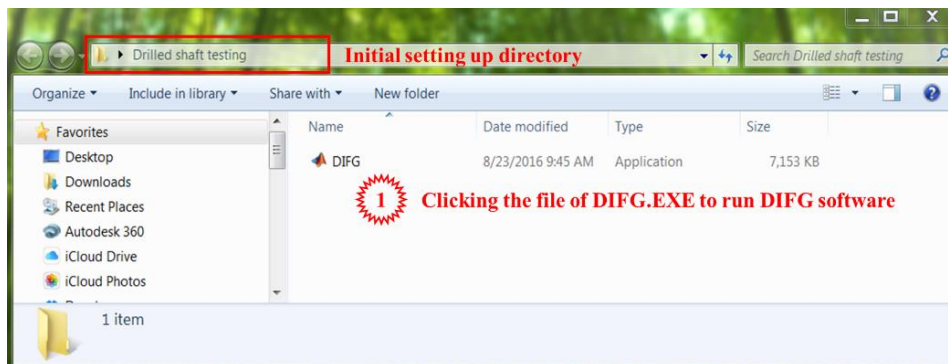


Figure N-22. Creating the folder and saving DIFG.EXE in it.

Click “DIFG.EXE” to open the software. The interface screen of DIFG will appear soon as shown in Figure N-23.

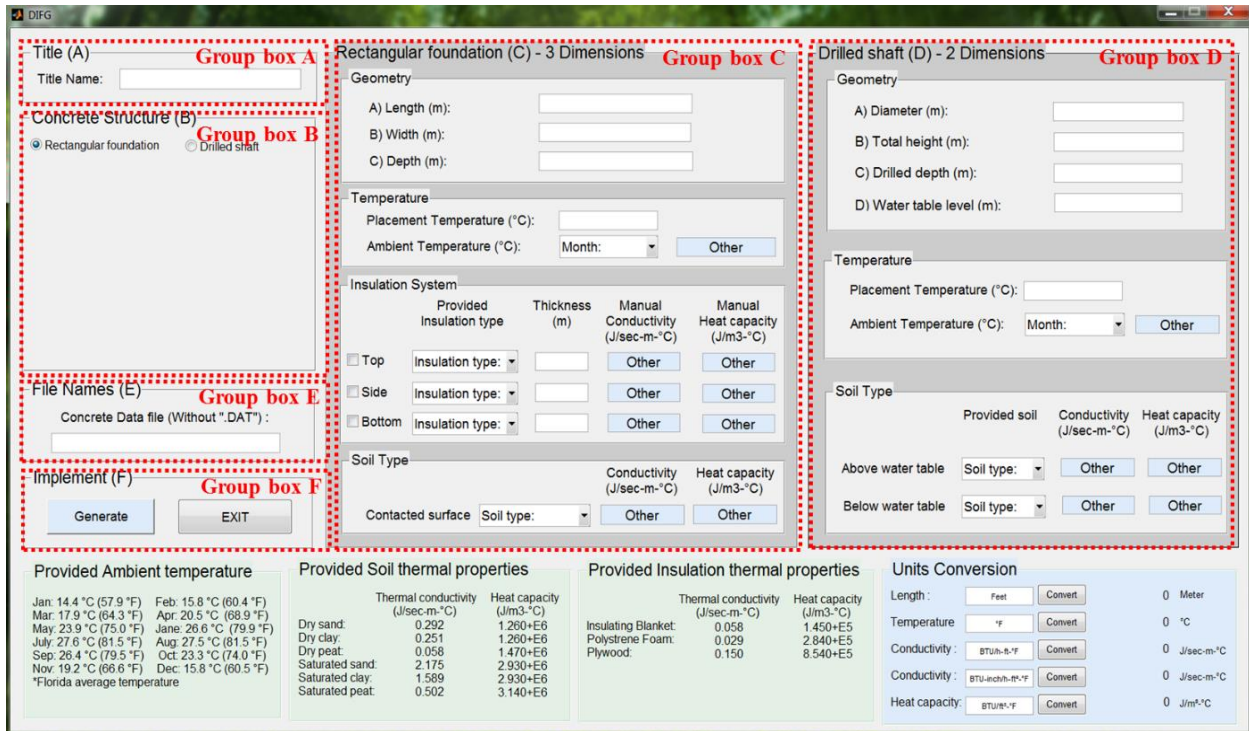
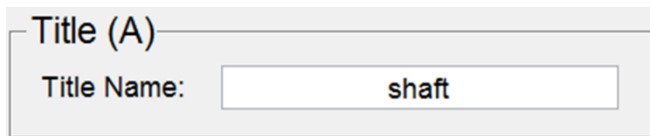


Figure N-23. Screen display upon running of DIFG interface software.

N.3.3 STEP 3: Inputting Parametric Values on DIFG Interface

In order to generate DIANA input files for analyzing a drilled shaft, Group box A, B, D, E, and F (Not including Group box C) should be entered as in the following steps. Firstly, the field of Title Name is entered as “shaft” in the Group box (A) as shown in Figure N-24.



Inputting “shaft” in field

Figure N-24. Inputting title name for analysis.

The DIFG has two choices for structure, which are rectangular foundation and cylindrical drilled shaft. In order to analyze a rectangular foundation, the user clicks the round button of “Drilled shaft” in Group box (B)” as illustrated in Figure N-25. When the structure type of “Drilled shaft” is selected, the figure of cylindrical geometry will appear, as shown in Figure N-25. The figure will also indicate the side dimension of drilled shaft as well as water table level under soil. Besides, it will activate the Group box (D)” while Group box (C)” will be deactivated.

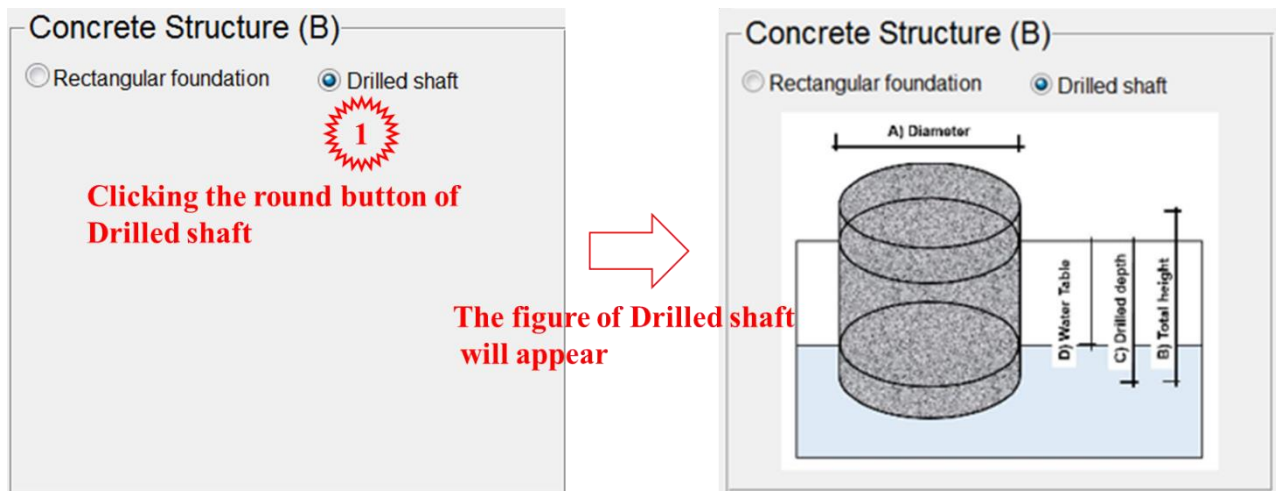


Figure N-25. Structure selection of drilled shaft.

The next step is inputting the parametric values — geometry dimensions, temperature and soil type — in Group box (D) as shown in Figure N-26.

Drilled shaft (D) - 2 Dimensions

Geometry

A) Diameter (m):

B) Total height (m):

C) Drilled depth (m):

D) Water table level (m):

Temperature

Placement Temperature (°C):

Ambient Temperature (°C):

Soil Type

	Provided soil	Conductivity (J/sec-m-°C)	Heat capacity (J/m3-°C)
Above water table	<input type="text" value="Sand"/>	<input type="button" value="Other"/>	<input type="button" value="Other"/>
Below water table	<input type="text" value="Sand"/>	<input type="button" value="Other"/>	<input type="button" value="Other"/>

- Enter a diameter of 1.8288 m , a total height of 2.1336 m, a drilled depth of 1.8288 m and a water table level of 1.2192 m
- DIFG will generate a model of half size of the whole shaft
- Enter 26.0 (°C) for the placement temperature
- Selecting “January” for the ambient temperature
- Select dry “Sand” and wet “sand” for surrounding soil types

Figure N-26. Inputting parametric values for drilled shaft.

In the next step, the user must input the name of concrete data file in Group box (E), as shown in Figure N-27. In this group box, these file names have the extension of “*.DAT”, but the file name should be entered without “.DAT”. The file name entered should match with actual name of the data file in the directory. The pre-created concrete property input file must include the thermal and mechanical properties of the concrete. The concrete data file used in this example is shown in Appendix I.

File Names (E)

Concrete Data file (Without ".DAT") :

Inputting “concrete” in field

Figure N-27. Inputting the name of concrete data file.

N.3.4 STEP 4: Saving Output Files and Closing DIFG

After all parameter values are determined and entered through the DIFG interface, the final step is that the user has to click the button of “Generate”, as shown in Figure N-28, in order for DIFG to generate four different input files. These four generated files include a batch file, pre-processing file, command file and post-processing file. These four files will be generated one-by-one sequentially. When each generated file appear, the user should click the “Save” button to save the file in the specified folder, as shown in Figure N-29. When all the files have been generated and saved, the user can click the “Exit” button to close the DIFG software.

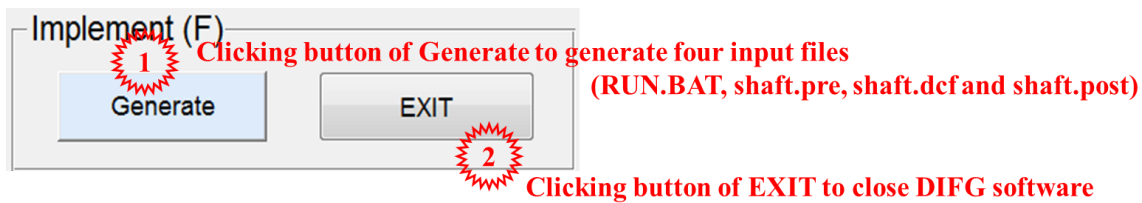
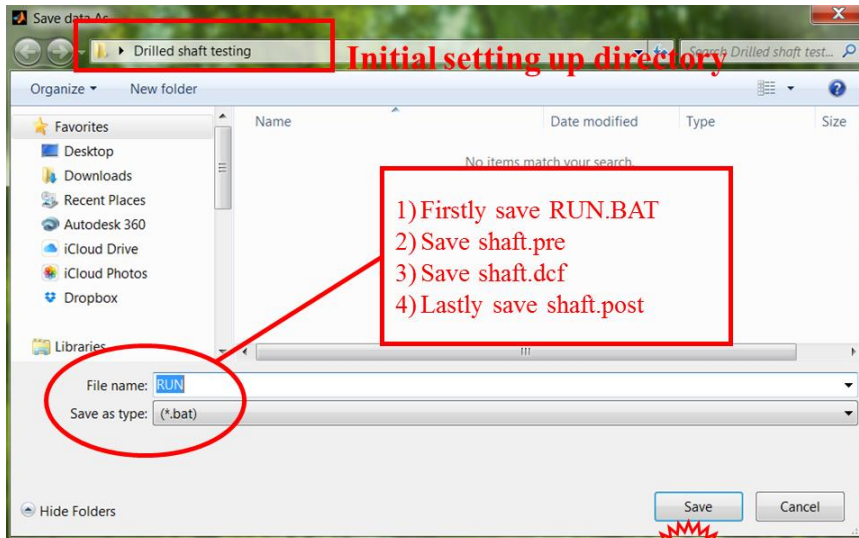


Figure N-28. Generating four input files and closing DIFG.



1 Clicking for saving files

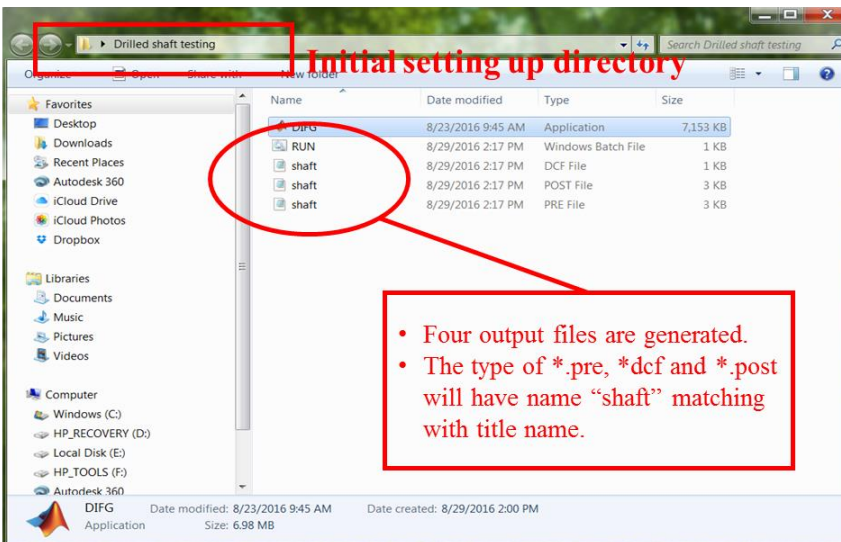



Figure N-29. Saving and generated input files in initial setting directory.

N.3.5 STEP 5: Pre-Setting before Operating DIANA

When the files are generated by DIFG as shown in Figure N-29, they are ready to be used in DIANA for thermal analysis. Once the user clicks the batch file of “RUN.BAT”, all the steps are going to execute automatically, including pre-processing, analysis and post-processing. After the batch file of “RUN.BAT” is clicked, thermal analysis starts and the results files are saved automatically. However, before clicking the batch file, it is necessary to set up one important thing as follows:

- iDIANA should be set in the initial directory as the same folder where all files have been saved in advance as shown in Figure N-30. This program can be opened by clicking this icon ( Diana) among the programs in user’s computer.
(Note: Directory: iDIANA → Tool → Options in iDIANA program)

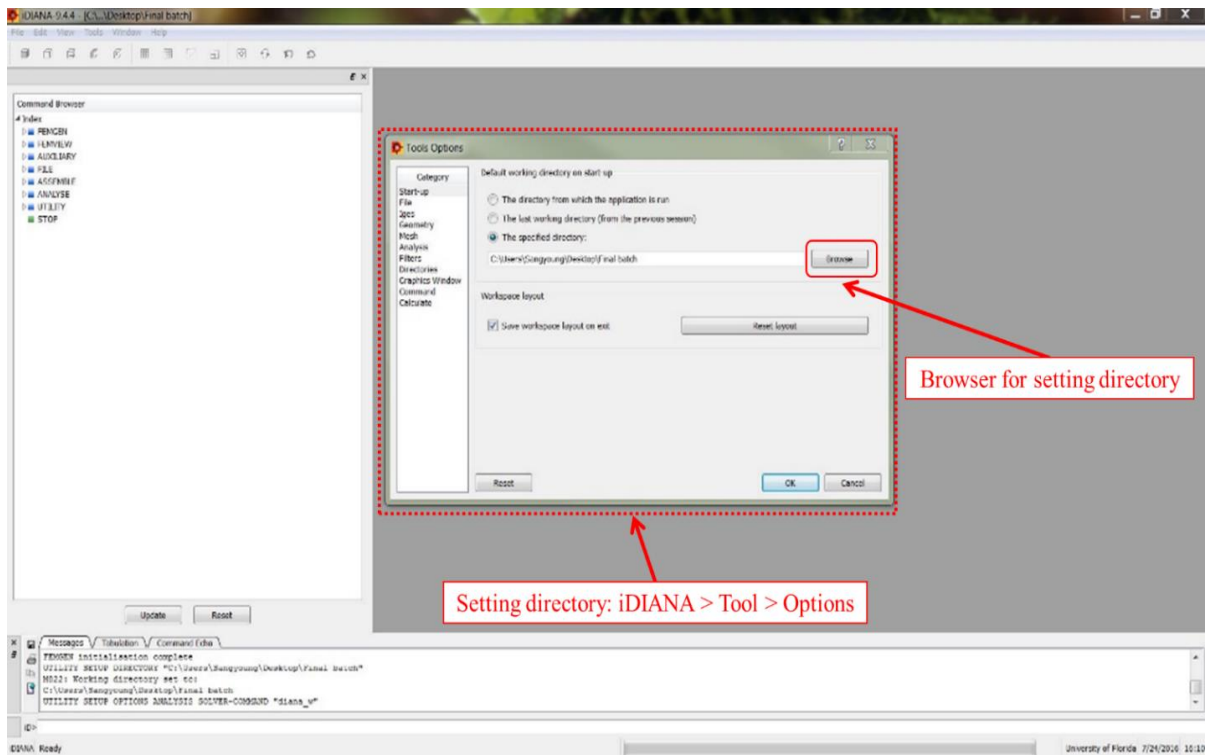


Figure N-30. Setting iDIANA in the initial directory where all files are located.

N.3.6 STEP 6: Running DIANA Automatically

After setting iDIANA in the initial directory as the same folder where all files have been saved in advance, the user can click the file of “RUN.BAT” as shown in Figure N-31 in order to run DIANA for analyzing thermal behavior of drilled shaft. Once DIANA starts to run, a screen display as shown in Figure N-32 will appear initially. It will be followed by a screen display as shown in Figure N-33 when it is performing the pre-processing step. It will then be followed by a screen display as shown in Figure N-34 when it is performing the analyzing step, and a screen display as shown in Figure N-35 when it is performing the post-processing step.

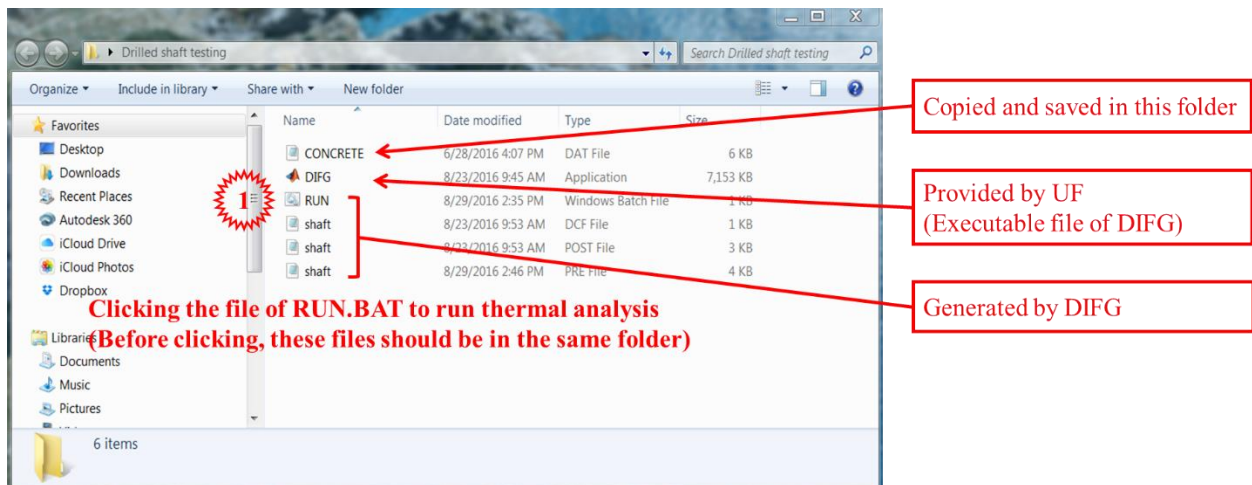


Figure N-31. All needed files for running thermal analysis using DIANA.

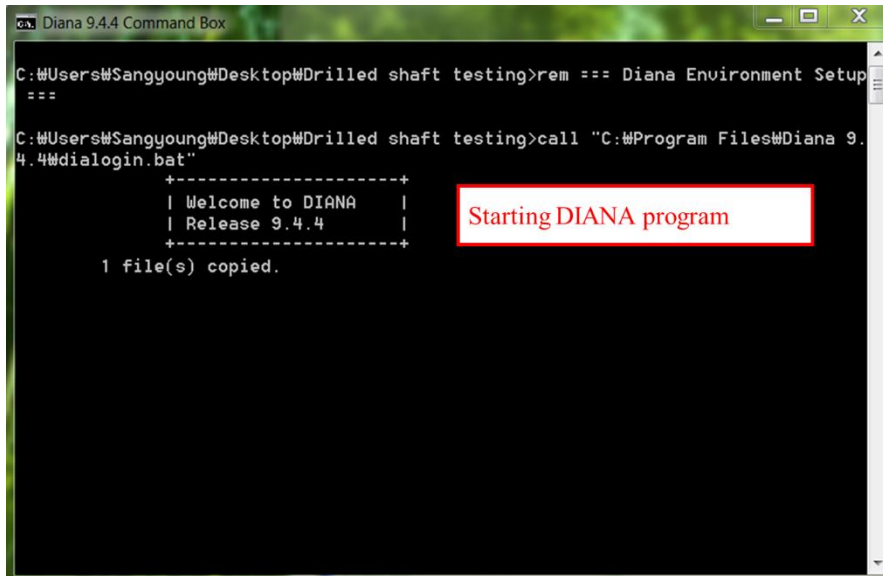


Figure N-32. Starting DIANA initially.

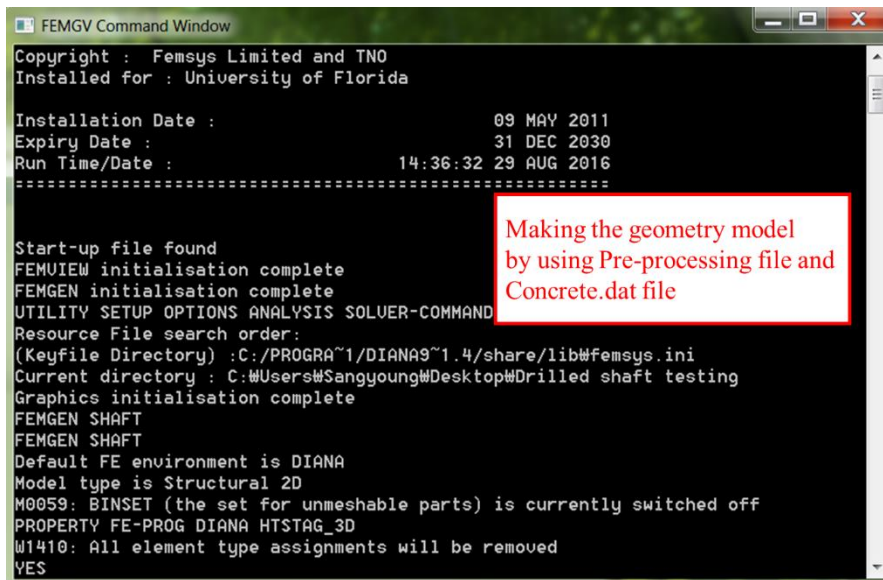


Figure N-33. Starting DIANA for pre-processing.

```
cx Diana 9.4.4 Command Box
C:\Users\Sangyoung\Desktop\Drilled shaft testing>rem === Diana Environment Setup
===
C:\Users\Sangyoung\Desktop\Drilled shaft testing>call "C:\Program Files\Diana 9.
4.4\dialogin.bat"
+-----+
| Welcome to DIANA |
| Release 9.4.4    |
+-----+
1 file(s) copied.
diana: working directory is C:\Users\Sangyoung\Desktop\Drilled shaft testing
diana: input file is shaft.dat
diana: command file is shaft.dcf
diana: output file is shaft.out
diana: filos file is diana.ff
```

Starting thermal Analysis
by using command file

Figure N-34. Starting DIANA for analyzing.

```
FEMGV Command Window
Installation Date : 09 MAY 2011
Expiry Date : 31 DEC 2030
Run Time/Date : 15:00:47 29 AUG 2016
=====
Start-up file found
FEMUIEW initialisation complete
FEMGEN initialisation complete
UTILITY SETUP OPTIONS ANALYSIS SOLUER-COMMAND "diana_w"
Resource File search order:
(Keyfile Directory) :C:/PROGRA~1/DIANA9~1.4/share/lib#Femsys.ini
Current directory : C:\Users\Sangyoung\Desktop\Drilled shaft testing
Graphics initialisation complete
FEMUIEW FLOW
FEMUIEW FLOW
M019: Loadcase < TR1 > step < 1 > selected
UIEW MESH CONC
EYE FRAME
EYE ROTATE TO 30 45 45
UIEW OPTIONS EDGES OUTLINE
RESULTS LOADCASE TR1 24
RESULTS NODAL PTE...S PTE
PRESENT CONTOUR LEVELS
```

Making output files (LRT, PS)
by using Post-processing file

Figure N-35. Starting DIANA for post-processing.

N.3.7 STEP 7: Reading the Output Files from DIANA Post-Processing

The results of the analysis after post-processing by DIANA are stored in thirteen (13) output files automatically. There are six output files with extension of “PRT” and seven output files with extension of “PS”. The six PRT files have file names of “Cold1”, “Cold2”, “Cold3”, “Cold4”, “Cold5”, and “Hot”. They contain the calculated temperature-time history of the concrete at five possible coldest points and one hottest point in the concrete structure. The locations of these five coldest points and one hottest points for the drilled shaft are shown in Figure N-36.

The seven output files with extension of “PS” have file names of “Day1”, “Day2”, “Day3”, “Day4”, “Day5”, “Day6, and “Day7”. They contain the temperature contour plots of the concrete structure at the end of the 1st, 2nd, 3rd, 4th, 5th, 6th, and 7th day after concrete placement.

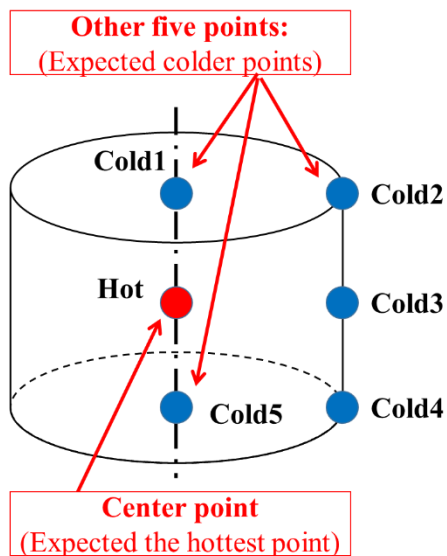


Figure N-36. Locations of coldest and hottest points in drilled shaft.

Figure N-37 presents the screen display showing all the thirteen output files from post-processing by DIANA. The contents of the six PRT files “Cold1”, “Cold2”, “Cold3”, “Cold4”, “Cold5”, and “Hot” are shown in Figures N-38. The temperature contour plots from the seven PS files “Day1”, “Day2”, “Day3”, “Day4”, “Day5”, “Day6, and “Day7” are shown in Figures N-39.

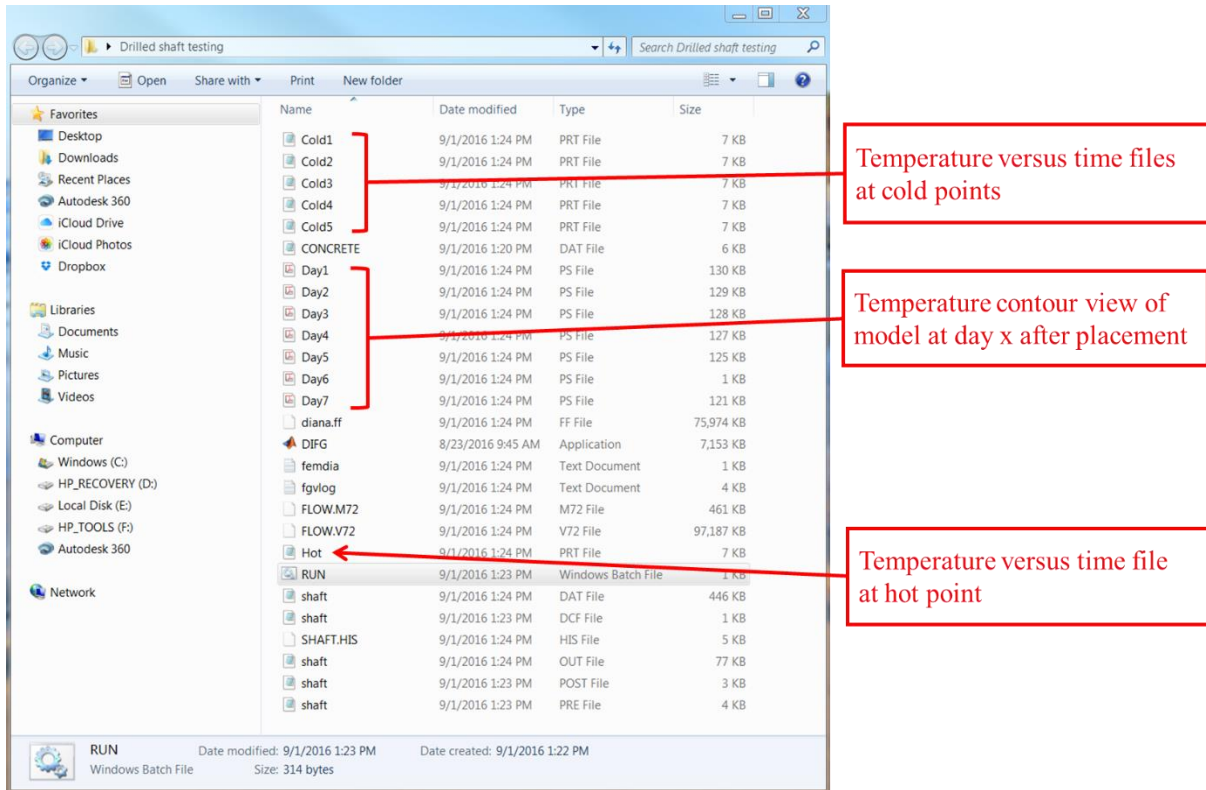


Figure N-37. Screen display showing all output files from DIANA.

Model: FLOW
 Nodal PTE....S PTE
 Graph begins
 Point no. X Y

1,	.36E4,	27.2
2,	.72E4,	28.4
3,	.108E5,	29.7
4,	.144E5,	31.4
5,	.18E5,	33.3
6,	.216E5,	35.4
7,	.252E5,	37.5
8,	.288E5,	39.9
9,	.324E5,	42.6
10,	.36E5,	44.9
11,	.396E5,	46.8
12,	.432E5,	48.4
13,	.468E5,	49.7
14,	.504E5,	51
15,	.54E5,	52.2
16,	.576E5,	53.3
17,	.612E5,	54.4
18,	.648E5,	55.4
19,	.684E5,	56.5
20,	.72E5,	57.5
- Line Skipped -		
164,	.59E6,	35
165,	.594E6,	34.9
166,	.598E6,	34.7
167,	.601E6,	34.6

Increment Time (hours) →

Irrelevant Data (DIANA internal Information) →

Temperature at corresponding time →

A

Model: FLOW			Model: FLOW		
Nodal PTE....S PTE			Nodal PTE....S PTE		
Graph begins			Graph begins		
Point no.	X	Y	Point no.	X	Y
1,	.36E4,	21.6	1,	.36E4,	18.7
2,	.72E4,	20.6	2,	.72E4,	17.3
3,	.108E5,	20.1	3,	.108E5,	16.6
4,	.144E5,	20	4,	.144E5,	16.3
5,	.18E5,	20.1	5,	.18E5,	16.2
6,	.216E5,	20.3	6,	.216E5,	16.2
7,	.252E5,	20.6	7,	.252E5,	16.1
8,	.288E5,	20.8	8,	.288E5,	16.2
9,	.324E5,	21.1	9,	.324E5,	16.2
10,	.36E5,	21.3	10,	.36E5,	16.2
11,	.396E5,	21.6	11,	.396E5,	16.2
12,	.432E5,	21.9	12,	.432E5,	16.2
13,	.468E5,	22.2	13,	.468E5,	16.2
14,	.504E5,	22.4	14,	.504E5,	16.2
15,	.54E5,	22.6	15,	.54E5,	16.3
16,	.576E5,	22.6	16,	.576E5,	16.3
17,	.612E5,	22.6	17,	.612E5,	16.3
18,	.648E5,	22.6	18,	.648E5,	16.3
19,	.684E5,	22.5	19,	.684E5,	16.3
20,	.72E5,	22.4	20,	.72E5,	16.3
- Line Skipped -			- Line Skipped -		
164,	.59E6,	16.4	164,	.59E6,	14.8
165,	.594E6,	16.4	165,	.594E6,	14.8
166,	.598E6,	16.4	166,	.598E6,	14.8
167,	.601E6,	16.4	167,	.601E6,	14.8

B

C

Figure N-38. Content of tabulation from analysis of example drilled shafts. A) Hot.PRT, B) Cold1.PRT, C) Cold2.PRT, D) Cold3.PRT, E) Cold4.PRT, and F) Cold5.PRT.

```

; Model: FLOW
; Nodal PTE....S PTE
;
; Graph begins
; Point no.      X      Y
;
1,      .36E4,    26.2
2,      .72E4,    26.6
3,      .108E5,   27.2
4,      .144E5,   28
5,      .18E5,    29
6,      .216E5,   30.1
7,      .252E5,   31.2
8,      .288E5,   32.3
9,      .324E5,   33.5
10,     .36E5,    34.9
11,     .396E5,   36.1
12,     .432E5,   37.1
13,     .468E5,   37.8
14,     .504E5,   38.5
15,     .54E5,    38.9
16,     .576E5,   39.3
17,     .612E5,   39.7
18,     .648E5,   40
19,     .684E5,   40.3
20,     .72E5,    40.6

- Line Skipped -

164,    .59E6,    28.8
165,    .594E6,   28.7
166,    .598E6,   28.6
167,    .601E6,   28.5
D

```

```

; Model: FLOW
; Nodal PTE....S PTE
;
; Graph begins
; Point no.      X      Y
;
1,      .36E4,    24.5
2,      .72E4,    23.8
3,      .108E5,   23.5
4,      .144E5,   23.5
5,      .18E5,    23.5
6,      .216E5,   23.6
7,      .252E5,   23.8
8,      .288E5,   23.9
9,      .324E5,   24.1
10,     .36E5,    24.3
11,     .396E5,   24.5
12,     .432E5,   24.7
13,     .468E5,   25
14,     .504E5,   25.2
15,     .54E5,    25.4
16,     .576E5,   25.5
17,     .612E5,   25.7
18,     .648E5,   25.7
19,     .684E5,   25.8
20,     .72E5,    25.9

- Line Skipped -

164,    .59E6,    24.6
165,    .594E6,   24.6
166,    .598E6,   24.5
167,    .601E6,   24.5
E

```

```

; Model: FLOW
; Nodal PTE....S PTE
;
; Graph begins
; Point no.      X      Y
;
1,      .36E4,    25.7
2,      .72E4,    25.7
3,      .108E5,   25.8
4,      .144E5,   26.2
5,      .18E5,    26.7
6,      .216E5,   27.3
7,      .252E5,   27.9
8,      .288E5,   28.6
9,      .324E5,   29.3
10,     .36E5,    30
11,     .396E5,   30.8
12,     .432E5,   31.6
13,     .468E5,   32.2
14,     .504E5,   32.7
15,     .54E5,    33.2
16,     .576E5,   33.5
17,     .612E5,   33.8
18,     .648E5,   34.1
19,     .684E5,   34.3
20,     .72E5,    34.5

- Line Skipped -

164,    .59E6,    27.7
165,    .594E6,   27.6
166,    .598E6,   27.6
167,    .601E6,   27.5
F

```

Figure N-38. Continued.

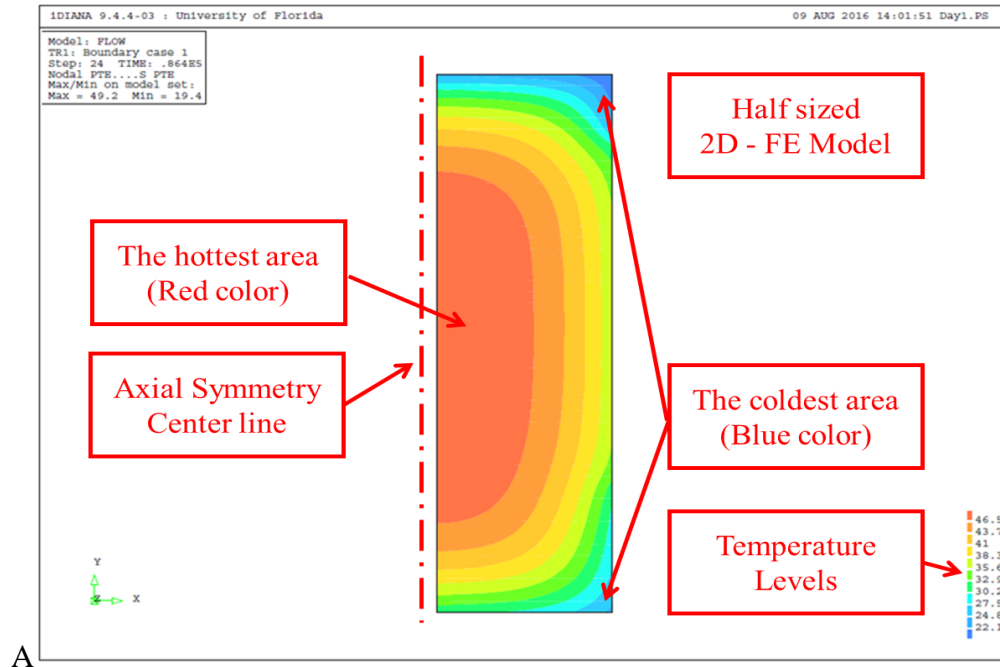


Figure N-39. Temperature contour view. A) day 1 after placement, B) day 2 after placement, C) day 3 after placement, D) day 4 after placement, E) day 5 after placement, F) day 6 after placement, and G) day 7 after placement.

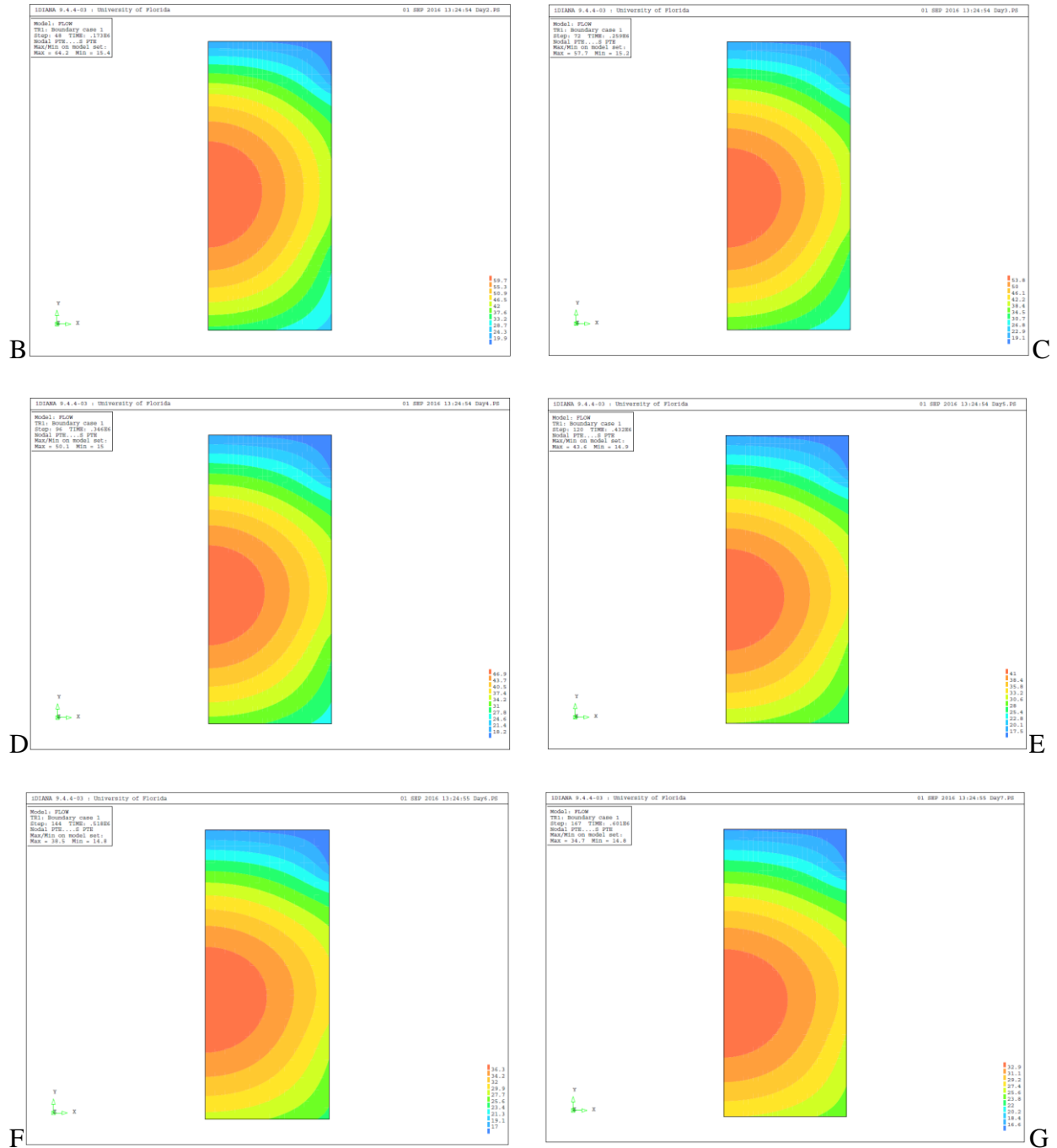


Figure N-39. Continued.